The effect of temperature on the protein corona around nanoparticles and the exocytosis of nanoparticles from cells

Dissertation

zur Erlangung des Grades
´Doktor rerum naturalium (Dr. rer. nat.)´
im Promotionsfach Chemie

am Fachbereich Chemie, Pharmazie, Geographie und Geowissenschaften der
Johannes Gutenberg-Universität in Mainz

vorgelegt von

Jennifer Oberländer

geboren in Wiesbaden-Dotzheim

Mainz, November 2022

Dekanin: Univ.-Prof. Dr. Tanja Schirmeister

1.Berichterstatter: Univ.-Prof. Dr. XXX

2.Berichterstatter: Univ.-Prof. Dr. XXX

Datum der mündlichen Prüfung: _____

The presented work was carried out from August 2019 until November 2022 at the Max Planck Institute for Polymer Research in Mainz in the department of Prof. Dr. XXX under the supervision of Prof. Dr. XXX.

I, Jennifer Oberländer, hereby declare that I wrote this dissertation entitled "The effect of temperature on the protein corona around nanoparticles and the exocytosis of nanoparticles from cells" independently and without any unauthorized external assistance. All used references and resources are completely indicated. I have not submitted the work for an examination and I have not submitted the work or any part thereof to any other faculty or department as a dissertation.

.....

Jennifer Oberländer

Mainz, November 2022

Content

Abstract

Chemically engineered nanoparticles that come into contact with biomolecules containing fluids rapidly become coated with biomolecules forming a biomolecular corona. This biomolecular corona changes the surface properties of the nanoparticles and thereby determines the therapeutic efficiency of the nanoparticles and their interactions *in vivo*. A lot of effort was spent on the analysis of the protein corona and the reduction of the amount of protein in the corona. Creating a so-called stealth effect on the nanoparticles by their functionalization with hydrophilic polymers was shown to prolong the blood circulation time and to reduce the unspecific uptake in immune cells. However, often *in vitro* studies analyzing the protein corona show a lack of consistency in the coating conditions and a thorough analysis of the coating conditions is needed.

Therefore, the first study aimed to analyze the influence of plasma concentration and temperature on the formation of the protein corona. Making use of a proteomic approach with liquid chromatography coupled to mass spectrometry (LC-MS) it was possible to show that the protein corona composition on polystyrene nanoparticles is dependent on the human blood plasma concentration and temperature. Additionally, it was shown that the differences in protein corona composition influence the uptake of the nanoparticles in human cervical cancer cells (HeLa) and human endothelial cells (HUVEC). Besides that, the temperature can also be used to force the protein corona to a specific composition of proteins in it. By using a temperature-responsive nanoparticle with a poly(N-isopropylacrylamide) (PNIPAM) shell, changes in the temperature can be used to specifically catch apolipoproteins from human blood plasma. Through the enrichment of the apolipoprotein J (clusterin) in the protein corona at lower temperatures, the uptake of the nanoparticles in murine macrophages (RAW2647) and HeLa cells can be reduced.

Nanomedicine and nanoparticle research have taken an important role due to its diverse range of applications for diagnosis and therapeutics. However, for most applications, specific cells must be targeted, and the nanoparticles must be taken up into the cell. To achieve the full therapeutic efficacy in these cells or long-term tracking of the nanoparticles during imaging, the nanoparticles must additionally remain in the cell for as long as needed and not be exocytosed. For the application in specific tissues, on the other hand, nanoparticles have to pass through cells and should be exocytosed. While the uptake of nanoparticles is well studied, the exocytosis of the nanoparticles has received little attention so far. We showed that a prolonged incubation time leads to a higher and more stable loading of gold nanoparticles in mesenchymal-like stromal cells. This higher loading resulted in a reduced exocytosis of the gold nanoparticles which would allow for a longer imaging period *in vivo*.

Since several intracellular mechanisms could lead to an exocytosis of nanoparticles, it is important to investigate and understand these processes. A lot of studies focused on the exocytosis pathway analysis

by imaging methods or blocking specific pathways. However, LC-MS proteomics have shown important insights into the intracellular trafficking of nanoparticles and therefore we wanted to extend this method to analyze the exocytosis pathways of nanoparticles. Although no influence of a human blood plasma protein corona on the exocytosis pathways could be shown, the method for the analysis was established and a first hint on the time dependency of the exocytosis pathways was shown. When combining this method with imaging methods in the future, a complete analysis of the intracellular pathways could be gained.

Overall, these findings will help to transfer the stealth properties on nanoparticles by using temperature-responsive nanoparticles and applying a precoating at the desired temperature. Moreover, with deeper knowledge about uptake times and exocytosis pathways, a better efficacy of the nanoparticles can be achieved.

Zusammenfassung

Chemisch hergestellte Nanopartikel, die mit Flüssigkeiten in Kontakt kommen, welche Biomoleküle enthalten, werden schnell durch diese ummantelt und bilden eine biomolekulare Korona aus. Diese biomolekulare Korona verändert die Oberflächeneigenschaften der Nanopartikel und bestimmt damit die therapeutische Effizienz der Nanopartikel und deren Wechselwirkungen *in vivo*. Es wurden viele Studien durchgeführt, um die Proteinkorona zu analysieren und die Menge an Protein in der Korona zu reduzieren. Es hat sich gezeigt, dass die Funktionalisierung der Nanopartikel mit hydrophilen Polymeren einen so genannten „Stealth-Effekt" erzeugt, der die Zirkulationszeit der Nanopartikel im Blut verlängert und die unspezifische Aufnahme in Immunzellen verringert. Allerdings mangelt es den *in-vitro*-Studien zur Analyse der Proteinkorona häufig an Konsistenz bei den Beschichtungsbedingungen, so dass eine gründliche Analyse der Bedingungen zur Proteinkorona Präparation erforderlich ist.

Ziel der ersten Studie war es daher, den Einfluss der Plasmakonzentration und der Plasmatemperatur auf die Bildung der Proteinkorona zu analysieren. Unter Verwendung eines proteomischen Ansatzes mit Flüssigchromatographie gekoppelt mit Massenspektrometrie (LC-MS) konnte gezeigt werden, dass die Zusammensetzung der Proteinkorona auf Polystyrol-Nanopartikeln von der Konzentration und Temperatur des verwendeten menschlichen Blutplasmas abhängig ist. Außerdem wurde gezeigt, dass die Unterschiede in der Zusammensetzung der Proteinkorona die Aufnahme der Nanopartikel in menschliche Gebärmutterhalskrebszellen (HeLa) und menschliche Endothelzellen (HUVEC) beeinflussen. Des Weiteren kann die Temperatur auch genutzt werden, um die Proteinkorona zu einer bestimmten Zusammensetzung von Proteinen zu drängen. Durch die Verwendung eines temperaturabhängigen Nanopartikels mit einer Poly(N-Isopropylacrylamid)-Hülle (PNIPAM) können Temperaturänderungen genutzt werden, um gezielt Apolipoproteine aus menschlichem Blutplasma einzufangen. Durch die Anreicherung des Apolipoproteins J (Clusterin) in der Proteinkorona bei niedrigeren Temperaturen kann die Aufnahme der Nanopartikel in murine Makrophagen (RAW2647) und HeLa-Zellen reduziert werden.

Die Nanomedizin und die Nanopartikelforschung sind aufgrund ihrer vielfältigen Einsatzmöglichkeiten für Diagnose und Therapie zu einem wichtigen Themengebiet geworden. Für die meisten Anwendungen müssen jedoch bestimmte Zellen ins Visier genommen werden und die Nanopartikel müssen in diese Zellen aufgenommen werden. Um eine volle therapeutische Wirksamkeit in diesen Zellen oder eine langfristige Verfolgung der Nanopartikel während der Bildgebung *in vivo* zu erreichen, müssen die Nanopartikel zudem möglichst lange in der Zelle verbleiben und sollten möglichst nicht exozytiert werden. Für die Anwendung in bestimmten tieferliegenden Geweben hingegen müssen die Nanopartikel die Zellen passieren und sollten exozytiert werden. Während die Aufnahme von Nanopartikeln gut untersucht ist, wurde der Exozytose der Nanopartikel bisher wenig Aufmerksamkeit geschenkt. Wir

haben gezeigt, dass eine längere Inkubationszeit zu einer höheren und stabileren Beladung von Gold-Nanopartikeln in mesenchymal-ähnlichen Stromazellen führt. Diese höhere Beladung führte zu einer geringeren Exozytose der Gold-Nanopartikel, was eine längere Bildgebungsdauer *in vivo* ermöglichen würde.

Da verschiedene intrazelluläre Mechanismen zu einer Exozytose von Nanopartikeln führen können, ist es wichtig, diese Prozesse zu untersuchen und zu verstehen. Viele Studien konzentrierten sich auf die Analyse der Exozytosewege durch bildgebende Verfahren oder die Blockierung bestimmter Wege. Es hat sich jedoch gezeigt, dass die LC-MS-Proteomik wichtige Erkenntnisse über den intrazellulären Transport von Nanopartikeln liefert, und deshalb wollten wir diese Methode auf die Analyse der Exozytosewege von Nanopartikeln erweitern. Obwohl kein Einfluss einer humanen Blutplasma-Proteinkorona auf die Exozytosewege gezeigt werden konnte, konnte hier die Methode für die Analyse etabliert werden und ein erster Hinweis auf die Zeitabhängigkeit der Exozytosewege gezeigt werden. Wenn diese Methode in Zukunft mit bildgebenden Verfahren kombiniert wird, könnte eine vollständige Analyse der intrazellulären Wege gewonnen werden.

Insgesamt werden diese Erkenntnisse dazu beitragen, den „Stealth-Effekt“ auf Nanopartikel zu übertragen, indem temperaturabhängige Nanopartikel verwendet und eine Vorbeschichtung bei der gewünschten Temperatur angewendet wird. Darüber hinaus kann mit einem tieferen Wissen über Aufnahmezeiten und Exozytosewege eine bessere Wirksamkeit der Nanopartikel erreicht werden.

Publication list

[1] XXX, XXX, **Jennifer Oberländer**, XXX, XXX, XXX. Modulating Protein Corona and Materials-Cell Interactions with Temperature-Responsive Materials. *Advanced Functional Materials*, **2021**, 32 (2), 2106353.

[2] **Jennifer Oberländer***, XXX*, XXX, XXX, XXX. Temperature, concentration, and surface modification influence the cellular uptake and the protein corona of polystyrene nanoparticles. *Acta Biomaterialia*, **2022**, 148, 271-278. (***shared first)**

[3] XXX*, **Jennifer Oberländer***, XXX, XXX, XXX, XXX, XXX, XXX, XXX. Temperature-Responsive Nanoparticles Enable Specific Binding of Apolipoproteins from Human Plasma. *Small*, **2021**, 18 (3), 2103138. (***shared first)**

[4] **Jennifer Oberländer**, XXX, XXX, XXX, XXX, XXX, XXX, XXX, XXX, XXX. Higher Loading of Gold Nanoparticles in PAD Mesenchymal-like Stromal Cells Leads to a Decreased Exocytosis. *Cells*, **2022**, 11 (15), 2323.

[5] XXX, XXX, XXX, **Jennifer Oberländer**, XXX, XXX, XXX, XXX, XXX. Amphiphilic dendrimers control protein binding and corona formation on liposome nanocarriers. *Chemical Communications*, **2020**, 56 (61), 8663-8666.

[6] XXX, XXX, XXX, **Jennifer Oberländer**, XXX, XXX, XXX, XXX, XXX, XXX, XXX, XXX. Transparent polycarbonate coated with CeO_2 nanozymes repel *Pseudomonas aeruginosa* PA14 biofilms. *Nanoscale*, **2022**, 14 (1), 86-98.

[7] XXX, **Jennifer Oberländer**, XXX, XXX, XXX, XXX. A new methodology combining QCM-D and proteomic profiling enables characterization of protein adsorption on 2D surfaces. *Journal of Colloid and Interface Science*, **2023**, 630, 965-972.

[8] XXX, XXX, **Jennifer Oberländer**, XXX, XXX, XXX. Proteomics-guided intracellular trafficking analysis reveals time-dependent protein corona changes and the intracellular pathway. To be submitted to *Small*.

[9] XXX, XXX, XXX, XXX, XXX, **Jennifer Oberländer**, XXX, XXX. Protein Corona Bio-Inspired Mesenchymal Stem Cells Derived Extracellular Vesicles for Specific Liver Cells Targeting. Submitted to *Nature Nanotechnology*.

[10] XXX*, **Jennifer Oberländer***, XXX, XXX, XXX. Formation of a protein corona on HCT116 extracellular vesicles leads to an increased uptake into human monocytes (preliminary title) (***shared first)**. To be submitted.

Introduction

Nanotechnology and nano-based drug delivery systems have become increasingly important for modern medicine in recent years. The use of nanoparticles as nanomedicine has many advantages compared to traditional drugs. Nanoparticles can serve as a vehicle for drugs to achieve a selective targeting to the site of interest[1]. This can help to overcome the poor bioavailability and stability as well as the toxicity of larger molecules that serve as potential drugs[2]. Moreover, besides the usage of nanomaterials for therapeutics, nanoparticles can also serve as imaging agents or contrast agents[3].

Nanomedicine has become even more important recently. Formulation of mRNA into lipid nanoparticles allowed a more potent immune response *in vivo* compared to naked mRNA[4] and an efficient delivery of the mRNA into cells compared to vaccination with a viral vector[5]. Due to the flexibility of the system of lipid nanoparticles and mRNA, it was possible to rapidly develop a vaccine against the COVID-19 virus and it offers the possibility to quickly adapt vaccines to other diseases in the future[6].

However, the translation from chemically designed nanoparticles to *in vitro* and *in vivo* studies often remains challenging. When nanoparticles come into contact with biological fluids such as blood, a so-called biomolecular corona forms around the nanoparticles. This biomolecular corona consists of various biological molecules such as proteins, lipids, and sugars[7]. These molecules can mask the original surface of the nanoparticles and thereby influence the interactions of nanoparticles with cells or their toxicity[8]. Through a proteomic approach the proteins in the protein corona were intensively investigated since it was shown that the proteins have a huge influence on the *in vivo* response of the nanoparticles[9]. However, the interactions between nanoparticles and proteins forming the protein corona are still not fully elucidated. Predicting what a protein corona and the biological fate of a particular nanocarrier would look like remains difficult.

Thus, this thesis focuses on the formation of the protein corona of nanocarriers and their interactions with cells. This thesis is divided into three subchapters and the first **Chapter A** deals with the temperature sensitivity of the protein corona and its cellular impact. In a first study, the influence of plasma concentration and temperature on the cellular uptake and protein corona of polystyrene nanoparticles is analyzed. In the second study of the chapter, the temperature-dependent binding of apolipoproteins from human plasma on temperature-responsive nanoparticles is investigated.

In **Chapter B** the intracellular formed protein corona is studied to track the intracellular fate and exocytosis behavior of nanoparticles. In the first study of the chapter, the exocytosis rate in dependence on the loading efficiency of gold nanoparticles in mesenchymal-like stromal cells is investigated. In order to quantify the amount of gold nanoparticles in the cells and supernatant, a new method using inductively coupled plasma-optical emission spectrometry was developed. The second part of the chapter deals with the exocytosis of magnetic dextran coated iron-oxide nanoparticles. Here, the protein

corona of exocytosed nanoparticles is used to predict the intracellular mechanisms by which the nanoparticles are eliminated from the cell.

Furthermore, I contributed to different other projects during my PhD. Therefore, the last **Chapter C** gives a short summary of these projects and shows further applications of the protein corona and the inductively coupled plasma-optical emission spectrometry.

Chapter A – The influence of temperature on the protein corona

The first chapter is divided into three subchapters. The first subchapter provides an introduction to the overall topic and the theoretical background. Parts of the introduction have been published in the review **[1]** showing the state of the art. In the second subchapter, the second publication **[2]** is presented, which demonstrates the influence of the temperature and the concentration of human plasma on the proteins adsorbed on polystyrene nanoparticles. The results shown were published in a peer-reviewed journal (Acta Biomaterialia) and the text is an almost identical reproduction of the published paper. The third publication **[3]** is introduced in the third subchapter and it shows that the protein adsorption on nanoparticles can be controlled by the use of a temperature-responsive polymer. All results and the text from the published paper in a peer-reviewed journal (Small) are shown in a nearly word-to-word reproduction.

[1] XXX, XXX, **Jennifer Oberländer**, XXX, XXX, XXX. Modulating Protein Corona and Materials-Cell Interactions with Temperature-Responsive Materials. *Advanced Functional Materials*, **2021**, 32 (2), 2106353.

[2] **Jennifer Oberländer***, XXX*, XXX, XXX, XXX. Temperature, concentration, and surface modification influence the cellular uptake and the protein corona of polystyrene nanoparticles. *Acta Biomaterialia*, **2022**, 148, 271-278. (***shared first)**

[3] XXX*, **Jennifer Oberländer***, XXX, XXX, XXX, XXX, XXX, XXX, XXX. Temperature-Responsive Nanoparticles Enable Specific Binding of Apolipoproteins from Human Plasma. *Small*, **2021**, 18 (3), 2103138. (***shared first)**

1. Theoretical background

The use of nanotechnology in modern medicine has been steadily expanded in recent years and has reached a wide range of applications[2]. By definition, only engineered structures with a size range of 1-100 nm are considered as nanotechnology[10]. However, in most areas and in biomedical applications larger structures of some hundred nanometers are also included in nanotechnology[10]. A large part of the research on nanotechnology is conducted on nanoparticles and over the last decades, many types of nanoparticles have been developed[11].

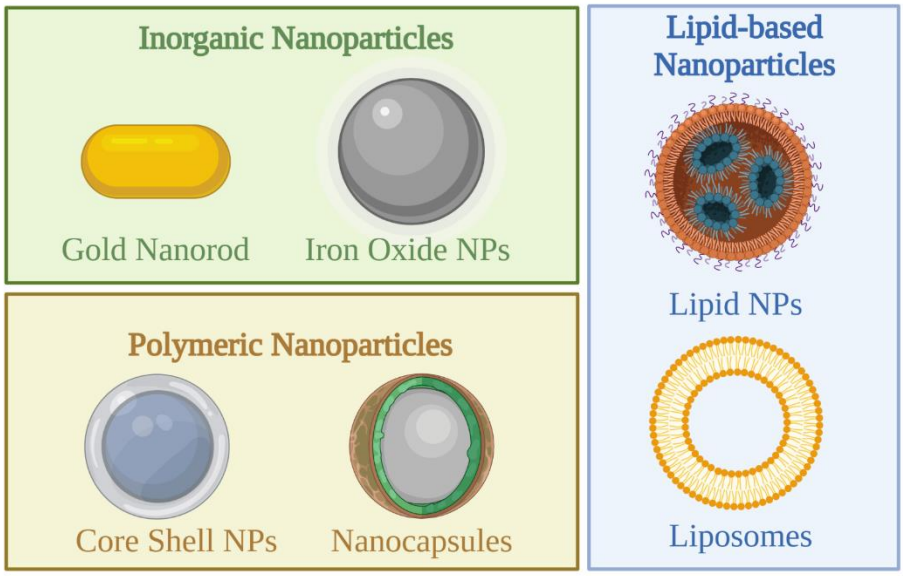

Figure 1.1. Three different classes of nanoparticles under investigation for nanomedicines. For each class, two examples of nanoparticle types are shown. Figure created with BioRender.com**.**

The broad applicability of nanoparticles (NPs) in medicine is due to their diverse compositions and properties (Figure 1.1). While lipid-based NPs captivate with their high biocompatibility and ability to carry large payloads, inorganic NPs convince with the possibility to synthesize various sizes and geometries and their good applicability for imaging applications[11]. On the other hand, e.g. polymeric NPs benefit from the advantage of controlled release of active drugs and a wide variety of characteristics and materials[12]. All these types of NPs have in common that they help to overcome biological barriers and improve the safety and efficacy of drugs[1]. However, despite their great potential as drug delivery agents, only a few formulations have been approved for patients yet[13, 14]. One reason for this is the interaction of NPs with proteins in the human body and the direct adsorption of proteins onto the surface of the NPs[8, 15]. This nano-bio interface is often not taken into account in the design of new NPs and therefore results in the fact that only a few new drugs based on nanotechnology are approved[14].

1.1 The biomolecular corona on nanoparticles

The adsorption of proteins onto the surfaces of NPs was first described in the 1960s by Vroman and colleagues[16]. Since that time, many studies have dealt with this effect. While Vroman investigated protein adsorption by gel electrophoresis at that time, analysis by mass spectrometry became more and more common and the name protein corona was established for protein adsorption[9]. Nowadays, the term has evolved even further and the protein corona is now increasingly referred to as biomolecular corona[17]. This should reflect the fact that, in addition to proteins, other biomolecules such as lipids and sugars also adsorb on the nanoparticles[18]. However, since proteins make up the largest proportion of the biomolecular corona, they have also been studied the most[17].

The adsorption of proteins on the surface of nanocarriers happens immediately after their contact with biological fluids[19, 20]. This spontaneous adsorption is driven by different attractive forces including Van der Waals interactions, hydrogen bonds, electrostatic forces, hydrophobic forces, and disulfide interactions (Figure 1.1.1)[18, 19, 21, 22]. First small proteins with a high diffusion rate and high concentration bind to the NPs. These loosely bound proteins are replaced over time by proteins with a higher affinity to the NPs and the hard protein corona forms with characteristic and strongly bound proteins[23, 24]. This effect is known as the Vroman effect[25]. The time until the proteins with the highest affinity have bound depends on the physicochemical properties of the NP but once formed, the protein corona remains stable for several hours or days[26-28]. Despite the high complexity and the great diversity of proteins in human plasma, only about 300 proteins were found in the protein corona of different NPs[26]. This clearly demonstrates that the protein corona is a complex system in which certain proteins bind with a high affinity[18]. Moreover, often the protein corona is described with two different layers, the hard corona and the soft corona. While the hard corona is described as the inner layer of proteins tightly bound directly to the surface of the NP, the soft corona is considered as an outer shell of loosely bound and rapidly exchanging proteins[20, 23, 24]. However, these two layers cannot be considered as two independent layers and the importance of the soft corona has not yet been clearly demonstrated[8, 9].

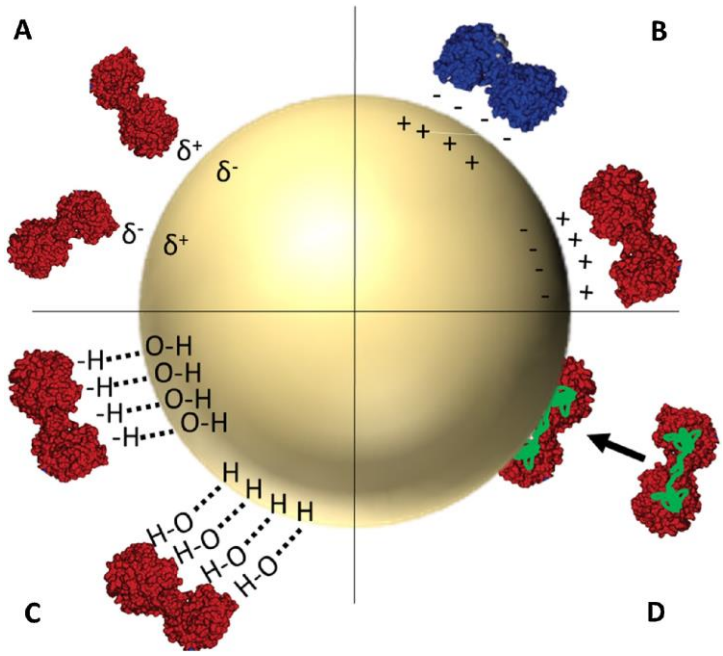

Figure 1.1.1. Schematic representation of the surface interactions between nanoparticles and proteins. The main interactions which drive protein adsorption on nanoparticles are Van der Waals interactions (A), electrostatic forces (B), hydrogen bonds (C), and hydrophobic forces (D). Figure reprinted with permission from Mahmoudi et al.[19]. Copyright © 2016, Elsevier.

Since the protein corona on NPs turns their chemical identity into a biological identity, it can alter the properties of an engineered NP mostly[18, 29, 30]. Through the protein corona on the NPs, the adhesion capacity of them on cell membranes can be reduced and therefore the uptake and internalization of NPs in cells can be reduced[31, 32]. On the opposite, specific proteins in the protein corona, such as immunoglobulins, can increase the uptake into certain cells[33]. Moreover, the protein corona can cover targeting moieties of the NP and thereby reduce its uptake into target cells[33, 34]. Despite that, the protein corona can even lead to unspecific uptake through receptor recognition of the proteins in the protein corona[35, 36]. In addition, the proteins in the corona can change their structure or denature, thereby promoting inflammation and toxicity[8, 37]. As the biomolecular corona is dependent on the properties of the NPs, it is important to understand these parameters to minimize or control protein adsorption.

1.2 Physicochemical properties

The surface of the NPs is the key factor influencing the formation of the biomolecular corona. And the surface of the nanomaterials is determined by the physicochemical properties of the nanomaterial. Some of these physicochemical properties influencing the protein adsorption on NPs are the size, shape, ligands, and surface charge[38, 39]. Some important correlations between the physicochemical properties and the protein adsorption have already been reported[8].

One of the most prominent and extensively studied key factors determining protein adsorption is the surface charge of the NP[40]. Since a majority of the blood proteins have mainly a negative charge, positively charged NPs bind higher quantities of protein, and the protein corona is thicker compared to negatively charged and neutral NPs[8, 41]. However, negatively charged NPs still attract a higher amount of proteins compared to neutral NPs due to interactions with positively charged proteins or positive regions of proteins[42-45]. Besides neutral NPs, zwitterionic NPs with an overall neutral surface charge at their isoelectric point showed a significantly reduced protein adsorption and were reported as promising low fouling materials[46, 47]. These protein adsorption properties of charged NPs have a dramatic influence on the behavior of the NPs *in vivo*. Positively charged NPs show a high uptake into cells through their ability to bind easily to the negatively charged cell membrane. However, due to their high protein binding, they show a high toxicity, a high uptake in macrophages, and in consequence a fast clearance of these NPs from the blood plasma[40]. The high uptake of charged NPs in macrophages can be explained by their preferential binding of opsonins (e.g. IgG, fibrinogen, albumin)[42, 48, 49]. In contrast, negatively charged and zwitterionic materials have shown that dysopsonins are enriched in their protein corona (e.g. clusterin) which leads to a reduced unspecific uptake in macrophages[49-53]. Moreover, since the surface of the NPs is still charged, the uptake into the desired cells is still high[40].

Besides the surface charge, the size and morphology of the NPs have a great influence on the protein adsorption. Smaller NPs have a higher surface-to-volume ratio and one could expect therefore that smaller NPs adsorb higher amounts of proteins per weight of NPs[40]. However, it could be shown for different NP systems that the actual trend is the opposite. It was shown for different polymeric[20, 54, 55] but also for silica[56], dendrimeric[57], and metal[58] NPs that more protein adsorbs on bigger nanoparticles compared to smaller ones. This is due to the lower curvature degree of bigger particles which makes the surface of the NP better accessible to the proteins[29, 40]. In addition, extremely small NPs with sizes smaller than 10 nm showed nearly no protein adsorption[8]. Nevertheless, although the size influences the amount of protein, the composition of the protein corona is very similar and almost the same for different sizes[56, 59]. Besides the size of the NPs, the surface roughness and the shape influence the curvature as well. Roughness of NPs leads to an irregular surface and an increased local surface curvature[40]. Therefore, the binding of the proteins is hindered and rough NPs have shown to bind less protein[60]. While for gold NPs it was shown that star shaped gold NPs bind more protein in comparison to rod shaped ones[61], for mesoporous silica NPs with rod shape the total amount of protein was higher than on

spherical NPs[62]. Moreover, the shape did not only affect the amount of protein, it also directly influenced the composition of the protein corona[61, 62].

Of course, the surface properties do not only depend on the charge and the size of the NPs. Another factor that drastically influences protein adsorption is hydrophobicity. Early studies have already shown that by increasing the amount of hydrophobic monomer in the polymer, the amount of protein adsorbed increased as well[29]. This trend that hydrophobic NPs tend to adsorb more proteins was confirmed by several studies later[63-66]. Moreover, it was also shown that specific proteins prefer to bind either to hydrophilic or hydrophobic NPs[40]. For example, it was shown that apolipoproteins, which are known as dysopsonins to induce the stealth effect on NPs, tend to adsorb more on hydrophobic NPs[67-69] but can also adsorb on hydrophilic NPs[70-72]. To improve the applicability of NPs *in vivo*, different polymeric coatings have been investigated to decrease the hydrophobicity but increase the adsorption of dysopsonins on the NPs[67]. Thereby polyethylene glycol (PEG) coating was most widely applied. PEGylation has shown to decrease the protein adsorption by creating a hydrophilic shell around the NP and to increase the circulation time by decreasing the clearance of the NPs by phagocytes[73-75]. Besides the hydrophilic character PEGylation provides a steric hindrance, so that proteins cannot penetrate to the NPs surface[8]. However, this effect strongly depends on the PEG chain length and density on the surface[74]. Longer PEG chains provide a bigger distance of the NPs to the proteins making protein binding less favored[8]. The PEG density influences the conformation which the PEG chains form on the NP surface. While at low PEG densities the mushroom conformation is the preferred one, at higher densities PEG forms a brush conformation which hinders protein adsorption[76, 77]. However, PEGylation does not prevent protein adsorption completely. In fact, certain proteins, mainly dysopsonins, still bind on the PEGylated nanoparticles and often they are responsible for the stealth effect of the NPs[18, 75, 78].

In addition to these physicochemical factors influencing the protein corona, the exposure conditions as e.g. the protein source can also influence the protein corona composition. Here, the species of the protein source has obviously a huge influence on the protein corona. It was shown that in human plasma one of the main adsorbed proteins on polystyrene NPs was clusterin followed by Apo-A1. On contrary, in mouse plasma, Apo E and Apo-A1 were the most abundant proteins in the protein corona[79]. Moreover, comparing human, mouse, and rabbit protein corona it was shown that the immunoglobulin content differed significantly between 1% for mice and 13% for humans[80]. Additionally, for the use of blood plasma an anticoagulant is needed but it was shown that this can influence the protein adsorption as well[14, 59]. Besides this, protein corona composition may vary also with temperature. Even in the physiological range, the protein corona can change depending on the incubation temperature[7]. This factor is often forgotten and must be taken into account, especially when working with temperature-responsive materials[81, 82].

1.3 Analytical methods for the protein corona

Since many different factors can affect the protein corona composition, the protein corona of each newly synthesized NP needs to be analyzed. Therefore, different approaches have been developed to analyze the protein corona. While initially proteins from protein corona were separated by Sodium dodecyl sulfate polyacrylamide gel electrophoresis (SDS-PAGE) and then single bands were analyzed by mass spectrometry, modern corona studies analyze the entire protein corona[83]. In the bottom-up proteomic approach the proteins are digested into peptides after collecting them and in the top-down approach the undigested and intact proteins are measured (Figure 1.3.1)[83, 84]. Bottom-up proteomics which is also called shotgun proteomics, is the most commonly used method for protein corona analysis and is therefore described in more detail here.

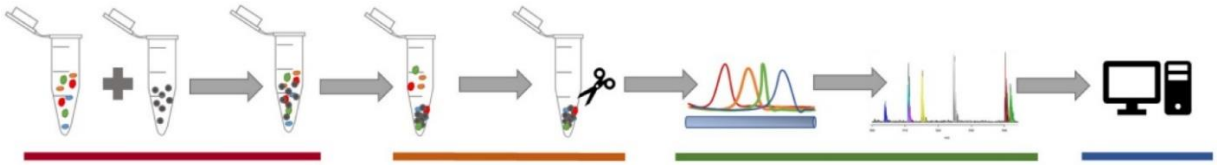

Figure 1.3.1. Bottom-up proteomic approach for the analysis of the protein corona. Protein corona characterization is divided into four different phases. 1) Nanoparticles incubation with biological fluids (red bar). 2) Protein isolation and digestion to peptides (orange bar). 3) Separation and characterization of peptides by liquid chromatography and mass spectrometry (green bar). 4) Protein identification using deconvolution software and protein databases (blue bar). Figure reprinted with the permission of Chetwynd et al[83]. Copyright © Elsevier 2019.

The first step during protein corona analysis with the bottom-up approach is the formation of the protein corona on the NPs. As previously described this is a critical step in corona analysis since the exposure conditions can already influence the protein corona significantly. To achieve the best possible results and to best understand the situation *in vivo*, it is necessary to consider e.g. the incubation temperature, pH, protein to nanoparticle ratio, or the shear stress for protein corona formation[85]. Especially the blood flow is a difficult factor to reproduce, but it can lead to distinct changes in the protein corona[86].

The next step in protein corona preparation and analysis is the isolation of the NPs and removal of unbound proteins. The most used method for the isolation of the NPs is centrifugation but magnetic separation or chromatographic methods have also been reported[86, 87]. Centrifugation is easy to perform and applicable for many different NP protein complexes[29, 87, 88]. However, centrifugation steps need to be adapted to each new NP protein system and protein aggregates may sediment during centrifugation as well[86]. Magnetic separation avoids this problem and is therefore described as less interfering. Aggregation of proteins does not falsify the results there, however, this purification method is limited to magnetic and thus a very small group of particles[45, 89]. Since for most issues the hard protein corona should be analyzed, washing of the NPs is needed in order to remove loosely bound proteins. For both methods, centrifugation and magnetic separation, loss of NPs and proteins is reported[59, 85]. However, for magnetic separation, a lower loss of analyte was reported[86]. The washing buffer can also influence the protein corona. Changes in pH, ionic strength, or temperature can alter the composition of the protein

corona[81, 87, 90]. Therefore, a good balance must be found for the washing step. Insufficient washing means too much contamination by weakly bound proteins, whereas too much washing can lead to the loss of actual bound proteins[8]. Asymmetric flow field-flow fractionation (AF4) is being used to analyze the more loosely bound proteins in the corona as well. This method is comparable to chromatographic methods and is therefore considered as a gentle purification method[87, 91, 92]. However, this method also has a few disadvantages, e.g. the high dilution of the samples or the time-consuming nature of the process[86, 93]. Other, but less frequently used isolation methods, are size exclusion chromatography and hydrodynamic chromatography[29, 61, 94, 95]. However, centrifugation and magnetic separation remain the most popular methods due to their ease of implementation[8, 85].

After washing the proteins from the protein corona, the NPs need to be separated. Therefore, mainly two different methods have been explored. Proteins can either be desorbed from the NPs surface or directly on the surface digested[66]. Mostly, desorption with different surfactants is applied to separate proteins and NPs. SDS has been widely applied and different protocols were developed with varying temperatures, desorption times or SDS concentrations[96-99]. Besides SDS also other desorption buffers have been developed e.g. using urea, Triton X, or dodecyltrimethylammonium bromide[8, 96]. Desorbing the proteins from the surface allows further investigations of the protein composition using the molecular weight or the charge of the proteins[8]. However, one must make sure that the proteins are completely desorbed and do not remain on the particle[99-101].

For the bottom-up proteomics approach, the proteins need to be digested into peptides before analysis by liquid chromatography and mass spectrometry (LC-MS). For a more efficient digestion the disulfide bonds of the proteins are often first reduced with reducing agents as 1,4-dithio-DL-threitol (DTT)[75, 85]. To avoid reformation of the disulfide bonds the free thiol groups are alkylated afterwards with an alkylation agent such as iodoacetamide (IAA)[102]. Protein digestion is then performed by the use of specific proteins e.g. trypsin[103]. Digestion can be carried out in three different ways: In-gel digestion, In-solution digestion, and on-particle digestion[85]. In-gel digestion was the method that was originally used a lot. Proteins are therefore separated by SDS PAGE and afterwards protein bands are cut out and digested. The resulting peptides can then be extracted from the gel[61, 104, 105]. However, with this method, only the highly abundant and visible proteins in the protein corona can be analyzed[85]. Therefore, nowadays the in-solution method is mostly used where the whole protein solution is analyzed[75, 102, 104, 106]. Here, the most critical step is the protein desorption from the NPs surface. However, with attention to the choice of desorption solutions, this method leads to a proper digestion and protein corona analysis[85]. The last method, the on-particle digestion, benefits from requiring fewer steps and no desorption buffer to obtain the peptides[8, 104]. However, cleavage sites of the proteins may not be accessible to trypsin, resulting in incomplete digestion. In addition, the peptides may reattach to the particles after digestion[104]. Nevertheless, it has been shown that this method is more sensitive and can detect more low abundant proteins than the in-gel method[104, 107, 108].

After the digestion of the proteins, in the next step the peptides are separated by LC and are analyzed by MS. Since in complex peptide solutions several peptides have similar masses, a separation of the peptides by e.g. chromatography is necessary[103]. During chromatographic separation the peptides are pushed through a hydrophobic packed column with a polar mobile phase. Since hydrophobic peptides will interact more with the hydrophobic column than hydrophilic peptides, the peptides are separated according to their hydrophobicity. With this separation it is possible to distinguish peptides with the same mass but different hydrophobicity[103]. After LC separation other separation techniques such as ion mobility separation can be applied where peptides collide with neutral gas and are by that separated according to their size and gas phase structure[109]. After separation, peptides are analyzed with a mass spectrometer where the mass to charge ration is measured. To further improve the resolution and analyte identification, mass spectrometers are often coupled to a quadrupole or time-of-flight (TOF) mass spectrometers are used[103, 109].

The last step of bottom-up proteomics is the analysis of the data where the proteins are identified from the mass spectrum of the LC-MS. With the use of a deconvolution software and databases containing all proteins and amino acid sequences of expected proteins, the peptides are assigned to the proteins. For human proteins often the whole known proteome is used for protein analysis. Therefore, the tryptic digestion of the proteins is simulated to create the peptide fragments. Theoretical fragmentation of the proteins is then compared to the measured data and the peptides are assigned to the proteins[103]. Prior to peptide matching, different data filtration steps can be added to reduce background noise or false discovery[110]. For the quantification of the proteins, either a label free approach or an isotope labeling can be applied[111]. Isotope labeling creates a shift in the mass to charge ratio of the peptide and through the comparison with the unlabeled peptide a quantification of the protein can be done[103]. However, labeling of the samples can be complicated and expensive and consequently label free approaches have been developed[111, 112]. With this method it is possible to absolutely quantify the amount of protein in solution by the use of an internal standard peptide[112]. Due to the complexity of this process, the data analysis, protein identification, and protein quantification are performed by the use of specified software.

Overall, previous studies have shown that the protein corona needs to be considered when developing new particles and that the protein corona preparation and analysis influence the results. Some factors influencing the corona e.g. size and surface hydrophobicity have been widely analyzed and their influence is well known. However, other factors such as the temperature are often not taken into account even when working at different temperatures. Therefore, it is important to analyze the influence of the temperature on the protein corona.

1.4 Temperature-responsive polymers in protein adsorption

Copyright:

[1] XXX, XXX, **Jennifer Oberländer**, XXX, XXX, XXX. Modulating Protein Corona and Materials-Cell Interactions with Temperature-Responsive Materials. *Advanced Functional Materials*, **2021**, 32 (2), 2106353.

Contribution:

XXX wrote the manuscript for publication. I assisted for biological questions and proteomics-related questions and I have proofread the manuscript. XXX, XXX, XXX, and XXX have proofread the manuscript and supervised the project.

1.4.1 Introduction

Proteins are composed of amino acids within some cases phosphate groups or lipids and oligosaccharide chains. The heterogeneous structures and functions of proteins hence lead to a complex pattern of adsorbed proteins[113]. The protein adsorption is a result of an overlap of transport, adsorption, and repulsion processes. It is a kinetic process, initiated by the adsorption of highly mobile proteins followed by replacement of initially adsorbed proteins by higher affinity proteins[25, 114]. Moreover, proteins undergo a conformational change when they are adsorbed on the surface due to protein-surface interactions. Van der Waals forces, hydrogen bonds as well as electrostatic interactions play a role on protein adsorption in case of charged surfaces[115]. In addition, external parameters such as temperature, pH value, and ionic strength can have a strong influence on protein adsorption around materials. The number of protein adsorbed around materials could be either increased or decreased upon increasing temperature, mainly due to change of protein conformation[116, 117].

Protein adsorption can be regulated using stimuli-responsive materials such as temperature-responsive polymers. For biomedical applications, temperature-responsive polymers of interest usually display a phase transition temperature (lower critical solution temperature – LCST or upper critical solution temperature – UCST) around body temperature (≈ 37 °C) in water, above which they are either collapsed or dissolved, respectively[118-120]. Polymers with a LCST in water in the physiological range such as poly(N-isopropylacrylamide) (PNIPAM) and its derivatives display a conformational change from a hydrophilic coil to a hydrophobic globule at T > LCST, due to changes in solvation of the polymer chains[121]. Other polymers (e.g. poly(N-acryloylglycinamide) and copolymers containing acrylamide units) displaying a UCST in the physiological range of temperatures in water and hence undergo precipitation below UCST[122].

The amount of protein adsorbed on the surface of temperature-responsive polymers was found to be strongly temperature-dependent. Indeed, the adsorption of bovine serum albumin (BSA) on PNIPAM brushes at 23 °C (T < LCST) was ≈ 3 times lower than its adsorption at 37 °C (T > LCST) after the swelling of PNIPAM chains in water. This resulted in the lift-off of proteins from the PNIPAM surface at T < LCST[123]. Temperature-responsive materials were used for separating specific proteins from a protein mixture[124]. Specific proteins, such as lysozyme and human serum albumin which were present in a protein mixture, were bound to temperature-responsive copolymers containing NIPAM units at T > LCST. The proteins were then retrieved by lowering temperature to T < LCST. Besides, temperature-responsive nanoparticles could be enriched with different proteins when altering incubation temperature due to the change of surface hydrophobicity[125, 126]. Protein adsorption on nanoparticles leads to rapid (<0.5 min) formation of protein corona[26, 127, 128]. The protein corona around the nanoparticles strongly influences cell uptake, biodistribution, and clearance of nanoparticles[28].

The uptake of temperature-responsive materials prepared with PNIPAM by cells significantly increased at 37 °C due to favored interactions between collapsed polymer chains and the cell membrane. Thus,

the temperature-responsive materials were applied for intracellular drug delivery[129]. The temperature-responsive materials were also used for growing cells at 37 °C and detaching them by reducing the temperature to T < LCST, without the need of chemical disruption that may harm cells[130-134].

1.4.2 Nanoparticles-Protein Interactions

It is known that protein corona plays a key role in biological response such as the recognition of nanoparticles by macrophages[28]. The protein corona on dextran-coated superparamagnetic iron oxide nanoparticles (SPIONs) was investigated at different temperatures[81, 82]. Dextran-coated SPIONs with positive, negative, and neutral surface charge were incubated in fetal bovine serum (FBS). According to liquid chromatography-mass spectrometry (LC-MS) measurements, the relative content of serum albumin, serotransferrin, apolipoprotein A1, and alpha-2-HS glycoprotein in the protein corona was dependent on the temperature (5–45 °C), although no clear trend could be identified[81]. Furthermore, differential centrifugal sedimentation results revealed that the amount of protein in the corona on SPIONs was also dependent on temperature, but with no noticeable trend[82]. Inactivation of proteins by heating fetal calf serum (FCS) affected the composition and amount of the proteins in the corona around nanoparticles[135, 136]. Typically, heating serum or plasma to 56 °C for 30 min is applied to inactivate heat labile proteins such as complement proteins, which can interfere with immunological assays[137]. The amount of proteins in the protein corona formed on polystyrene nanoparticles in FCS preheated to 56 °C was larger than for the nanoparticles incubated in a serum that was not heated[135].

Clusterin, a protein providing stealth properties to nanoparticles, was the major protein (>50%) identified in the protein corona of polystyrene nanoparticles stabilized with Lutensol AT-50 incubated in human serum or plasma at 37 °C for 1 h[136]. The amount of clusterin in the protein corona was reduced to ≈ 3% when incubating the nanoparticles with heat-inactivated human plasma or serum. 40% clusterin was unfolded during the heat inactivation procedure (56 °C for 30 min), as measured by scanning fluorometry. The relative amount of complement C3 protein in the protein corona was reduced from ≈ 6.8% to ≈ 0.8% when incubating hydroxyethyl starch nanocapsules with inactivated serum at 37 °C for 1 h instead of incubating the nanoparticles with the native serum[136]. Therefore, the type and amounts of proteins in the protein corona around nanoparticles are influenced by temperature. Moreover, the protein corona can be tuned by inactivating serum or plasma with a heat treatment. Controlling temperature during protein corona formation is hence crucial.

1.4.3 Interactions between Proteins and Temperature-Responsive Polymers

The hydrophobicity of temperature-responsive materials is altered upon temperature change. At T < LCST, temperature-responsive polymer chains are in the hydrophilic state due to their solvation in water, resulting in less interactions between protein and polymer, and hence less proteins are adsorbed.

On the contrary, higher protein adsorption is obtained at T > LCST than at T < LCST due to more hydrophobic interactions between polymer and protein. The change of surface hydrophobicity can hence be used for regulating the amount of proteins adsorbed. The surface hydrophobicity of flat surfaces can be determined by water contact angle measurement[123, 138]. For nanoparticles, the surface hydrophobicity can be determined based on the adsorption of organic molecules[49, 139-141], by evaluating the partition coefficient between octanol and water phases[141], and by measuring their maximum optical density upon dispersion in solvents with different surface tensions[142].

Protein Adsorption Amount Regulated by Temperature-Dependent Surface Hydrophobicity

PNIPAM is the most reported polymer for controlling protein adsorption by change of hydrophobicity as a consequence of a change of temperature. This peculiar ability of PNIPAM has been applied for controlling adsorption of BSA[123, 138, 143], fibrinogen[144], FBS[145], and human plasma on various surfaces[125]. BSA is the most abundant protein found in bovine serum. BSA was adsorbed before fibronectin on poly(allylamine) surface immersed in a mixture of BSA and fibronectin. This phenomenon was attributed to the lower molecular weight and higher abundancy of BSA compared with fibronectin[146]. BSA on the surface was then replaced by fibronectin (a protein promoting cell adhesion and spreading), following the Vroman effect. Therefore, BSA was employed as a model protein to prescreen whether PNIPAM-based surfaces can be applied for cell culture with an ability to detach cell sheets at T < LCST. The adsorbed amount of ^{3}H-BSA (BSA labeled by ^{3}H-acetic anhydride) on glass coated with PNIPAM (LCST = 32 °C) at 37 °C was ≈ 0.6 times larger than at 10 °C[138]. On the contrary, no significant difference in ^{3}H-BSA adsorption at 10 and 37 °C was observed for PNIPAM-co-N-tert-butylacrylamide (LCST = 20 °C) and PNIPAM-co-acrylamide (LCST = 42 °C) surfaces. The density and molecular weight of PNIPAM played a role on the amount of adsorbed BSA at T > LCST[123]. Indeed, adsorption of ^{125}I-BSA (BSA labeled by iodine-125) on PNIPAM surface at 37 °C with a higher molecular weight and grafting density (126 kDa and 0.11 nm^{-2}) ([^{125}I-BSA] ≈ 35 ng/cm^{2}) was lower than for the surface with a lower molecular weight and grafting density (85 kDa and 0.09 nm^{-2}) ([^{125}I-BSA] ≈ 45 ng/cm^{2}). The amount of adsorbed protein at T > LCST on the PNIPAM surface increased because the protein was capable of penetrating into the tightly PNIPAM brushes to extensively interact with PNIPAM chains. Moreover, the adsorbed amount of ^{125}I-BSA at 23 °C (T < LCST) was ≈ 20 ng/cm^{2} for surfaces of PNIPAM with different molecular weights and densities, suggesting that the density and molecular weight of PNIPAM on the surface did not regulate protein adsorption when PNIPAM was hydrophilic.

BSA was also used as model protein for determining the thermoresponsive protein separation feature of PMMA/PNIPAM nanofibrous mats[143]. The equilibrium concentration of BSA adsorbed on PMMA/PNIPAM mats was ≈ 8 times larger at 37 °C than at 25 °C. Moreover, 85% of BSA could be released from the mats when lowering temperature from 37 to 25 °C. Thus, PNIPAM-based nanofibrous mats can find a potential application for bioseparation because no chemicals were required to detach proteins from the mats. Fibrinogen is a highly abundant protein in blood plasma, possessing the ability

to promote adhesion of blood platelets and cells to surfaces[147]. Therefore, the amount of fibrinogen reflects whether cells successfully grow on a surface. The amount of adsorbed fibrinogen at 37 °C (T > LCST) on a PNIPAM surface containing hydrophobic dodecyl trithiocarbonate terminal group was 7 times larger than for the PNIPAM surface with a carboxylic acid terminal group[144]. On the contrary, fibrinogen was adsorbed on the surface at T < LCST in negligible amount, without noticeable difference between the PNIPAM with different terminal groups.

The adsorption of FBS on PNIPAM surfaces has also been reported. FBS was selected because it is widely used as a supplement in cell culture media, and thus its adsorption on PNIPAM-coated surfaces could enhance cell adhesion. The adsorption of FBS on gold substrates grafted with PNIPAM and alkanethiols with different end groups at 25 and 37 °C increased with increasing hydrophobicity and the electron withdrawing ability of the alkanethiol's end group (-COOH > -CH3 >-OH > oligo(ethylene glycol))[145]. Moreover, FBS could be almost completely recovered from the surface when lowering temperature from 37 to 25 °C, when increasing density of PNIPAM on the surface from 0.07 to 0.15 chains per nanometer square. Therefore, surface hydrophobicity, surface functional groups, and PNIPAM density are important parameters for designing temperature-responsive cell culture surfaces.

Serum and plasma contain many types of protein, which can bind onto foreign surfaces to yield a protein corona. The amounts and types of proteins in the protein corona depend, among other properties, on surface hydrophobicity[63]. The variation of the protein corona on temperature-responsive surfaces has been demonstrated with PNIPAM nanoparticles[148]. Below the LCST, the interactions between proteins and PNIPAM chains were reduced due to the solvation of PNIPAM, increasing the energy required for forming tightly bound proteins (hard corona) around nanoparticles. Proteins hence were loosely bound around nanoparticles (soft corona) at this temperature range. On the contrary, the interactions between proteins and PNIPAM chains increased when PNIPAM chains were in the hydrophobic state (T > LCST). These interactions lowered the energy to form a hard corona around nanoparticles, resulting in more protein adsorption. To prove that the change of surface hydrophobicity of PNIPAM by temperature controls the formation of the protein corona, protein amounts on magnetic beads coated with PNIPAM were measured after incubating the beads in human plasma at 25 and 37 °C for 2 h[125]. The concentration of human plasma on the beads at T > LCST was slightly larger (105 μg/mL) than at T < LCST (90 μg/mL). Temperature could be used to control the amount of proteins bound to PNIPAM-based surfaces when incubating the surfaces in protein mixtures. PNIPAM is not a bio-inert polymer because its amide moieties can strongly bind with proteins via hydrogen bonding[149]. To overcome these limitations, temperature-responsive polymers composed of poly(ethylene glycol) (PEG) such as poly[di(ethylene glycol) methyl ether acrylate], poly[oligo(ethylene glycol) methyl ether methacrylate], and poly[2-(2-methoxyethoxy)ethyl methacrylate] were developed because PEG is non-cytotoxic and less susceptible to hydrogen bonding than PNIPAM[150]. The LCST of poly[2-(2-methoxyethoxy) ethyl methacrylate] (PME2MA) was 25 °C[151]. Thereafter, the glass surface grafted with PME2MA was incubated in BSA, human immunoglobulin G, or bovine plasma fibrinogen for 1 h at 25 and 37 °C. The

amount of adsorbed protein on the surface at 37 °C was ≈ 1.5, 2, and 2.5 times higher than at 25 °C for BSA, human immunoglobulin G, and bovine plasma fibrinogen, respectively. The PME2MA surface hence displayed a protein repellent property at T < LCST. The amount of adsorbed protein on PME2MA surfaces was ≈ 2 times and ≈ 5 times larger at 37 °C than at 22 °C for fibrinogen and fibronectin, respectively[152]. These two proteins promote cell adhesion on surfaces and the PME2MA surfaces could hence be used as cell culture scaffold.

Poly(glycidyl methyl ether-co-glycidyl ethyl ether) is a temperature-responsive polymer with a biocompatibility and a bio-inertia comparable to PEG. Gold substrates grafted with this polymer were investigated as cell culture scaffold[153]. The amount of fibrinogen on poly(glycidyl methyl ether-co-glycidyl ethyl ether) surfaces, a protein promoting cell adhesion, measured by surface plasmon resonance (SPR), was higher at T > LCST (40 °C) than at T ≤ LCST (25–37 °C), making these substrates potentially interesting as cell scaffolds. Similarly to PME2MA surfaces, the ability of the scaffold to release cells from the surface needs however to be investigated.

Poly(2-alkyl-2-oxazoline) are thermoresponsive pseudopeptide biocompatible polymers showing low accumulation in organs[154]. Poly(2-isopropyl-2-oxazoline) with a LCST ≈ 30 °C was processed as nanoparticles for drug-delivery applications[155]. The total protein concentration on nanoparticles in bovine serum after incubation for 1 h was ≈ 2 times larger at 37 °C than at 20 °C (5.6×10^{-14} mg/NP at 20 °C and 9.9×10^{-14} mg/NP at 37 °C), indicating that change of surface hydrophobicity upon temperature controlled the amount of protein adsorbed on NPs surface. In summary, the amount of adsorbed protein on temperature-responsive surfaces depends on the variation of surface hydrophobicity by temperature change, polymer grafting density, and hydrophobicity of end groups. Temperature-responsive surfaces were then applied for cell culture, membranes for protein separation, and drug delivery carriers (Table 1.4.3.1). A multiple reusability of temperature-responsive surfaces for adsorbing proteins without loss of performance is an interesting challenge to tackle.

Table 1.4.3.1. Temperature-responsive surfaces prepared with poly(N-isopropylacrylamide) (PNIPAM), poly[2-(2-methoxyethoxy)ethyl methacrylate], poly(glycidyl methyl ether-co-glycidyl ethyl ether), and poly(2-isopropyl-2-oxazoline) with various transition temperatures on different substrates for controlling protein adsorption amount by changing temperature.

Polymeric material	Substrate	$T_{transition}$ [°C]	Protein	Ref
PNIPAM-based surfaces				
PNIPAM	Silicon wafer	32	Bovine serum albumin	[123]
PNIPAM and PNIPAM-PAA	Silicon wafer	29-30	Fibrinogen	[144]
PNIPAM	Gold	32	Fetal bovine serum	[145]
PNIPAM copolymers	Glass	20, 32, 42	Bovine serum albumin	[138]
PEG-based surfaces				
Poly[2-(2-methoxyethoxy)ethyl methacrylate]	Glass	25	Bovine serum albumin, human immunoglobulin G and bovine plasma fibrinogen	[151]
Poly[2-(2-methoxyethoxy)ethyl methacrylate]	Poly(ethylene terephthalate)	22	Fibrinogen and fibronectin	[152]
Glycerol-based surface				
Poly(glycidyl methyl ether-*co*-glycidyl ethyl ether)	Gold	29, 33, 35	Fibrinogen	[153]
Particles				
PNIPAM	Magnetic beads	32	Human plasma	[125]
Poly(2-isopropyl-2-oxazoline)	Poly(organosiloxane) nanoparticles	30	Bovine serum	[155]
Nanofibers				
PMMA/PNIPAM	Nanofibrous mats	n.a.	Bovine serum albumin	[143]

Changes of Protein Coating Compositions/Specific Protein Adsorption

The composition of adsorbed proteins when incubating temperature-responsive materials in protein mixtures can be altered upon temperature, due to the change of surface hydrophobicity. At 25 °C, PNIPAM beads were mostly enriched with transport/ binding proteins (16 proteins from 28 detected proteins) after incubation in human plasma, while they were enriched with transport/binding proteins and immune response related proteins (18 proteins from 27 detected proteins) after incubation at 37 °C[125]. Besides, the amount of adsorbed immunoglobulin light chains on PNIPAM-based nanogels after incubation in human serum was larger at 37 °C than at 25 °C[126].

It should be noted that the human plasma or serum used in these experiments was obtained from multiple donors. However, recent findings revealed that the protein composition in the plasma rely on several factors such as sex, age, and individual health status[156]. For instance, the amount of growth hormone is typically ≈ 11 times larger in female plasma than in male plasma. In addition, the concentration of proteins in female's plasma is altered during menstruation, pregnancy, lactation state, and menopause. The difference of protein composition of the protein corona due to sex was investigated by incubating SiO_2 nanoparticles (diameter = 70 nm) in the plasma of male and female zebrafish[157]. The SiO_2 nanoparticles were enriched with vitellogenin (an egg yolk protein) after incubating the nanoparticles in plasma of female zebrafish, whereas this phenomenon was not attributed after incubation in the plasma of male zebrafish. The uptake of nanoparticles incubated in plasma of female zebrafish by leukocytes was ≈3 times larger than for nanoparticles incubated in plasma of male zebrafish. Thus, the source of serum and plasma affects strongly the protein composition around the nanoparticles.

In the previous section, it was shown that the amount of adsorbed proteins on temperature-responsive materials at T > LCST was larger than at T < LCST due to increased surface hydrophobicity. Because of this characteristic, temperature-responsive materials can be applied for harvesting specific proteins from protein mixtures and preventing protein denaturation upon heating.

1.4.4 Cellular Uptake of Temperature-Responsive Materials

Uptake of nanoparticles by cells is found to increase with the hydrophobicity of the nanoparticles[158]. Because PNIPAM becomes more hydrophobic above the LCST than below, cell uptake is hence increased at higher temperature[159]. The uptake of PNIPAM by RAW 264.7 cells at 37 °C (T > LCST) was ≈ 30 times larger than at 25 °C (T < LCST)[160]. This remarkable increase of cellular uptake at T > LCST was attributed to the dehydration of PNIPAM chains, leading to an increase of hydrophobic interactions between cell membranes and PNIPAM. Thus, temperature-responsive polymers such as PNIPAM are suitable for intracellular drug delivery systems because they enhance the uptake of nanoparticles by cells at physiological temperatures compared with conventional polymers such as poly(lactic acid)[161]. Short interfering RNA (siRNA), as the therapeutic macromolecule used in gene therapy, was encapsulated into liposomes grafted with PNIPAM in order to increase the uptake of siRNA by cells[129]. The gene silencing activity caused by internalized siRNA was quantified by flow cytometry measurements after incubating PNIPAM-based liposome loaded with siRNA in HeLa Luc cells at different temperatures. The gene silencing at 37 °C (T > LCST) was ≈ 7 times larger than at 30 °C (T < LCST), because of an enhanced adhesion between collapsed PNIPAM chains and cell membranes at T > LCST.

2. Temperature, concentration, and surface modification influence the cellular uptake and the protein corona of polystyrene nanoparticles

Copyright:

[2] **Jennifer Oberländer***, XXX*, XXX, XXX, XXX. Temperature, concentration, and surface modification influence the cellular uptake and the protein corona of polystyrene nanoparticles. *Acta Biomaterialia*, **2022**, 148, 271-278. (***shared first)**

Aim:

The formation of the protein corona around different types of nanoparticles has been analyzed in several studies during the last decades. Thereby different key factors that influence the composition of the protein corona have been identified. However, the influence of temperature or concentration has received little attention so far. This study, therefore, aimed to analyze the effect of the temperature and concentration on the formation of the protein corona on polystyrene nanoparticles and in consequence the influence on the cellular uptake of these nanoparticles. Moreover, to achieve better comparability to other publications, we tested different surface modifications and surfactants to give a systematic representation of the effects. In the future this will help to better compare publications where different conditions have been chosen.

Contribution:

The project was divided into the temperature-responsive protein corona and the concentration-responsive protein corona. I performed the cell experiments with the HeLa cells (Flow cytometry, cell viability, and cLSM), protein corona (Pierce Assay, SDS-PAGE, and LC-MS), and characterizations (DLS and Zeta potential) of the temperature-responsive protein corona. XXX analyzed and characterized the concentration-dependent protein corona (DLS, Zeta potential, Pierce Assay, SDS-PAGE, and LC-MS) and cell uptake (Flow cytometry and cell viability). XXX performed the cell studies with the HUVEC cells (Flow cytometry and cell viability). Nano DSF measurements were performed by XXX and PCD by XXX. Manuscript preparation was done by XXX and me. The project was supervised by XXX and XXX.

2.1 Abstract

The composition of the protein corona varies depending on several parameters and influences the cellular fate of the nanocarriers. Here, we investigated the influence of three key parameters (surface charge, temperature, and plasma concentration) on the formation and composition of the protein corona of polystyrene nanoparticles and ultimately on the cellular uptake of pre-coated nanoparticles. At a fixed temperature and concentration, the surface charge, and surfactant influence its composition. We observed that the composition of the corona formed at low temperatures (4 °C) is different from that formed at physiological temperatures (37 °C). While fibrinogen is enriched in the protein corona at 4 °C, clusterin, serum albumin, and vitronectin is enriched at 37 °C. At low plasma concentrations (up to 25%), the corona consists of more diverse proteins than at higher concentrations. Finally, we concluded that regardless of the nanoparticle formulation, the degree of uptake by model cancer and endothelial cells of the nanoparticles decreased when pre-coated at increasing temperature or plasma concentration.

2.2 Introduction

Research groups around the world have developed their own polymer, silica, or gold nanoparticles and more recently liposomal formulations, to improve drug delivery to cells[162, 163]. Pre-coating nanoparticles with a defined protein corona has been investigated and successfully applied[164, 165]. However, consistency regarding coating conditions (type of plasma, plasma concentration, temperature…) is not always achieved, making it difficult to cross-reference results[20, 35, 166]. The formulation of a nanoparticle has been at the core of studies carried out over the last decade regarding the protein corona composition[167]. Key parameters such as size, charge, surface hydrophobicity, or the addition of polyethylene glycol (PEG) to the surface have been changed to provide important insights into protein corona and cellular uptake[59, 75, 168].

In addition to formulation considerations, the pre-coating conditions are also critical during pre-clinical testing of new nanoparticles. The protein source (human vs mouse, serum vs plasma) is known to influence the cellular uptake[169]. The temperature used during the coating has been investigated for temperature-responsive nanomaterials[123, 170], yet it is not clear if it is relevant for other, non-temperature-responsive materials. Temperature-responsive nanoparticles have been used for the catch and release of proteins[171]. Moreover, small changes in incubation temperature, close to the physiological temperature, have been shown to influence the adsorption of individual proteins[81]. Furthermore, heat inactivation of serum resulted in a different protein corona composition and therefore in a different cellular uptake[135, 136]. However, an analysis of the temperature-dependent protein corona in human plasma is still missing.

Similarly, the concentration of plasma used for pre-coating has been varied; and changes in the protein corona have been studied in the past[20, 33, 59, 172-174], however such studies were limited to one type of nanoparticles and no cellular uptake tests were performed. Dawson's group did several studies on this topic using silica and polystyrene nanoparticles concluding that the plasma concentration influences the protein content in the corona[20, 59]. However, they did not relate these results to the effect on cellular uptake. Gräfe et al. demonstrated that the protein concentration used for the pre-coating of positively charge magnetic nanoparticles altered their uptake into brain endothelial cells[172]. Yet, different groups still use different concentrations during their pre-clinical assays without always clearly explaining the reasons for their choices.

To address some concerns about pre-coating conditions, we test here five nanoparticles formulations stabilized with three different surfactants: CTMA-Cl, Lutensol, and SDS, and having surface charge ranging from +40 mV to -40 mV. Each nanoparticle from this panel is incubated either at 4 °C, 25 °C, or 37 °C in presence of undiluted human citrate plasma, or at 37 °C with 10%, 25%, 40%, 60%, or 100% plasma. Through these extensive and systematic tests, we are able to evaluate and conclude on the effect of temperature and concentration on the pre-coating step in regard to the protein corona composition and more importantly their impact on the cellular uptake. We demonstrate that increasing the human plasma concentration or increasing the coating temperature leads to a decrease of the uptake of

nanoparticles into HeLa and HUVEC cells. This can be attributed to an increase in the ratio of clusterin in the protein corona for most formulations.

2.3 Materials and methods

Synthesis of PS nanoparticles. Polystyrene nanoparticles (PS NPs) were synthesized by free-radical miniemulsion polymerization as mentioned in a previous work for the CMTA-NH_2 and SDS-COOH[175].

PS-CTMA-NH_2. The macro emulsion was composed of an aqueous continuous phase containing 2-aminoethyl methacrylate hydrochloride (3 %wt. to styrene) and cetyl trimethyl ammonium chloride (25 %wt. in water) in sterile Milli-Pore water. The organic dispersed phase contained distilled styrene, BODIPY 523/535 as fluorescent dye, and 2,2′-Azobis(2-methylpropionamidine) dihydrochloride in hexadecane. The continuous phase was added slowly to the dispersed phase under constant stirring. The macro emulsion was stirred for 1 hour at high speed. The emulsion was then passed through a microfluidizer (Microfluidics USA, LM10). The miniemulsion obtained was directly transferred into a flask and let to polymerize under stirring condition for 18 h at 72 °C. The dispersion was purified by filtration followed by successive centrifugations at 13,200 g. The supernatant was removed and the pellet was dispersed in sterile Milli-Pore water. The purification step was repeated twice.

PS-Lut-NH_2. The same procedure as for PS-CTMA-NH_2 was followed, yet Lutensol AT50 replaced cetyl trimethyl ammonium chloride in the continuous phase. The dispersion was purified by successive centrifugations at 20,000 g. Half of the supernatant was removed and replaced by sterile Milli-Pore water. The purification step was repeated four times.

PS-SDS-COOH. For these particles, acrylic acid was used as a co-monomer along with styrene in the disperse phase. In addition, sodium dodecyl sulphate was added to the continuous phase as surfactant. The emulsion and polymerization was carried as described for the amine nanoparticles. The purification was done by dialysis for 3 days against Milli-Pore water using 14000 kDa MWCO dialysis bags.

PS-Lut-COOH. The same procedure as for PS-SDS-COOH was followed, yet Lutensol AT50 replaced sodium dodecyl sulfate in the continuous phase. The dispersion was purified by successive centrifugations at 20,000 g. Half of the supernatant was removed and replaced by sterile Milli-Pore water. The purification step was repeated four times.

PS-Lut. The same procedure as for PS-Lut-COOH was followed, except no acrylic acid was used as co-monomer.

Characterization of PS nanoparticles. The nanoparticles were characterized in terms of surface charge using a Zetasizer Nano Z instrument (Malvern, Germany), size using a Zetasizer S90 instrument (Malvern, Germany), and fluorescence intensity using an Infinite M1000 plate reader (Tecan, USA). The characterization of the nanoparticles with protein corona was performed after preparation, centrifugation, and washing of the nanoparticles as described for the cellular experiments. The particle charge was determined using a particle charge detector (PCD, Mütek PCD 03 pH) as previously described[176].

Protein corona preparation. Human blood plasma was taken from healthy donors at the Department of Transfusion Medicine Mainz after physical examination and after obtaining written informed consent in accordance with the Declaration of Helsinki. Plasma of 10 donors was pooled and stored at -20 °C. The study was approved by the local ethics committee "Landesärztekammer Rheinland-Pfalz"(Bearbeitungsnummer: 837.439.12 (8540-F)). The protein corona experiments were performed as previously described by our group[102, 175]. To ensure comparability between the different types of PS nanoparticles, a constant ratio between the particle surface and plasma concentration was chosen. Therefore, 0.0625 m² of nanoparticles were incubated in 1 mL of human plasma for 1 h to allow the formation of a stable protein corona. In order to study the concentration-dependency of the protein corona, the incubation was performed at 37 °C in human plasma diluted with Dulbecco's Modified Eagle Medium to a final concentration of 10%, 25%, 40%, 60%, and 100%. The temperature-dependent protein corona formation was performed with undiluted plasma at the incubation temperatures of 4 °C, 25 °C, and 37 °C. Following the incubation, nanoparticles were isolated by centrifugation (20,000 g, 1 h, 4 °C) and washed three times with 1 mL PBS. Proteins from the hard protein corona were desorbed from the NP surface by adding 100 µL of 2% SDS in 62.5 mM Tris-HCl solution followed by incubation at 95 °C for 5 min. Proteins and nanoparticles were separated by centrifugation and the supernatant containing the protein was labeled as "hard protein corona" and used for protein quantification, SDS PAGE, and LC-MS analysis. As negative controls we incubated plasma in the same tubes as for the experiment but without adding nanoparticles. Washing and centrifugation was performed as described for the protein corona preparation and the proteins desorbed from the tubes were further processed the same way as the protein corona samples.

Protein quantification and SDS PAGE. The protein quantification was performed using the Pierce 660 nm Protein Assay (Thermo Fisher, Germany) according to the manufacturer's manual. Adsorption was measured with a Tecan Infinite M1000 plate reader using bovine serum albumin (Merck, Germany) for a calibration curve. Following quantification, the proteins were separated with a SDS PAGE and the proteins were revealed by Silver Staining or SimplyBlue™ SafeStain (Thermo Fisher, Germany) according to the manufacturer's recommendations. The hard corona proteins recovered from the nanocarriers were separated on a NuPAGE 10% Bis-Tris Bolt® polyacrylamide gel. A fix amount of hard corona proteins (2.5 µg for silver staining and 7.5 µg for Coomassie staining) was mixed with 26 µL water, 4 µL NuPage Reducing Agent, and 10 µL NuPage LDS Sample Buffer. SeeBlue Plus2 Pre Stained Standard (Invitrogen, Germany) was used as a marker. After protein denaturation for 10 min at 70 °C, the samples were loaded the gel and run in 1x NuPage MES SDS for 1.25 h at 100 V. The gel was either stained using Pierce Silver Staining Kit or SimplyBlue™ SafeStain according to the manufacturer's protocol. If not otherwise mentioned, materials were obtained from Thermo Fisher Scientific.

Protein preparation for mass spectrometry. SDS was removed before digesting the proteins using Pierce Detergent Removal Spin Columns (Thermo Fisher Scientific, Germany). The proteins were precipitated using ProteoExtract protein precipitation kit (CalBioChem, USA). Afterwards, the proteins were isolated by centrifugation (14 000 g; 10 min) and re-solubilized with 50 mM RapiGest SF (Waters, Germany) in ammonium bicarbonate buffer. The proteins were reduced in 5 mM dithiothreitol (Sigma-Aldrich, USA) for 45 min at 56°C and alkylated with 15 mM iodacetamide (Sigma-Aldrich, USA) for 1 h at room temperature in the dark. The tryptic digestion was carried out at a protein:trypsin ratio of 50:1 at 37 °C. After 18 h, digestion was stopped by lowering the pH with hydrochloric acid (Sigma-Aldrich, USA) and the samples were centrifuged (14 000 g; 15 min; 4 °C) in order to remove degradation products.

In solution digestion, sample preparation and liquid chromatography mass spectrometry (LC MS). The in-solution digestion and liquid chromatography-mass spectrometry was performed according to former protocols from our group[67, 177]. For the measurement, 0.1% formic acid was added to the sample and to allow absolute protein quantification, samples were spiked with 50 fmoL/µl Hi3 E.coli. (Waters, Germany). LC-MS measurements were performed using a nanoACQUITY UPLC system coupled to a Synapt G2-Si mass spectrometers based on a previous protocol[112]. Shortly, the system was operated in a positive resolution mode performing data-independent acquisition for the electrospray ionization source. The samples were injected with a flow rate of 0.3 µL/min and Glu-Fibrinopeptide (150 fmol/µL) and Leu-Enkephalin (200 pg/µL) were used as reference. The data was acquired using MassLynx 4.1. Proteins were analyzed using Progenesis QI 2.0 (thresholds for noise reduction were set at 120, 25, and 750 counts for low energy, high energy, and peptide intensity) and identified based on a reviewed database downloaded from Uniprot. For protein identification, at least two assigned peptides and five assigned fragments are required. The peptide identification needs three assigned fragments.

Nano DSF for protein stability. Nano differential scanning fluorimetry (nano DSF) was performed to confirm the stability of fibrinogen incubated at 4, 25, and 37 °C. Therefore, fibrinogen was solved in water to a concentration of 1.5 mg/mL. Measurements were performed 10 µL in standard capillaries (NanoTemper Technologies, Germany) and a NanoDSF Prometheus NT48 device. The data processing and analysis was performed with the PR.CONTROLL Data Analysis Software (v1.12.3, NanoTemper Technologies). The stability of fibrinogen was analyzed at the wavelength of 330 and 350 nm.

Cell culture. Human cervix carcinoma cells (HeLa) were cultured in Dulbecco's modified eagle medium (DMEM), supplemented with 10% FBS and 2 mM glutamine. Human umbilical vein endothelial cells (HUVECs) were cultured with Medium 200, supplemented with 1X large vessel endothelial supplement (LVES). Both media were supplemented with 100 U/mL penicillin and 100 mg/mL streptomycin. The cells were grown at 37 °C and 5% CO_2 in a humidified incubator and 0.25% Trypsin-EDTA was used for cell passaging and harvesting (all reagents from Gibco, Germany). The cell count and viability were determined using a 1:1 dilution with trypan blue. To ensure cell stability, the passage number was kept below 20 for HeLa and 8 for HUVEC.

Flow cytometry. HeLa and HUVEC cells were seeded at a density of 80,000 cells per well in 24 well plates (Greiner, Germany) and incubated over night at 37 °C and 5% CO_2. One hour before the uptake experiment, DMEM with FBS was removed, the cells washed with PBS, and DMEM without FBS was added. The plasma-coated nanoparticles were prepared as described above with two centrifugation steps to remove the excess proteins before dispersing them in DMEM without FBS. One mL nanoparticles solution (40 μg/mL) was incubated with the cells for 24 h at 37 °C in a cell incubator. Afterwards, cells were washed with PBS and collected using 0.25% Trypsin-EDTA. The cells were centrifuged (300 g, 5 min) and the pellet was suspended in PBS for measurements. The BODIPY signal of the nanoparticles was recorded using the BL1 channel of the Attune™ Nxt (Thermo Fisher Scientific, Germany) Flow Cytometer with an excitation laser of 488 nm and a band-pass filter of 530/30 nm. Cell debris was excluded by selecting a cell population in an FSC/SSC scatter plot processing the data with Attune™ NxT Software. The uptake experiments were carried out twice as independent experiments and within an experiment, for each condition, the cells were seeded as a triplicate.

Cell viability. Briefly, cells were seeded at a density of 5,000 cells per well in white bottom 96 well plates and incubated over-night at 37 °C and 5% CO_2. On the next day, the cells were treated in the same way as for the flow cytometry experiments. Additionally, cells were treated with a solution of 20% DMSO as a positive control. After 24 h of incubation, a volume of CellTiter-Glo®Reagent (Promega, Germany) equal to the volume of cell culture media present was added to the cells as recommended by the manufacturer. The luminescent signal was recorded with a Tecan Infinite M100 plate reader. The viability was calculated based on the average luminescent signal intensity (n=3) for the non-treated cells.

Confocal laser scanning microscopy. Visualization of the intracellular localization of nanoparticles was performed using confocal laser scanning microscopy (cLSM) with a Leica Microscope (LSM SP5 STED Leica, Germany). Bodipy signal of nanoparticles was measured using the Argon laser with an excitation at 514 nm and emission at 530–570 nm. The cell membrane was stained shortly before measurement using a 1000-fold diluted CellMask™ Deep Red solution (5 mg/mL, ThermoFisher Scientific, Germany). The signal was detected at 660-680 nm after excitation using the He-Ne Laser at 633 nm. Images were taken using LAS AF 3000 software and processed using Image J. For the confocal analysis, cells were seeded at a density of 50,000 cells per well in 8-well IbiTreat dishes and incubated overnight. Afterwards, cells were treated in the same manner as for the flow cytometry uptake and viability experiments.

Statistical analysis. GraphPad Prism v9.02 was used for the statistical analysis of the cellular uptake extent. The p-values generated after an unpaired t-test (n=3) were used to determine the significance of the difference between samples. Values $p > 0.12$ were considered non-significant, p-values < 0.033 were reported with $*$, p-values < 0.002 were reported with $**$, and p-values < 0.001 were reported with $***$on the graph for each condition in ESI.

2.4 Results and discussion

To establish the stability of the nanoparticles in the plasma solution, we measured the change in hydrodynamic diameter after coating at different temperatures or with different concentrations of plasma. To ensure that free proteins did not interfere with the measurements, the particles were centrifuged after the formation of the protein corona and washed with PBS. We observed that upon exposure to a concentration of 25% plasma or higher, the size of the nanoparticle increases from 130 nm on average to 160-170 nm indicating the formation of a protein corona around them (Table 2.6.1). For low plasma concentrations (10%) the size of CTMA-NH_2, Lut, and SDS-COOH nanoparticles increased to 470, 221, and 226 nm respectively. The larger size at 10% hP indicates the presence of aggregates, possibly due to the lower protein concentration surrounding the NPs at any given time. For highly charged NPs this means that the stabilization provided by the proteins is overcome by the destabilization brought on by the salts present in the buffer. Nevertheless, the size of the nanoparticles stabilized with 25% plasma. This could be a first hint that the protein corona around the nanoparticle changes with different plasma concentrations. In addition to the increased mean diameter of the NPs with protein corona, the presence of plasma, even at low concentration or low temperature, resulted in a negative ζ-potential around -18 mV, independently of the original ζ-potential of the pristine nanoparticles (Table 2.6.2). All these parameters confirmed that the coated nanoparticles are stable in solution (except for 10% hP) for future cellular uptake experiments. All NPs were synthesized with Bodipy 523 as fluorophore for cellular uptake tracking. The fluorescence intensity of the pristine NPs was determined to enable normalization of the uptake across NPs (Table 2.6.3). Additionally, the number of functional groups (NH_2 or COOH) on the nanoparticles was determined with a particle charge detector (Table 2.6.4). For both functional groups, the amount of amine or carboxyl groups per nm^2 was in the same order of magnitude within a particle type. The amount differed between amine and carboxyl group with SDS-COOH nanoparticle having the most groups on their surface and CTMA-NH_2 the lowest.

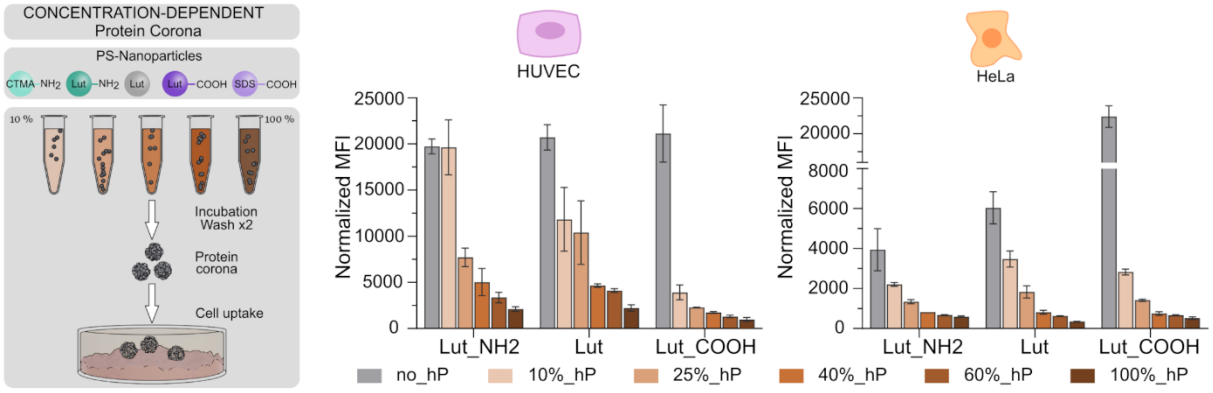

Figure 2.4.1. Schematic representation of the coating procedure leading to the cellular uptake displayed. HUVEC and HeLa cells were incubated for 24 h in media without protein with 40 µg/mL pre-coated polystyrene nanoparticles. The pre-coating of the NPs was done at 37°C here. The „no_hP" corresponds to pristine NPs incubated with the cells. The error bars represent the standard deviation between the means of a triplicate.

After we have ensured the quality of the coated NPs, we tested the uptake of the five polystyrene nanoparticles by HeLa and HUVEC cells after 24 h incubation in media without proteins. First, we focused on the impact of citrate plasma dilution on the cellular uptake. The pre-coating of the NPs was always done at 37°C for this series of experiments. We observed that the coating of the NPs induced a reduction of the uptake across cell types and was dependent on the plasma concentration of the coating solution (Figure 2.4.1). For the Lutensol stabilized NPs, the uptake is similar across surface functionalization for the cervix adenocarcinoma when the NPs are coated with 40% up to 100% plasma. Indeed, the broad range of uptake extent seen for the pristine NPs based on their surface modification subsides in the presence of increasing protein in the coating solution (Figure 2.6.1 and Figure 2.6.2). Additionally, the trend observed for Lutensol-stabilized NPs is also observed for CTMA- and SDS-stabilized NPs. For all NPs tested, the increase of the protein concentration in the coating solution led to a significant decrease of the uptake in the HeLa cells. It is worth noting that the uptake is strongly decreased between 10%_hP, 25%_hP, and 40% and tends to level out afterwards with more minute changes in the uptake level (Figure 2.6.3). Meanwhile, HUVEC are more sensitive and the increased plasma concentration in the coating solution leads to a more constant decrease of the uptake. We also verified the absence of toxicity induced by the NPs and confirmed good cell viability after incubation for all conditions, even though the pristine NPs tend to be more toxic to the cells (Figure 2.6.4). Finally, we confirmed by confocal laser microscopy the internalization of the NPs by the cells and not just their adsorption on the cell membrane, as shown by the red dots inside the membrane-stained cells (Figure 2.6.5).

Next, we investigated the protein corona composition to explain the uptake pattern observed. The change in uptake between pristine NPs (no_hP) and coated NPs was expected [67, 75, 102]; however the change for plasma concentration of 25% and above was interesting. Since the size and apparent surface charge did not change much within this plasma concentration range (25%-100%), we looked into the protein corona composition. First, we checked if the amount of protein adsorbed on the NPs varied with the coating concentration. We found no correlation between the original protein concentration and the amount adsorbed on each NPs. The amount varied based on the surfactant and surface functionalization as expected (Figure 2.6.6). The amount of protein desorbed from the tube in the negative control was for all conditions minimal indicating that this should have no effect on the proteins determined in the protein corona (Figure 2.6.7). We also checked the protein corona composition by SDS-PAGE analysis. We observed a clear difference in the composition of the protein corona for the carboxy-functionalized NPs compared to the amino- or un-functionalized ones. The differences between the concentrations were not as obvious. For example, for the CTMA-NH_2 NPs we could see a decrease in the band intensity for the serum albumin at 62 kDa. However, since the staining method used here is a non-quantitative method, it is not possible to draw a direct conclusion from the band intensities to the protein concentration in the protein corona. Overall, no new band appeared at different concentrations for any NPs (Figure 2.6.8) which suggests that no new proteins are appearing but rather that the relative concentration of each

proteins in the protein corona may be changing. This also counts for the negative controls (Figure 2.6.9 and Figure 2.6.10). Only for the 10% plasma condition the protein concentration desorbed from the tube was too low in order to load enough protein on the SDS PAGE. Therefore, the band intensities are weaker for this condition.

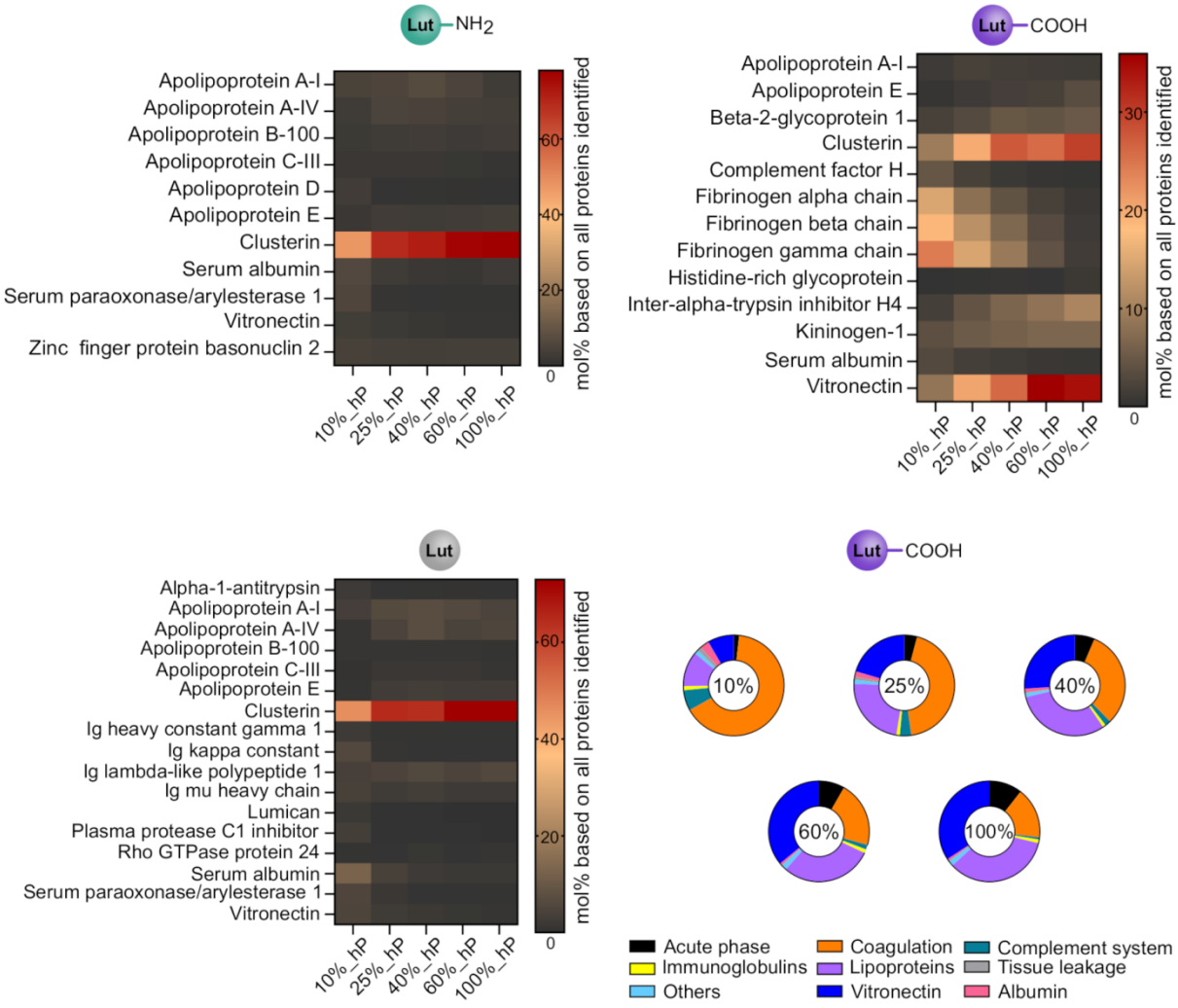

Figure 2.4.2. Combined top10 proteins identified in the corona of the NPs and category affiliation of the proteins for the Lut_COOH NP. The top10 proteins for each condition within a NP were combined to the final heatmap shown here.

Therefore, we moved on to proteomic analysis of the whole protein corona recovered from the NPs or the tube. The results of the negative controls and the composition of the human plasma are shown in Figure 2.6.11 and Figure 2.6.12. For the Lutensol-stabilized NPs, we observed that the fraction of clusterin in the corona increases with increased plasma concentration (Figure 2.4.2). However, it does not account for the same fraction of the corona for each NPs. Here, the surface modification has a higher impact compared to the cellular uptake. Apolipoproteins constitute a large part of the proteins identified, with clusterin and ApoE found in the top10 identified proteins across all five NPs. The Lut_COOH NP has the most complex corona out of the three Lutensol-stabilized NPs in terms of the category to which

the most abundant proteins belong. Indeed, for the other two, about 60% to 80% of the corona was made of apolipoproteins leaving little space for other types of proteins. In contrast, the corona evolved quite interestingly for the Lut_COOH NPs with a change from coagulation proteins (fibrinogen) at low plasma concentrations to a tripartite composition involving coagulation proteins, apolipoproteins, and vitronectin at higher concentrations (Figure 2.4.2). A similar trend is observed with SDS_COOH NPs for which when the proportion of coagulation proteins decreases, the proportion of vitronectin increases with the plasma concentration. For these NPs as well as the CTMA_NH_2, apolipoproteins account for a very small portion of the corona (Figure 2.6.13). Taking into account that for the SDS_COOH nanoparticles the cellular uptake decreases with increasing plasma concentration, we would expect to see an increasing concentration of apolipoproteins and especially of clusterin which is known to reduce the cellular uptake of nanoparticles[75, 174]. However, for this type of nanoparticle apolipoproteins and clusterin play only a minor role in the protein corona.

We can conclude that for all the NPs tested, the composition of the protein corona evolves with the amount of plasma in the coating solution (Figure 2.6.14). It is worth noting that the use of Lutensol, a non-ionic PEGylated surfactant, led to a protein corona enriched with apolipoproteins for all the NPs. The corona composition seems to be dictated as much by the surfactant as by the surface functionalization. Indeed, the carboxy-functionalized NPs showed enrichment with coagulation proteins compared to the amino ones. Based on these observations, we propose that the presence of carboxy-groups on the NPs are more important than the surfactant, while the surfactant is more important than the presence of amino-groups on the NPs.

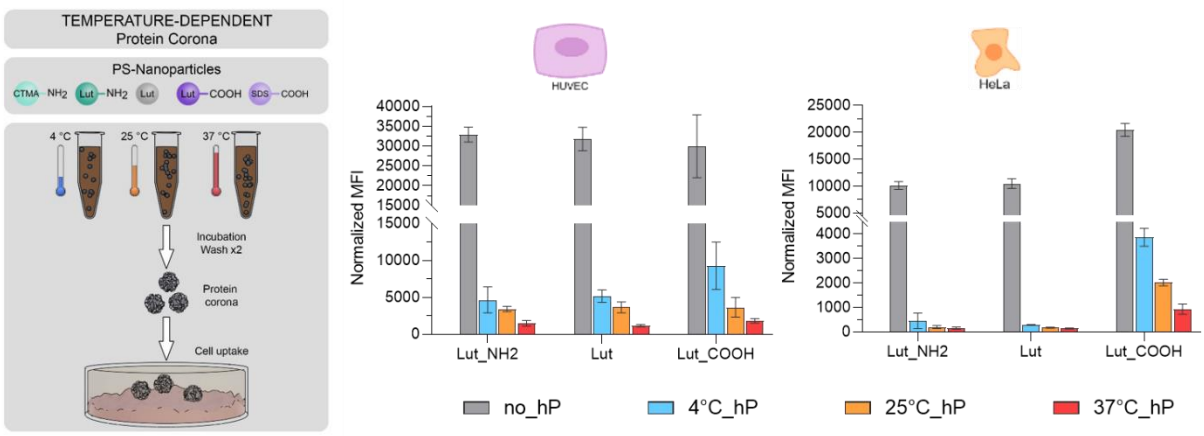

Figure 2.4.3. Schematic representation of the formation of the protein corona and the uptake into HUVEC and HeLa cells. HUVEC and HeLa cells were incubated for 24 h in media without protein with 40 µg/mL pre-coated polystyrene nanoparticles. Pre-coating was done in 100% plasma. The „no_hP" corresponds to pristine NPs incubated with the cells. The error bars represent the standard deviation between the mean of a triplicate.

Besides the influence of different plasma concentrations on the protein corona, we also focused on different incubation temperatures. Here we kept the concentration of plasma for the pre-coating stable at 100%. The coating of the nanoparticles with human plasma induces a reduction of the uptake in

HUVEC and HeLa cells. For Lutensol stabilized NPs, it can be seen that the uptake is reduced with increasing temperature (Figure 2.4.3). Additionally, this trend is observed for CTMA-stabilized NPs (Figure 2.6.15 and Figure 2.6.16). For these NPs the decrease of the uptake from 4 °C to 37 °C is mainly significant while the difference between 4 °C to 25 °C and 25 °C to 37 °C is only minor. These trends can be seen in both cell lines tested. However, the HUVEC cells seemed to be more sensitive to the presence of protein coating which leads to a higher decrease between coated and uncoated NPs. For the SDS-stabilized carboxylic NPs a different trend can be observed. As for the other particles, a reduced uptake from pristine to coated particles can be seen. However, with increasing temperature an increase in cellular uptake for HUVEC and HeLa cells was observed (Figure 2.6.15 and Figure 2.6.16). These trends can also be seen in confocal laser scanning microscopy images (Figure 2.6.17). Besides verifying the uptake of the particles into the cells, it can also be observed that for the CTMA-stabilized amine particles the uptake was reduced with increasing temperature and for the SDS-stabilized carboxylic particle the uptake increased with increasing temperature. We tested the toxicity induced by the NPs as well for these conditions. For most conditions, we additionally confirmed here the absence of toxicity to both cell types (Figure 2.6.18). For the pristine CTMA-stabilized amine particle we saw a toxic effect mostly on HeLa cells but also slightly on HUVEC cells. The toxic effect is no longer present when a protein coating was applied.

To investigate the reason for the uptake change, we analyzed the protein corona composition. Since the size and surface charge do not change significantly between the different temperatures, we focused on the protein analysis of the protein corona on the particles. Protein quantification with Pierce assay resulted in no obvious correlation between temperature and amount of protein adsorbed except for the CTMA stabilized amine NP (Figure 2.6.19). For the CTMA_NH_2 NPs the highest protein amount desorbed can be observed at 4 °C and it decreases at 37 °C. However, SDS-PAGE analysis showed a temperature-dependent difference in protein composition on the particles (Figure 2.6.20). Especially for the SDS-stabilized carboxylic and the CTMA-stabilized amine particles, an increase of the band intensity at 38 kDa was observed. But also for the Lutensol-stabilized NPs a slight increase of the band intensity between 38 kDa and 49 kDa was observed. However, a clear appearance or disappearance of the bands cannot be observed. Comparing the different particles, as expected, a difference in protein corona composition can be seen between the different surface functionalizations but also between different surfactants.

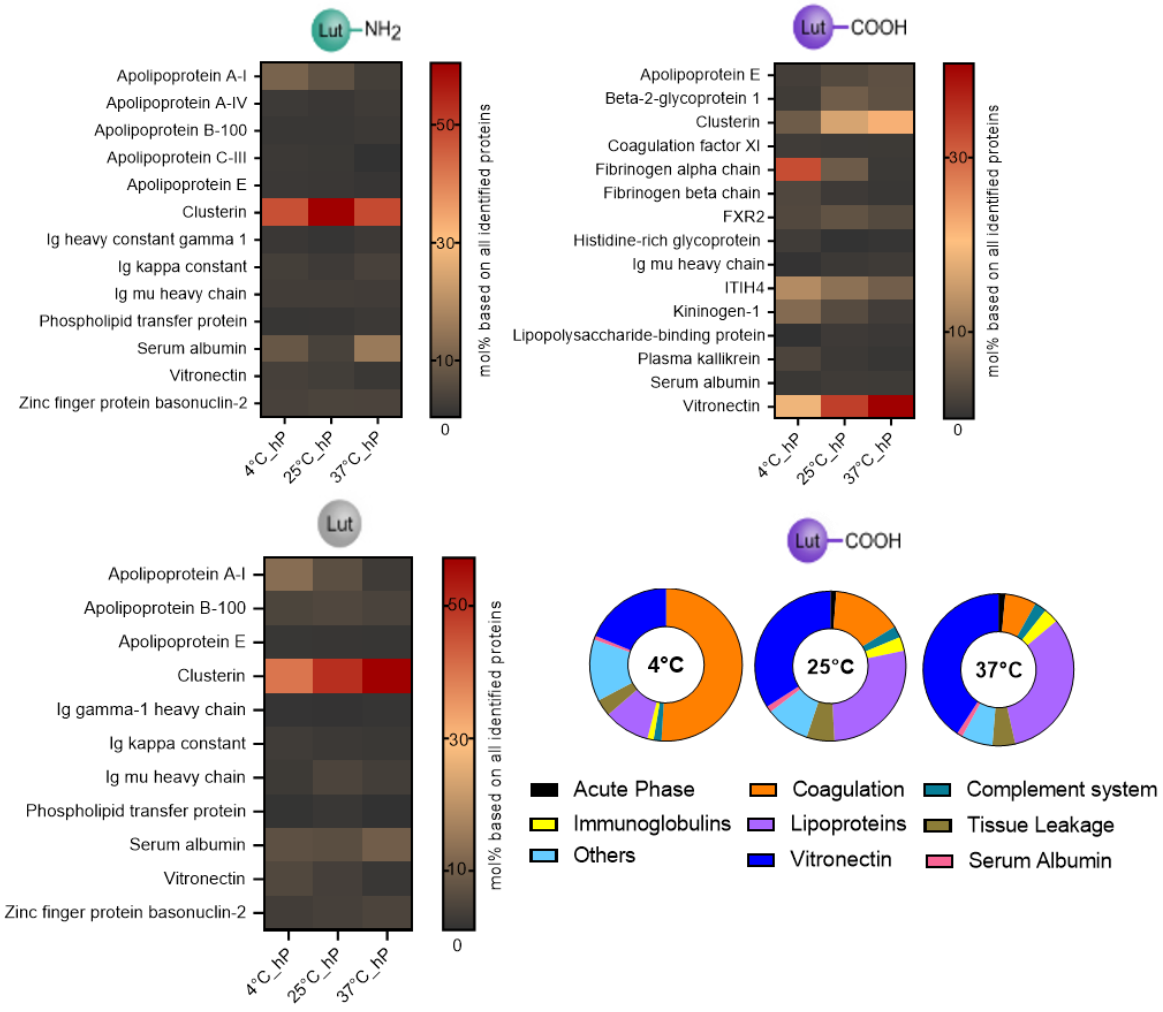

Figure 2.4.4. Combined top10 proteins identified in the corona of the NPs and category affiliation of the proteins for the Lut_COOH NP. The top10 proteins for each condition within a NP were combined to the final heatmap shown here.

Afterwards, we had a deeper look at the composition of the protein corona *via* LC-MS analysis. As already shown previously, the surface modification had a huge influence on the composition of the protein corona (Figure 2.4.4). However, it can be seen that for the Lutensol-stabilized nanoparticles the amount of clusterin in the protein corona increased with increasing temperature while the amount of ApoA1, ApoE, and fibrinogen decreased with increasing temperature. Interestingly, for the Lutensol-stabilized carboxylic nanoparticles we saw an additional increase in the amount of vitronectin in the protein corona. While the coagulation proteins were the dominant protein group in the protein corona at 4 °C, the lipoproteins and the vitronectin were the dominant proteins in the protein corona at 37 °C (Figure 2.6.21). This trend can also be observed for the SDS-stabilized carboxylic nanoparticle. The CTMA-stabilized amine nanoparticles showed additionally a temperature-dependent increase of serum albumin in the protein corona with increasing temperature (Figure 2.6.22). From that, we can conclude that the protein corona composition is temperature dependent.

One concern when measuring the temperature-dependent protein corona could be that the stability of proteins changes at the different temperatures. Therefore, we decided to use temperatures between 4 °C and 37 °C where we do not expect to have protein denaturation. In order to evaluate if in this temperature range protein stability changes, we performed nano differential scanning fluorimetry (nano DSF) measurements. Since the determination of protein stability in full plasma is complex, we performed nano DSF with fibrinogen as a model protein. Fibrinogen showed a temperature-dependent behavior with a higher amount adsorbed at lower temperatures. It can be seen, that the stability of the fibrinogen does not change by incubation at 4, 25, and 37°C (Figure 2.6.23). Also, after an additional 24 h after the incubation time the fibrinogen is still stable in solution. We therefore confirmed that the protein stability, at least for fibrinogen, is not the major effect which influences the temperature-dependent adsorption of the proteins.

We demonstrated that the cellular uptake of pre-coated polystyrene NPs by cancer and endothelial cells steadily decreases with increasing plasma concentration in the coating solution. This stealth effect appears to be more pronounced at low protein concentrations, with the extent of uptake flattening above 40% of plasma. Given our results here, it would be a good practice to not go below 40% plasma in a medium when pre-coating or actively incubating NPs with cells. This highlights the need to choose a sufficiently high plasma concentration when performing *in vitro* studies aiming to mimic *in vivo* conditions. In the human body, blood is composed of about 55% plasma with cells accounting for the other 45% [178]. We would like to point out that this 45% of non-plasma volume is not readily accessible for NPs and therefore we would argue that the NPs "see" only the pure plasma (100%). Nevertheless, other groups prefer to dilute their plasma, however diluting plasma often begs the questions*: which diluent should be used? Should water, PBS, or cell culture media be used? Which one would bring the least amount of artifacts into the system?* Although we still observe a statistically significant difference in uptake at a high plasma concentration, the difference between 40% and 100% does not appear to be clinically relevant, meaning that the uptake is more uniform at this point and using any plasma concentration above 40% should not drastically alter the outcome of the cellular uptake. If diluent is used this introduces an additional variability and hence, using 100% of plasma could solve the issue of the diluent without bias to the resulting cellular uptake.

Still, the decrease of the uptake could not be explained by the change in size of surface charge and is therefore due to the evolution of the protein corona. The increase of plasma concentration leads to an increase of clusterin in the corona for most NPs, except for SDS_COOH. The proportion of clusterin in the corona varies from NP to NP, but the trend endures. Clusterin is a well-known dysopsonin protein and was shown to improve the stealth of nanoparticles in macrophages [75, 174]. Yet, clusterin alone cannot explain the trend observed for the SDS_COOH NP. Indeed, the percentage of clusterin in the corona of this NP is very low (about 2%) and the same at all concentrations. However, the percentage of fibrinogen and vitronectin fluctuates greatly based on the concentration and could be somehow involved in the change of cellular uptake. We could also point out to the difference in coverage of the nanoparticles

with proteins at the different coating concentrations to explain the change in cellular uptake. The question of the protein density would in turn raise the question of the orientation of the absorbed proteins, which could change depending on the densely or sparsely populated protein regions. However, the analysis of single proteins on the surface of nanoparticles is challenging, even more so for a complex protein mixture and is beyond the scope of the present study. Other groups performed studies to evaluate the impact of low or high plasma concentrations on the protein corona as well[20, 35, 172]. Salvati's group showed a higher uptake of silica nanoparticles with a lower plasma concentration and the group of Dawson demonstrated changes in the protein corona composition with different plasma concentrations[20, 35]. However, in most cases these studies were only performed on one type of nanoparticles and the impact on the cellular uptake was not always shown.

Besides the concentration-dependent uptake of PS nanoparticles in the cells, we also showed that the uptake of NPs in HeLa and HUVEC cells decreases with increasing temperature during protein corona formation. For a protein corona formed at 4 °C, the uptake of the Lutensol stabilized nanoparticles was significantly higher than for a protein corona formed at 37 °C. This also applies to the CTMA stabilized amine nanoparticles. However, for the SDS stabilized carboxylic nanoparticles a slightly increased uptake has been observed at the highest temperature of 37 °C. In most studies, protein corona formation and cellular uptake of nanoparticles are performed at 37 °C in order to be as close as possible to the *in vivo* conditions. Nevertheless, especially when working at low temperatures[81, 82] or when working with temperature sensitive materials, this must be taken into account[123, 171].

Furthermore, we showed that the protein corona changes with the incubation temperature and that this is very likely the reason for the temperature-dependent uptake behavior. At 4 °C, we observed a low amount of lipoproteins but an increased amount of coagulation proteins in the protein corona. This changed when we increased the temperature to 37 °C. At this temperature, the lipoproteins, serum albumin, and vitronectin became more prominent in the protein corona. However, it can also be seen that the protein corona of the Lutensol and SDS stabilized carboxylic as well as the CTMA stabilized amine nanoparticles show a stronger dependence on temperature than the Lutensol stabilized unfunctionalized and amine nanoparticles. Since the amount of total proteins bound in the protein corona does not differ much between the different incubation temperatures, we assume that the difference in the protein corona is not due to a reduced interaction of the proteins with the nanoparticles. It is more likely that the affinity of specific proteins for the nanoparticles is temperature dependent. It is known that proteins can consist of multiple binding sites which can interact with surfaces and that conformational stability of proteins depends on temperature, among other factors[179]. However, the protein corona consists of different proteins, and for most of them the protein structure is not yet known. A prediction of binding affinities in dependence on temperature, therefore, remains challenging. Yet, this field is relatively unexplored and requires further research. Moreover, we analyzed here the proteins bound in the hard protein corona. When considering protein affinities, we could also suggest that with a change in the hard protein corona the protein affinities in the soft corona could change. However, the

analysis of the soft protein corona remains complicated. Previously it has been shown that for a short incubation time the uptake of pre-coated liposomes did not differ between hard and soft protein corona[91]. We therefore do not expect an impact of the soft protein corona and its difference with temperature or concentration on the uptake of the nanoparticles.

2.5 Conclusion

We demonstrated that the protein corona composition varies with plasma concentration and temperature. Five NPs with different surface functionalization and surfactants were similarly impacted proving the universality of the effect. Additionally, the change in the protein corona composition directly affected the extent of cellular uptake of the pre-coated NPs. In cervix adenocarcinoma and in endothelial cells, a decrease of the uptake was observed with the increase of the plasma concentration of the coating solution. Hence, we recommend always performing experiments using a plasma content of at least 40% to ensure the full stealth effect induced by a mature protein corona. This recommendation is aimed at pre-clinical studies to provide consistent results when proceeding with animal-based studies. We have also shown a decrease in the cellular uptake of the nanoparticles with an increase in temperature during protein coating. This should be considered when using different incubation temperatures for pre-coating and in *in vitro* experiments.

2.6 Supporting Information

Table 2.6.1. Mean hydrodynamic diameter (nm) of the pre-coated NPs treated as for cellular uptake experiment. The values reported correspond to the mean of a triplicate measurement. The value in parenthesis corresponds to the standard deviation between the mean diameters of the triplicate. The "no hP" condition corresponds to the pristine NCs dispersed in DPBS before coating with plasma. The nanoparticles with protein corona were centrifuged and washed with DPBS after formation of the protein corona in plasma.

	no hP (37 °C)	**10% (37 °C)**	**25% (37 °C)**	**40% (37 °C)**	**60% (37 °C)**	**100% (37 °C)**	**100% (25 °C)**	**100% (4 °C)**
CTMA-NH_2	124 (1.5)	470 (35)	178 (2.7)	166 (1.5)	167 (1.6)	164 (3.9)	169 (0.5)	144 (16.8)
Lut-NH_2	125 (3.5)	197 (2.5)	161 (1.4)	159 (1.1)	154 (3.1)	151 (3.8)	150 (2.4)	162 (18.8)
Lut	136 (0.8)	221 (9.6)	199 (5.4)	192 (9.2)	188 (1.4)	165 (9.1)	162 (3.0)	185 (2.7)
Lut-COOH	131 (3.8)	170 (3.7)	168 (0.6)	162 (3.5)	166 (3.4)	164 (2.4)	156 (1.6)	143 (14.1)
SDS-COOH	102 (1.3)	226 (4.2)	165 (0.4)	157 (2.2)	158 (2.2)	160 (4.8)	151 (1.6)	141 (14.2)

Table 2.6.2. Mean ζ-potential (mV) of the pre-coated NPs treated as for cellular uptake experiment. The values reported correspond to the mean of a triplicate measurement. The value in parenthesis corresponds to the standard deviation between the mean ζ-potential of the triplicate. The "no hP" condition corresponds to the pristine NCs dispersed in DPBS before coating with plasma. The nanoparticles with protein corona were centrifuged and washed with DPBS after formation of the protein corona in plasma.

	no hP (37 °C)	**10% (37 °C)**	**25% (37 °C)**	**40% (37 °C)**	**60% (37 °C)**	**100% (37 °C)**	**100% (25 °C)**	**100% (4 °C)**
CTMA-NH_2	33.3 (0.5)	-19.8 (1.2)	-21.3 (1.1)	-21.9 (1.0)	-21.1 (0.7)	-21.0 (0.3)	-13.8 (0.6)	-12.0 (0.8)
Lut-NH_2	-1.1 (0.9)	-14.1 (1.3)	-16.5 (0.6)	-14.9 (0.9)	-13.5 (1.5)	-13.2 (1.7)	-12.8 (1.1)	-13.2 (0.9)
Lut	-1.3 (0.4)	-18.6 (1.2)	-23.0 (1.3)	-22.6 (1.5)	-21.5 (0.9)	-20.8 (0.8)	-20.0 (1.3)	-8.7 (0.6)
Lut-COOH	-8.3 (0.5)	-11.3 (1.3)	-12.2 (0.5)	-11.3 (0.7)	-15.0 (1.5)	-16.2 (1.0)	-12.6 (1.3)	-20.5 (0.4)
SDS-COOH	-42.4 (1.5)	-21.3 (1.0)	-21.4 (0.6)	-14.6 (0.6)	-20.8 (1.2)	-19.4 (1.4)	-15.8 (0.6)	-13.2 (0.9)

Table 2.6.3. Mean fluorescence intensity of the pristine polystyrene NPs as measured on a plate reader (excitation at 488 nm and emission 530 nm with a bandpass of 10 nm). The values were measured as a triplicate at a concentration of 40 µg/mL. The "Lut" NC was chosen as reference for the normalization of the flow cytometry data. The value in parenthesis corresponds to the standard deviation between the mean fluorescence intensity of the triplicate.

	CMTA-NH_2	**Lut-NH_2**	**Lut**	**Lut-COOH**	**SDS-COOH**
Fluorescence intensity - Pristine NC (no hP)	17342 (100)	10335 (150)	12847 (230)	17029 (140)	13589 (280)

Table 2.6.4. Particle charge of charged polystyrene NPs measured with a particle charge detector. The charge of the nanoparticles was measured in order to determine the amount of groups per particle. For the nanoparticles with charged surfactant (CTMA and SDS) the measurements were carried out at two different pHs.

Particle type	pH	Groups / gram of polymer	Groups / particle	Groups / nm^2
CTMA_NH2	2.5 and 10	1.41E+19	20.7	3.41E-04
Lut_NH2	9	2.26E+19	33.15	5.46E-04
Lut_COOH	2.5	5.51E+19	80.91	1.33E-03
SDS_COOH	2.5 and 9	1.50E+20	220.11	3.63E-03

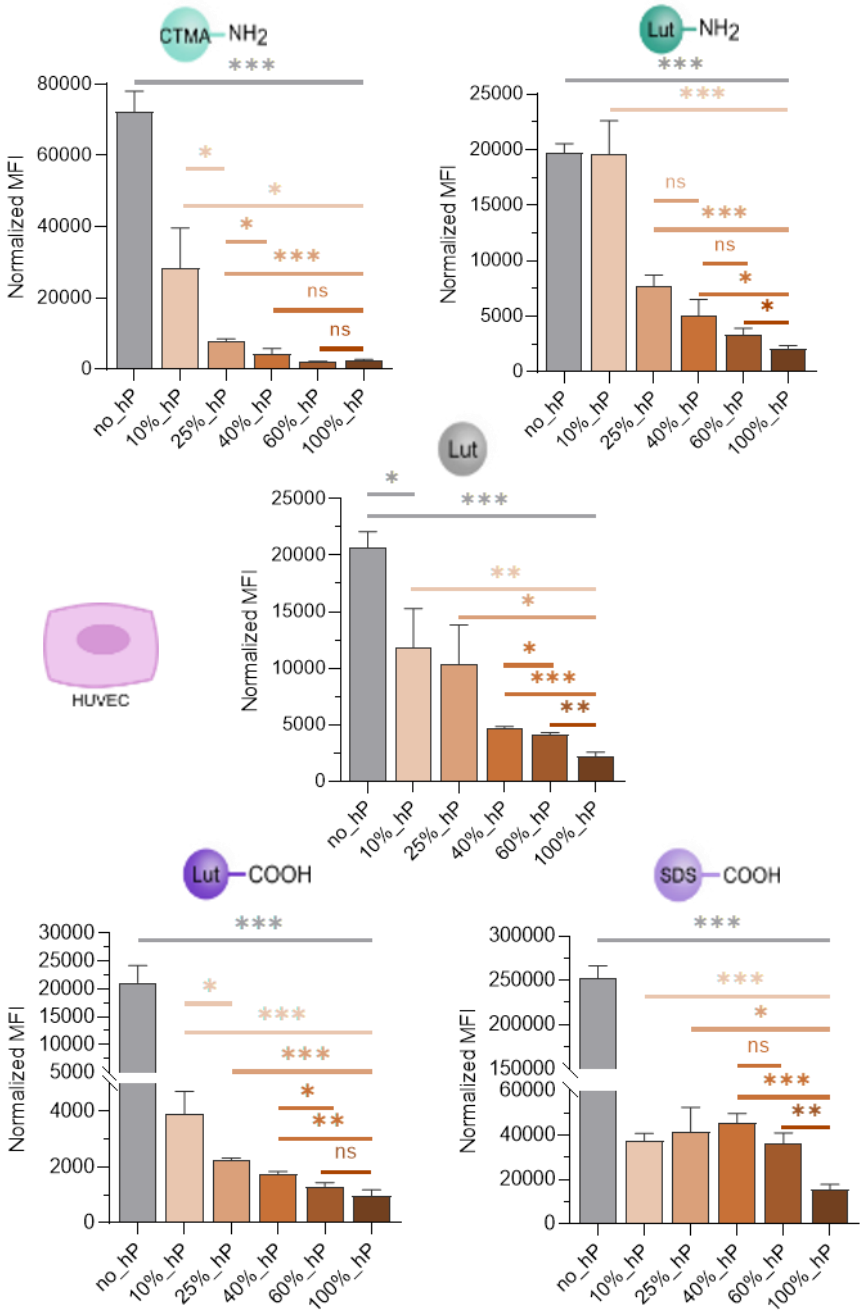

Figure 2.6.1. Cellular uptake extent of the pre-coated NPs with different concentrations by HUVEC cells after 24 h incubation at 37 °C. The cells were incubated with a solution containing 40 µg/mL NPs. The difference of intrinsic fluorescence intensity of the NPs tested was accounted for by normalizing the median fluorescence intensity recording by the flow cytometer based on the fluorescence intensity of the "Lut" NPs. The statistical significance of the difference between samples was determined by unpaired t-test. P-values > 0.12 were non-significant (n.s.), p-values < 0.033 correspond to *, p-values < 0.002 correspond to **, and p-values < 0 .001 correspond to ***

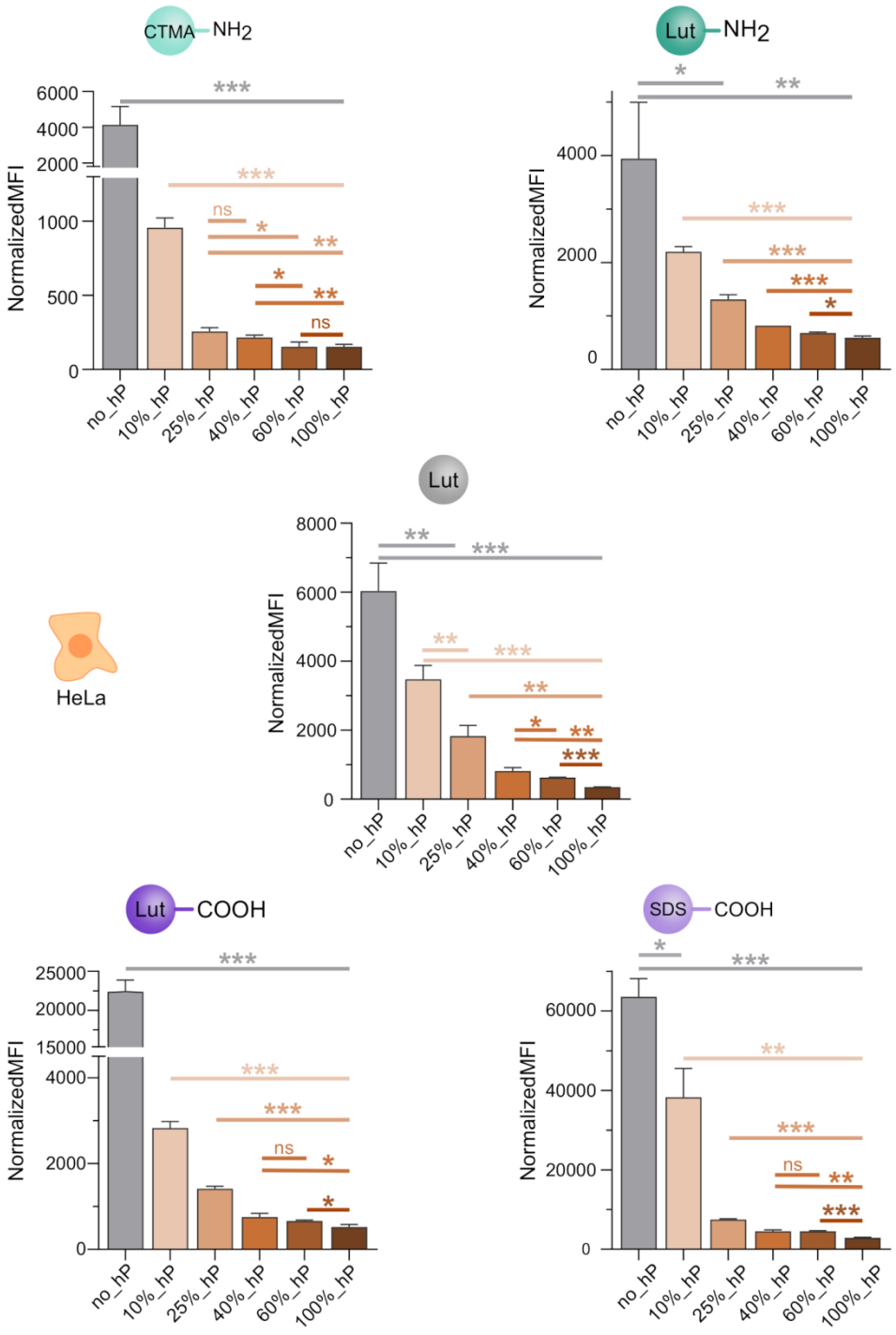

Figure 2.6.2. Cellular uptake extent of the pre-coated NPs with different concentrations by HeLa cells after 24 h incubation at 37 °C. The cells were incubated with a solution containing 40 µg/mL NPs. The difference of intrinsic fluorescence intensity of the NPs tested was accounted for by normalizing the median fluorescence intensity recording by the flow cytometer based on the fluorescence intensity of the "Lut" NPs. The statistical significance of the difference between samples was determined by unpaired t-test. P-values > 0.12 were non-significant (n.s.), p-values < 0.033 correspond to *, p-values < 0.002 correspond to **, and p-values < 0 .001 correspond to ***

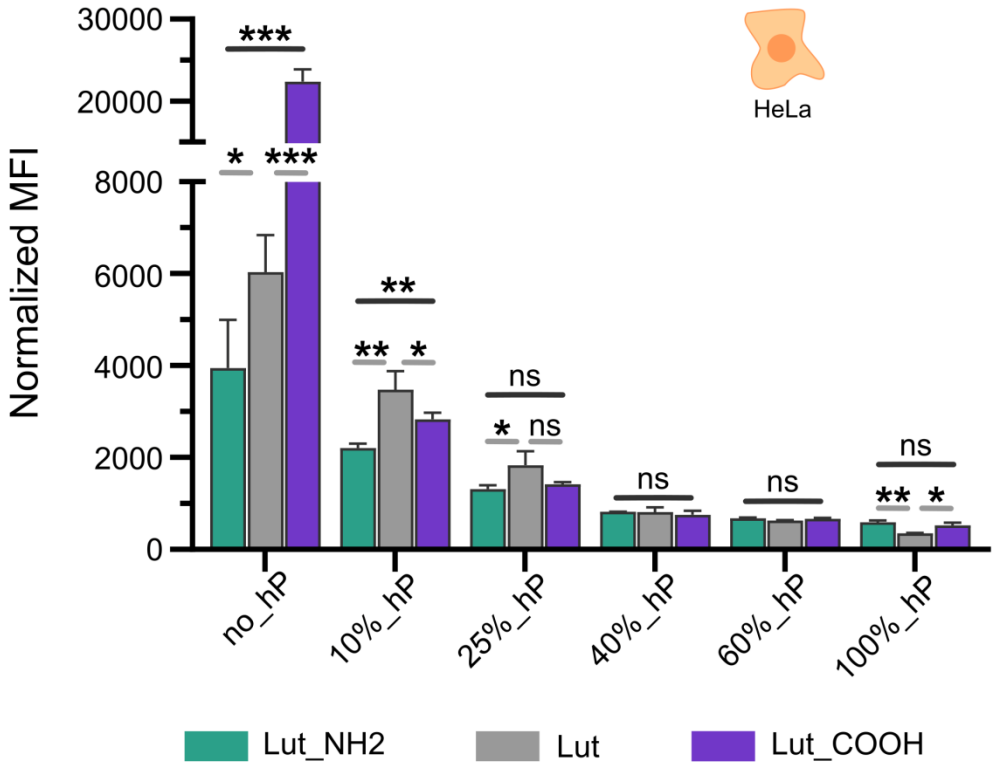

Figure 2.6.3. Cellular uptake of pre-coated Lutensol stabilized NPs with different concentrations of plasma (hP) after 24 h incubation in DMEM. The difference of intrinsic fluorescence intensity of the NPs tested was accounted for by normalizing the median fluorescence intensity recording by the flow cytometer based on the fluorescence intensity of the "Lut" NPs. The statistical significance of the difference between samples was determined by unpaired t-test. P-values > 0.12 were non-significant (n.s.), p-values < 0.033 correspond to *, p-values < 0.002 correspond to **, and p-values < 0 .001 correspond to ***

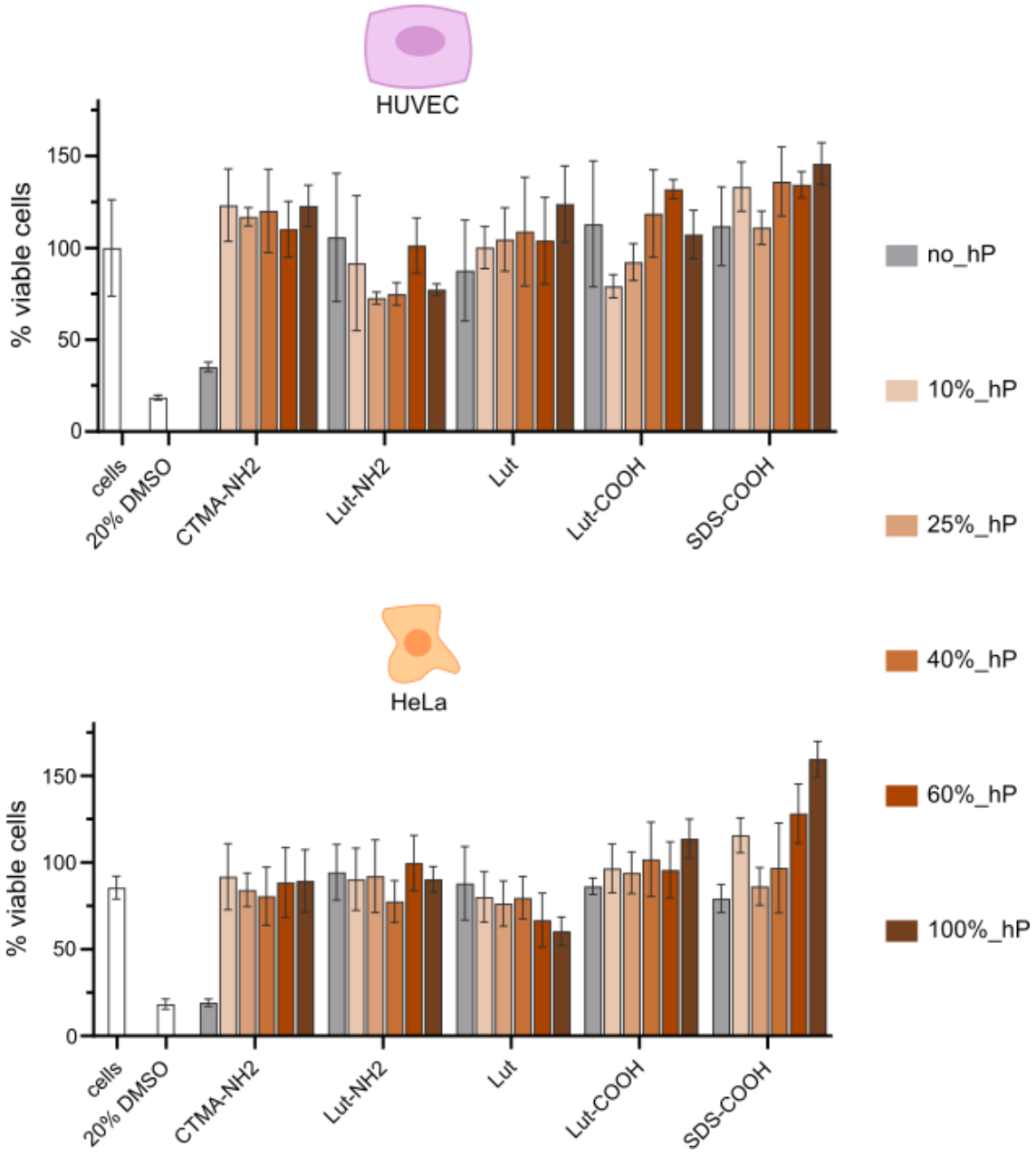

Figure 2.6.4. Cellular viability after incubation for 24 h in presence of 40 µg/mL NPs. The sample labeled "cells" corresponds to the untreated cells incubated in DMEM media without NPs, the sample labelled "20% DMSO" corresponds to cells treated for 24 h with a DMEM media containing 20% DMSO. These samples are used as controls to validate the assay. The error bars represent the standard deviation between the viability of three samples treated with the same nanoparticle solution.

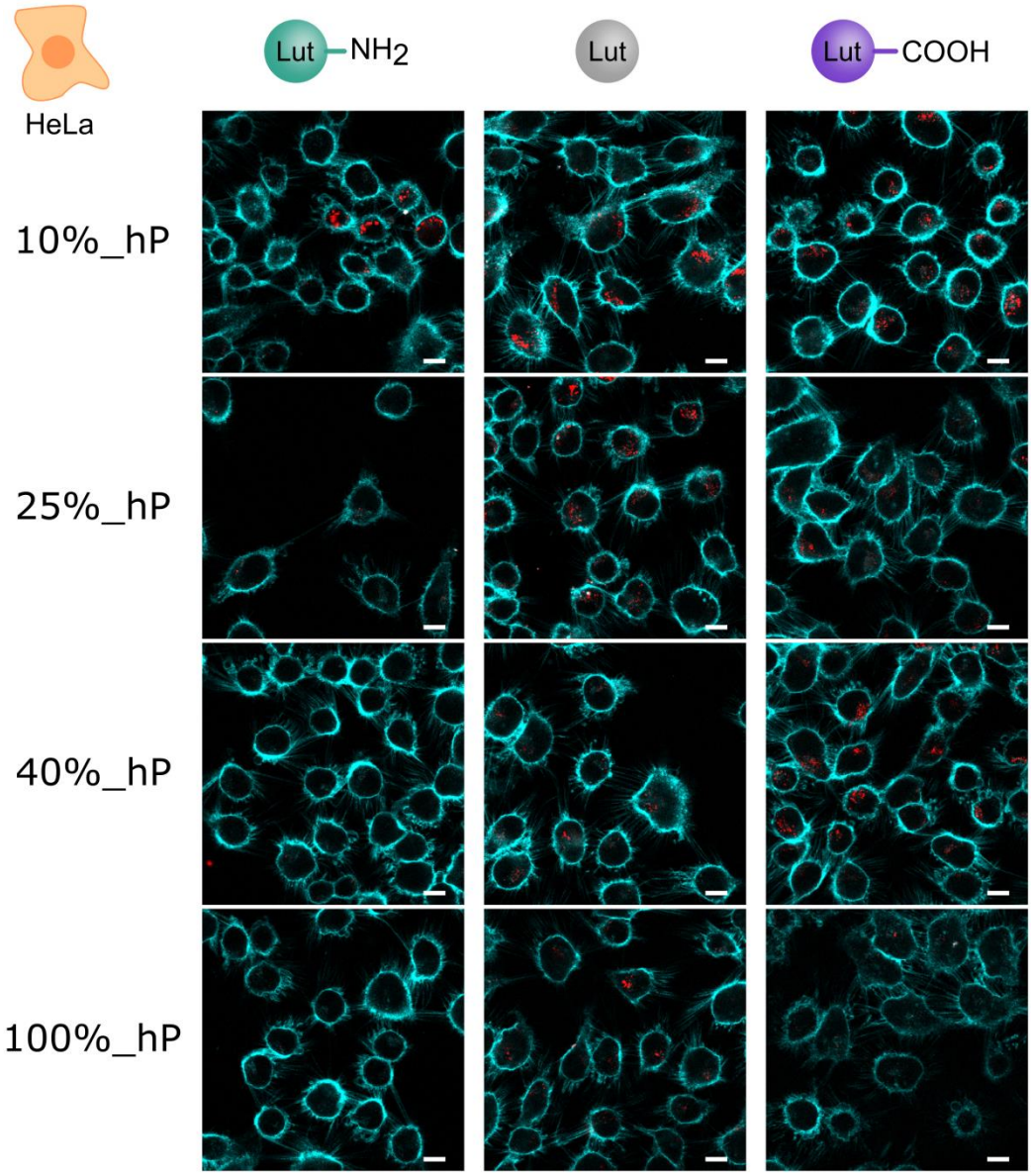

Figure 2.6.5. Imaging of the interaction between Lutensol stabilized NPs and HeLa cells in the presence of different concentrations of plasma (hP) after 24 h incubation at 37 ˚C. The image represents the overlay of the nanoparticles (red) and the cell membrane (light blue). The first column corresponds to the amino functionalized NPs, the middle one corresponds to the un-functionalized NPs, and the last column to the carboxyl functionalized NPs. The scale bar represents 10 µm.

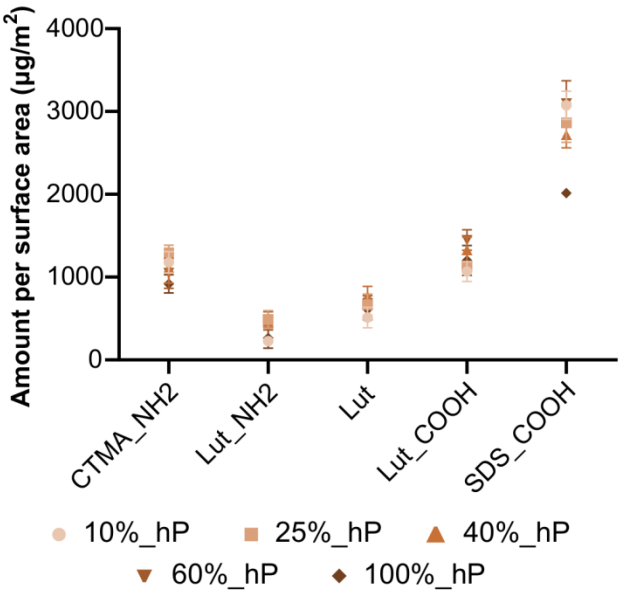

Figure 2.6.6. Hard corona protein amount recovered from the nanoparticles after coating in different concentrations of plasma. For accurate comparison between conditions, the amount of proteins is normalized based on the surface area. The nanoparticles were incubated with 10% hP (dot), 25% hP (square), 40% hP (triangle), 60% hP (inverted triangle), and 100% hP (diamond). The error bars represent the standard deviation between the amounts of proteins in a triplicate measurement.

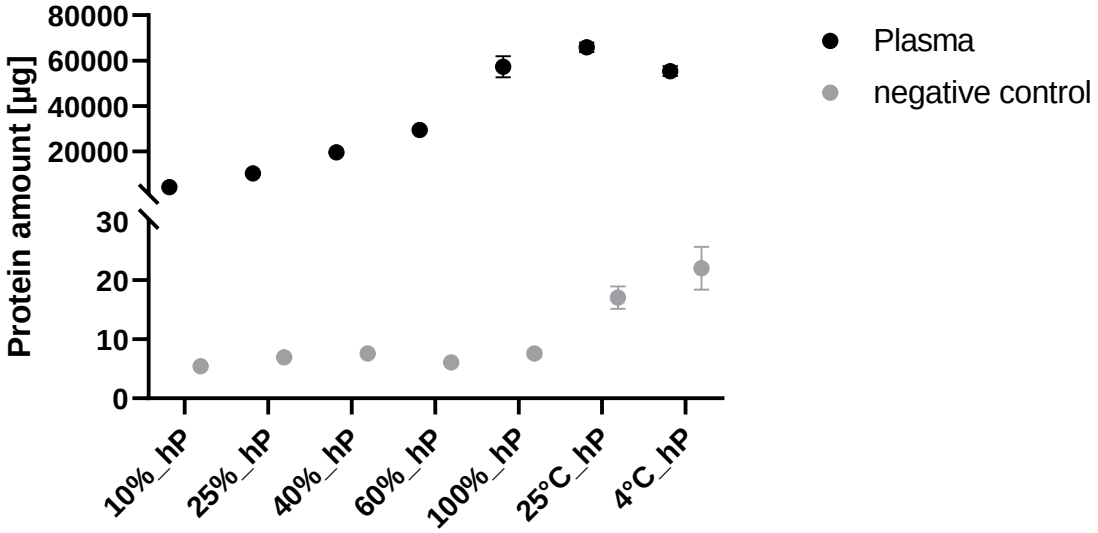

Figure 2.6.7. Protein amount in 1 mL human plasma used for the incubation of the nanoparticles (black) and protein amount in the negative control desorbed from the tube after plasma incubation and washing (grey). The error bar represents the standard deviation between the amounts of proteins in a duplicate measurement.

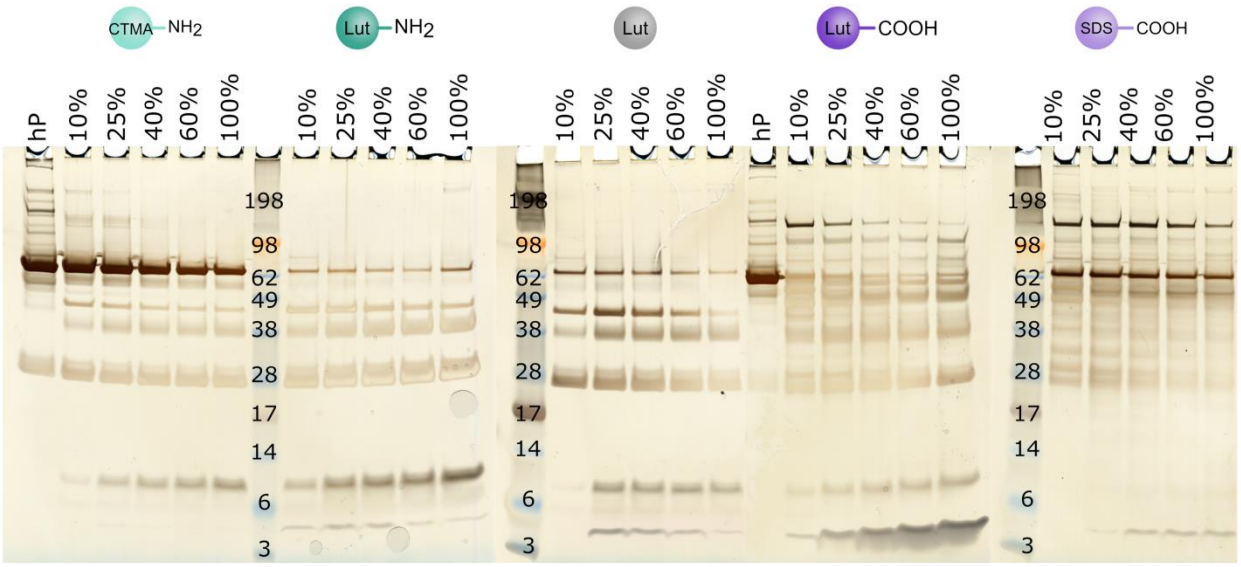

Figure 2.6.8. Separation of the hard corona proteins by SDS-PAGE revealed by silver staining for the different pre-coated NPs using five plasma concentrations. The lanes labeled as "hP" correspond to loading of pure plasma. The samples were loaded from left to right based on an increased amount of plasma (10%, 25%, 40%, 60%, and 100%) used in the NPs coating step.

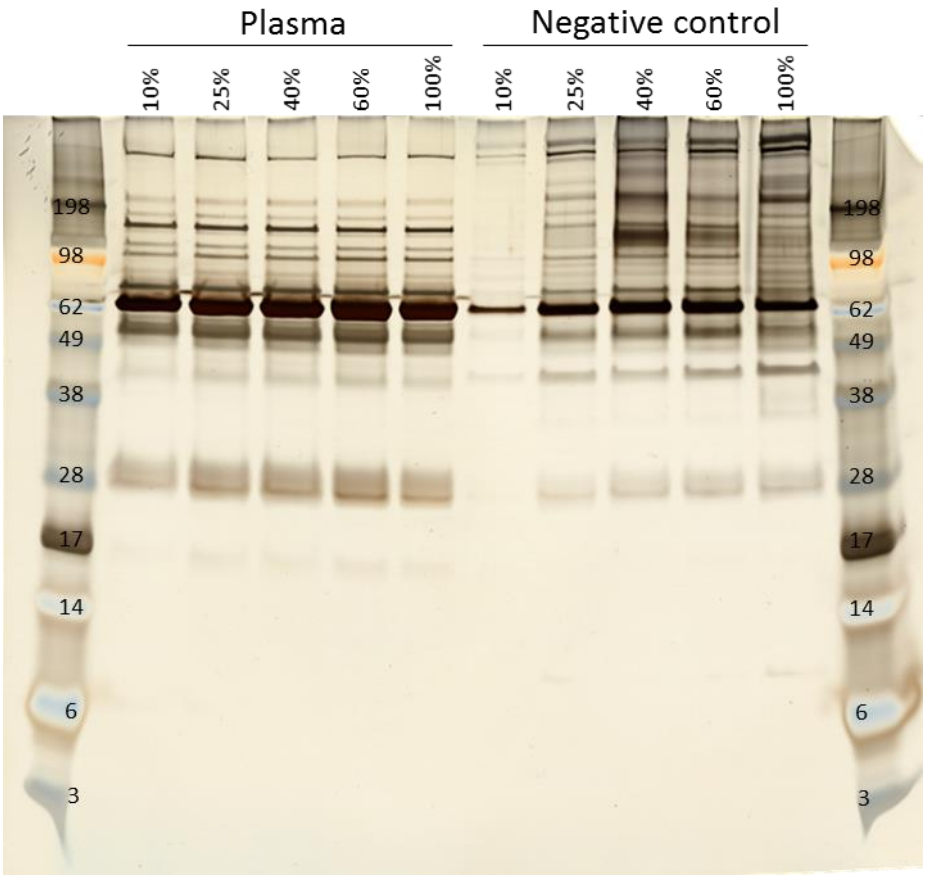

Figure 2.6.9. Separation of the proteins by SDS-PAGE revealed by silver staining for the different diluted plasma samples and for the negative controls. The lanes are labelled with the different dilutions from left to right with an increasing plasma concentration.

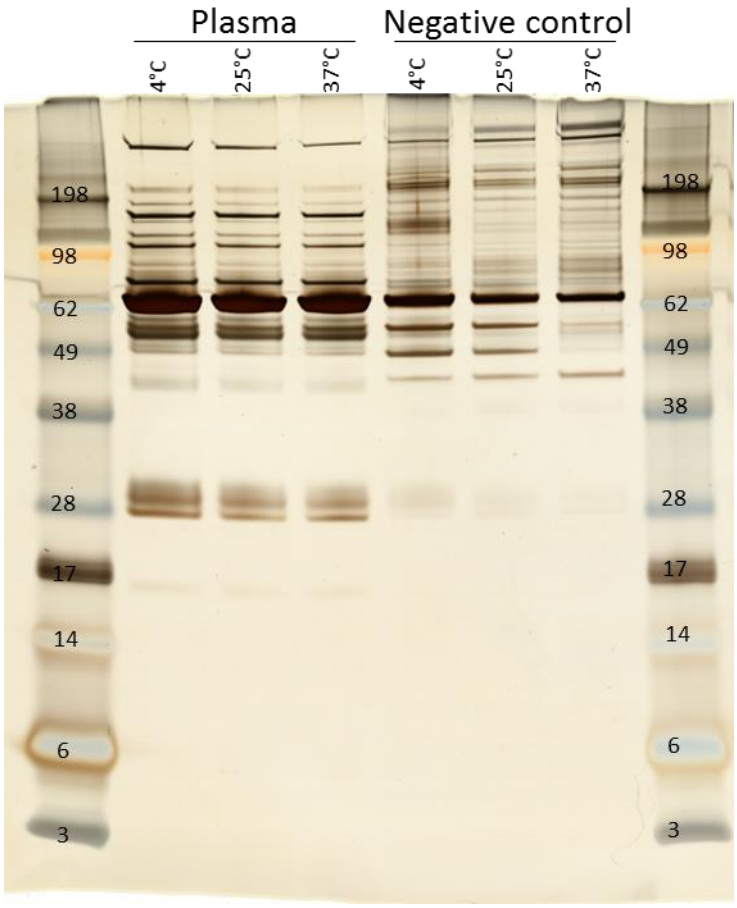

Figure 2.6.10. Separation of the proteins by SDS-PAGE revealed by silver staining for the different temperatures of the plasma samples and for the negative controls. The lanes are labelled with the different temperatures from left to right with an increasing plasma temperature.

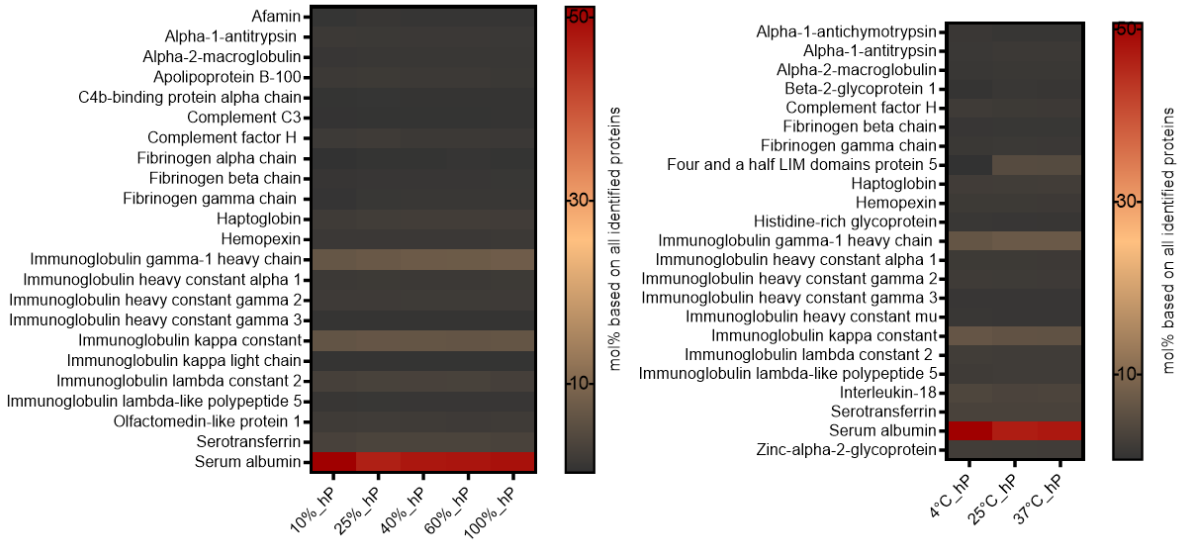

Figure 2.6.11. Combined top20 proteins identified in human plasma after incubation at the given concentration or temperature. The top20 proteins for each condition were combined to the final heatmaps.

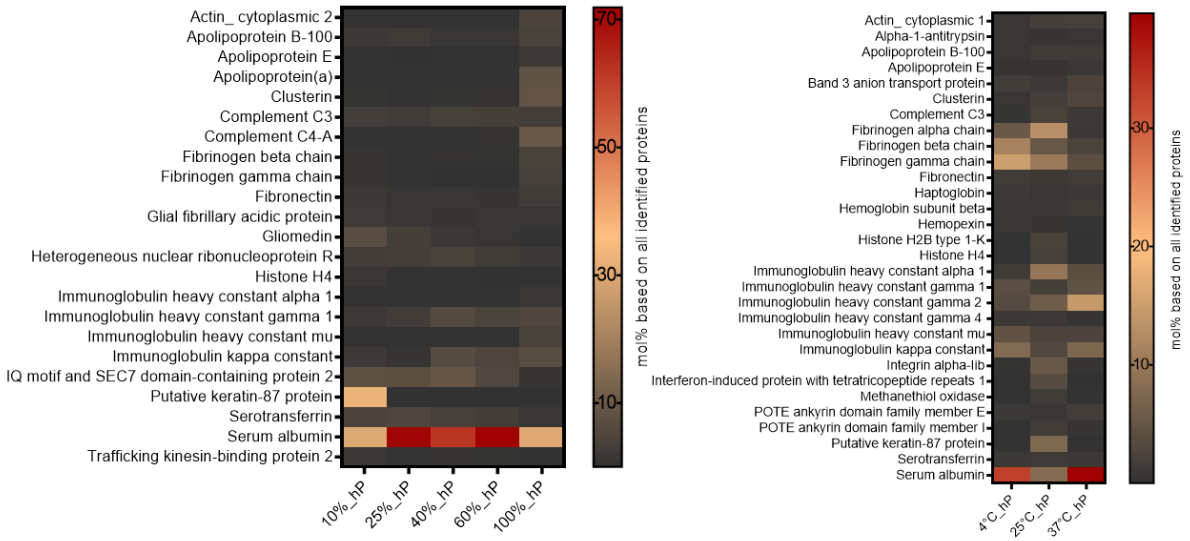

Figure 2.6.12. Combined top20 proteins identified in the negative controls after incubation of human plasma in the tube and washing as described. For the different concentrations, all 23 identified proteins are shown here and for the different temperatures the combined top20 proteins are shown in the heatmaps.

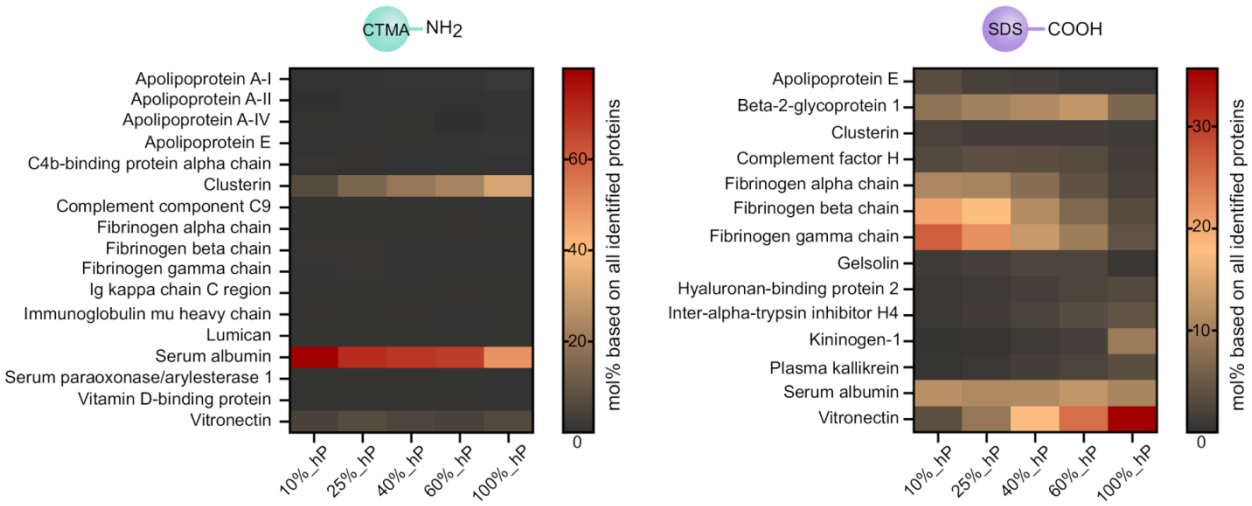

Figure 2.6.13. LC-MS analysis of the hard protein corona of CTMA-NH_2 and SDS-COOH NPs after coating with five different plasma concentrations. The values reported correspond to the %mol of the total protein identified in the corona and only the combined top10 proteins of each samples are plotted on the heatmap.

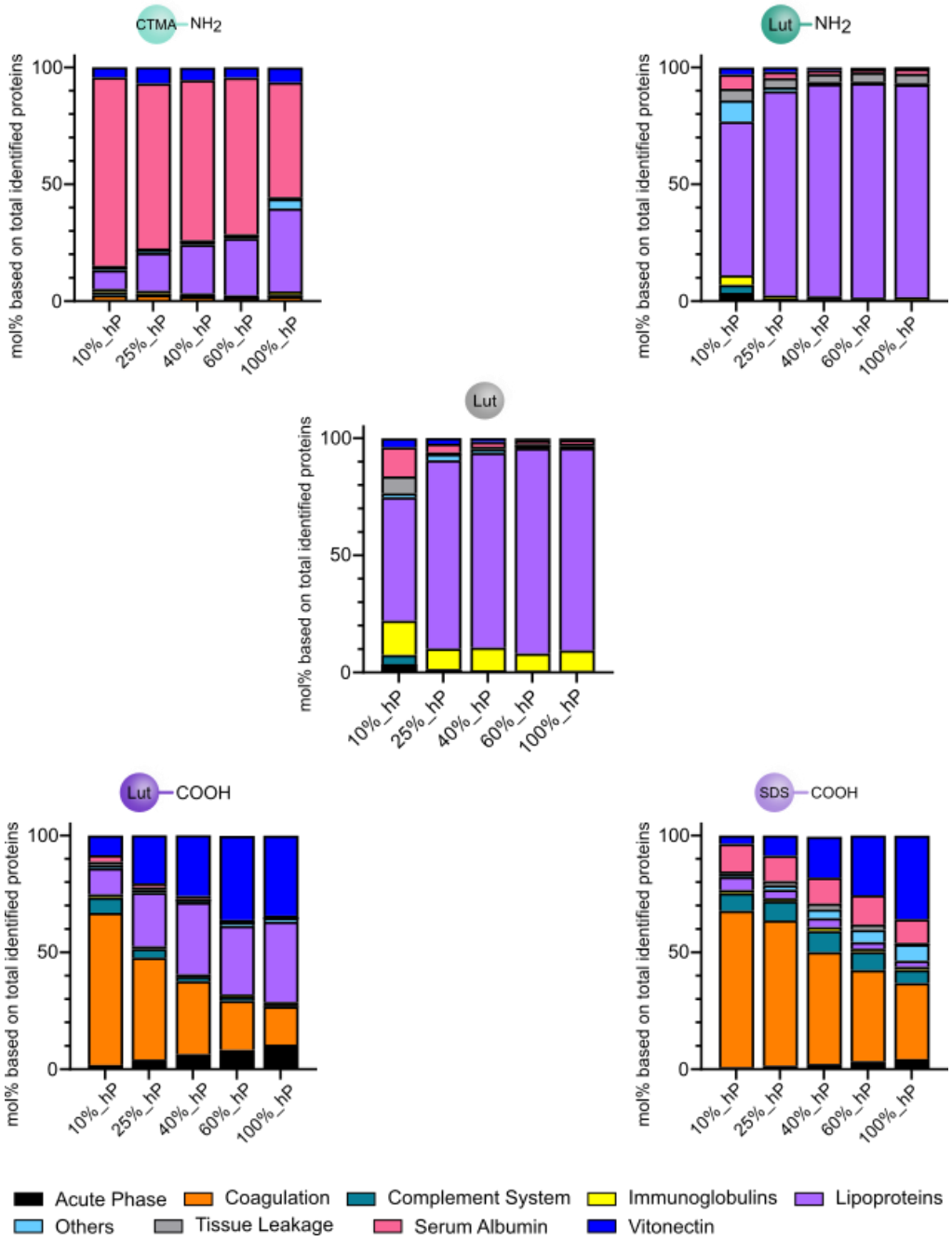

Figure 2.6.14. LC-MS analysis of the hard protein corona of NPs after coating with five different plasma concentrations. All the proteins identified were sorted based on their affiliation to one of the following categories: Acute Phase, Coagulation, Complement System, Immunoglobulins, Lipoproteins, Others, Tissue Leakage (staked from bottom to top on the graphics). Additionally, 2 single proteins (Serum Albumin and Vitronectin) with a high %mol present in the protein corona were also plotted.

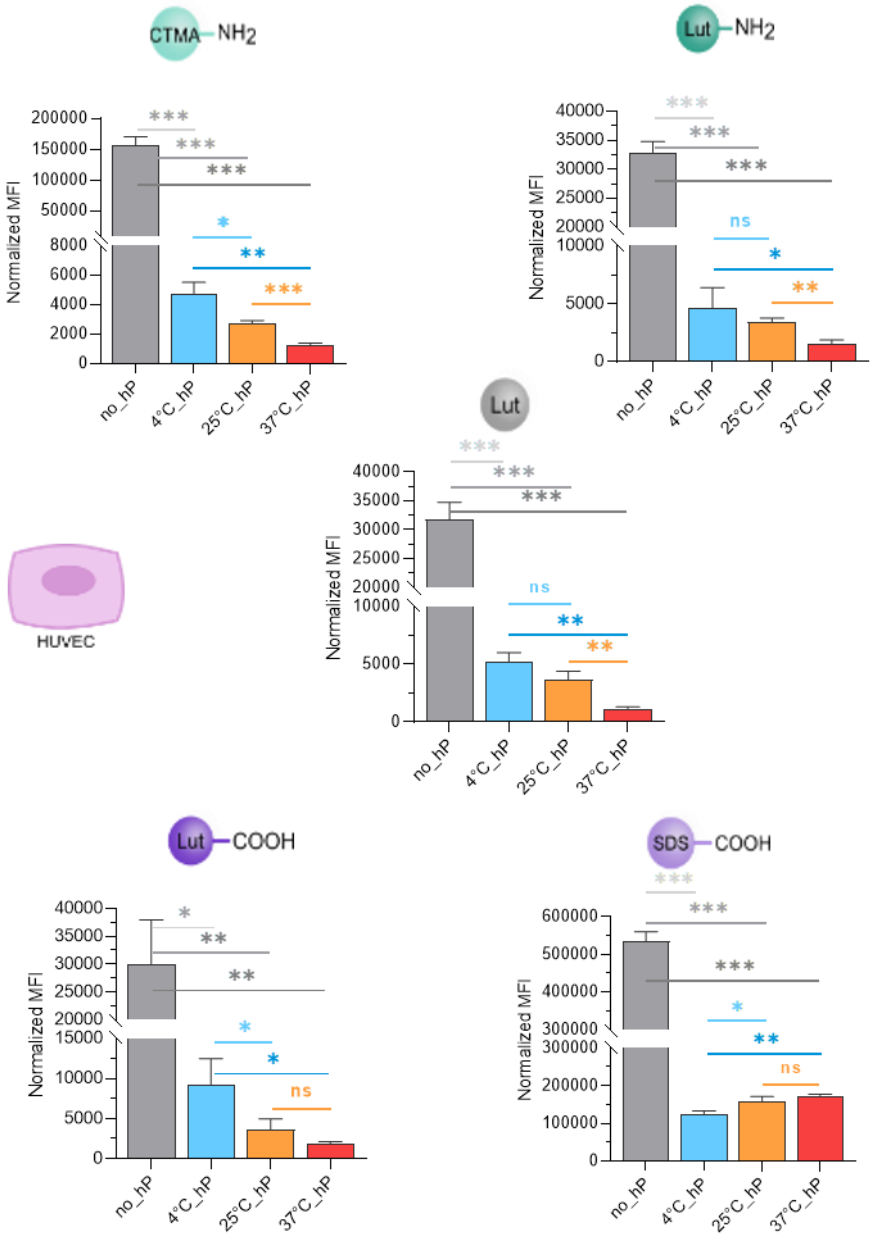

Figure 2.6.15. Cellular uptake extent of the pre-coated NPs with different temperatures by HUVEC cells after 24 h incubation at 37 °C. The cells were incubated with a solution containing 40 µg/mL NPs. The difference of intrinsic fluorescence intensity of the NPs tested was accounted for by normalizing the median fluorescence intensity recording by the flow cytometer based on the fluorescence intensity of the "Lut" NPs. The statistical significance of the difference between samples was determined by unpaired t-test. P-values > 0.12 were non-significant (n.s.), p-values < 0.033 correspond to *, p-values < 0.002 correspond to **, and p-values < 0 .001 correspond to ***

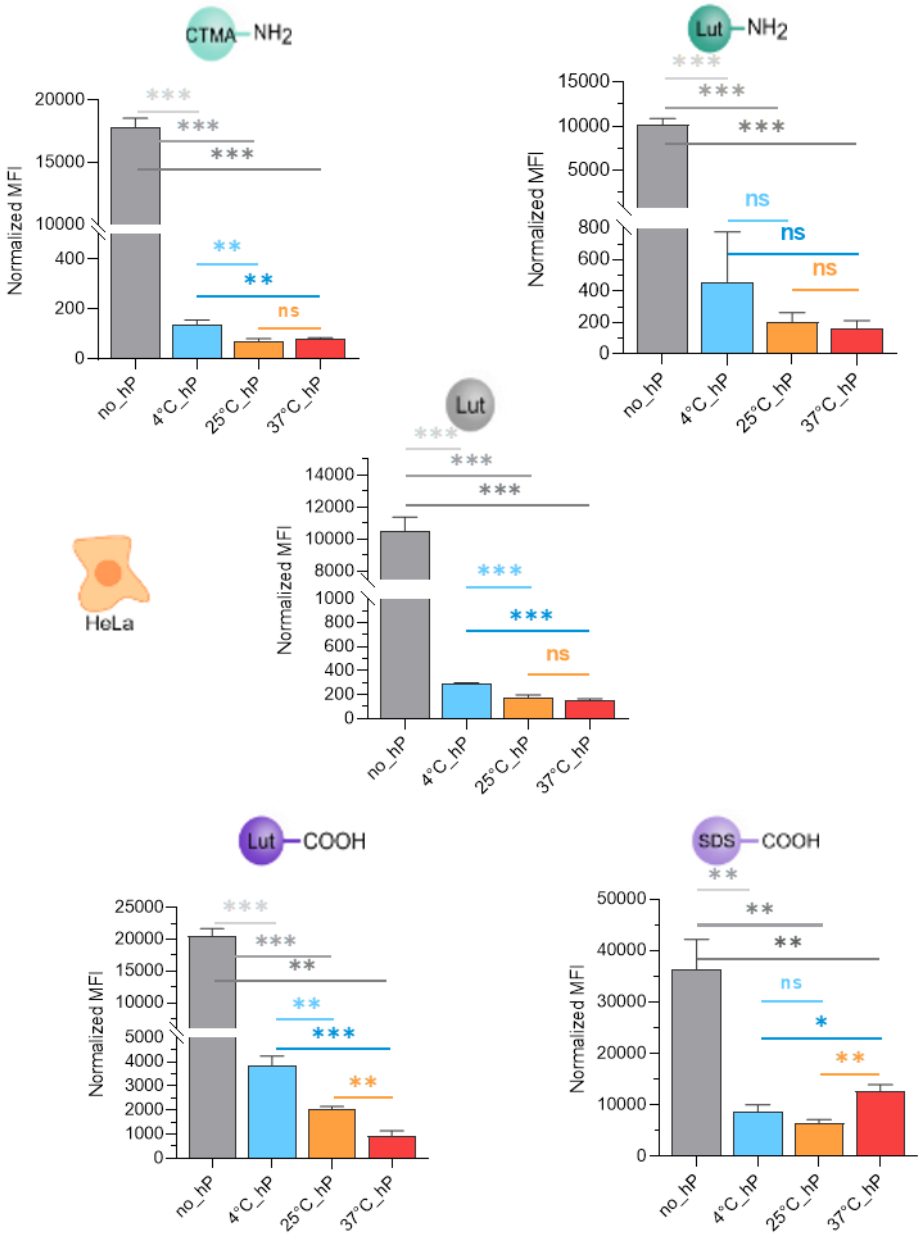

Figure 2.6.16. Cellular uptake extent of the pre-coated NPs with different temperatures by HeLa cells after 24 h incubation at 37 °C. The cells were incubated with a solution containing 40 µg/mL NPs. The difference of intrinsic fluorescence intensity of the NPs tested was accounted for by normalizing the median fluorescence intensity recording by the flow cytometer based on the fluorescence intensity of the "Lut" NPs. The statistical significance of the difference between samples was determined by unpaired t-test. P-values > 0.12 were non-significant (n.s.), p-values < 0.033 correspond to *, p-values < 0.002 correspond to **, and p-values < 0 .001 correspond to ***.

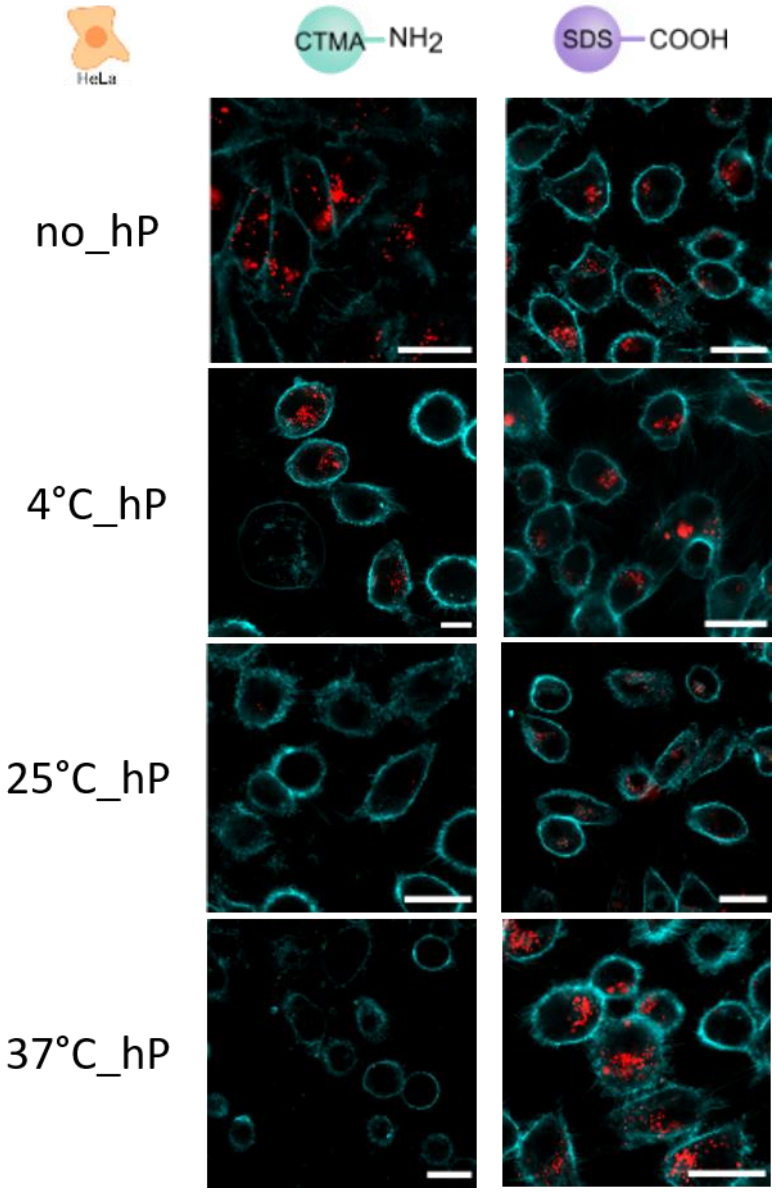

Figure 2.6.17. Images of the interaction between plasma pre-coated CTMA- and SDS- stabilized NPs at different temperatures (4 ˚C, 25 ˚C, and 37 ˚C) and HeLa cells after 24 h incubation at 37 ˚C. The image represents the overlay of the nanoparticles (red) and the cell membrane (light blue). The first column corresponds to the amino functionalized NPs and the last column to the carboxyl functionalized NPs. The scale bar represents 25 µm.

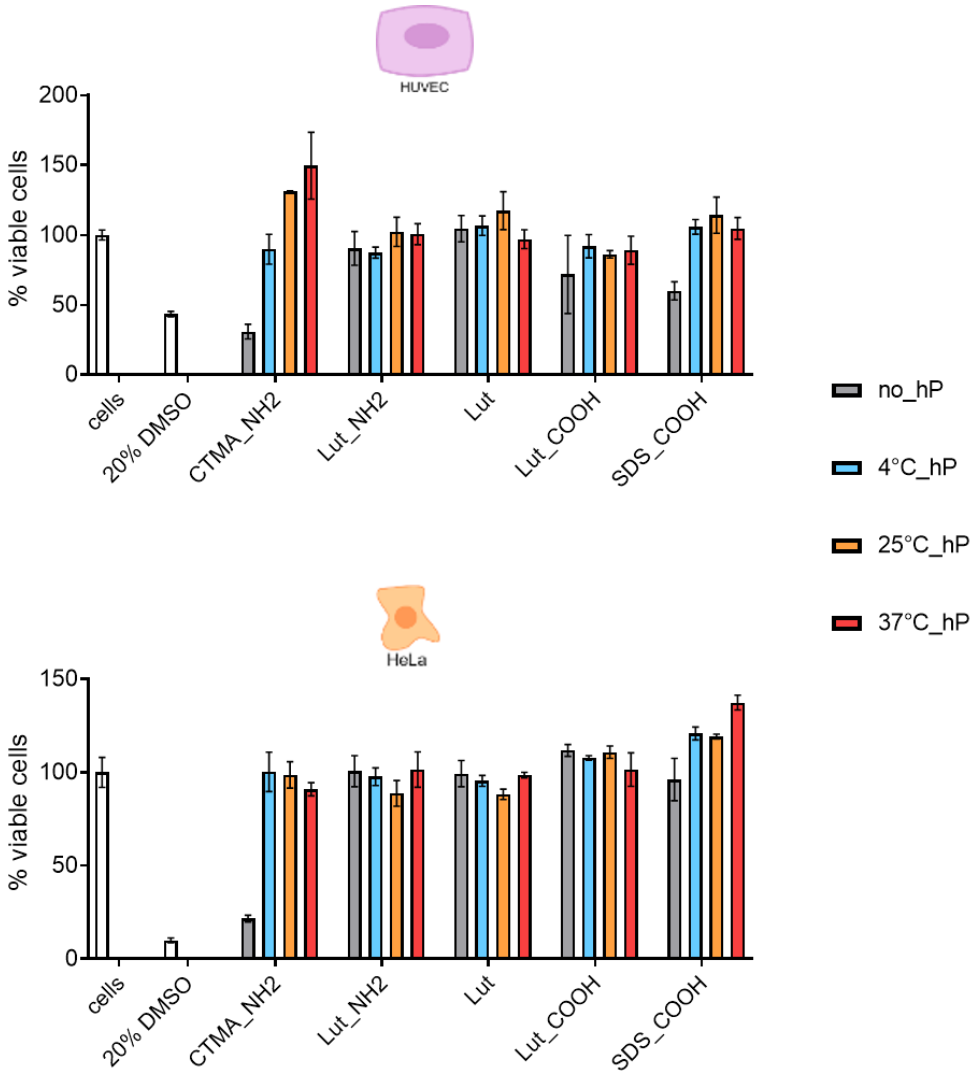

Figure 2.6.18. Cellular viability after incubation for 24 h in presence of 40 µg/mL NPs. The sample labeled "cells" corresponds to the untreated cells incubated in DMEM media without NPs, the sample labelled "20% DMSO" corresponds to cells treated for 24 h with a DMEM media containing 20% DMSO. These samples are used as controls to validate the assay. The error bars represent the standard deviation between the viability of three samples treated with the same nanoparticle solution.

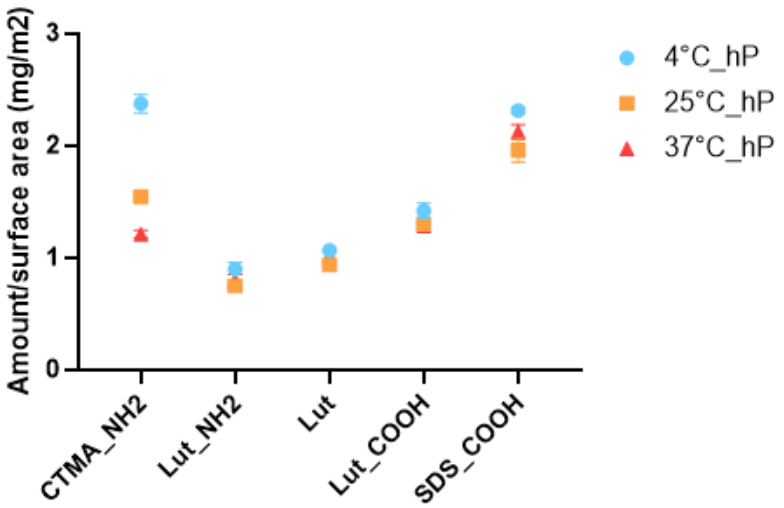

Figure 2.6.19. Hard corona protein amount recovered from the nanoparticles after coating at different temperatures with plasma. For accurate comparison between conditions, the amount of proteins is normalized based on the surface area. The nanoparticles were incubated at 4 °C hP (blue dot), 25 °C hP (orange square), and 37 °C hP (red triangle). The error bars represent the standard deviation between the amounts of proteins in a triplicate measurement.

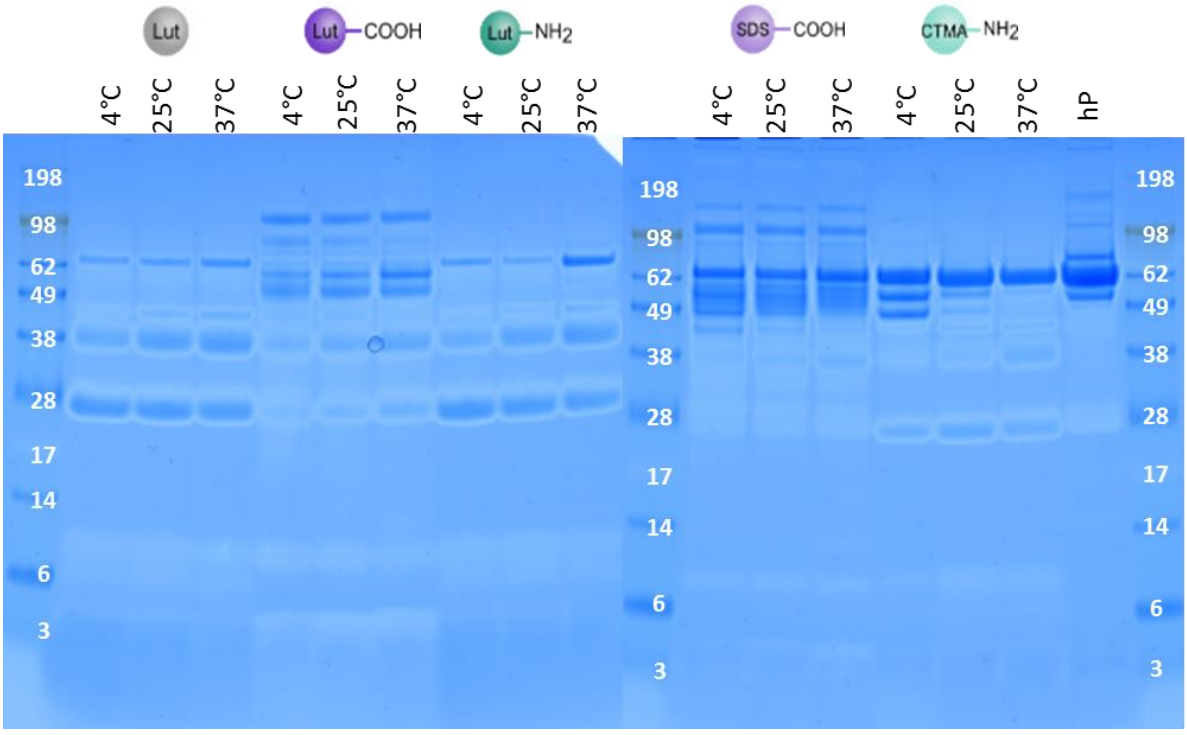

Figure 2.6.20. Separation of the hard corona proteins by SDS-PAGE revealed by Coomassie Blue for the different pre-coated NPs using three temperatures. The lane labeled as "hP" corresponds to loading of pure plasma. The samples were loaded from left to right based on an increased temperature (4 ˚C, 25 ˚C, and 37 ˚C) used in the NPs coating step.

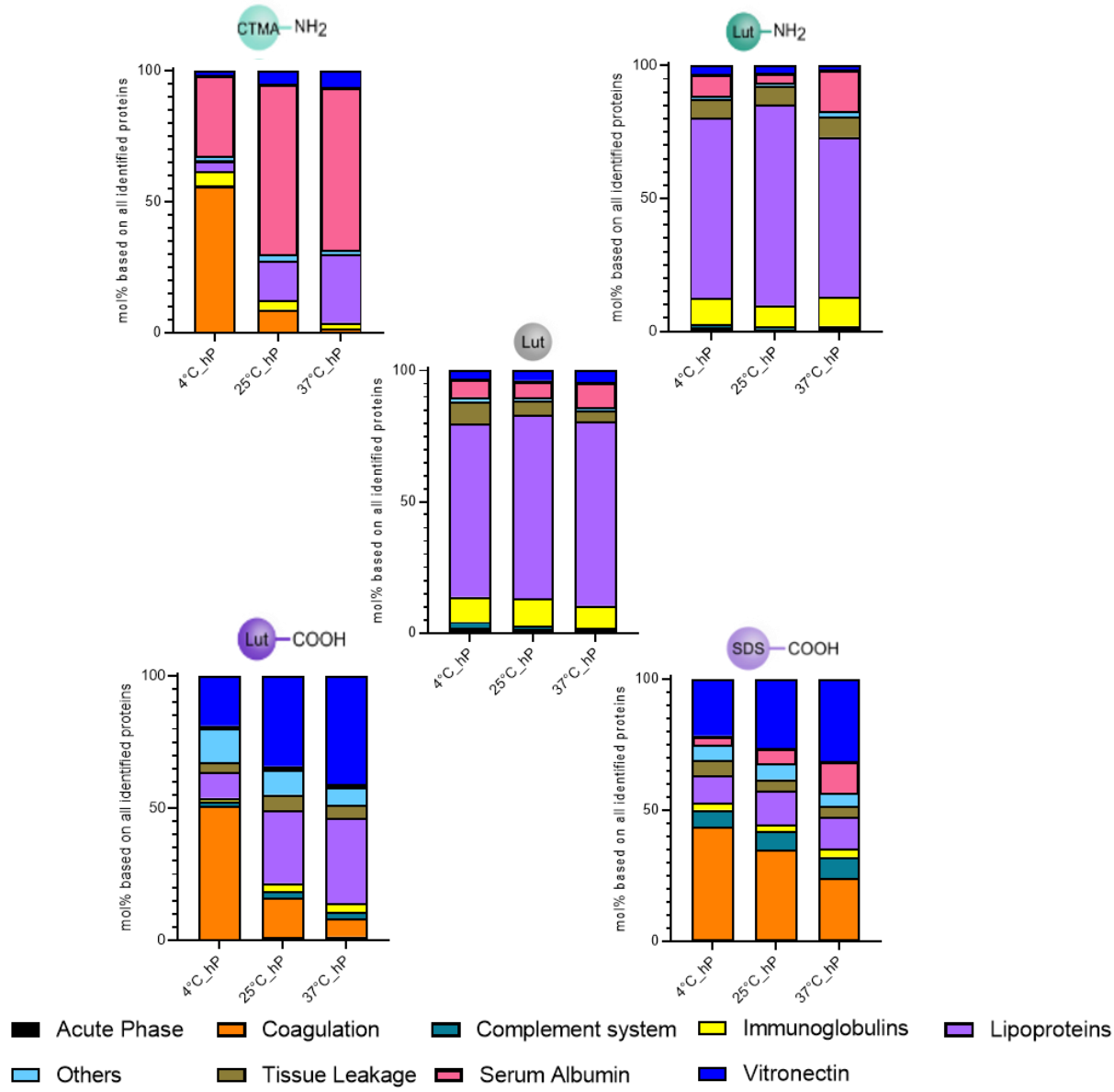

Figure 2.6.21. LC-MS analysis of the hard protein corona of NPs after coating with plasma at three different temperatures. All the proteins identified were sorted based on their affiliation to one of the following categories: Acute Phase, Coagulation, Complement System, Immunoglobulins, Lipoproteins, Others, Tissue Leakage (staked from bottom to top on the graphics). Additionally, two single proteins (Serum Albumin and Vitronectin) with a high %mol present in the protein corona were also plotted.

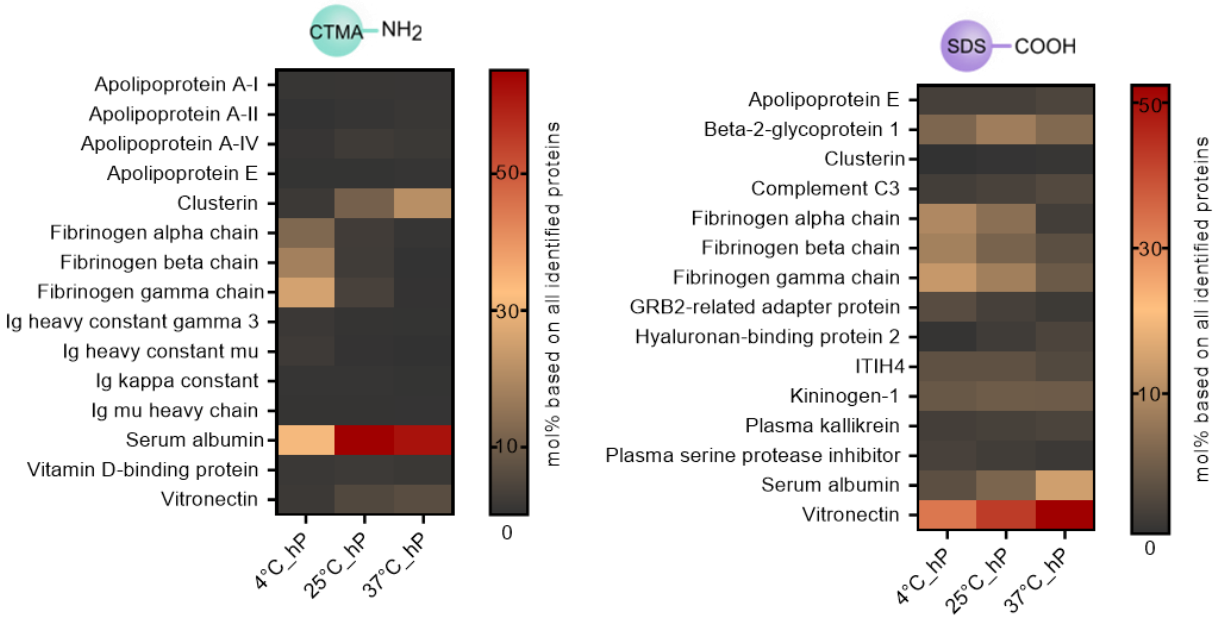

Figure 2.6.22. LC-MS analysis of the hard protein corona of CTMA-NH$_2$ and SDS-COOH NPs after coating with plasma at three different temperatures. The values reported correspond to the %mol of the total protein identified in the corona and only the combined top10 proteins of each samples are plotted on the heatmap.

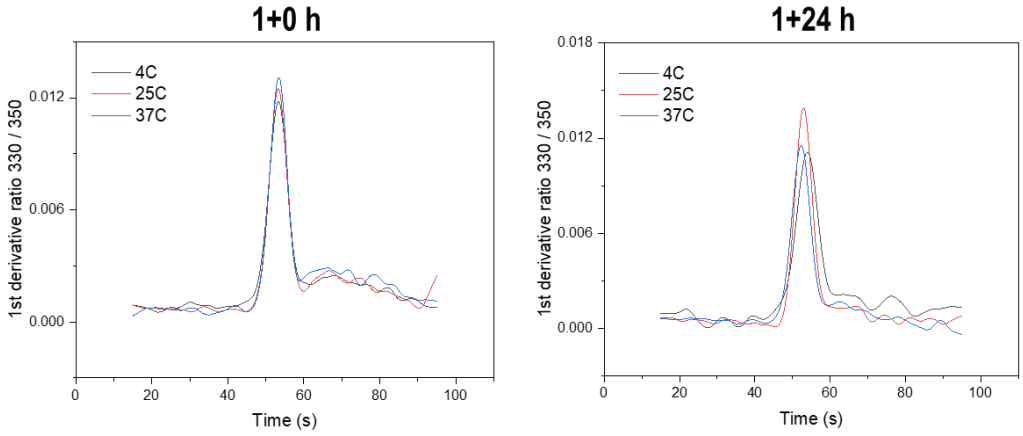

Figure 2.6.23. Stability of fibrinogen incubated at three different temperatures determined with nano DSF. Fibrinogen was incubated at a concentration of 1.5 mg/mL in water for 1 h at the given temperature. Afterwards the stability was either directly or after 24 h measured with nano DSF.

3. Temperature-Responsive Nanoparticles Enable Specific Binding of Apolipoproteins from Human Plasma

Copyright:

[3] XXX*, **Jennifer Oberländer***, XXX, XXX, XXX, XXX, XXX, XXX, XXX. Temperature-Responsive Nanoparticles Enable Specific Binding of Apolipoproteins from Human Plasma. *Small*, 2021, 18 (3), 2103138. **(*shared first)**

Aim:

Understanding and controlling the protein corona formed around nanocarriers after injection into the human blood stream is of great importance for their successful application in drug delivery processes. Apolipoproteins have been previously shown to provide a so-called stealth effect on nanocarriers whereby the blood circulation time of nanocarriers is increased and their unspecific uptake in immune cells is decreased. This study aimed to control the apolipoprotein adsorption on a nanoparticle by using a temperature-dependent polymer. This will help to design future nanoparticle surfaces in such a way that a specific protein corona and thus improved targeting can be achieved.

Contribution:

I performed the complete protein corona analysis including Pierce Assay, SDS-PAGE, and LC-MS analysis as well as the analysis of the cellular uptake of the nanoparticles (flow cytometry and cLSM). XXX synthesized the nanoparticles and performed the characterization of the nanoparticles. The manuscript was prepared by XXX and me. The synthesis of the Bodipy-methacrylate was done by XXX and the solid state ^{13}C NMR characterization by XXX. XXX performed the multi-angle DLS measurements under the supervision of XXX. XXX, XXX, XXX, and XXX supervised the project.

3.1 Abstract

Apolipoproteins are an important class of proteins because they provide a so-called stealth effect to nanoparticles. The stealth effect on nanocarriers leads to a reduced unspecific uptake into immune cells and thereby to a prolonged blood circulation time. Herein, a novel strategy to bind apolipoproteins specifically on nanoparticles by adjusting the temperature during their incubation in human plasma is presented. This specific binding, in turn, allows a control of the stealth behavior of the nanoparticles. Nanoparticles with a well-defined poly(N-isopropylacrylamide) shell are prepared, displaying a reversible change of hydrophobicity at a temperature around 32 °C. It is shown by label-free quantitative liquid chromatography-mass spectrometry that the nanoparticles are largely enriched with apolipoprotein J (clusterin) at 25 °C while they are enriched with apolipoprotein A1 and apolipoprotein E at 37 °C. The temperature-dependent protein binding is found to significantly influence the uptake of the nanoparticles by RAW264.7 and HeLa cells. The findings imply that the functionalization of nanoparticles with temperature-responsive materials is a suitable method for imparting stealth properties to nanocarriers for drug-delivery.

3.2 Introduction

Apolipoproteins are lipid binding proteins in human plasma and are mostly responsible for generating the so-called "stealth effect" around nanoparticles. The stealth effect enables a prolonged circulation time of nanoparticles in the blood after injecting nanoparticles into the body[180]. Currently, research on nanoparticles is of growing interest as they are used as drug delivery agents in nanomedicine[181]. However, the main problem when injecting nanoparticles into a bloodstream is the clearance of nanoparticles from the blood caused by an unspecific protein adsorption and fast uptake into immune cells like macrophages[182]. Therefore, controlling the protein adsorption around nanoparticles and in consequence controlling the stealth effect is of great importance[167]. Herein, we report a method for preparing a specific protein corona on nanoparticles, which significantly imparts them with a stealth effect.

The most straightforward method to provide a stealth effect to nanoparticles is to coat them with apolipoproteins prior to injection[75]. However, isolated apolipoproteins are costly, and therefore, this approach cannot be easily scaled up. Another approach relies on the enrichment of protein corona on the surface of materials with apolipoprotein by incubating functionalized nanoparticles with plasma[173]. The coating of nanocarriers with poly(ethylene glycol) (PEG) or polyphosphoesters was found to favor the adsorption of apolipoproteins[67, 75].

The protein adsorption on nanoparticles is known to be temperature-dependent[81, 82]. However, no clear correlation between the composition of protein corona and the temperature could be derived[81]. Because the temperature varies in the human body, it is necessary to incubate the nanoparticles ex vivo prior to their use in vivo, in order to prepare a stable and reproducible protein corona.

Some reports have investigated the temperature dependence of the relationship between the protein adsorption and polymers, which undergo a transition from hydrophilic to hydrophobic properties above a lower critical solution temperature (LCST). Around two times more bovine serum albumin was adsorbed on the poly(N-isopropylacrylamide) (PNIPAM) surface at T > LCST (37 °C) compared to T < LCST (23 °C)[123]. Because the LCST of PNIPAM is in the physiological range, it was used to prepare materials for biomedical applications. Thin films or beads containing PNIPAM were used for cell culture[131]. Cells spread and proliferate on the surfaces at 37 °C (T > LCST) and cell sheets could be detached and collected at T < LCST. Furthermore, beads containing PNIPAM were employed for protein separation[131]. Specific proteins in protein mixtures were adsorbed on the beads at T > LCST and eluted after lowering the temperature below LCST. PNIPAM was also used to impart a temperature-modulated release function to nanocarriers[120]. Moreover, cellular uptake of nanocarriers containing PNIPAM increased significantly at T > LCST due to favored interactions between collapsed PNIPAM chains and the cell membrane[129].

Previously, PNIPAM-based nanoparticles with a LCST of ≈ 11 °C were used to isolate lysozyme, a natural antibacterial agent located in the white extract of chicken egg[171]. The nanoparticles were incubated in the extract at room temperature to catch lysozyme. Finally, apolipoproteins were found to be the major proteins detected on PNIPAM-based nanoparticles which were incubated in human plasma[170]. However, there are no reports investigating the type of preferentially adsorbed proteins on temperature-responsive nanoparticles at different temperatures and its relationship with the cell uptake.

We synthesized well-defined temperature-responsive polystyrene (PS)-PNIPAM core-shell nanoparticles with a controllable shell thickness and studied the adsorption of proteins from human plasma at various temperatures. Our hypothesis was that the incubation above or below the volume phase transition temperature (VPTT) of PNIPAM would favor a specific adsorption of certain types of apolipoproteins, which play a crucial role in imparting a stealth effect to nanocarriers. Our hypothesis was tested and verified by studying the uptake of temperature-responsive nanocarriers by RAW264.7 and HeLa cells.

3.3 Materials and methods

Materials. 4-Hydroxybenzaldehyde (98%, Aldrich), trifluoroacetic acid (TFA, 99%, Aldrich), methacryloyl chloride (97%, Aldrich), 2,3-dichloro-5,6-dicyano-p-benzoquinone (DDQ, 98%, Aldrich), anhydrous dichloromethane (DCM, 99.8%, Aldrich), methanol (99.9%, Aldrich), cyclohexane (99.5%, Aldrich), petroleum ether (puriss, Aldrich), (99.8%, Aldrich), toluene (99.8%, Aldrich), 3-ethyl-2,4-dimethylpyrrole (97%, TCI Chemicals), triethylamine (99.5%, Carl Roth), N,N-diisopropylethylamine (DIPEA, 99.5%, Carl Roth), sodium sulfite (98%, Carl Roth), sodium sulfate (98.5%, Carl Roth), 1,8-diazabicyclo[5.4.0]undec-7-en (DBU, for synthesis, Merck), boron trifluoride etherate (for synthesis, Merck), SDS (≥ 90%, Fluka), aluminum oxide (Al2O3, for chromatography, Acros Organics), potassium peroxydisulfate (KPS, ≥ 99%, Merck), N-isopropylacrylamide (NIPAM, 98%, Acros Organics), N,N′-methylenebisacrylamide (BIS, 99%, Alfa Aesar), Stains-All (95%, Sigma Aldrich), isopropanol (99.96%, Fisher Scientific), and formamide (extra pure, Applichem) were used as received. Styrene (99%, Acros Organics) was purified through an aluminum oxide column prior to reaction. Unless otherwise noted, Milli-Q water was used throughout experiments.

Human blood was taken from healthy donors at the Department of Transfusion Medicine Mainz after physical examination and after obtaining written informed consent in accordance with the Declaration of Helsinki. The study was approved by the local ethics committee “Landesärztekammer Rheinland-Pfalz” (Bearbeitungsnummer: 837.439.12 (8540-F)).

Synthesis of Phenol-BODIPY (2,6-diethyl-1,3,5,7-tetramethyl-8-(4-hydroxyphenyl)-BODIPY. 4-Hydroxybenzaldehyde (244 mg, 2 mmol) and 3-ethyl-2,4-dimethylpyrrole (492 mg, 4 mmol) were dissolved in 100 mL of absolute DCM under Ar atmosphere. Three drops of TFA were added, and the solution was stirred at room temperature overnight in the dark. Dry 2,3-dichloro-5,6-dicyano-p-benzoquinone (DDQ) (400 mg) was added, and stirring was continued for 2 h. Triethylamine (2 mL) was added and the organic phase was washed with aqueous sodium sulfite (3%, 2 × 100 mL). Organic layers were separated, dried over anhydrous sodium sulfate, and evaporated. N,N-diisopropylethylamine (DIPEA) (3 mL) and 100 mL of absolute DCM were added under an Ar atmosphere, and the solution was stirred at room temperature for 10 min. BF3·OEt2 (3 mL) was added, and stirring was continued for 2 h. The reaction mixture was washed with an aqueous solution of NaHCO3 (5%, 2 × 100 mL) and deionized water (100 mL). The combined organic extracts were dried over Na2SO4, filtered, and evaporated. Column chromatography with silica gel and dichloromethane as eluent afforded phenol-BODIPY which was evaporated and recrystallized from DCM/methanol to give red crystals after drying under vacuum. Yield: 642 mg (81%). 1H NMR (250 MHz, CD2Cl2, δ): 7.15 (d, J = 8.7 Hz, 2H), 6.97 (d, J = 11.3 Hz, 2H), 5.08 (s, 1H), 2.48 (s, 6H), 2.32 (q, J = 7.5 Hz, 4H), 1.37 (s, 6H), 1.01 (t, J = 7.6 Hz, 6H); λ_{max} (toluene, ε) = 526 nm (63 000); fluorescence (toluene): λ_{max} = 542 nm (ϕ = 72%); MS (ESI) m/z [M+Na]: calcd for C23H27BF2N2NaO2 419.27; found 419.24.

Synthesis of the Polymerizable BODIPY (2,6-diethyl-1,3,5,7-tetramethyl-8-(4-methacryloyloxyphenyl)-BODIPY. Phenol-BODIPY (397 mg, 1 mmol) was dissolved in 50 mL of anhydrous dichloromethane and flushed with argon. Then DBU (305 mg, 2 mmol) was slowly added. The resulting mixture was cooled with ice-water and methacryloyl chloride (156 mg, 1.5 mmol) in dry dichloromethane (10 mL) was added dropwise. The mixture was stirred at room temperature during 24 h, and then concentrated under vacuum at room temperature. The residue purified by chromatography on silica gel (dichloromethane/petroleum ether: 70/30 vol/vol), afforded 352 mg of product (76% yield).The monomer was dissolved in cyclohexane and freeze-dried, the resulting powder was stored in the freezer at −20 °C. 1H NMR (250 MHz, CD2Cl2, δ):7.31 (d, J = 6.2 Hz, 1H), 6.37 (s, 1H), 5.81 (s, 1H), 2.49 (s, 3H), 2.33 (q, J = 7.5 Hz, 2H), 2.08 (s, 1H), 1.36 (s, 3H), 0.99 (t, J = 7.5 Hz, 3H); λ_{max} (toluene, ε) = 528 nm (64 000); fluorescence (toluene): λ_{max} = 545 nm (ϕ = 81%); MS (ESI) m/z [M+Na]: calcd for C27H31BF2N2NaO2 487.23; found 487.21.

Synthesis of Polystyrene-Poly(N-isopropylacrylamide) (PS-P0.05) Core Nanoparticles. Styrene (30 g, 288.05 mmol), NIPAM (1.63 g, 14.40 mmol), SDS (0.3 g, 1.04 mmol), polymerizable BODIPY (0.05 g, 0.105 mmol), and 200 mL water were charged into a 500 mL round-bottom flask. Nitrogen was bubbled through the mixture to remove oxygen for 10 min. KPS (0.3 g, 1.11 mmol) dissolved in 20 mL water was then fed into the mixture. The polymerization was performed at 80 °C for 8 h with the stirring speed of 1000 rpm. The nanoparticles were purified by dialysis to remove excessive SDS. 100 mL of the nanoparticle dispersion was placed into a dialysis tube (MWCO ≈ 14 kDa). The dialysis was performed against 10 L deionized water for 24 h while water was changed 5 times. The feed molar ratio of styrene to NIPAM was 1:0.05 and the obtained nanoparticles are denoted as PS-P0.05.

Synthesis of Core-Shell Polystyrene-Poly(N-isopropylacrylamide) Nanoparticles. To prepare PS-PNIPAM nanoparticles with varied PNIPAM shell thickness, 12.3 mL of PS-P0.05 dispersion (solid content = 10.4 wt%) was fed into a 100 mL round-bottom flask. The dispersion was diluted with 40 mL water to obtain a dispersion with a solid of 2.45 wt%. Known amounts of NIPAM and crosslinker BIS were added into the dispersions (Table 3.6.1). The mixture was deoxygenized by N2 bubbling for 10 min. Certain amounts of KPS were dissolved in 2 mL water, and the solution was then added to the dispersions to initiate polymerization. The polymerization was performed at 80 °C for 4.5 h with a stirring speed of 1000 rpm. Thereafter, the dispersions were dialyzed against 5 L deionized water for 24 h while changing water 5 times (MWCO ≈ 14 kDa) to remove SDS. Samples with styrene to NIPAM molar ratios of 1:0.10, 1:0.15, and 1:0.20 are denoted as PS-P0.10, PS-P0.15, and PS-P0.20, respectively. The measured residual surface concentrations of SDS in the dialyzed dispersions are shown in Table 3.6.1.

Quantification of Poly(N-isopropylacrylamide) in the Core-Shell Particles by Using Solid State Nuclear Magnetic Resonance Spectroscopy. The quantitative cross polarization magic-angle spinning nuclear magnetic resonance (NMR) spectra of the nanoparticles were recorded on a 300 MHz Bruker AVANCE II spectrometer at 10 KHz MAS spinning frequency[183]. The molar ratio between NIPAM to styrene units of the particles was obtained from the NMR spectra by signal integration of the NIPAM-CH3 units at 22 ppm and the quaternary aromatic site at 146 ppm, connecting the phenyl ring of PS to its aliphatic main chain. The PNIPAM shell thickness was calculated by assuming the PS and the PNIPAM formed a core and a shell in a concentric spherical structure with an external diameter equal to the hydrodynamic diameter in water determined by dynamic light scattering (DLS). The thickness of PNIPAM shell was then calculated by considering the amounts of NIPAM units determined by NMR spectroscopy for the PS-P0.10, PS-P0.15, and PS-P0.20 subtracted with the amounts of NIPAM units found in PS-P0.05, the weighted amount of styrene, the molar mass of NIPAM and styrene, and the density of both polymers which were assumed to be the density in bulk (ρPS = 1.04 g/mL and ρPNIPAM = 1.10 g/mL).

Stability of the Core-Shell Nanoparticles in Human Plasma. The multi-angle DLS measurements were performed on an ALV spectrometer consisting of a goniometer and an ALV-5004 multiple-tau full-digital correlator (320 channels). A He-Ne laser (wavelength of 632.8 nm) was used as a light source. For temperature-controlled measurements, the light scattering instrument was equipped with a thermostat (Julabo). Before the measurement, water, PBS, or undiluted human plasma were filtered through Millex-GS filters (Merck Millipore, Billerica, USA) with a 200 nm pore size into quartz cuvettes with an inner radius of 9 mm (Hellma, Müllheim, Germany). Prior to use, the quartz cuvettes were cleaned with acetone using a Thurmond apparatus[184]. The nanoparticles and the plasma, water, or PBS were separately incubated at 25 °C or at 37 °C before mixing (1 µL of 2 wt% NPs in 1 mL solution of plasma, water, or PBS). Then, the mixture was incubated at 25 or 37 °C for 1 h. For data analysis, a robust multicomponent fit method reported by Rausch et al. was used[185].

The correlation functions of nanoparticles in water and PBS at 25 and 37 °C, $g_{1,\,np(t)}$, could be fitted by a sum of two exponentials:

$$g_{1,np}(t) = a_{1,np}\, x\, exp\left(-\frac{t}{\tau_{1,np}}\right) + a_{2,np}\, x\, exp\left(-\frac{t}{\tau_{2,np}}\right) \quad (1)$$

where a_i is amplitude and $\tau_i = 1/(q2D_i)$ is decay time, q is the absolute value of the scattering vector ($q = 4\pi n \sin(\theta/2)/\lambda 0$) and D_i is the diffusion coefficient of particle.

Because human plasma contains many proteins and lipids with various sizes, the fit of correlation functions of pure plasma, $g_{1,p}(t)$, was more complex and hence required a sum of three exponentials:

$$g_{1,p}(t) = a_{1,p}\, x\, exp\left(-\frac{t}{\tau_{1,p}}\right) + a_{2,p}\, x\, exp\left(-\frac{t}{\tau_{2,p}}\right) + a_{3,p}\, x\, exp\left(-\frac{t}{\tau_{3,p}}\right) \quad (2)$$

When no aggregation occurred, the ACFs of nanoparticles in human plasma could be fitted by a force fit of the sum of the individual correlation functions:

$$g_{1,m}(t) = f_p\, g_{1,p}(t) + f_{np}\, g_{1,np}(t) \quad (3)$$

The variable factors in the experiments are amplitude (f_p and f_{np}). When the nanoparticles were aggregated in human plasma, the Equation (4) was extended by adding an additional aggregate term:

$$g_{1,m}(t) = f_p\, g_{1,p}(t) + f_{np}\, g_{1,np}(t) + f_{agg}\, g_{1,agg}(t) \quad (4)$$

where f_{agg} is the amplitude weighted by intensity of the aggregates, and the unknown correlation function of the aggregates ($g_{1,agg}$ (t)) was described as:

$$g_{1,np}(t) = a_{1,agg}\, x\, exp\left(-\frac{t}{\tau_{1,agg}}\right) \quad (5)$$

Accordingly, the diffusion coefficient of the aggregates is obtained for each scattering angle (all different scattering vectors q). After extrapolation to q = 0, the average hydrodynamic radius of the aggregates ($R_{h,\,agg}$) was then be calculated from the Stokes-Einstein equation.

$$R_h = \frac{kT}{6\pi\eta_0 D_{q=0}} \quad (6)$$

where k is the Boltzmann's constant (k = 1.38 × 10−23 JK−1), T is temperature, and η_0 is the kinematic viscosity of the medium.

Protein Corona Preparation. Protein corona experiments were performed as previously described from our group[67, 102, 175]. A constant amount of nanoparticles was chosen in order to ensure reproducibility. Therefore, 1 mg of each nanoparticle was incubated in 1 mL of human citrate plasma for 1 h either at 25 or 37 °C under constant agitation (300 rpm). Afterward, nanoparticles were centrifuged (20 000 g; 1 h; 25/37 °C) and resuspended in 1 mL PBS. For the removal of unbound and loosely bound proteins, the nanoparticles were washed 3 times with PBS. Hard corona proteins were detached from the particles using 2% (w/v) SDS and 62.5 mm Tris*HCl at 95 °C for 5 min. The protein containing supernatant was collected after centrifugation (20 000 g; 1 h; 25/37 °C) and used for protein quantification, SDS-PAGE and LC-MS analysis.

Protein Quantification. The protein concentration was determined by the Pierce 660 nm protein Assay (Thermo Scientific) according to the manufacturer's instructions. The adsorption was measured at 660 nm with a Tecan Infinite M1000 plate reader using bovine serum albumin as standard.

Sodium Dodecyl Sulfate-PAGE. The protein separation with SDS PAGE was performed using a NuPAGE 10% BisTris Gel, SeeBlue Plus2 Pre-Stained Standard (Invitrogen) as a marker, and NuPAGE MES SDS as running buffer. An absolute amount of 2 µg in 26 µL hard corona proteins were mixed with 4 µL NuPage Reducing Agent and 10 µL NuPage LDS Sample Buffer. The samples were loaded onto the gel and ran for 1.25 h at 100 V. Gels were stained with the Pierce Silver Stain Kit according to the manufacturer's manual (all materials from Thermo Fisher Scientific)

In Solution Digestion. The proteomic analysis was performed as previously described from our group[67, 102]. Prior to digestion, SDS was removed from the protein solution using the Pierce Detergent Removal Spin Columns (Thermo Fisher Scientific). Afterward, the protein precipitation was performed via the ProteoExtract protein precipitation kit (CalBioChem) according to the manufacturer's manual. Proteins were isolated by centrifugation (14 000 g; 10 min) and resuspended with RapiGest SF (Waters) in ammonium bicarbonate (50 mm) buffer. The reduction of the proteins was performed using dithiothreitol (Sigma-Aldrich) (5 mm) for 45 min at 56 °C followed by alkylation with iodacetoamide (Sigma-Aldrich) (15 mm) for 1 h at rt in the dark. A protein: trypsin ratio of 50: 1 was used for tryptic digestion (18 h; 37 °C) and stopped by lowering the pH with 2 µL hydrochloric acid (Sigma-Aldrich). Degradation products of RapiGest SF were removed by centrifugation (14 000 g; 15 min; 4 °C).

Liquid Chromatography Mass Spectrometry Analysis. For absolute protein quantification, samples were diluted with 0.1% formic acid and spiked with 50 fmol/µL Hi3 E. coli (Waters). The peptide solution was applied to a nanoACQUITY UPLC system coupled to a Synapt G2-Si mass spectrometer. The electrospray ionization (ESI) was operated in positive mode with a NanoLockSpray source. A sample flow rate of 0.3 µL/min was used and the reference Glu-Fibrinopeptide (150 fmol/µL) at a flow rate of 0.5 µL/min was injected into the system. Synapt G2-Si was operated in resolution mode performing data-independent acquisition (MSE) experiments. Data analysis was performed with MassLynx 4.1. Proteins were identified using Progenesis QI (2.0) and a reviewed human database downloaded from Uniprot. Noise reduction thresholds were set for low energy, high energy, and peptide intensity to 120, 25, and 750 counts. For the protein and peptide identification, the following parameters were used: Maximum protein mass 600 kDa, one missed cleavage, fixed carbamidomethyl modification for cystein, variable oxidation for methionine and false discovery rate of 4% for proteins. For the protein identification, at least two assigned peptides and five assigned fragments are required. The peptide identification needs three assigned fragments. The TOP3/Hi3 approach provided the amount of each protein in fmol[112].

Cell Culture. RAW 264.7 cells and Human cervix carcinoma cells (HeLa) were cultured in Dulbecco's modified eagle medium (DMEM) supplemented with 10% FBS, 100 U/mL penicillin, 100 mg/mL streptomycin, and 2 mm glutamine. Cells were grown in a humidified incubator at 37 °C and 5% CO_2. The cell passaging and harvesting was performed using 0.25% Trypsin-EDTA for 5 min at 37 °C, 5% CO_2 (all reagents from Thermo Fisher Scientific). The cell viability and count were determined by using trypan blue and measuring by an automated cell counter (TC10, Bio-Rad, Germany).

Flow Cytometry. The nanoparticle uptake and cytotoxicity experiments were performed by flow cytometry. Therefore, HeLa and RAW 264.7 cells were seeded at a density of 150 000 cells per well in 24 well plates (Greiner) and incubated over night at 37 °C and 5% CO2. Prior to the uptake experiment, DMEM was removed and cells were incubated for 1 h in DMEM without FBS. Nanoparticles were incubated for 1 h for the protein corona formation. The cell incubation with the nanoparticles (75 µg/mL) was performed for 4 h at 37 °C and 5% CO2 in DMEM without FBS. Afterward, cells were washed with PBS and detached from the cell culture plate using 0.25% Trypsin-EDTA. The viability staining was performed using Zombie Aqua (Biolegend) according to the manufacturer's manual. For the flow cytometry measurement cells were suspended in 1 mL PBS and 10 000 events recorded on Attune NxT Flow Cytometer. The BODIPY signal of nanoparticles was detected using the BL1 channel with an excitation laser of 488 nm and a 530/30 nm band pass filter and Zombie Aqua signal using VL2 channel with an excitation laser of 405 nm and a 512/25 nm band pass filter for emission. Data analysis was performed with Attune NxT Software selecting a cell population using a FSC/SSC scatter plot and excluding cell debris. Events were analyzed as percentage of gated events/cells and as median fluorescent intensity.

Confocal Laser Scanning Microscopy. In order to verify the intracellular localization of nanoparticles, the cLSM experiment was conducted using a Leica Laser Scanning Confocal Microscope (LSM SP5 STED Leica, Germany) equipped with a multi-laser combination and five detectors (range of 400–800 nm). Nanoparticles were detected using the 514 nm laser detecting at 530–600 nm. The cell membrane was stained shortly before measurement using 1:1000 dilution CellMask DeepRed (5 mg/mL ThermoFisher Scientific), excited with the 633 nm laser and detected at 655–755 nm. Images were taken using LAS AF 3000 software and processed using Image J. For the confocal analysis, cells were seeded at a density of 50 000 cells per well in 8-well ibidi dishes and incubated overnight. The cell incubation with nanoparticles was performed in the same manner as in the flow cytometry experiment.

Analytical Tools. ^{1}H-NMR spectra were recorded on a Bruker Avance 250 spectrometer. Chemical shifts are denoted in ppm. Mass spectra were recorded with an Advion Expression L spectrometer. UV-vis and fluorescence spectra were recorded at room temperature on a Duetta absorbance and fluorescence spectrometer (Horiba). Fluorescence quantum yields were determined by the relative method using Lumogen Red (BASF) as reference[186]. The average size and the size distribution of the nanoparticles were measured by DLS at 25 and 37 °C using a Malvern Zetasizer Nano S90 (Malvern Instruments, UK) with a scattering angle of 90°. The samples were diluted with water to a concentration of ≈0.3 mg/mL. The zeta potential of the nanoparticles was measured with a Zeta Sizer Nano Series (Malvern Instruments, UK) at 25 °C. The nanoparticles were diluted with a 1 mm potassium chloride aqueous solution to a concentration of ≈ 0.5 mg/mL. The residual concentration of SDS in the dispersions was determined by using Stains-All assay[187]. The Stains-All was dissolved in isopropanol:water (1:1 v:v) at a concentration of 1 mg/mL. Thereafter, the Stains-All solution was mixed with 1 mL formamide and 18 mL water to prepare a working solution. A working solution without Stains-All was also prepared as a control. 1 µL of NPs dispersion was added to 200 µL working solution (or control solution). The absorbance was recorded at 438 nm by a Tecan INFINITE M1000 (Tecan Group Ltd., Switzerland). The measurements were performed in triplicate. The concentration of SDS (mg/L) was determined using a calibration curve for SDS prepared in the range of 0–721 mg/L water.

3.4 Results and discussion

PS-PNIPAM core-shell nanoparticles displaying a controlled PNIPAM shell thickness were prepared in order to impart the nanoparticles surface with a variable degree of hydrophilicity. Indeed, hydrophilicity has been shown to strongly affect the protein adsorption and hence, the composition and amount of protein corona[63, 67, 76, 188]. The PS-PNIPAM nanoparticles were synthesized in two steps. First, core nanoparticles were synthesized by copolymerizing styrene with 5 mol% NIPAM to provide a chemical compatibility and lower the interfacial energy between the core's polymer and the outer PNIPAM shell[189]. The anionic surfactant sodium dodecyl sulfate (SDS) was used in the first step to stabilize the droplets of styrene in water by reducing the interfacial tension between styrene and the continuous phase of the emulsion. In a second step, the PNIPAM shell was formed around the core particle by free-radical polymerization of NIPAM with 2.6 mol% of the crosslinker N,N'-methylenebis(acrylamide). The amount of NIPAM in the second step was varied (Table 3.6.1) to obtain core-shell nanoparticles with different PNIPAM-shell thickness.

The content of PNIPAM in the nanoparticles was quantified by solid-state 13C NMR spectroscopy. The resonance of -CH3 of NIPAM unit (δ = 22 ppm) was compared with the signal of the aromatic carbon atom (of styrene unit) next to the methanetriyl unit at δ = 146 ppm (Figure 3.4.1,Figure 3.6.1). The measured ratio between NIPAM and styrene units in the nanoparticles increased from 0.04 to 0.15 as their feed ratio increased from 0.05 to 0.20 (Table 3.4.1). The corresponding thickness of the PNIPAM shell, calculated from the amount of NIPAM units determined by 13C NMR spectroscopy and the density of PNIPAM (ρ = 1.10 g/mL), increased from $\approx$ 1.2 to 2.0 nm (Figure 3.4.1b)[189].

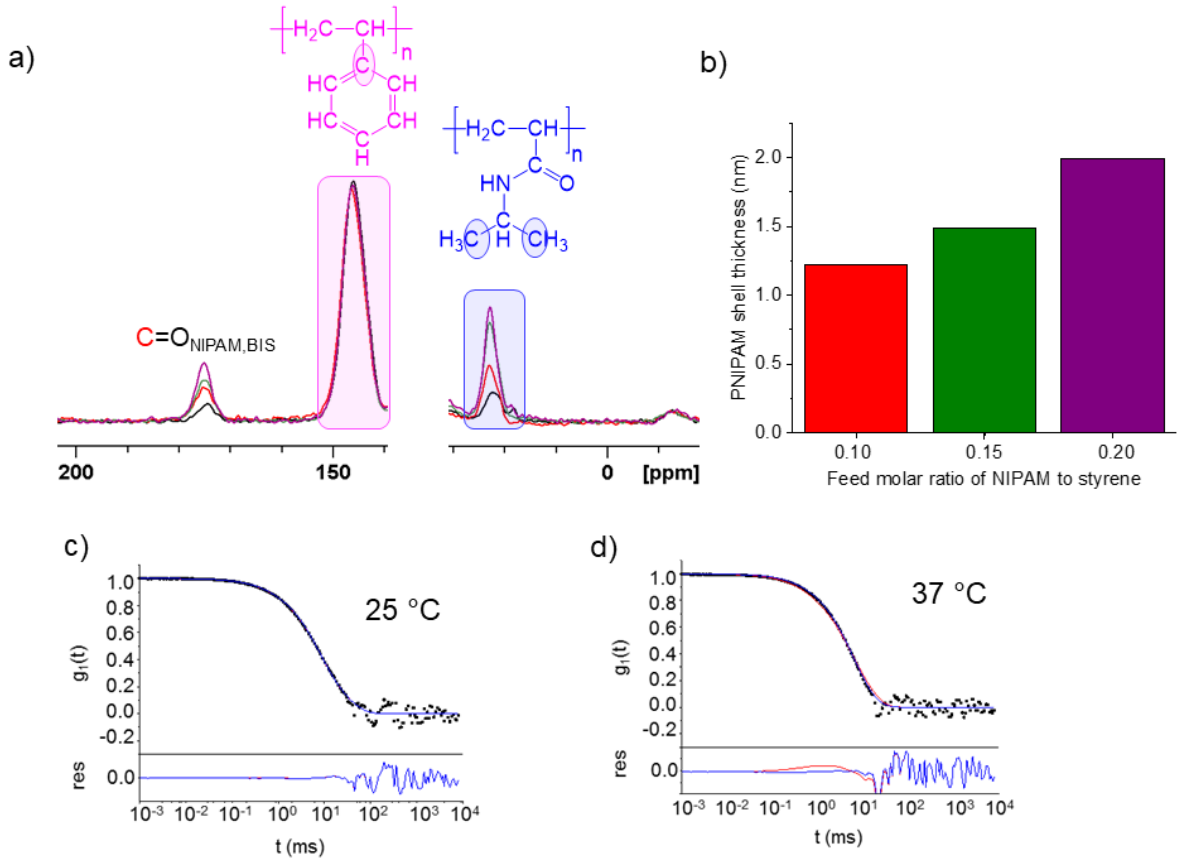

Figure 3.4.1. Characterization of the core-shell PS-PNIPAM nanoparticles with different PNIPAM shell thickness. a) Solid-state 13C CP-MAS NMR spectra for determining the molar ratio of NIPAM to styrene in the nanoparticles by comparing the resonance of -CH3 of NIPAM unit (δ = 22 ppm) with the signals attributed to the aromatic carbon atom next to the methanetriyl unit (δ = 146 ppm); PS-P0.05 (black), PS-P0.10 (red), PS-P0.15 (green), and PS-P0.20 (purple). b) Evolution of PNIPAM shell thickness against feed molar ratios of NIPAM to styrene. Intensity autocorrelation functions (ACFs) of sample PS-P0.10 in human plasma at c) 25 °C and d) 37 °C measured by multi-angle light scattering with a scattering angle of 30°. Upper graphs: ACFs of PS-P0.10 in human plasma, including data points (•), forced fit of ACFs of PS-P0.10 and proteins (red curve), and fit with additional aggregate function (blue curve). Lower graphs: Corresponding residuals resulting from the difference between data and the two fits.

Table 3.4.1. Feed molar ratios of NIPAM to styrene (nNIPAM/nstyrene), molar ratios of NIPAM units to styrene units in the nanoparticles measured by solid-state 13C-NMR spectroscopy (nNIPAM units/nstyrene units), hydrodynamic diameter (D_h) and polydispersity index (PDI) of nanoparticles at 25 and 37 °C in water, and ζ-potential of nanoparticles at 25 °C in 1 mM KCl.

Entry	$n_{NIPAM}/n_{styrene}$ (mol)	$n_{NIPAM\ units}/n_{styrene\ units}$ (mol)	D_h (PDI) (nm) 25 °C	D_h (PDI) (nm) 37 °C	ζ-potential (mV)
PS-P0.05	0.05	0.04	97 (0.10)	100 (0.09)	-46 ±1
PS-P0.10	0.10	0.10	102 (0.02)	102 (0.01)	-41 ± 1
PS-P0.15	0.15	0.14	98 (0.08)	99 (0.01)	-40 ± 1
PS-P0.20	0.20	0.15	104 (0.05)	103 (0.02)	-30 ± 2

Because the PNIPAM shell thickness was small, the nanoparticles did not show any significant change of average hydrodynamic diameter (D_h) upon temperature change (Table 3.4.1). Hence, the shell thickness was limited so that the average diameter of nanoparticles at various temperatures remains approximately the same, and therefore, the available surface area for protein adsorption stays constant.

Because the presence of surfactant strongly affects the protein binding on nanoparticles[190], the nanoparticles were extensively purified. The concentration of the remaining surfactant measured by the Stains-All assay was very low (≈ 0.1–0.2 molecules per nm^2, Table 3.6.1), so that the influence of surfactant on the protein corona is minimized.

The stability of nanoparticles in protein solutions is a prerequisite for investigating the protein adsorption. Indeed, the aggregation of nanoparticles can influence the protein adsorption profiles (e.g. amount and composition)[191]. We measured the stability of PS-PNIPAM nanoparticles in human plasma by multi-angle light scattering. The VPTT of PNIPAM in solution was found to be unaffected by the presence of human serum albumin[192], the most abundant protein in human plasma. Therefore, we assumed that the transition temperature of the PNIPAM shell would also not be altered during incubation in human plasma. The stability of nanoparticles in human plasma was evaluated based on a differential analysis of the autocorrelation functions (ACFs) obtained from multiangle light scattering experiments performed at 25 and 37 °C (Figure 3.4.1 c,d) according to the procedure described by Rausch et al[185]. First, the ACFs for pure human plasma and nanoparticles dispersion in water were determined separately. Thereafter, mixtures of nanoparticles dispersion and human plasma were evaluated with a forced fit (red line) - a sum of the individual ACFs of nanoparticles and proteins. In case that the forced fit was not sufficient to describe the measured data of the NP-protein mixture, a third aggregate term was added to the fit, shown by the blue curve. An overlapping of these two fits (blue and red curves) indicated that no aggregation occurred in the dispersion. PS-PNIPAM nanoparticles were stable in human plasma at 25 and 37 °C (Figure 3.4.1 c,d, Figure 3.6.2). Only for PS-P0.20, significant aggregation with aggregate sizes between 500 and 1000 nm was observed when incubated with human plasma at 37 °C. However, the size of aggregates should have no influence on cellular uptake.

In order to investigate the temperature-dependent formation of the protein corona, PS-PNIPAM nanoparticles were incubated in human plasma at either 25 or 37 °C for 1 h to allow the formation of a protein corona (Figure 3.4.2). To allow for comparable protein corona determination, the amounts of nanoparticles were fixed to 1 mg/mL plasma. Temperatures of 25 and 37 °C, the first below and the latter above VPTT, were selected to investigate the influence of hydrophobicity of PS-PNIPAM nanoparticles on protein adsorption. Moreover, protein denaturation does not occur at these temperatures. Proteins were quantified by the Pierce assay before being analyzed by liquid chromatography mass spectrometry (LC-MS). The incubation of nanoparticles at 37 °C resulted in an increased amount of total adsorbed protein in comparison to the incubation at 25 °C (Figure 3.6.3). Protein adsorption is known to increase with increasing surface hydrophobicity[63, 188]. The reduction of

the protein adsorption below the VPTT is the first indication that the temperature change and the surface hydrophilicity change provided a stealth behavior to the nanoparticles.

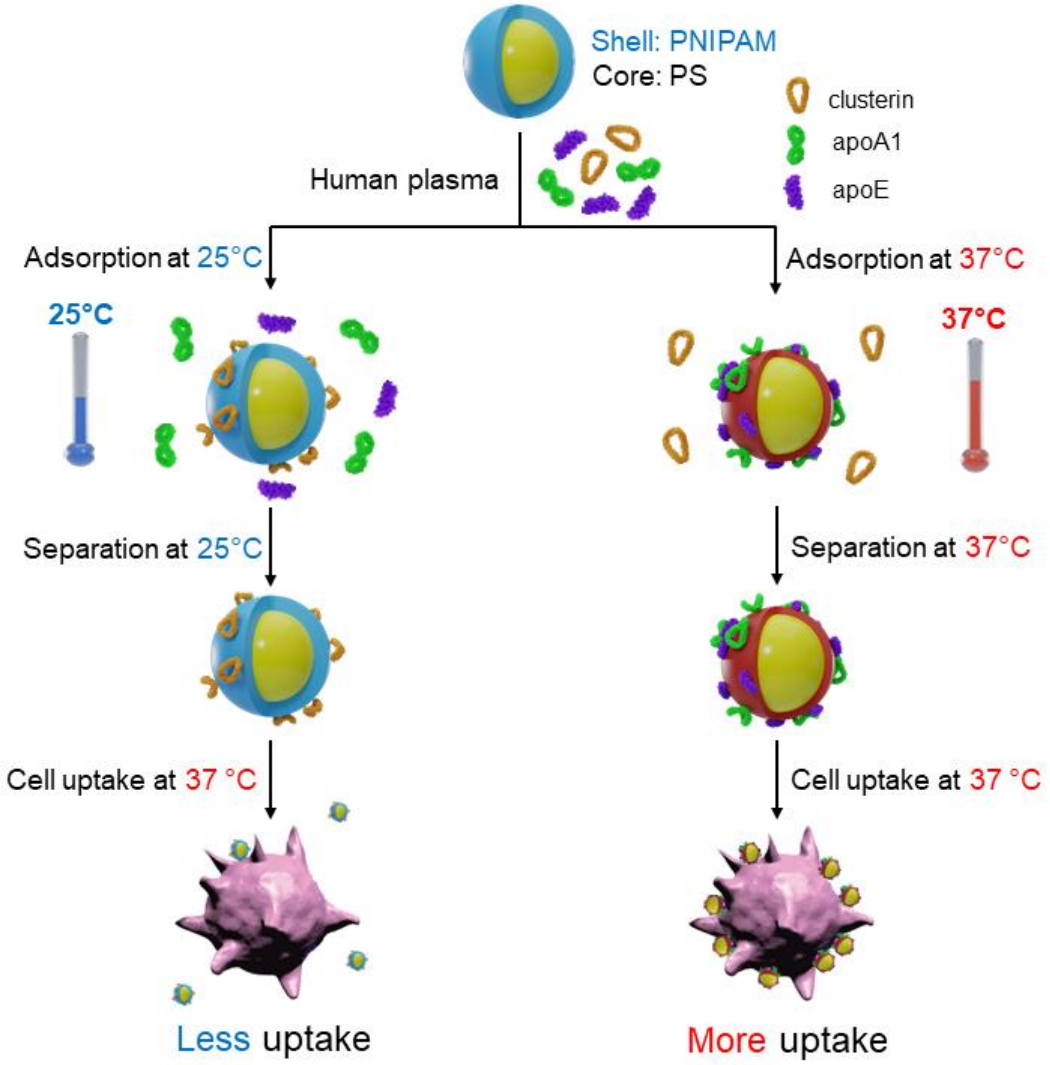

Figure 3.4.2. The catching of apolipoproteins (apolipoprotein J/clusterin, or apolipoprotein A1 and apolipoprotein E) from human plasma by temperature-responsive PS-PNIPAM nanoparticles. Apolipoprotein J is obtained in large amounts after incubating the nanoparticles in human plasma at 25 °C (T < VPTT) while apolipoprotein A1 and apolipoprotein E are adsorbed when incubating the nanoparticles in human plasma at 37 °C.

The most abundant hard corona proteins and the protein composition at 25 and 37 °C were determined by LC-MS (Figure 3.4.3). A list of identified proteins and their relative amounts is available in the corresponding publication. At 25 °C, below the VPTT, the PS-PNIPAM nanoparticles were enriched with Apo J (≈ 40% of the hard protein corona). On the contrary, the surface of PS-PNIPAM nanoparticles were enriched with apolipoprotein E and apolipoprotein A1 at 37 °C (above the VPTT). In line with previous reports[63, 188], it can be shown that changing the surface hydrophilicity influences the composition of protein corona on nanocarriers. The protein corona of nanocarriers coated with a hydrophilic polymers such as PEG were enriched with Apo J and other apolipoproteins[177]. However, coating with a hydrophobic polymer led to an enrichment with fibrinogen and immunoglobulins[67].

Herein, PNIPAM has the advantage to provide different hydrophobicity while keeping the same chemical structure. The protein corona on the surface of the nanoparticles was dependent on the PNIPAM shell thickness. No temperature dependence of Apo J binding was observed for the PS-P0.05 (very low concentration of PNIPAM) whereas the difference in enrichment of Apo J on PS-P0.20 (highest concentration of PNIPAM) was more than 40% (Figure 3.4.3b). The same trend was observed for Apo E. Indeed, with an increasing PNIPAM shell thickness the difference in Apo E enrichment at the hydrophobic state also increased, with the highest difference of ≈ 26% for PS-P0.20 (Figure 3.4.3c). However, a different effect in Apo A1 binding was observed (Figure 3.4.3d). Indeed, the amount of Apo A1 was the largest on the PS-P0.05 nanoparticles. With increasing PNIPAM concentration, the amount of Apo A1 in the protein corona decreased.

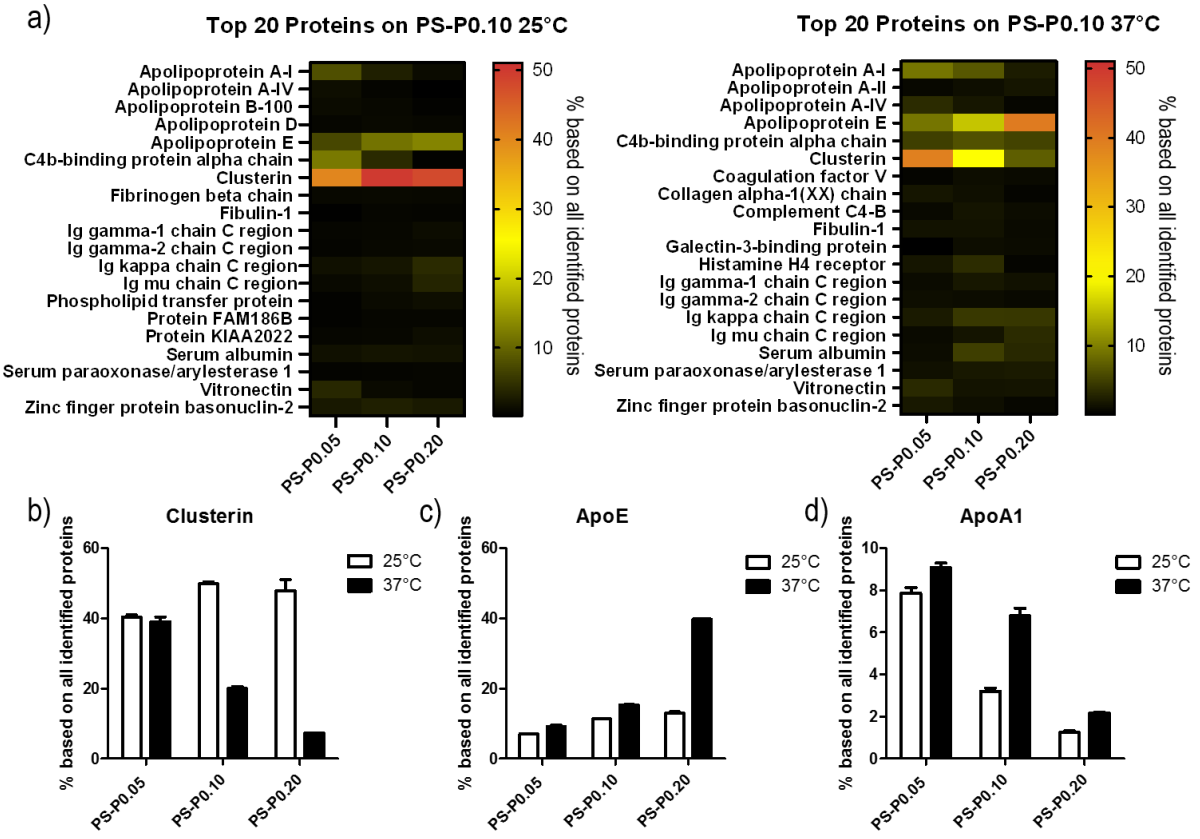

Figure 3.4.3. Proteomic analysis of protein corona on the surface of PS-PNIPAM nanoparticles. a) Heatmap displaying the most abundant hard corona proteins on nanoparticles either at 25 °C or at 37 °C identified by LC-MS. b) Relative amount of Apo J (clusterin) on the surface, which is enriched on the hydrophilic surface at 25 °C. c,d) Apolipoprotein E and A1 are enriched at the hydrophobic state of nanoparticles at 37 °C. A detailed list of all identified proteins is supplemented in an excel sheet. All values are displayed as mean ± SD (n = 3).

The reason why some proteins preferentially attach at certain temperatures remains unclear. A possible explanation is the stability of the 3D structure at different temperatures. Serum/plasma proteins tend to have hydrophilic amino acids on the outside of their structure and hydrophobic amino acids on the inside. Therefore, the probability to unfold depending on temperature should play a major role on adsorption at different temperatures. As for the proteins of interest here (ApoA1, ApoE and

ApoJ/Clusterin), no experimentally determined 3D structures were available so that it is difficult to predict in which location of the protein structure such an unfolding would occur. This is clearly a challenging but crucial task to be investigated in further research.

Furthermore, we determined whether a protein corona formed at a given temperature can be altered by a second incubation at another temperature (below and above the VPTT of PNIPAM), as it may occur during cell culture incubation. The dispersions that were previously incubated at 25 °C were centrifuged at 25 °C, re-dispersed in PBS at room temperature, and incubated in PBS at 37 °C for 24 h. Similarly, the dispersions that were previously incubated at 37 °C were centrifuged at 37 °C, re-dispersed in PBS at room temperature, and incubated in PBS at 25 °C for 24 h. The Pierce assay revealed that the trend about the difference between total concentration of adsorbed proteins at the two different temperatures was conserved even after the second incubation at another temperature. Indeed, the total protein amount bound on the nanoparticles subjected to a second incubation was larger when the nanoparticles were first incubated at 37 °C in comparison to when the nanoparticles were first incubated at 25 °C (Figure 3.6.3). After the second incubation, the amount of protein was slightly reduced compared with the amount detected after the first incubation. We attributed this slight loss to the additional purification step. After the desorption and digestion of the proteins in the protein corona, the protein composition was analyzed by liquid chromatography and mass spectrometry. As shown in Figure 3.6.4, the composition of the protein corona before and after the second incubation was not significantly different. Therefore, preferential desorption of Apo A1, Apo E, and Apo J was not observed, confirming that they are tightly bound to the nanoparticles, hence conferring stealth properties even after a change of temperature of the external media.

The adsorption of apolipoproteins, especially the adsorption of Apo J, is known to induce a prolongation of blood circulation time of nanoparticles and to reduce their unspecific uptake by immune cells such as macrophages[75]. Therefore, we investigated the cellular uptake of the PS-PNIPAM nanoparticles into RAW264.7 macrophages by flow cytometry and confocal laser scanning microscopy (cLSM). In order to analyze the effect of the temperature dependence on the protein corona composition, the nanoparticles were incubated at 25 or 37 °C in human plasma prior to cell uptake. Flow cytometry measurements showed a reduced uptake of nanoparticles incubated in human plasma compared with non-incubated nanoparticles, independently from the incubation temperature (Figure 3.4.4, Figure 3.6.5). This is consistent with previous literature showing a reduced uptake of nanoparticles after their incubation with plasma or serum[67, 168]. PS-P0.10 and PS-P0.20 nanoparticles incubated at 25 °C, which adsorbed the largest amount of Apo J, showed the lowest uptake into both RAW264.7 macrophages as well as into HeLa cells. For PS-P0.05 the Apo J amount in the protein corona at 25 and 37 °C was nearly the same, leading into no difference of uptake into cells. Interestingly, PS-P0.20 incubated at 37 °C showed a relatively low amount of Apo A1 and a high amount of Apo E in the protein corona. For these nanoparticles incubated at 37 °C, the difference of uptake between incubated and non-incubated nanoparticles was not as large as for the PS-P0.10 nanoparticles. This nanoparticle displayed the thickest

PNIPAM shell and showed the lowest total protein amount on the surface. This shows hence that the reduced amounts of total proteins were not responsible for the stealth behavior. The stealth effect was mainly induced by specific apolipoproteins, namely Apo J (clusterin) and Apo A1. Conversely, the enrichment of the protein corona with Apo E led to an increased uptake (Figure 3.6.5a).

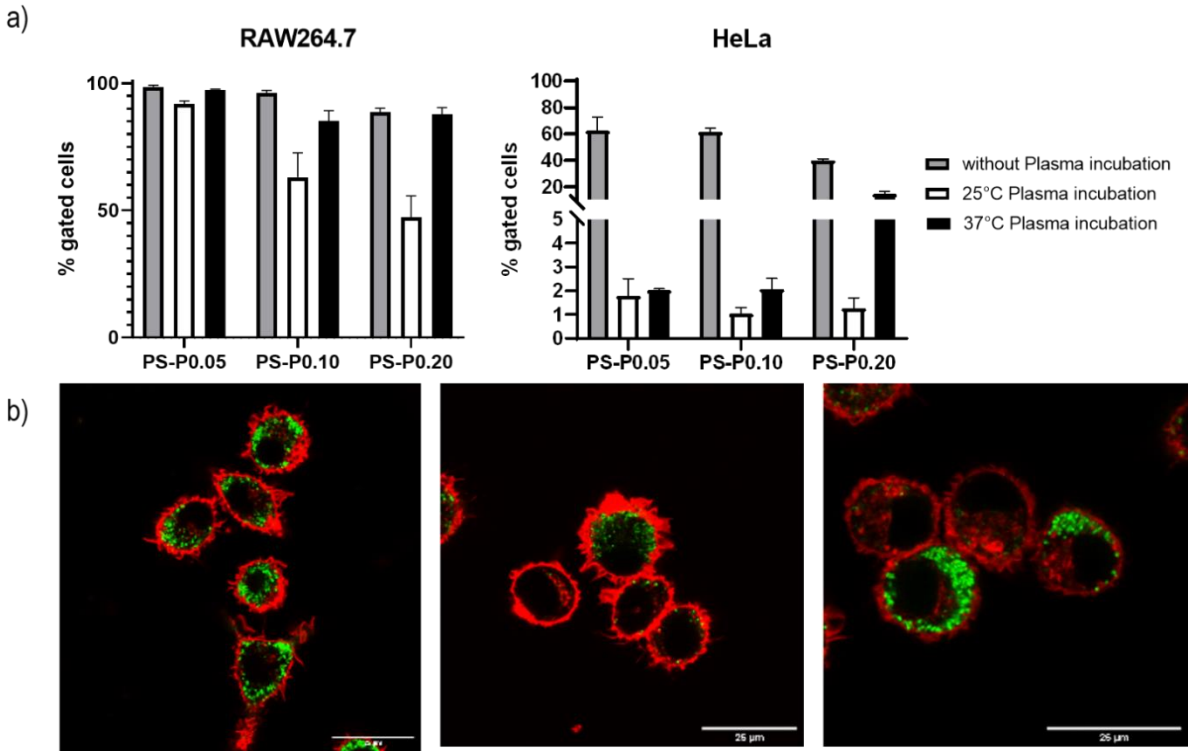

Figure 3.4.4. Cellular uptake of PS-PNIPAM nanoparticles without and after the incubation in plasma at 25 and 37 °C. a) Flow cytometry analysis of cells labelled with PS-PNIPAM nanoparticles after 4 h. Values are expressed as mean ± SD. b) Confocal laser scanning microscopy images of RAW264.7 cells incubated with PS-P0.10 nanoparticles. Left picture without plasma incubation, middle with plasma incubation at 25 °C, and right with incubation in plasma at 37 °C. The cell membrane was stained with Cellmask Deep Red and is pseudocolored in red. Nanoparticles are pseudocolored in green. Scale bars: 25 µm.

The cLSM confirmed the internalization of the nanoparticles into the cells (Figure 3.4.4b, Figure 3.6.5c). Without plasma incubation, the nanoparticles were strongly internalized. However, with Apo J and Apo A1 on their surface, the uptake was reduced. Cell viability was measured by flow cytometry using Zombie Aqua staining (Figure 3.6.5b). Independently from the incubation temperature, all nanoparticles showed no toxicity on both cell lines. In addition, the high uptake of nanoparticles without plasma incubation did not show any influence on the viability of the cells.

3.5 Conclusion

We demonstrated that the stealth behavior of temperature-responsive nanoparticles can be controlled by adjusting the incubation temperature in human plasma, resulting in a change of composition of the protein corona. The protein corona was enriched with the stealth protein apolipoprotein J (clusterin) when incubating the nanoparticles in human plasma at 25 °C, that is, at a temperature below the VPTT of the nanoparticles. Besides, the protein corona was enriched with apolipoproteins A1 and E after incubation at 37 °C (T > VPTT). Among the prepared nanoparticles, a thickness of 1.2 nm PNIPAM was optimal for adsorbing the largest amount of Apo J at 25 °C. Furthermore, the uptake of nanoparticles after incubating in human plasma at 25 °C by RAW264.7 and HeLa cells was significantly lower than with native nanoparticles. Ultimately, we presented a novel method to prepare stealth nanoparticles by simply incubating temperature-responsive nanoparticles in human plasma at 25 °C. It is hence a suitable method for imparting stealth properties to nanocarriers for drug delivery applications.

3.6 Supporting information

Table 3.6.1. Feed molar ratio and weighted amounts of styrene, NIPAM, KPS, and BIS, and residual SDS concentration of the dialyzed samples.

Entry	Feed molar ratio				Mass (g)				SDS	
	styrene	NIPAM	KPS	BIS	styrene	NIPAM	KPS	BIS	Molecules /nm^2	Molecules /NP
PS-P0.05	1	0.05	0.004	0	30	1.63	0.3	0	0.12 ± 0.04	3,635 ± 1,221
PS-P0.10	1	0.10	0.0026	0.0015	1.28	0.14	0.005	0.005	0.16 ± 0.02	5,069 ± 519
PS-P0.15	1	0.15	0.0039	0.0023	1.28	0.21	0.007	0.008	0.18 ± 0.05	5,506 ± 1,650
PS-P0.20	1	0.20	0.0052	0.0030	1.28	0.28	0.010	0.010	0.18 ± 0.03	5,950 ± 946

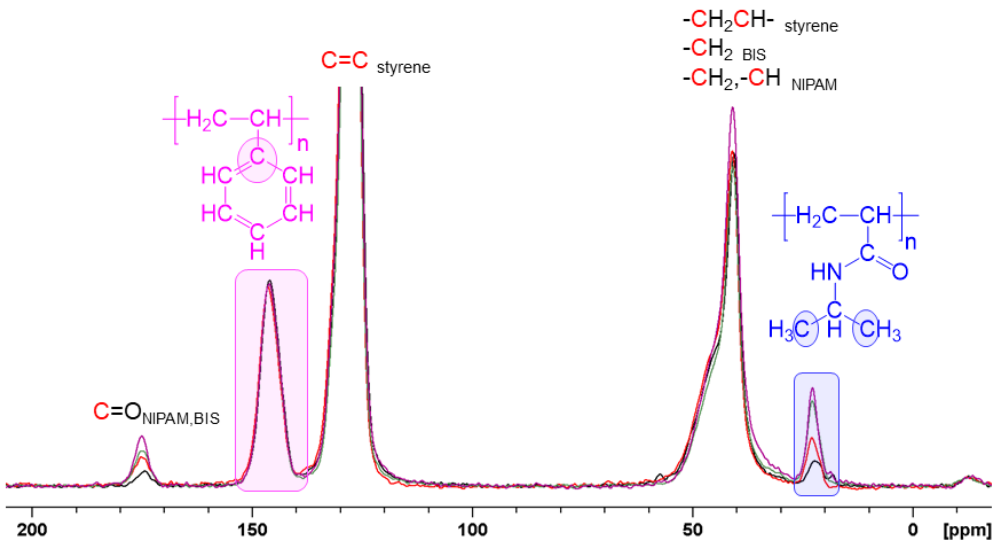

Figure 3.6.1. Solid state ^{13}C NMR spectra of the core-shell PS-PNIPAM nanoparticles with different PNIPAM shell thickness. The molar ratio of NIPAM to styrene unit in the nanoparticles were determined by comparing the resonance of -CH_3 of NIPAM unit (δ = 22 ppm) with the signals assigned to the quaternary aromatic carbon atom (δ = 146 ppm) next to the methanetriyl unit; PS-P0.05 (black), PS-P0.10 (red), PS-P0.15 (green), and PS-P0.20 (purple).

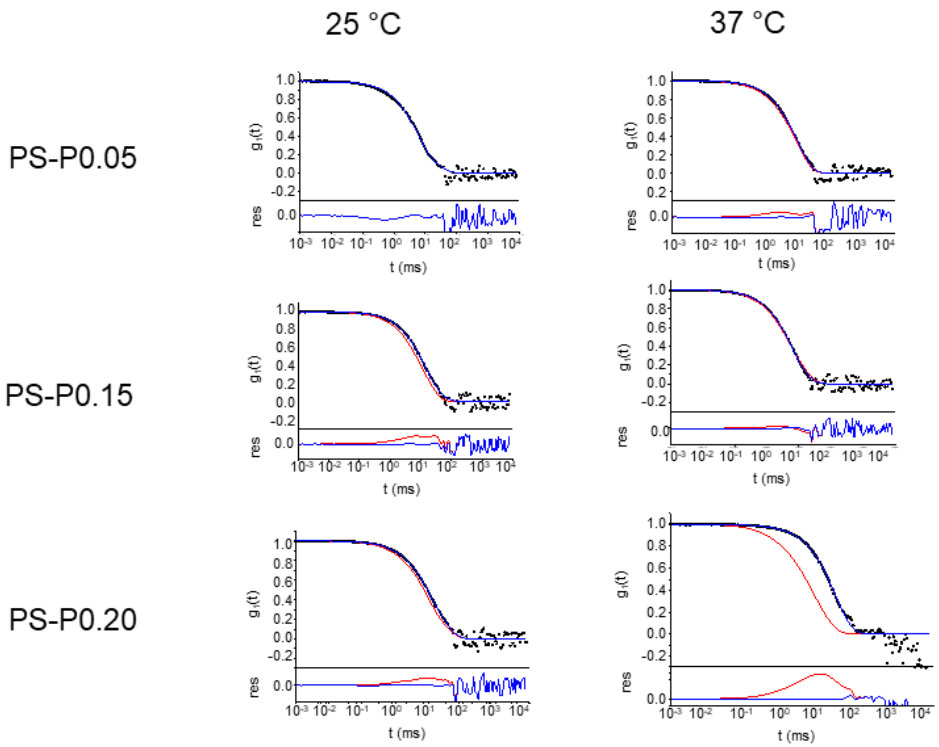

Figure 3.6.2. Intensity autocorrelation functions (ACFs) of PS-P0.05, PS-P0.15, and PS-P0.20 in human plasma at the scattering angle of 30° at 25 and 37 °C. Upper graphs: ACFs of PS-P0.05, PS-P0.15, and PS-P0.20 in human plasma including data points (•), forced fit of ACFs of nanoparticles and proteins (red curve), and fit with additional aggregate function (blue curve). Lower graphs: corresponding residuals resulting from the difference between data and the two fits.

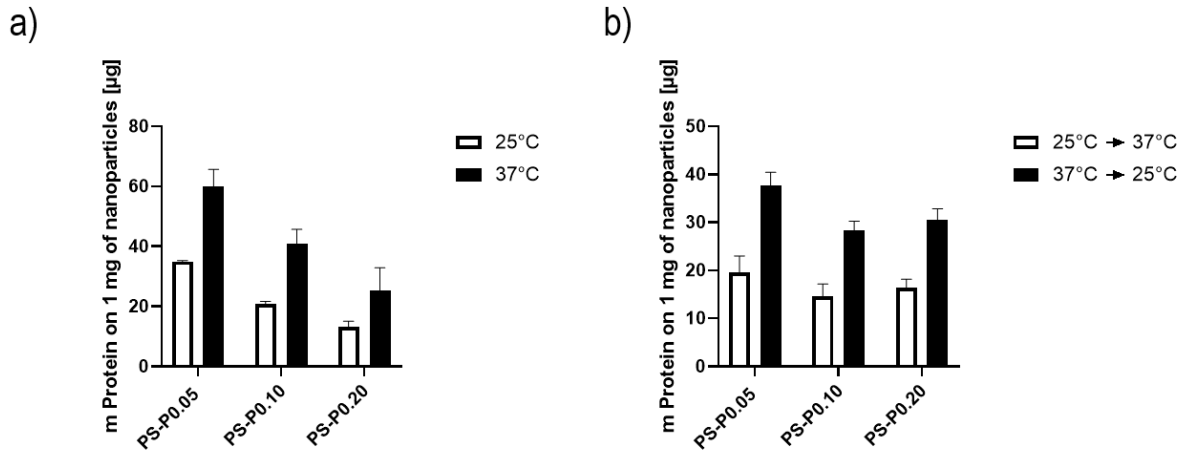

Figure 3.6.3. Absolute amount of corona proteins on PS-PNIPAM nanoparticles determined by Pierce Assay. All values are displayed as mean ± SD (n=2). b) Absolute amount of corona proteins after first incubation in human plasma and a second incubation in PBS where the temperature has either been increased from 25 °C to 37 °C or decreased from 37 °C to 25 °C. All values are displayed as mean ± SD (n = 2).

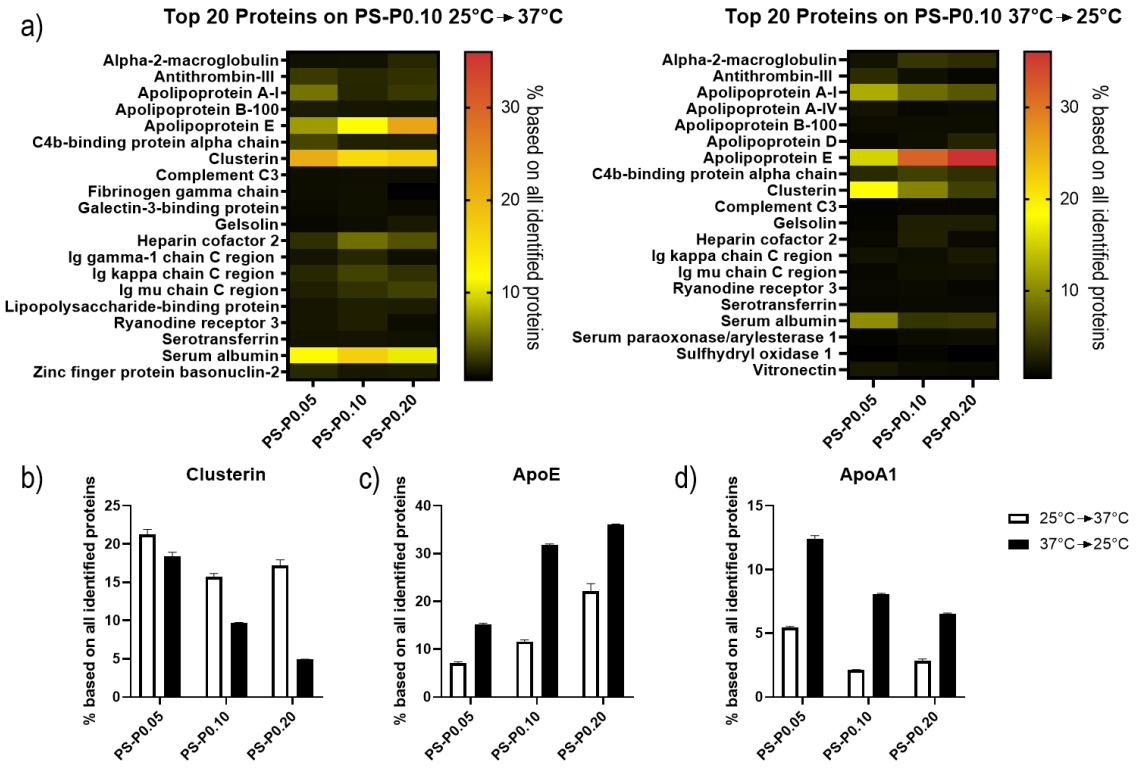

Figure 3.6.4. Proteomic analysis of protein corona on the surface of PS-PNIPAM nanoparticles after a first incubation in human plasma and a second incubation in PBS where the temperature has either been increased from 25 °C to 37 °C or decreased from 37 °C to 25 °C (a) Heatmap displaying the most abundant hard corona proteins on nanoparticles at 25 °C or at 37 °C identified by LC-MS. (b) Relative amount of apolipoprotein J (clusterin) on the surface, which is not desorbed by changing the temperature from 25 to 37 °C. (c)-(d) The protein corona is enriched with apolipoprotein E and A1 after incubation of nanoparticles at 37 °C and cooling to 25 °C. A detailed list of all identified proteins is given as a supplementary excel sheet. All values are displayed as mean ± SD (n = 3).

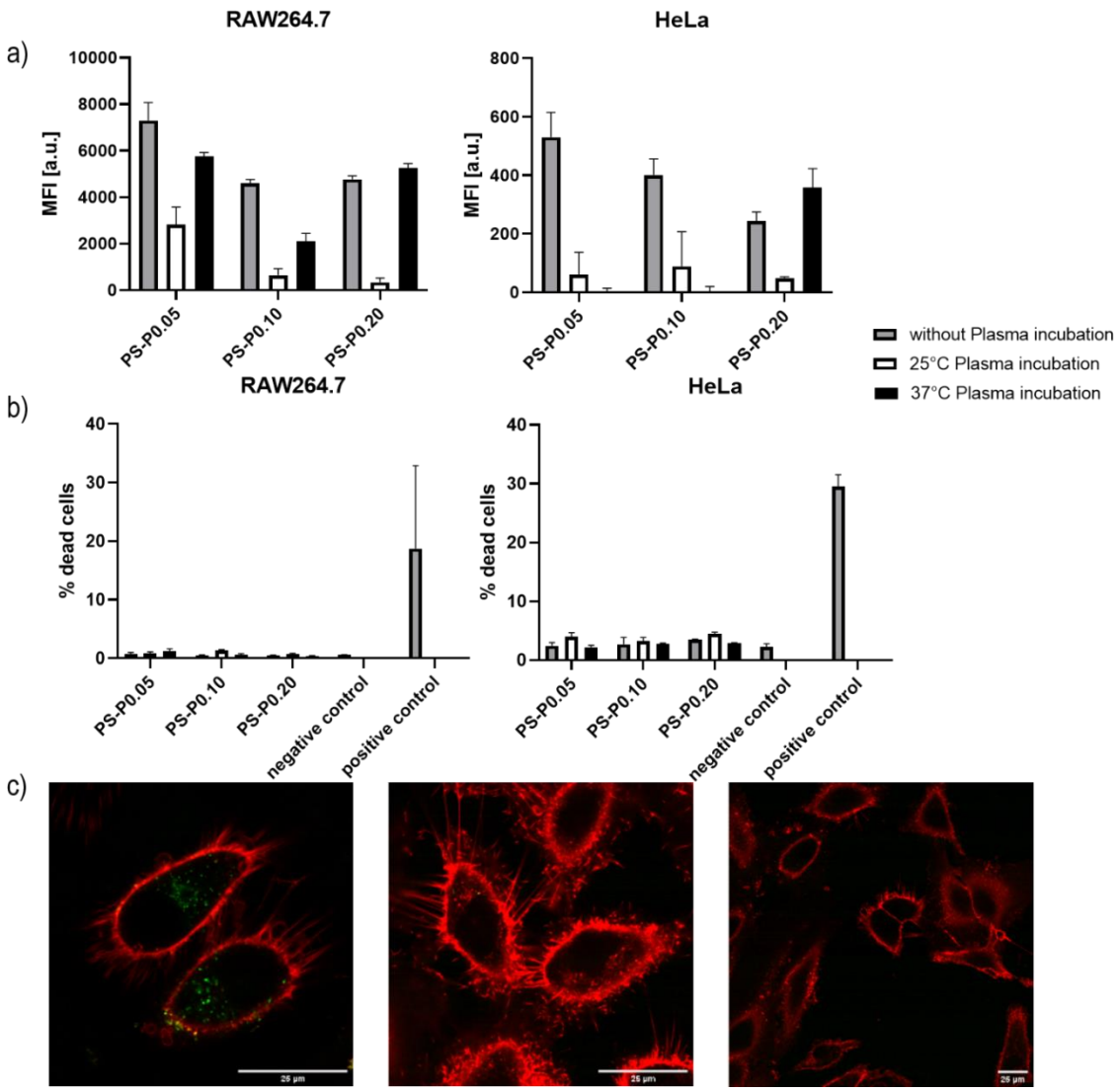

Figure 3.6.5. Cellular uptake of PS-PNIPAM nanoparticles without and with plasma incubation at 25 °C and 37 °C. a) Cell uptake of PS-PNIPAM nanoparticles displayed as median fluorescence intensity (MFI) of Cy5 positive cells analyzed by flow cytometry. Values are expressed as mean ± SD (n=3). b) The cell viability shown as % dead cells measured by flow cytometry using a Zombie Aqua™ staining. Values are expressed as mean ± SD (n=2). c) Confocal laser scanning microscopy images of HeLa cells incubated with PS-P0.10 nanoparticles. Left picture without plasma incubation, middle with plasma incubation at 25 °C and right with plasma incubation at 37 °C. Cell membrane was stained with Cellmask Deep Red and is pseudocolored in red. Nanoparticles are pseudocolored in green. Scale bars: 25 µm.

Chapter B – The exocytosis of nanoparticles from cells

The second chapter of this dissertation is divided into three subchapters. The fourth subchapter offers an introduction to the theoretical background of the topic and the methods used. The fifth subchapter presents the fourth publication **[4]** where the exocytosis rate of gold nanoparticles is investigated. The results and the text were published in a peer-reviewed journal (Cells) and the subchapter represents an almost identical word-to-word reproduction of the published paper. The sixth subchapter provides an insight into the determination of exocytosis pathways of magnetic dextran nanoparticles by LC-MS proteomics. The data shown in this subchapter represent unpublished results that can possibly be used for publication in the future.

[4] **Jennifer Oberländer**, XXX, XXX, XXX, XXX, XXX, XXX, XXX, XXX, XXX. Higher Loading of Gold Nanoparticles in PAD Mesenchymal-like Stromal Cells Leads to a Decreased Exocytosis. *Cells*, **2022**, 11 (15), 2323.

4. Theoretical Background

Nanotechnology offers a wide range of new possibilities for the diagnosis and treatment of different diseases[11]. With the use of different approaches, nanomedicine makes it even possible to combine diagnosis and therapy within the same NPs[193]. Through these so-called "theranostics" it is possible to follow the *in vivo* biodistribution and drug delivery of the NPs with a non-invasive approach[17, 193]. However, clinical useful imaging applications are limited and research to develop new nanomedicines for imaging is ongoing[193].

4.1 Nanotechnology for imaging

The imaging of NPs administered *in vivo* is highly useful to better understand the biodistribution and properties of the NPs[193]. However, NPs have to be developed which can be imaged by clinically used imaging methods. Thereby commonly targeted imaging systems for NPs are magnetic resonance imaging (MRI), computed tomography (CT), positron emission tomography (PET), and single photon emission tomography (SPECT)[194]. For example, MRI makes use of the proton spin of different elements when an external magnetic field is applied[194]. To enhance the contrast for MRI, superparamagnetic iron oxide nanoparticles (SPIONs) have shown promising results[195]. Thereby, a magnetic iron oxide core serves for the imaging contrast and a surface decoration with different targeting molecules for the addressing to the specific sites of interest[196-198]. On the other hand, CT imaging makes use of the X-ray attenuation of the tissue and gold NPs have shown to be promising imaging tools for it[199]. Gold NPs have been used for the labelling of tumor cells or red blood cells[200, 201]. Moreover, gold nanoclusters encapsulated in liposomes have been functionalized with Her2 antibody for the detection of breast cancer[202]. NPs thereby help to overcome non-specific distribution and fast metabolism of traditional contrast agents due to their targeting possibilities[194]. Besides the imaging of specific tissues, it is also possible to apply a functional targeting and a functional imaging e.g. by targeting specific integrins as biomarkers for angiogenesis[203].

So that NPs can serve as imaging reagents, they need to reach and accumulate at the site of interest. Therefore, two ways of targeting can be used, the passive and the active targeting[204]. Passive targeting makes use of the enhanced permeability and retention effect (EPR effect)[205]. NPs tend to specifically accumulate in tumor tissues due to the higher permeability of their blood vessels and their lack of a lymphatic drainage[205, 206]. However, to make use of this effect, NPs need to have a long circulation time in the human blood plasma since no active transport to the site of interest is involved[194]. On the opposite, for active targeting, the surface of the NPs is loaded with ligands that specifically can bind to receptors at the targeted tissue[207]. As ligands e.g. antibodies, peptides, saccharides, nucleic acids, or aptamers can be used[205]. This targeting strategy allows besides the imaging of a tumor also the imaging of other tissues. However, after the achievement of a targeting, in the next step, the NPs must also be taken up and remain in the corresponding cells.

4.2 Uptake and Exocytosis of nanoparticles

The uptake of NPs into the cells is an important step to achieve their diagnostic or therapeutic goals[158]. The uptake mechanisms of NPs into cells are well investigated[158, 208, 209]. The uptake of NPs is mainly driven through endocytosis pathways since the NPs are not able to diffuse through the cell membrane[210, 211]. Endocytosis is an energy-dependent process by which usually biomolecules enter the cells[212]. Thereby the NPs are engulfed into membrane invaginations forming an endocytic vesicle which is then transported intracellular[158, 213]. The main endocytosis mechanisms are phagocytosis, clathrin-mediated endocytosis, caveolin-mediated endocytosis, clathrin/caveolin-independent endocytosis, and macropinocytosis[158, 208, 209]. While phagocytosis is mainly limited to phagocytic cells, the other mechanisms, which are also grouped to the term pinocytosis, can take place in almost all other cell types[214].

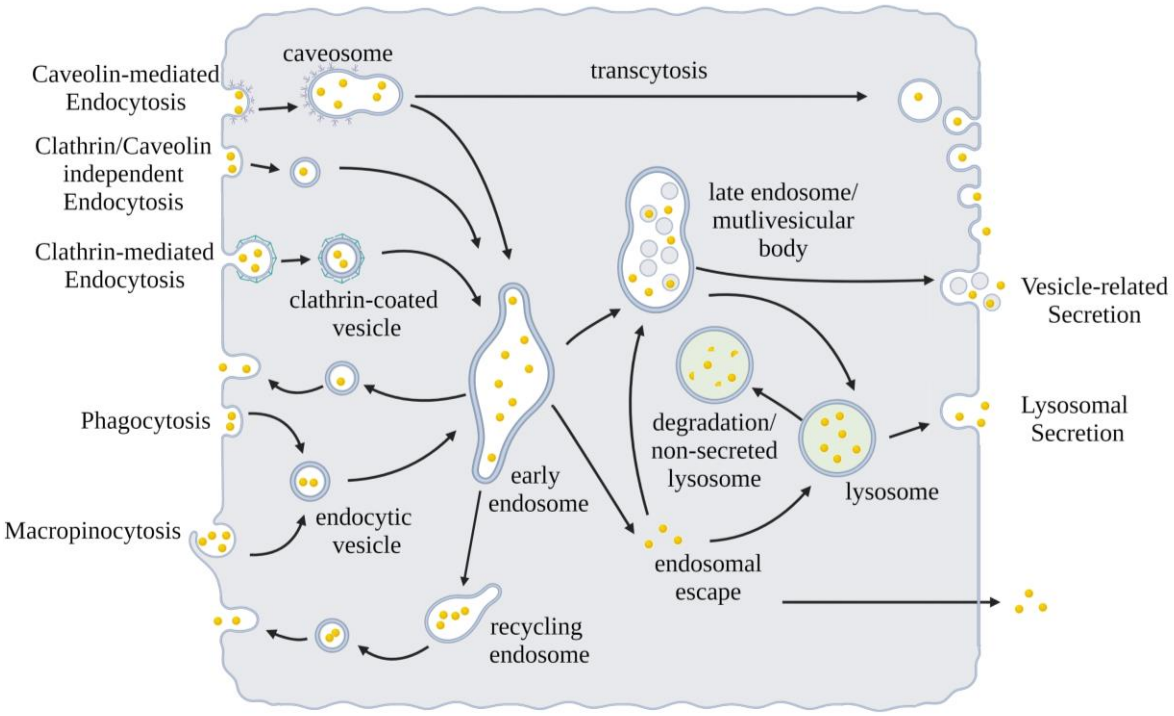

Figure 4.2.1. Scheme of the main endocytosis and exocytosis pathways of nanoparticles (NPs) from cells. NPs are taken up into the cells *via* five different pathways: caveolin-mediated endocytosis, clathrin/caveolin-independent endocytosis, clathrin-mediated endocytosis, phagocytosis, and macropinocytosis. After the uptake the NPs are transported through vesicles to the early endosome. From the early endosome the NPs can either be directly or indirectly recycled back to the plasma membrane or can get further internalized to the late endosome. From the late endosomes they can be directly secreted *via* the vesicle-related secretion or the late endosomes fuses with lysosomes whose contents are then released during lysosomal secretion. An alternative exocytosis pathway is the transcytosis after uptake into a caveosome by caveolin-mediated endocytosis. Figure created with BioRender.com.

The phagocytosis uptake mechanism is mainly used by phagocytes e.g. macrophages, dendritic cells, and monocytes and is used to take up larger NPs with sizes above 250 nm[215]. Since these phagocytes are cells belonging to the immune system and immune response, the phagocytosis of NPs can be increased by opsonins in the protein corona such as immunoglobulins or complement proteins due to

receptor recognition[216-218]. During clathrin-mediated endocytosis, specific molecules like nutrients and plasma membrane components can be taken up into the cells[219, 220]. The mechanism can either occur as a receptor specific uptake due to receptor binding or as a receptor-independent uptake due to hydrophobic or electrostatic interactions[158, 221]. After receptor binding, the complex out of receptor and NPs moves to a clathrin-rich region of the plasma membrane where the NPs get engulfed by clathrin-coated vesicles. These vesicles fuse intracellular with early endosomes and get further internalized[222, 223]. The caveolin-dependent endocytosis is mainly involved in cell signaling, transcytosis, and the regulation of membrane proteins and lipids[214, 224, 225]. Caveolin-dependent endocytosis includes flask-shaped invaginations of the plasma membrane driven by the membrane protein caveolin-1[225, 226]. Thereby caveosomes are formed which can avoid lysosomes and trigger transcytosis. Therefore, this pathway is often targeted for nanomedicines[208, 221, 227]. For cells without clathrin or caveolin in the cell membrane, uptake takes place via clathrin/caveolin-independent endocytosis. Thereby, growth hormones, extracellular fluids or folic acid are taken up into the cells and this pathway can be specifically addressed by conjugating these molecules onto NPs[158, 208]. The last common pathway for the uptake of NPs is the macropinocytosis. Thereby usually large vesicles in micron scale are formed to take up high volumes of extracellular fluids. Through these pathways, bigger NPs can be taken up independently from specific receptor binding[158].

After the uptake, the NPs are further transported in the cells by endosomes which determine the diagnostic or therapeutic efficiency of the NPs. Endosomes can be classified into early endosomes, late endosomes, and recycling endosomes[228]. After the detachment of the endocytic vesicles from the plasma membrane, the vesicles fuse with early endosomes which are dictating the intracellular pathways of the cargo[228, 229]. These early endosomes mature then into late endosomes. However, parts of their cargo can be recycled to the plasma membrane by fusing with recycling endosomes[230]. The late endosomes can either fuse with the cell membrane and release their cargo or they can fuse with lysosomes forming endolysosomes. When late endosomes fuse with lysosomes, the cargo and the NPs get exposed to hydrolytic enzymes and the NPs can get degraded[211]. Furthermore, late endosomes can continue to mature to become multi-vesicular bodies (MVB). Fusion of MVBs with the cell membrane lead to the exosome-associated NP release[211, 228, 229, 231].

Besides the pathway through endosomal stages, NPs can also escape from the endosomes at any stage which leads to their release into the cytoplasm. Thus, lysosomal degradation can be bypassed and the NPs can end up in the cytoplasm or other intracellular compartments[232, 233]. However, during autophagy cytoplasmic content is delivered to lysosomes for degradation and thus NPs can also end up in lysosomes despite their escape from the endosomal process[234, 235]. Besides the uptake pathway, also physicochemical properties, cell type, and the protein corona can influence the intracellular trafficking of the NPs[236, 237]. The presence of a protein corona and its influence as well as the influence of the protein source of the protein corona may affect the intracellular pathway of NPs and therefore need to be better addressed in the future[158].

At several stages of the intracellular processing, the NPs can get released from the cells. NPs can be recycled back to the cell membrane directly after entering the early endosomes. NPs that remain in the endosomes will be transported to late endosomes and lysosomes[238]. Lysosomal secretion has been reported to be the main exocytosis pathway for mesoporous silica NPs[239]. However, for gold NPs it has been shown that they can be secreted by unconventional secretion with exosomes[240]. Depending on the uptake mechanism different endocytosis pathways can be involved. In general, entering a fast exocytosis pathway as reported for recycling endosomes, means a fast secretion of the NPs while entering a long pathway as escape from endosomes or transport to lysosomes, means a slow exocytosis or persistence in the cells[238]. However, in most reports, only the exocytosis rate has been investigated and only a small share has investigated the exocytosis pathways[238].

4.3 Protein corona in determination of intracellular fate

Currently, the most used way to detect the intracellular localization and the intracellular pathway of NPs are microscopic methods. With increasingly sophisticated microscopes with very high resolutions, many intracellular interactions can be visualized[158]. However, protein adsorption on NPs can trigger specific uptake and intracellular mechanisms determining the fate and exocytosis rate of NPs. These proteins cannot easily be imaged by microscopic methods and therefore proteomic approaches have been developed in order to analyze the proteomic fingerprint and the intracellular fate of NPs[241]. This method takes advantage of the fact that the protein corona is a dynamic process and due to a constant change of the protein environment intracellular, the protein corona composition changes as well, depending on the intracellular fate of the NPs[242]. Indeed with a proteomic approach it could be shown that iron oxide NPs entered the cells via a macropinocytotic-like pathway and were guided through an endolysosomal pathway to lysosomes[243]. In another study, it was reported that gold NPs were taken up mainly through a clathrin-mediated endocytotic mechanism leading as well to the endolysosomal pathway[242]. In both publications, a final retention of NPs in lysosomes was suspected and in case of the gold NPs only negligible exocytosis could be observed. However, that NPs get released from cells is known for various NPs[238] but only minor attention was put onto that in this publication. In general, the uptake mechanisms have been very well analyzed. There is more and more awareness for the intracellular pathways, but the exocytosis and release of nanoparticles have been rather neglected until now.

4.4 ICP-OES for cell uptake and exocytosis analysis

Inductively coupled plasma optical emission spectrometry (ICP-OES) has become an important method for elemental analysis and is used for a wide range of applications[244, 245]. During ICP-OES a nobel gas, mostly argon, is ionized which leads to the formation of a plasma. In this so-called fourth state of matter, positively charged argon ions can move independently from the negatively charged electrons[246, 247]. In the plasma, the analyte is atomized, ionized, and excited due to the high energy of the plasma and the collision of the atoms with free electrons. After the excitation of the analyte, the excited electrons fall back to an energetically lower orbital and thereby emit electromagnetic radiation with specific wavelengths that can be used for the quantification of the analyte[244]. Due to its high capability to analyze a broad range of analytes in a short time, it became an important elemental analysis method and was thus also used for the analysis of cells and nanoparticles.

Calcium was one of the first elements determined in different cell samples by the use of elemental analysis and ICP-OES[248]. However, at this time sensitivity of the ICP-OES systems was too low to quantify other elements like Na, K, or Mg[249]. Then, in 2000, Prohaska et al. reported the use of ICP-OES for the analysis of multi trace elements (Ca, Mg, Fe, Cu, and Zn) in blood plasma, erythrocytes, and lymphocytes[250]. Haraguchi introduced the use of the term metallomics, in accordance with the terms proteomics and genomics, for the elemental analysis of biological systems[251]. Afterwards, several studies focused on the use of ICP-OES for the determination of the uptake of metals into cells or the intracellular metal concentration[252-254]. Liu et al. quantified the uptake of gold NPs in cells by ICP-OES in 2007[255]. Since then, ICP-OES became one of the main analytical tools for the analysis of NPs cell uptake and release[238, 256, 257]. For example, in 2012 Yanes et al. analyzed the intracellular and extracellular silicon amount with ICP-OES to determine the exocytosis of silica nanoparticles from human adenocarcinomic cells[239]. Compared to fluorescent microscopy and flow cytometry, ICP OES offers the advantage of being independent from fluorescent dyes. Fluorescent labeling of NPs can change their surface properties or the fluorescent labels can be detached from the NPs due to the enzymatic activity in the cells[238]. However, ICP-OES cannot differentiate between different cell types or intracellular compartments. In addition, only inorganic NPs can be determined and not NPs which consist of materials that occur naturally in cells[238]. Therefore, often combinations of elemental analysis by ICP-OES and imaging methods such as transmission electron microscopy or combinations with fluorescence based methods are used[239, 240, 258-260].

Overall exocytosis of NPs from cells is poorly understood but an important factor influencing the effectiveness of NPs. With the elemental analysis by ICP-OES and proteomic analysis by LC-MS it is possible to quantify and analyze uptake and exocytosis pathways of NPs from cells. To increase the efficacy of NPs in the future and to enable a better transition from synthetically engineered NPs to nanomedicines and theranostics, the exocytosis of NPs needs to be better investigated.

5. Higher Loading of Gold Nanoparticles in PAD Mesenchymal-like Stromal Cells Leads to a Decreased Exocytosis

Copyright:

[4] **Jennifer Oberländer**, XXX, XXX, XXX, XXX, XXX, XXX, XXX, XXX, XXX. Higher Loading of Gold Nanoparticles in PAD Mesenchymal-like Stromal Cells Leads to a Decreased Exocytosis. *Cells*, **2022**, 11 (15), 2323.

Aim:

Labelling of cells for different applications e.g. for the imaging of cells after transplantation, has received increasing attention in the last years. Hereby, nanoparticles have emerged as one possibility for the loading of the cells. Nevertheless, in order to serve as a contrast reagent for imaging applications, the particles must remain stable in the cells and must not be secreted after a short time. In here, we analyzed the exocytosis behavior of glucose-PEG-coated gold nanoparticles from human mesenchymal-like stromal cells in order to achieve a high and stable labelling of the cells. This will help to better visualize the remaining cells and their function after they have been injected into a body.

Contribution:

I performed the ICP-OES measurements for uptake and exocytosis, Zeta-potential measurements, nanoparticle uptake preparation for TEM with the low loading protocol, protein quantification, SDS PAGE, and protein digestion. XXX and XXX performed the viability measurements, cell loading efficiency experiments, and the TEM experiments for the high loading protocol. XXX prepared the protein corona for intracellular trafficking and analyzed the protein corona dataXXX, XXX, and XXX prepared the nanoparticles. XXX and XXX manufactured the cells. DLS measurements have been performed by XXX and TEM imaging for low loading protocol by XXX. XXX performed the graphical design. The manuscript was written by me and proofread by XXX, XXX, XXX, XXX, and XXX. The project was supervised by XXX, XXX, XXX, and XXX.

5.1 Abstract

Cell therapy is an important new method in medicine and is being used for the treatment of an increasing number of diseases. The challenge here is the precise tracking of cells in the body and their visualization. One method to visualize cells more easily with current methods is their labeling with nanoparticles before injection. However, for a safe and sufficient cell labeling, the nanoparticles need to remain in the cell and not be exocytosed. Here, we test a glucose-PEG-coated gold nanoparticle for the use of such a cell labeling. To this end, we investigated the nanoparticle exocytosis behavior from PLX-PAD cells, a cell type currently in clinical trials as a potential therapeutic agent. We showed that the amount of exocytosed gold from the cells was influenced by the uptake time and loading amount. This observation will facilitate the safe labeling of cells with nanoparticles in the future and contribute to stem cell therapy research.

5.2 Introduction

The idea of using cells as a therapeutic agent for various diseases has widely expanded over the past years[261]. However, the therapeutic mechanisms and the distribution of the cells in the organism often remain unclear. As methods for tracking cells in the human body are very limited, imaging and contrast agents like nanoparticles have been developed to increase the visibility of the cells in vivo[3, 262, 263]. To date, cell tracking is often performed using either radionuclides for scintigraphy, PET (positron emission tomography), and SPECT (single photon emission computer tomography), or using superparamagnetic iron oxide nanoparticles for MRI (magnetic resonance imaging)[199, 264, 265]. Radionuclide imaging has the main advantage of high sensitivity and very small amounts of label can be detected. However, radionuclides with short half-lives make this method very expensive and make long-term tracking impossible[265]. On the other hand, MRI does not use ionizing radiation and tissue can be well visualized. Nevertheless, this method is also relatively cost-intensive and the acquisition time is slow[199, 265]. Therefore, there is increasing effort to develop cell tracking markers for CT (computed tomography). These have the benefit that the technology is cost-effective with a fast temporal resolution[199]. Thereby, gold nanoparticles or gold-iron nanoparticles have proven to be very promising tracking tools. Gold features strong contrast properties for CT imaging and, in combination with iron for MRI, a wide range of analysis methods can be covered when combining both materials[263]. Furthermore, gold nanoparticles are already very well studied materials of low toxicity to cells, making them even more promising as a contrast agent for cell therapy labeling[266-268]. However, for good CT tracking, a high amount of gold nanoparticles need to be taken up by the cells and, for long-term tracking, the nanoparticles need to remain stable in the cells[269]. While high loading of cells could previously be achieved, the reduction of the exocytosis of gold nanoparticles from cells still remains a challenge[269-271].

One type of cell that is currently considered as a potential therapeutic agent against different diseases is the PLX-PAD cell[272-282]. PLX-PAD cells are a cell therapy product under development containing placental expanded (PLX) placenta-derived mesenchymal-like adherent stromal cells[274, 279, 283]. It has previously been shown that these cells secrete relevant factors as a response to muscle trauma or inflammation to trigger the natural repair mechanisms of the body[274]. Therefore, these cells are currently used in different clinical studies for the treatment of injured muscle.

For a combination of particles and cells to be effective as a therapeutic and imaging reagent, the particles must remain stable in the cells. One factor that can influence the uptake in cells is the so-called protein corona. Furthermore, surface modifications and the size and shape of the particles, among other things, can affect the uptake and exocytosis rate of particles[238, 260, 284]. When nanoparticles come into contact with biological fluids, proteins directly attach to the surface of the particles and form a protein corona. Previously, it has been shown that the protein corona can alter the uptake of particles into cells, but it can also influence the exocytosis rate of particles from cells[75, 238]. To use the nanoparticles as a reliable imaging reagent, it is crucial to keep the exocytosis rate as low as possible to allow long-term tracking

of the cells. Besides influencing the uptake into cells, changes in the protein corona composition can also be used to learn about the intracellular pathway followed by the nanoparticles. The type of proteins bound in the corona, therefore, reflects a fingerprint of the intracellular pathway taken by the nanoparticles[242, 243]. This intracellular protein corona can be used to predict whether particles are more likely to be exocytosed or to remain inside the cell.

In this study, we analyzed the exocytosis rate of glucose-coated and PEGylated gold nanoparticles from loaded PLX-PAD cells. As the combination of cells and particles should be used in the future for long-term tracking of cells in the human body, it is important to reach a high loading efficiency together with a low exocytosis rate of the GNPs from the cells. Here, we tested two different in vitro loading protocols, one with a lower loading efficiency and another with a higher loading efficiency of GNPs. Afterwards, we analyzed the amount of exocytosed gold and characterized the intracellular protein corona to predict which protocol reached a more stable loading of nanoparticles in the cells.

5.3 Materials and Methods

Synthesis of GNPs. PEGylated and glucose coated gold nanoparticles (GNPs) were synthesized according to previously described methods in a three-step process[263]. The nanoparticles were synthesized by heating $HAuCl_4$ solution (50%; 82.345 mL) in ultrapure water (39.78 L) until boiling. Then sodium citrate solution (10%; 803.556 mL) was introduced and the solution was stirred for 10 min at 1200 rpm. Particles were purified and concentrated via cross-flow filtrations with a 10 kDa PES membrane to a final volume of 1193.4 mL. In a second step PEG (PEG7, 50 mg/mL, 198.9 mL) was added and together with the particles stirred for 30 min at 1200 rpm followed by an incubation at 4 °C for 24 h. Purification was again performed via cross-flow filtration reaching a final volume of 688.5 mL. In the third step, the glucose was attached to the nanoparticles. Therefore, the PEGylated particles were stirred together with 1-Ethyl-3-(3-dimethylaminopropyl)carbodiimid (EDC; 0.2M; 68.85 mL) and N-hydroxysuccinimide (NHS; 0.2M; 344.25 mL) for 30 min at 1200 rpm. Then, the active ester from PEG can react in an amidation reaction with the NH_2 groups of the glucosamine (24 mg/mL; 688.5 mL). After the addition of the glucosamine, the solution was stirred again for 30 min at 1200 rpm and then incubated at 4 °C for 24 h. Final purification was again performed by cross flow filtration and particles were filtrated through a 0.22 µm filter.

Characterization of GNPs. After the synthesis, the gold concentration of the nanoparticles was determined by ICP-OES or ICP-MS. The size of the particles was determined via multi-angle DLS and TEM[285]. For multi-angle DLS an ALV spectrometer consisting of a goniometer and an ALV-5004 multiple-tau full digital correlator (320 channels) was used. This allows measurements over an angular range from 30° to 150°. A He-Ne laser (wavelength of 632.8 nm) was used as the light source. Temperature was adjusted through a thermostat from Julabo. Before the measurement, the GNPs were filtrated through a 0.2 µm filter so that no larger particles or dust interfered with the measurement. TEM images were taken with a Jeol JEM 1400 at 120 kV to determine the primary size. For the drop casting, undiluted GNPs were added on a 300 mash copper grid coated with a 20-30 nm carbon layer. Excess sample dispersion was blotted with a filter paper[285]. The size was determined using Image J software and counting 100 particles. The gold concentration was determined *via* ICP-OES (SpectroGreen, Spectro/Ametek). 10 µL GNPs were diluted in 1 mL aqua regia (3:1 hydrochloric acid: nitric acid) for digestion of nanoparticles. Afterwards, the samples were diluted up to 10 mL with MilliQ water, and the gold concentration was determined with ICP-OES. The calibration curve was prepared by using 0.1, 0.5, 1, 5, and 20 ppm gold standard solution (stock 1000 mg/L Au TraceCERT®, Sigma Aldrich).

Production and Cell Culture of PLX-PAD Cells. PLX-PAD cells were produced by Pluristem Therapeutics, Ltd. (Haifa, Israel) as previously described [272, 283]. Production of PLX PAD cells was performed in a state-of-the-art clean room facility according to GMP regulations. Human placentas were

collected from healthy donors and cut into pieces. After enzymatic digestion of the tissue, cells were seeded as 2D cultures in a culture flask followed by 3D cultivation in a bioreactor. Before characterization of the cells, 3D cultures were harvested and cryopreserved in liquid nitrogen. Characterization was performed by staining the cells with MSC-positive and MSC-negative markers and analyzed by flow cytometry[279].

Cell culture. PLX-PAD cells were cultured in Dulbecco's modified eagle medium (DMEM) supplemented with 10% FBS, 100 U/mL penicillin, 100 mg/ml streptomycin, and 2 mM glutamine. Viability and count were measured with trypan blue by an automated cell counter (TC10, Bio-Rad). Cells were grown in a humidified incubator at 37 °C and 5% CO_2. Cells were either thawed one day before the experiment and seeded at the recommended density for the experiments or cultured in flasks and sub-cultured once a week when they reached around 80% confluence.

Uptake and Exocytosis. Two different protocols for the uptake of GNPs were tested. For both protocols, the PLX-PAD cells were seeded at a density of 500,000 cells per well in a six-well plate (Greiner, Pleidelsheim, Germany) and incubated overnight. All incubation steps were performed in a humidified incubator (37 °C, 5% CO_2). Afterwards, the cells were incubated with a nanoparticle solution of 300 µg/mL in isotone NaCl (B.Braun, Melsungen, Germany) for 30 min (low loading protocol) or with 300 µg/mL nanoparticles in DMEM (Thermo Fisher Scientific, Waltham, MA, USA) with 10% FBS for 24 h (high loading protocol). After the incubation time, the cells were washed twice with PBS (Thermo Fisher Scientific, Waltham, MA, USA) and then either incubated again in DMEM with 10% FBS for exocytosis measurements or harvested with Trypsin-EDTA (Thermo Fisher Scientific, Waltham, MA, USA) for uptake measurements.

The exocytosis of the GNPs was also determined using two different protocols. Either the collected DMEM was not replaced or the DMEM volume collected was replaced. When keeping the same supernatant during the entire time, the DMEM and the corresponding cells were collected after 2, 6, 24, or 48 h (without supernatant replacement). For the second protocol with supernatant replacement, the supernatant was exchanged with fresh supernatant after collecting it from the cells at the same time point as for the protocol without supernatant replacement. Here, the cells and the supernatant were harvested for analysis as well.

ICP-OES Analysis. Before the analysis of the gold content in the cells and in the supernatant, the cells were digested. Therefore, after trypsinization, cells were centrifuged (300× *g*, 5 min) and the supernatant was discarded. Afterwards, cells were diluted with 1 mL of aqua regia (3:1 hydrochloric acid/nitric acid) and incubated at room temperature overnight on an orbital shaker (300 rpm) followed by dilution with

MilliQ water to 10 mL before measurement. The cell culture supernatants for the determination of exocytosed gold content were collected from the cells and treated with aqua regia followed by incubation and dilution to 10 mL with water. The gold concentration was determined by ICP-OES (SpectroGreen, Spectro/Ametek, Kleve, Germany). The calibration curve was prepared using 0.1, 0.5, 1, 5, and 20 ppm gold standard solution (stock 1000 mg/L Au TraceCERT®, Sigma Aldrich, St. Louis, MO, USA). Untreated cells and cell culture media were used to deduct background signals. The amount of gold was calculated using the concentration resulting from the ICP OES and the volume of the sample.

ICP-MS Analysis. ICP-MS analysis was used to determine the cell loading efficiency. After incubation of PLX-PAD cells with GNPs, incubation cell culture media, washing media, and GNP exposed cells were digested in 1 mL aqua regia (3:1 hydrochloric acid/nitric acid). The obtained digestion solutions were properly diluted to be analyzed by ICP-MS (7500, Agilent, Santa Clara, CA, USA) in duplicates. The quantification was carried out by interpolation in a standard curve obtained from a commercial 1000 ppm gold standard (Inorganic Ventures, INYCOM, Zaragoza, Spain).

Cell Viability Evaluation. The viability of PLX-PAD cells exposed to GNPs was measured with the Alamar Blue™ (Thermo Fisher Scientific, Waltham, MA, USA) assay. PLX-PAD cells were seeded at a density of 10,000 cells per well in 96-well plates and grown in a humidified incubator (37 °C, 5% CO_2) for 24 h. GNPs were diluted in DMEM with FBS at different concentrations (25, 50, 100, 200, 400, 800, and 1200 µg/mL) and incubated in the incubator with the cells for 24 h. After cell exposure, the cell media was removed and wells were washed twice with PBS. Then, cells were exposed to Alamar Blue™ reagent for 1 to 3 h. After the incubation time, an aliquot of the supernatant was transferred into a new plate and the fluorescence (530/590 nm) was measured with a microplate fluorometer. The fluorescence signal of untreated cells was set as 100% and the viability was calculated as a function of this.

Nanoparticle cell uptake analysis by TEM. For the imaging of the cell uptake with the high loading protocol, PLX-PAD cells were washed with PBS after the incubation period and fixed with glutaraldehyde (2.5%) for 1 h. The cells were detached from the Petri dish by scraping and afterwards centrifuged (4 °C, 1000× *g*, 5 min) to obtain a compact pellet. Cells were harvested after the incubation time by scrapping and centrifugation. After washing the cell pellet with phosphate buffer (PB, 0.1M), the cells were stained with OsO4 (1%) for 2 h and washed again with PBS. The cells were dehydrated at 4 °C through a series of acetone concentrations (50%, 70%, 90%, 96%, and 100%), prior to being progressively (25%, 50%, 75%, and 100%) embedded in Epon resin. After resin curing (60 °C, 48 h), sections with a thickness of 50 nm were cut with an ultramicrotome and placed on Formvar carbon-

coated Cu grids. Finally, these grids were further contrasted with uranyl acetate and lead citrate. All electron micrographs were obtained with a TEM (Jeol JEM 1010 MT), operating at 80KV. Images were obtained with AnalySIS (SIS, Munster) on a Megaview III CCD camera.

To observe the internalization and exocytosis of the GNPs for the low loading protocol, the cells were seeded at a density of 50,000 cells per well in 24-well plates and incubated overnight. Before seeding, the plates were equipped with 3 mm plasma-sterilized sapphire discs (M. Wohlwend GmbH, Sennwald, Switzerland) covered with a 20 nm carbon layer. Incubation of the cells with the GNPs was performed for the exocytosis protocol without supernatant replacement to image intracellular localization of the GNPs over time. After the incubation period, the GNPs were removed, the cells were washed with PBS, and the cells were further processed for TEM imaging. After incubation with the low loading protocol, the GNPs were removed and the sapphire discs with cells were frozen under high pressure (2100 bars) with a high-pressure freezing machine (Engineering Office M. Wohlwend GmbH) for a good preservation of the cellular structures. The sapphire discs were locked in a small volume between two specimen carriers and introduced into the specimen pressure chamber with liquid nitrogen as the cooling medium. Additionally, a freeze substitution and resin embedding were added. Therefore, the cryo-fixed samples were dehydrated at -90 °C in a freeze substitution machine (EM, AFS 2, Leica Microsystems) by water substitution with an organic solvent (0.2% osmium tetroxide, 0.1% uranyl acetate, and 5% water in acetone). Afterwards, samples were rinsed in acetone at room temperature and with EPON 812 infiltrated. On the next day, polymerization was performed at 60 °C and then ultrathin sections using a Leica ultramicrotome were produced. All electron micrographs were either obtained with a Jeol JEM 1400 or with a FEI Tecnai F20 TEM at 120 kV and 200 kV respectively.

Intracellular Trafficking. For the intracellular trafficking of the GNPs, PLX-PAD cells were seeded at a density of 400,000 cells per well in six-well plates. On the next day, incubation with GNPs was carried out at a GNP concentration of 300 µg/mL for 4 and 24 h. Additionally, a pulse-chase experiment was performed where the PLX-PAD cells were incubated with the GNPs for 4 h followed by an exchange to fresh cell culture medium and a subsequent 20 h incubation. After the incubation time, cells were harvested with Trypsin-EDTA (Thermo Fisher Scientific, Waltham, MA, USA). For each condition, three wells were pooled after harvesting to reach enough intracellular GNPs. PLX-PAD cells were centrifuged (300× *g*, 5 min) and the supernatant was discarded. For cell lysis, cells were suspended in PBS with protease inhibitor (Thermo Fisher Scientific) and EDTA at 4 °C. Cell lysis was carried out through sonication (QSonica Q800R3, QSonica, Newton, CT, USA) at an amplitude of 70% and pulsation frequency of 30 s. Sonication was performed in total for 7 min at 4 °C. Cell debris and nuclei were removed by centrifugation (1000× *g*, 4 °C, 10 min) and, afterwards, the GNPs were collected by centrifugation (5000× *g*, 4 °C, 30 min). To remove unbound and loosely bound proteins, the nanoparticles were washed three times with PBS containing protease inhibitor and EDTA. Afterwards,

the hard corona proteins were detached from the nanoparticles using 2% (*w*/*v*) SDS and 62.5 mm Tris-HCl, as previously described by our group [67, 102]. Proteins and nanoparticles were separated via centrifugation (5000× *g*, 4 °C, 30 min) and protein-containing supernatant was used for protein quantification, SDS PAGE, and LC-MS analysis.

Protein Quantification and SDS-PAGE. Proteins were quantified by the Pierce 660 nm Protein Assay (Thermo Fisher Scientific) according to the manufacturer's manual. The adsorption was measured with a Tecan Infinite M1000 plate reader using bovine serum albumin (Merck, Kenilworth, NJ, USA) for a calibration curve.

After quantification, the proteins were separated with SDS-PAGE and stained by Silver Staining according to the manufacturer's recommendations. A total of 2 µg protein in 26 µL total volume was mixed with 4 µL NuPage Reducing Agent and 10 µL of NuPage LDS Sample Buffer (Thermo Fisher Scientific). The sample was loaded on a 10% Bis-Tris-Protein Gel using SeeBlue Plus2 Pre-Stained (Invitrogen, Waltham, MA, USA) as a molecular marker and NuPage MES SDS Running Buffer. Gels were stained with Pierce Silver Stain Kit (Thermo Fisher Scientific) according to the manufacturer's protocol.

In-Solution Digestion, Liquid Chromatography-Mass Spectrometry (LC-MS), and Protein Identification. The in-solution digestion, liquid chromatography-mass spectrometry, and protein identification were performed as previously described by our group with slight modifications [67, 102, 175]. Prior to digestion, SDS was removed from the protein mix using Pierce Detergent Removal Spin Columns (Thermo Fisher Scientific). Afterwards, the proteins were precipitated via the ProteoExtract protein precipitation kit (Merck) and solubilized in RapiGest SF (Waters) in ammonium bicarbonate butter (50 mM). The Proteins were reduced with dithiothreitol (5 mM, Sigma-Aldrich) and alkylated with iodoacetamide (15 mM, Sigma-Aldrich) followed by an overnight tryptic digestion at a protein:trypsin ratio of 50:1. To allow absolute protein quantification, samples were diluted with 0.1 % formic acid and spiked with 50 fmol/µL Hi3 *E.coli.* (Waters), following a published protocol[286].

Peptides were measured using a nanoACQUITY UPLC system coupled to a Synapt G2-Si mass spectrometer. The system was operated in a positive resolution mode, performing data-independent acquisition with additional ion mobility separation (IMS-MSE) with a mass to charge range of 50-2000 Da, scan time of 1 s, ramped trap collision energy from 20 to 40 V, and data acquisition of 120 min. The samples were injected with a flow rate of 0.3 µL/min and as a reference Glu-Fibrinopeptide (150 fmol/µL) and Leu-Enkephalin (200 pg/µL) were used and injected with a flow rate of 0.5 µL/min.

Data processing was performed using MassLynx 4.1 and Progenesis QI 2.0 with a reviewed database downloaded from Uniprot. Thresholds for noise reduction were set at 120, 25, and 750 counts for low energy, high energy, and peptide intensity. For protein identification, at least one assigned fragment per peptide, three assigned fragments per protein, and one assigned peptides per protein were required. The TOP3/HI3 approach provided the amount of each protein in fmol[112].

Protein Annotation. After protein identification, we identified all corona proteins with an enrichment of 1.5-fold compared with the lysate proteins. The enriched corona proteins were forwarded to an analysis with the functional annotation tool DAVID (Version 6.8, https://david.ncifcrf.gov/home.jsp accessed on 15th November 2021) [287, 288]. The enriched proteins were analyzed by functional annotation clustering, implementing the database for GOTERM_CC_FAT with medium classification stringency to consider the cellular compartments. The following GOTERMS were considered for the study: extracellular vesicle, cell surface, secretory vesicle, endoplasmatic reticulum, early endosome, cytoplasmic region, endocytic vesicle, and nucleosome.

5.4 Results and Discussion

For the purpose of evaluating the influence of the loading amount on nanoparticles on their exocytosis, glucose-PEG-coated gold nanoparticles (GNPs) were synthesized. In this study, we focused on one type of nanoparticle to demonstrate changes in the nanoparticle exocytosis behavior independently from particle size or surface functionalization. Gold nanoparticles were chosen as a widely used type of nanoparticle and as a particle type that could be used in the future as an imaging reagent for stem cells. To achieve a higher stability of the nanoparticles under physiological conditions, the GNPs were surrounded with HS-PEG-COOH via gold–thiol interactions. Carboxylic functionalization of PEG was then used for coupling of glucose on the nanoparticles to achieve an increased uptake of the GNPs into cells [262]. In Figure 5.4.1, an illustration of the surface functionalization of the nanoparticles can be seen, as well as a representative transmission electron microscopy (TEM) picture. TEM showed an average size of the gold nanoparticles of 12.0 ± 2.8 nm. Dynamic light scattering (DLS) revealed a significantly larger size of the GNPs of 75 nm (Figure 5.6.1). However, using TEM, only the size of the gold nanoparticle core is measured (e.g. without the PEG and glucose coating contributing to the size measurement). In contrast in DLS, where the whole hydrodynamic diameter of the particles is measured. As the PEGylated and glucose-coated nanoparticles show a negative ζ-potential, the particles can, in addition, build up more electrostatic interactions in liquid dispersion, and thus show a larger diameter size than that measured by TEM images.

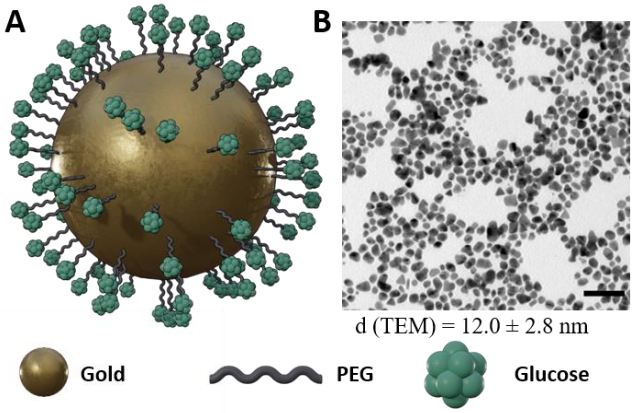

C **Physicochemical propertries**

Parameters	Values
d_H (DLS)	75 nm
PDI	0.387
ζ-Potential	-29.8 mV

Figure 5.4.1. (A) Schematic representation of PEGylated and glucose-coated gold nanoparticles. (B) Representative TEM images of GNPs. The size of the nanoparticles is given in nm ± SD. Scale bar = 50 nm. (C) Physicochemical properties of the GNPs.

To evaluate the exocytosis of the GNPs from PLX-PAD cells, we used two different uptake and exocytosis protocols. For a lower loading of nanoparticles in the cells, we used a protocol with a short incubation time (30 min). However, to still have a sufficient uptake of nanoparticles in cells for this protocol, we incubated the cells without any proteins in isotone NaCl solution, as it was previously shown that the protein corona that formed in cell culture media with FBS reduces the uptake of nanoparticles into cells [168]. This phenomenon, known as the *stealth effect*, was intended to be avoided

in this protocol by incubating the cells without the presence of proteins in the exposure media [75]. In the second protocol, we incubated the GNPs with the PLX-PAD cells for 24 h in DMEM with FBS. There, we expected to have a higher uptake and intracellular internalization of the nanoparticles because of the longer incubation time, despite the presence of proteins. The FBS was added to the cell culture media to avoid potential damage or change in cell functions due to the long incubation time without proteins.

Determination of the gold concentration in the cells was carried out using ICP-OES and ICP-MS. ICP-OES is mainly used to determine the concentration of metals in complex solutions. For the analysis, the samples are first atomized and ionized in an argon plasma. Then, the ions and atoms are excited and emit electromagnetic radiation, which can be assigned to the different elements as discrete lines and by that quantified [244]. In ICP-MS, ions are extracted from the plasma and separated based on their mass-to-charge ratio in order to quantify the concentration. For the injection of the samples into the plasma, the samples are sprayed into a nebulizer in order to form small droplets. As cells and cell clumps in the sample could result in an inhomogeneous solution and lead to poor aerosol formation, the cells were previously dissolved overnight in aqua regia. Afterwards, the gold concentration in the cell solutions was determined for both uptake protocols and exocytosis protocols.

In Figure 5.4.2A, a schematic representation of the different protocols used for the incubation can be seen. Figure 5.4.2B shows that the different incubation protocols indeed resulted in different amounts of gold in the cell suspension, suggesting that the uptake of GNPs was higher for the high loading protocol than for the low loading protocol. It can be seen at time point 0, which displays the measurement directly after uptake of the nanoparticles, that the amount of gold in the high loading protocol was 165 pg per cell, while for the low loading protocol, it was 15 pg per cell. Therefore, the high loading protocol led to a particle amount 10 times higher in the cell than the low loading protocol. Additionally, the recovery rate of the gold in comparison with the incubation solution was determined. Therefore, the amount of gold was analyzed in the supernatant of the washing steps and in the cells via ICP-MS. Here, we showed that, for the low loading protocol, only 6.4% of the available gold from the incubation solution was taken up in the cells (Table 5.6.1). On the other hand, with the high loading protocol, 27.9% of the gold was taken up by the cells. As longer incubation protocols and longer exposures to nanoparticles could cause damage or toxicity to cells [289], we determined the viability of the PLX-PAD cells with different concentrations of the GNPs (Figure 5.6.2). Thereby we demonstrated that the particles do not have toxic effects on the cells and nearly 100% of the cells were viable after a long incubation.

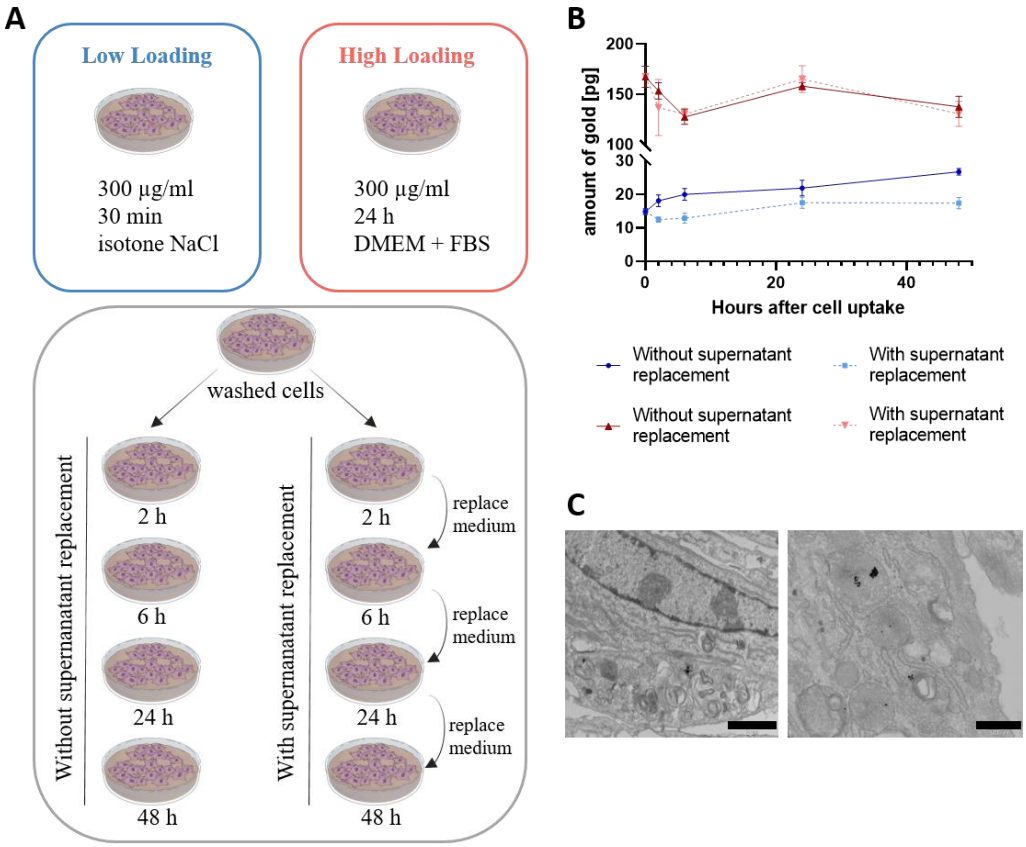

Figure 5.4.2. (A) Schematic representation of the different incubation protocols used for incubation. PLX-PAD cells were incubated either for 30 min with 300 µg/mL GNPs in isotone NaCl solution (blue) or for 24 h with 300 µg/mL GNPs in DMEM with FBS (red). After uptake of GNPs, the cells were further incubated in DMEM with FBS for up to 48 h either with regular exchange of the medium (grey box right) or kept in the same medium (grey box left). (B) Calculated gold concentration per cell. Cells were harvested after incubation with GNPs and after incubation with DMEM, respectively. Afterwards, cells were analyzed with ICP-OES and the amount of gold per cell was calculated. Mean values ± SD. *n* = 3 (C) Representative TEM images of PLX-PAD cells after uptake of 300 µg/mL GNPs in DMEM + FBS. Images show the internalization of the GNPs in the PLX-PAD cells. Left scale bar represents 2 µm, right scale bar 500 nm.

After uptake of the nanoparticles, the cells were incubated again with DMEM for analysis of the exocytosis of the nanoparticles. First, we determined the amount of gold in the cells when the cell culture media was kept the same the whole time (Figure 5.4.2A, grey box left). However, what the behavior might be in vivo should always be considered. There, exocytosed particles would be removed relatively quickly by other cells or body fluids. Thus, it is unlikely that exocytosed particles reabsorb on the cells and are taken up again. The amount of gold in the cells was also analyzed after replacing the supernatant regularly (Figure 5.4.2A grey box right). In Figure 5.4.2B, it can be seen that the intracellular gold concentration does not increase or decrease drastically for both protocols. However, looking deeper into the results, it can be seen that the amount of gold increases slightly with time for the low loading protocol both without and with supernatant replacement. This indicates that, after the uptake time, particles could be still attached to the surface of the cells and were available to be taken up with further incubation time. By washing and harvesting for ICP-OES analysis, particles that are attached to the surface might be lost. With supernatant replacement, this increase stopped after 24 h and the intracellular gold concentration leveled off at a gold amount of 17 pg per cell. Without supernatant replacement, the gold amount increases up to 26 pg per cell, which may indicate a further uptake either of exocytosed GNPs or GNPs

from the cell surface. For the high loading protocol, no difference could be observed with or without supernatant replacement. Here, a small decrease in the gold amount can be seen after 2 and 6 h. This could be due to a release or exocytosis of nanoparticles from the cells. However, after 24 h, the gold amount increases to the same level as before and decreases afterwards again slightly to 130 pg per cell. The increase in the gold amount could also be due to an uptake of GNPs that were still attached to the surface and reuptake of exocytosed GNPs occurred. Because, in TEM pictures (Figure 5.4.2C), no GNPs could be observed on the cell surface with the high loading protocol, uptake of attached particles on the surface seems to be improbable and reuptake of exocytosed GNPs seems to be more likely. Therefore, the amount of exocytosed gold in the supernatant of the cell was further analyzed.

To further determine the exocytosis of the GNPs from PLX-PAD cells, we analyzed the amount of gold in cell culture media after allowing exocytosis from the cells. In Figure 5.4.3A, the calculated exocytosed gold concentration per cell can be seen. To facilitate a comparison between intracellular gold concentration and that in the supernatant, the amount of gold was also given per cell here. Considering the samples without supernatant replacement, it is noticeable that the amount of gold in the supernatant increased for both protocols (low and high loading) until 6 h, then decreased up to 24 h before it increased again up to 48 h. As the supernatant was kept and harvested at the recommended time point, it is very probable that the particles, which were previously released from the cell, were taken up again. Looking at the intracellular gold concentration, an increase in the concentration for the high loading protocol could be observed, which supports the re-uptake theory when the particles are not removed from the cell culture media. This has also been observed previously for gold particles [284]. There, after a short time, a plateau was reached where exocytosis and re-uptake were in equilibrium [284]. However, under in vivo conditions, it is more probable that the exocytosed particles are removed from the surrounding area of cells by other cells (e.g. phagocytic cells). It is also important to pay attention to additional physiological dynamic removal processes that can occur. Considering this for the protocol, we observed that, with regular supernatant replacement, the amount of exocytosed gold decreased over time. Most of the gold was measured in cell culture media after 2 h and decreased rapidly to 6 h. After 24 h and 48 h, only a small amount of gold was measured in the supernatant. Therefore, in accordance with previous studies on different cell types, the exocytosis of nanoparticles seems to be fast, but decreases with time [284].

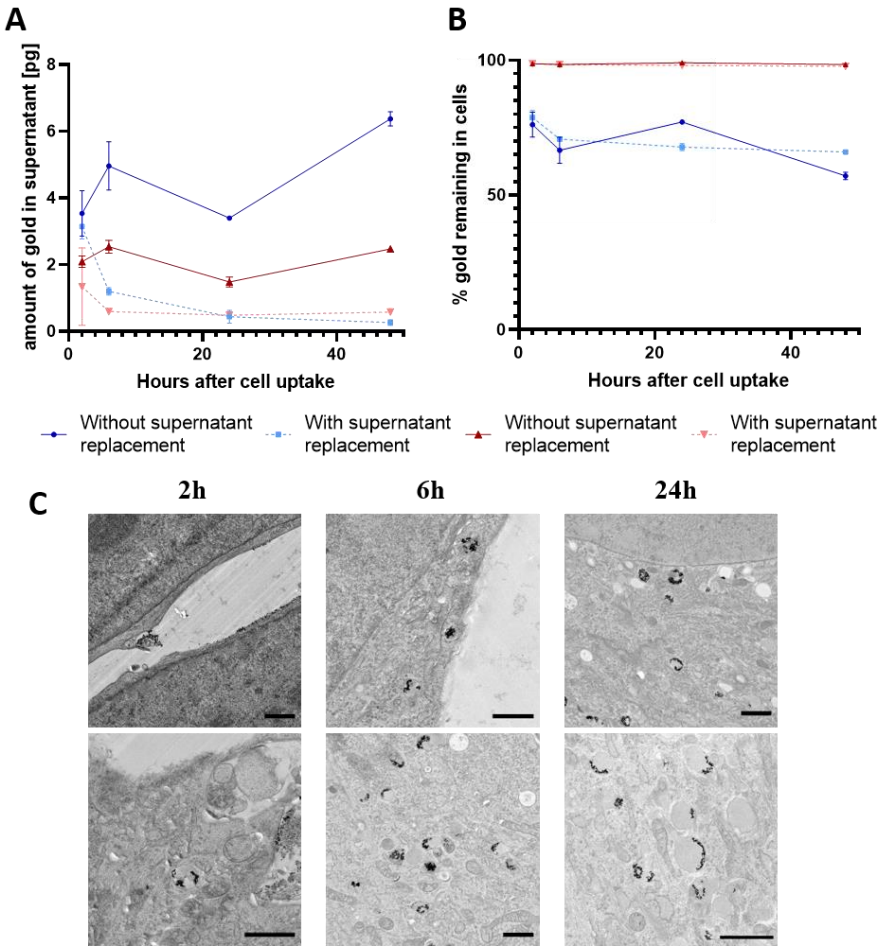

Figure 5.4.3. (A) Calculated amount of gold in supernatant determined by ICP-OES after incubation of PLX-PAD cells with GNPs and further incubation with cell culture media. The low loading protocol is shown in blue and the high loading protocol in red. The amount of gold is given in pg exocytosed per cell as mean ± SD. *n* = 3 (B) Calculated gold amount remaining in PLX-PAD cells after allowing for exocytosis given in percent. Values are displayed as mean ± SD. *n* = 3. (C) Representative TEM images of PLX-PAD cells after a first incubation with low loading protocol followed by a second incubation (2 h, 6 h, or 24 h) in cell culture media allowing for internalization and exocytosis. Scale bars are 1 µm.

To allow a better comparison of the exocytosis rate between the different loading protocols, the percent of gold remaining in the cells was calculated (Figure 5.4.3B). Therefore, the amount of gold quantified after the uptake of the particles and the amount quantified in the supernatant was used for calculation. While 98% of the gold remained in the cells for the high loading protocol, only 80% remained after 2 h and 66% remained after 48 h for the low loading protocol. Particles could either be released from the cell surface or excreted from the cells. A higher loading of the GNPs in the PLX-PAD cells (by means of a more prolonged incubation protocol) also seems to reduce the exocytosis of the loaded particles from the cells. This can be seen by consideration of the total amount of gold exocytosed and by looking at the amount of exocytosed gold given in percent. These observations could also be confirmed in the TEM images (Figure 5.4.3C, Figure 5.6.4, Figure 5.6.5, and Figure 5.6.6). To visualize internalization, TEM images were made for the low loading protocol after uptake and additional incubation in cell culture media for 2, 6, and 24 h. While, after 2 h, a high number of particles could be still seen on the cell surface (Figure 5.6.4), after 24 h, nearly no more particles attached to the cell surface were observed. In addition, after 6 and 24 h, increasingly more particles seemed to be located in lysosomes, which

suggests that the particles were internalized into the cells. Previously, Yu et al. synthesized temperature-responsive GNPs for long-term tracking of stem cells. Here, by adjusting the temperature, an increased uptake and a reduced exocytosis could be observed. However, still, a non-negligible amount of GNPs was secreted within 24 h, which could lead in vivo to a loss of signal or unspecific signal from other cells [269]. During other studies, GNPs were coated using poly-l-lysin or PEG coupled to a trans-activator of transcription peptide to increase the uptake of GNPs in stem cells, and thereby increase the CT signal. However, increased uptake did not lead to a decreased exocytosis of GNPs, which makes long-term tracking still problematic [270, 271]. Using our glucose-PEG-coated GNPs and adapting the incubation protocol, the exocytosis rate was significantly reduced, and a high loading of the stem cells could still be achieved. This could be used in the future for better long-term tracking of stem cells.

The next step was to analyze whether proteins attached to the surface of the GNPs indicate if particles stay intracellular or if they are exocytosed. Therefore, we incubated the particles with the PLX-PAD cells, harvested and lysed them, and collected the proteins in the protein corona around the GNPs. The protein corona develops dependently on proteomic milieu around the particle. Therefore, with this method, it is possible to determine the pathway to which the GNPs belong [242, 243]. As it is necessary for this analysis that the nanoparticles were internalized into the cell and were no longer on the surface, the protocol was adapted. Instead of an incubation of 30 min in isotone NaCl solution, the GNPs were incubated for the low loading protocol for 4 h in DMEM with FBS at the same concentration. Therefore, we ensured that we still have a lower and shorter loading of GNPs in the cells but reach a sufficient amount of particles in the cells to isolate them in the protein corona analysis. Additionally, a 4 + 20 h condition was analyzed to ensure internalization and processing for a possible exocytosis of the GNPs. The proteins were visualized via SDS-PAGE (Figure 5.6.3) and analyzed via LC-MS (Figure 5.4.4 and Figure 5.6.7). A detailed list of all identified proteins is provided in the respective publication. No clear differences between the conditions via SDS PAGE were observed. However, a clear distinction between the protein corona composition of the GNPs and the lysate of the PLX-PAD was noticed. This difference confirms that the protein corona of the GNPs was efficiently isolated from the cell lysate.

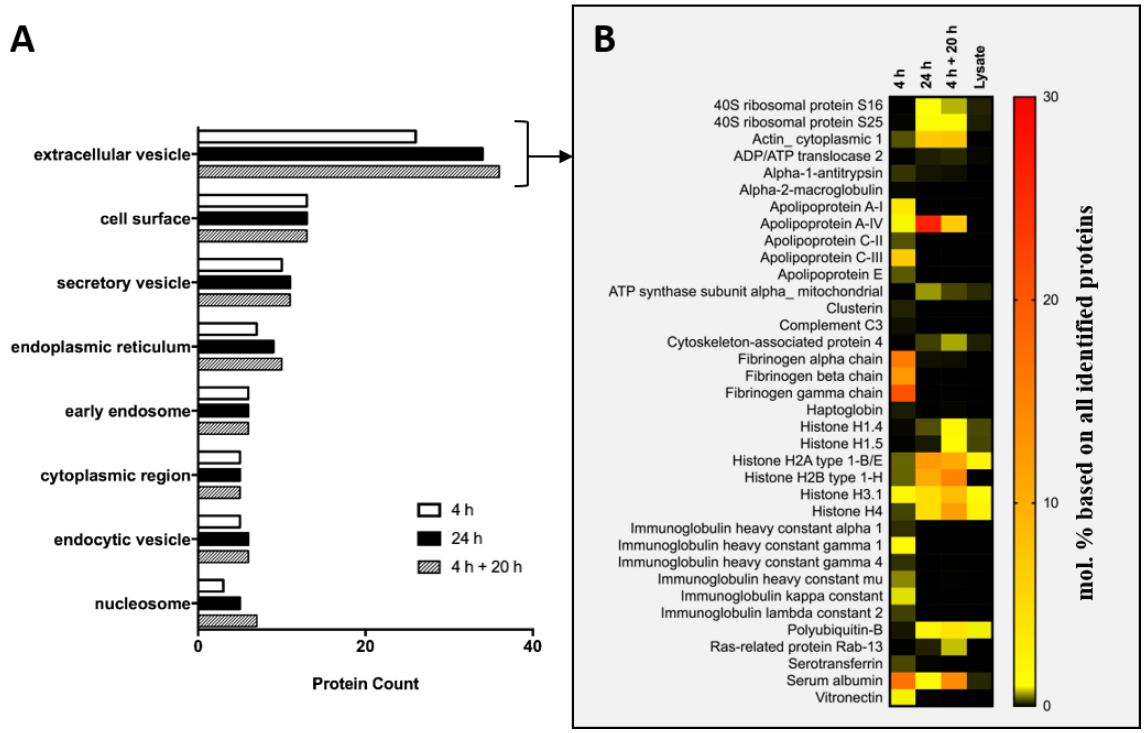

Figure 5.4.4. (A) Annotation of the proteins bound on the particles to intracellular compartments. Proteins were desorbed from GNPs after incubation and lysis of the PLX-PAD cells. The protein corona was analyzed by LC-MS and proteins assigned to selected intracellular compartments using DAVID-based functional annotation clustering by GOTERM_CC_FAT. (B) Heatmap of all proteins assigned to the extracellular vesicle GOTERM. Different incubation time points are displayed in comparison with cell lysate of PLX PAD cells. A detailed list of all proteins found in the protein corona and annotation to the intracellular GOTERMs can be found in the respective publication.

After the analysis of the SDS-PAGE, the protein corona was additionally analyzed via LC-MS. A bottom-up proteomic approach was used for this protein analysis [103]. Therefore, proteins were desorbed from nanoparticles followed by digestion into peptides with trypsin. Peptides were separated by liquid chromatography and ionized by electrospray ionization. In the mass spectrometer, the mass-to-charge ratio of the ionized peptides was recorded. With the use of a deconvolution software and protein databases, these signals can be assigned to specific proteins, and through this, the composition of protein mixtures can be determined [103]. Here, we used this proteomic approach to analyze the intracellular fate of the GNPs. First, we considered the TOP 10 proteins in the protein corona for all conditions. Thereby, it can be seen that the TOP proteins binding on the GNPs after 4 h differ from the proteins binding after 24 h and 4 + 20 h. After 4 h incubation, serum proteins, namely fibrinogen and serum albumin, were predominantly measured. After more prolonged incubation, this protein adsorption pattern changed towards intracellular proteins e.g. histones and actin.

Next, we analyzed to which intracellular compartments the proteins in the protein corona belong. Therefore, the enrichment factor of the proteins in the protein corona compared with cell lysate was calculated. Only proteins with a 1.5-fold enrichment were considered for annotation to an intracellular compartment. First, we used DAVID to assign the number of the enriched proteins of each condition to the different cellular compartments (Figure 5.4.4A). We observed that most of the enriched proteins of all conditions are associated with extracellular vesicles. The highest protein count for extracellular

vesicle proteins can be seen in the 4 + 20 h condition and the least protein count in the 4 h condition. For the categories cell surface, secretory vesicles, early endosomes, cytoplasmic region, and endocytic vesicles, no difference between the different conditions was observed. The higher protein count for the 4 + 20 h condition comes from the fact that, in total, more proteins were enriched in the corona for this condition, indicating that these particles traversed longer through the cells and encountered a more complex protein milieu.

In order to determine whether the protein corona indicates if a particle is exocytosed or not, we analyzed the proteins annotated to the extracellular pathway (Figure 5.4.4B). Here, again, the proteins found in the protein corona after 4 h of incubation clearly differ from the proteins in the corona after 24 h and 4 + 20 h. Many proteins that were already found under the TOP 20 list were observed here again, but some proteins that are not that highly represented could also be annotated to this group. After 4 h of incubation time, more apolipoproteins and vitronectin could be seen in the protein corona. However, after further incubation (e.g. 24 h and 20 + 4 h), the protein composition changed, and the amount of intracellular proteins increased. Moreover, only one representative of the proteins involved in the exocytosis, namely Rab-13, could be detected in a small amount in the protein corona after 24 h. However, Rab-13 is involved in the formation of intracellular vesicles and involved in both endocytotic and exocytotic processes, and cannot be unequivocally assigned as an exocytosis marker [290, 291]. The fast exocytosis of the GNPs observed for the low loading protocols is probably due to the protein corona, which was mainly formed by extracellular proteins. The obtained results suggest that prolonged nanoparticle incubation protocols allow intracellular protein corona changes and lead to a deeper and longer internalization in the cells.

5.5 Conclusion

Here, we demonstrated that a longer incubation protocol allows for higher loading of gold nanoparticles in PLX-PAD cells and leads to reduced exocytosis of these nanoparticles from the cells. Moreover, with the analysis of the protein corona, we showed that, with a prolonged incubation time, the serum proteins in the protein corona are exchanged to intracellular proteins, which probably leads to the reduced exocytosis. A low exocytosis rate of gold nanoparticles is absolutely necessary for long-term tracking of stem cells in vivo as background signals from other cells are reduced and the signal intensity of the stem cells remains stable over time. These findings could help to better understand the in vivo fate of stem cells and intracellular biokinetics of glucose-PEG-coated gold nanoparticles. It can also support on the design of nanoparticles' uptake protocols for the labelling and tracking of cells used as therapeutic agents.

5.6 Supporting Information

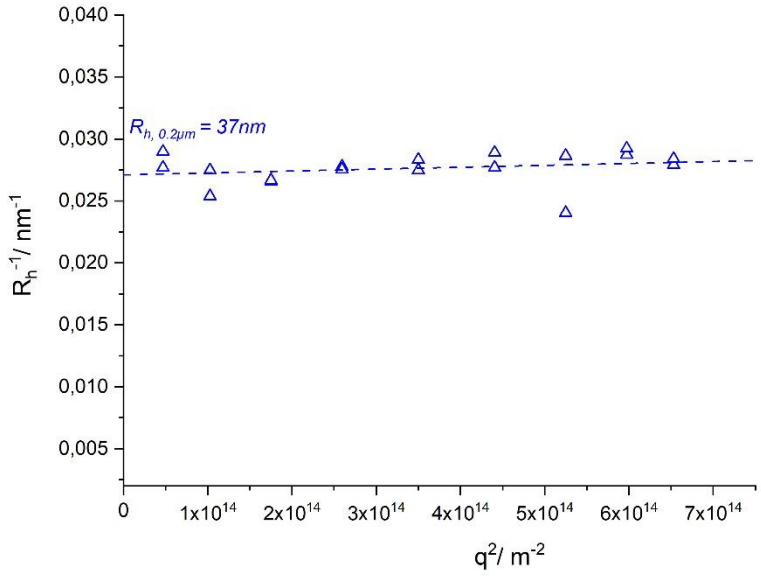

Figure 5.6.1. Dynamic light scattering of GNPs. Multi-angle dynamic light scattering of GNPs after filtration with a 0.2 µm filter, showing the size of the GNPs of 74 nm in diameter.

Table 5.6.1. Cell loading efficiency determined by ICP-MS. PLX-PAD cells were either incubated with 1 h or 24 h with 400 µg/mL GNPs for the low loading and high loading protocol respectively. Afterwards, gold amount in GNP exposed cells was quantified *via* ICP-MS analysis and the percentage of recovered gold as a function of total exposed gold was calculated.

	Low Loading		High Loading	
	Recovery of Au vs Total Au (%)	SD	Recovery of Au vs Total Au (%)	SD
Supernatant 1	86.5	3.1	66.6	9.2
Supernatant 2 (1st wash)	7.2	1.7	4.3	0.8
Supernatant 3 (2nd wash)	n.a	n.a	1.0	0.2
Cells	6.4	0.3	27.9	7.7
Total Au recovered (%)	104.9	5.4	105.0	3.8

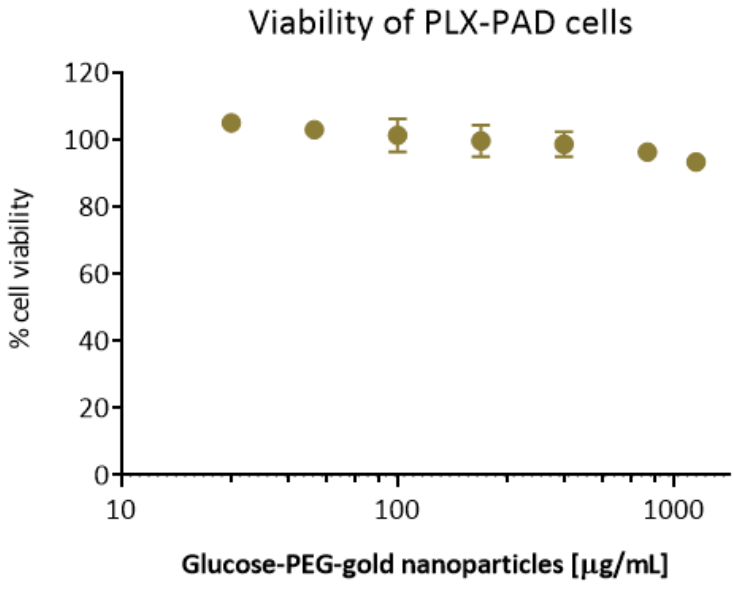

Figure 5.6.2. Cellular viability of PLX PAD cells after incubation with different concentrations of GNPs. PLX PAD cells were incubated with 25-1200 µg/mL GNPs for 24 h in full DMEM and the percentage of viable cells was determined with an Alamar Blue Assay. Results are shown as mean ± SEM of three independent assays.

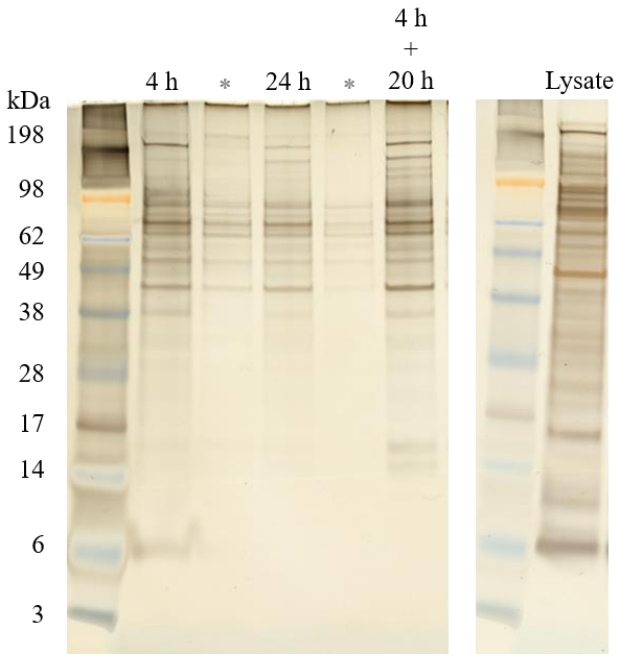

Figure 5.6.3. Hard corona proteins separated by SDS-PAGE and stained by a silver staining. The lanes are labelled according to the incubation time and Lysate corresponds to the cell lysate of PLX PAD cells. Lanes labelled with * are not relevant here.

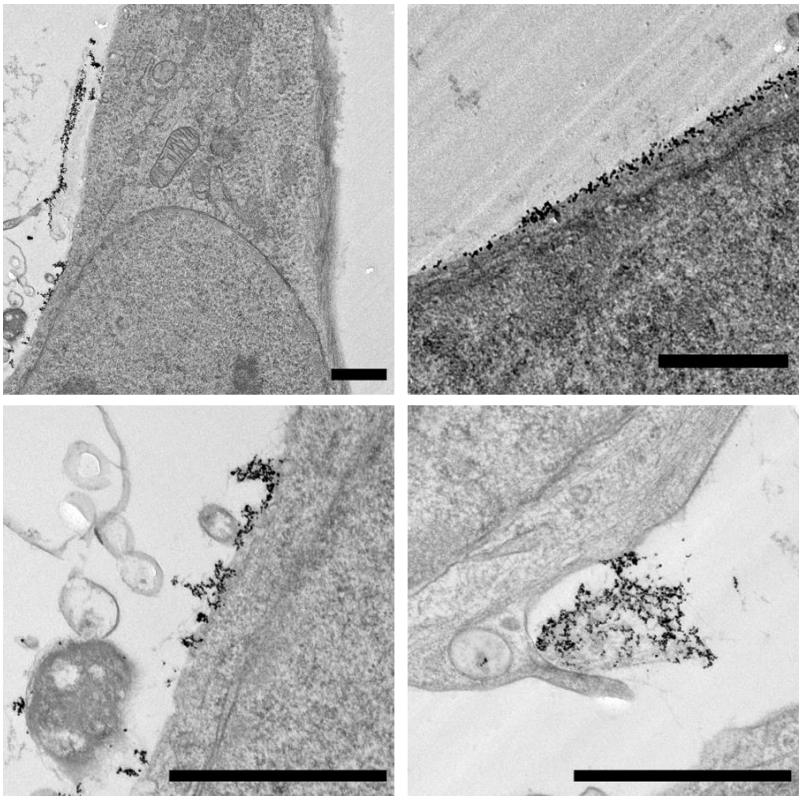

Figure 5.6.4. Representative TEM images of PLX PAD cells after first incubation with the low loading protocol followed by a second incubation for 2 h. The scale bars represent 1 µm.

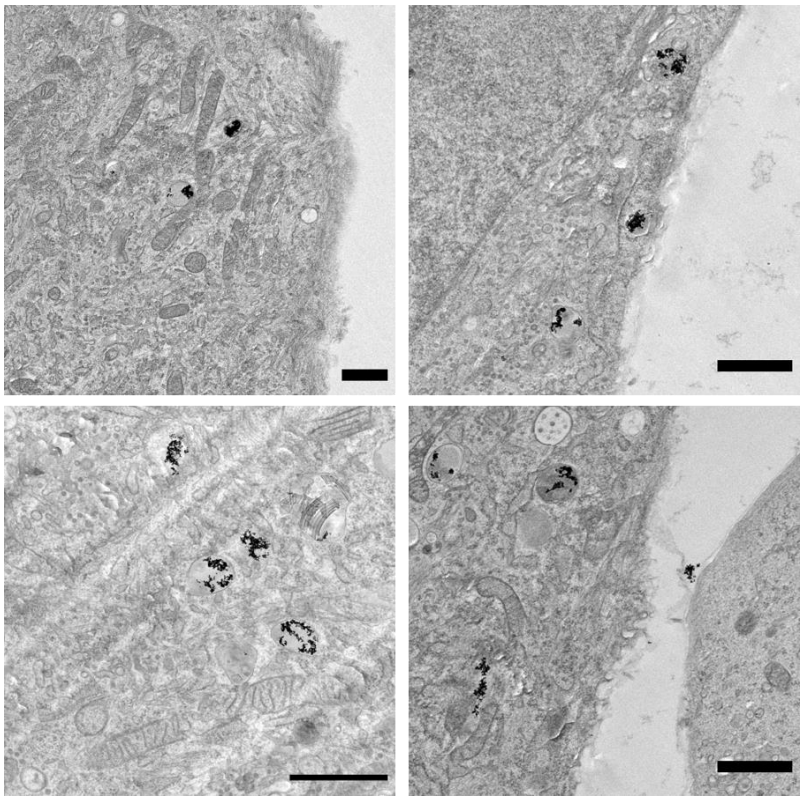

Figure 5.6.5. Representative TEM images of PLX PAD cells after first incubation with the low loading protocol followed by a second incubation for 6 h. The scale bars represent 1 µm.

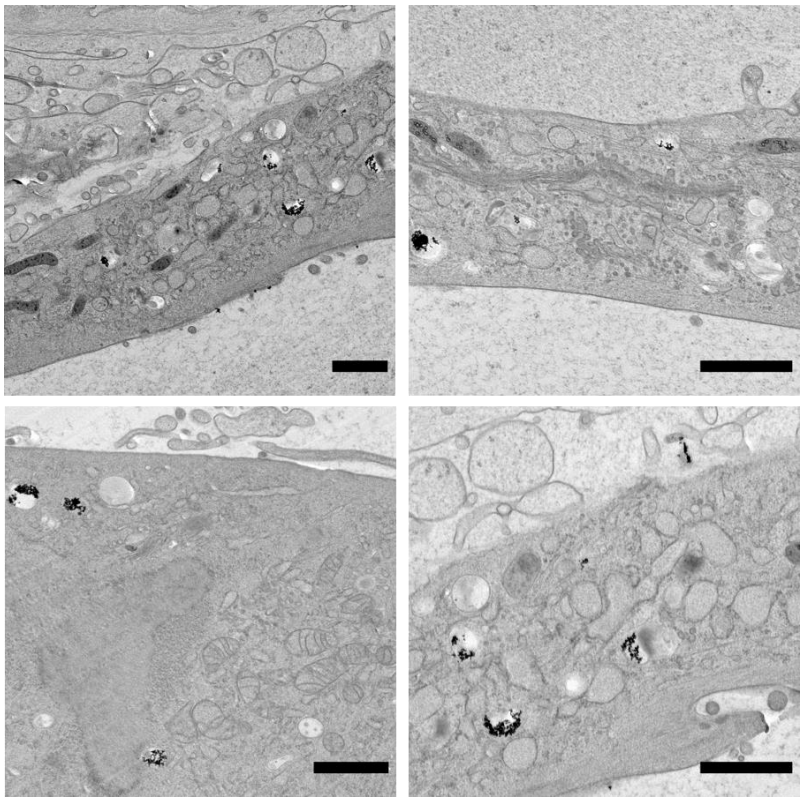

Figure 5.6.6. Representative TEM images of PLX PAD cells after first incubation with the low loading protocol followed by a second incubation for 24 h. The scale bars represent 1 µm.

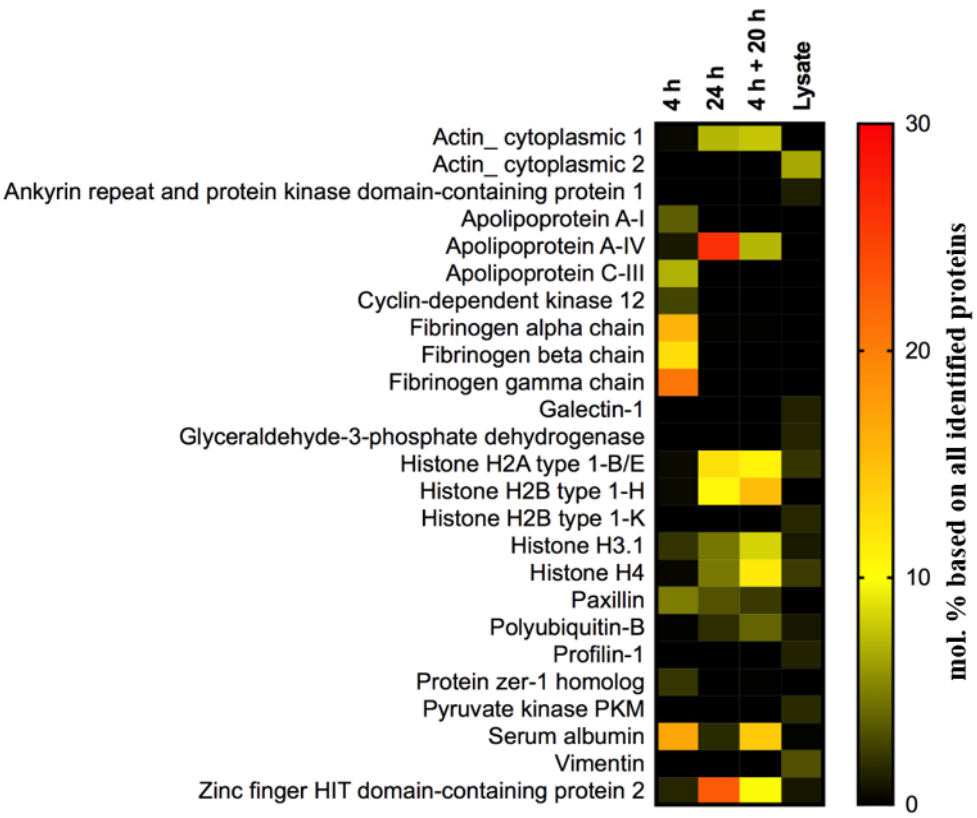

Figure 5.6.7. Proteomic analysis of the protein corona on the surface of GNPs after uptake in PLX PAD cells. The heatmap is displaying the combined TOP 10 proteins of each condition (25 proteins in total) identified by LC-MS. The values are reported as the mol% based on all identified proteins in the protein corona.

Table 5.6.2. List of enriched proteins in the protein corona identified by LC-MS. Displayed are the 1.5-fold enriched proteins compared to the proteins of the lysate

Uniprot Accession	Protein Name
P62249	40S ribosomal protein S16
P62851	40S ribosomal protein S25
P60709	Actin_ cytoplasmic 1
P12235	ADP/ATP translocase 1
P05141	ADP/ATP translocase 2
P01009	Alpha-1-antitrypsin
P01023	Alpha-2-macroglobulin
P02647	Apolipoprotein A-I
P06727	Apolipoprotein A-IV
P02655	Apolipoprotein C-II
P02656	Apolipoprotein C-III
P02649	Apolipoprotein E
O43150	Arf-GAP with SH3 domain_ ANK repeat and PH domain-containing protein 2
P25705	ATP synthase subunit alpha_ mitochondrial
P25098	Beta-adrenergic receptor kinase 1
P10909	Clusterin
P01024	Complement C3
Q9NYV4	Cyclin-dependent kinase 12
Q07065	Cytoskeleton-associated protein 4
P04843	Dolichyl-diphosphooligosaccharide--protein glycosyltransferase subunit 1
P02671	Fibrinogen alpha chain
P02675	Fibrinogen beta chain
P02679	Fibrinogen gamma chain
P00738	Haptoglobin
Q8WYB5	Histone acetyltransferase KAT6B
P10412	Histone H1.4
P16401	Histone H1.5
P04908	Histone H2A type 1-B/E
Q93079	Histone H2B type 1-H
P68431	Histone H3.1
P62805	Histone H4
Q14520	Hyaluronan-binding protein 2
P01876	Immunoglobulin heavy constant alpha 1
P01857	Immunoglobulin heavy constant gamma 1
P01861	Immunoglobulin heavy constant gamma 4
P01871	Immunoglobulin heavy constant mu
P01834	Immunoglobulin kappa constant
P0DOY2	Immunoglobulin lambda constant 2
Q5T7N2	LINE-1 type transposase domain-containing protein 1
P49023	Paxillin
P0CG47	Polyubiquitin-B
Q13045	Protein flightless-1 homolog
P61619	Protein transport protein Sec61 subunit alpha isoform 1
Q7Z7L7	Protein zer-1 homolog
P51153	Ras-related protein Rab-13
P02787	Serotransferrin
P02768	Serum albumin
P0DPH7	Tubulin alpha-3C chain
P04004	Vitronectin
Q9UHR6	Zinc finger HIT domain-containing protein 2
P21506	Zinc finger protein 10

Table 5.6.3. List of proteins annotated to the GOTERM "extracellular vesicle" by DAVID. Proteins were identified *via* LC-MS proteomics workflow and annotated to the corresponding intracellular compartment with DAVID. Displayed are the Uniprot Accession number and the protein name of each protein.

Extracellular Vesicle	
Uniprot Accession	**Protein Name**
P62249	40S ribosomal protein S16
P62851	40S ribosomal protein S25
P60709	Actin_ cytoplasmic 1
P05141	ADP/ATP translocase 2
P01009	Alpha-1-antitrypsin
P01023	Alpha-2-macroglobulin
P02647	Apolipoprotein A-I
P06727	Apolipoprotein A-IV
P02655	Apolipoprotein C-II
P02656	Apolipoprotein C-III
P02649	Apolipoprotein E
P25705	ATP synthase subunit alpha_ mitochondrial
P10909	Clusterin
P01024	Complement C3
Q07065	Cytoskeleton-associated protein 4
P02671	Fibrinogen alpha chain
P02675	Fibrinogen beta chain
P02679	Fibrinogen gamma chain
P00738	Haptoglobin
P10412	Histone H1.4
P16401	Histone H1.5
P04908	Histone H2A type 1-B/E
Q93079	Histone H2B type 1-H
P68431	Histone H3.1
P62805	Histone H4
P01876	Immunoglobulin heavy constant alpha 1
P01857	Immunoglobulin heavy constant gamma 1
P01861	Immunoglobulin heavy constant gamma 4
P01871	Immunoglobulin heavy constant mu
P01834	Immunoglobulin kappa constant
P0DOY2	Immunoglobulin lambda constant 2
P0CG47	Polyubiquitin-B
P51153	Ras-related protein Rab-13
P02787	Serotransferrin
P02768	Serum albumin
P04004	Vitronectin

Table 5.6.4. List of proteins annotated to the GOTERM "cell surface" by DAVID. Proteins were identified *via* LC-MS and annotated to the corresponding intracellular compartment with DAVID. Displayed are the Uniprot Accession number and the protein name of each protein.

Cell Surface	
Uniprot Accession	**Protein Name**
P02647	Apolipoprotein A-I
P06727	Apolipoprotein A-IV
P10909	Clusterin
P02671	Fibrinogen alpha chain
P02675	Fibrinogen beta chain
P02679	Fibrinogen gamma chain
P01876	Immunoglobulin heavy constant alpha 1
P01857	Immunoglobulin heavy constant gamma 1
P01861	Immunoglobulin heavy constant gamma 4
P01871	Immunoglobulin heavy constant mu
P01834	Immunoglobulin kappa constant
P0DOY2	Immunoglobulin lambda constant 2
P02787	Serotransferrin

Table 5.6.5. List of proteins annotated to the secretory vesicle pathway by DAVID. Proteins were identified *via* LC-MS and annotated to the corresponding intracellular compartment with DAVID. Displayed are the Uniprot Accession number and the protein name of each protein.

Secretory Vesicle	
Uniprot Accession	**Protein Name**
P01009	Alpha-1-antitrypsin
P01023	Alpha-2-macroglobulin
P02647	Apolipoprotein A-I
P10909	Clusterin
Q07065	Cytoskeleton-associated protein 4
P02671	Fibrinogen alpha chain
P02675	Fibrinogen beta chain
P02679	Fibrinogen gamma chain
P51153	Ras-related protein Rab-13
P02787	Serotransferrin
P02768	Serum albumin

Table 5.6.6. List of proteins annotated to the endoplasmatic reticulum by DAVID. Proteins were identified *via* LC-MS and annotated to the corresponding intracellular compartment with DAVID. Displayed are the Uniprot Accession number and the protein name of each protein.

Endoplasmatic Reticulum	
Uniprot Accession	**Protein Name**
P01009	Alpha-1-antitrypsin
P02647	Apolipoprotein A-I
P06727	Apolipoprotein A-IV
P02649	Apolipoprotein E
P10909	Clusterin
Q07065	Cytoskeleton-associated protein 4
P04843	Dolichyl-diphosphooligosaccharide--protein glycosyltransferase subunit 1
P61619	Protein transport protein Sec61 subunit alpha isoform 1
P02768	Serum albumin
P04004	Vitronectin

Table 5.6.7. List of proteins annotated to the early endosome pathway by DAVID. Proteins were identified *via* LC-MS and annotated to the corresponding intracellular compartment with DAVID. Displayed are the Uniprot Accession number and the protein name of each protein.

Early Endosome	
Uniprot Accession	**Protein Name**
P02647	Apolipoprotein A-I
P06727	Apolipoprotein A-IV
P02655	Apolipoprotein C-II
P02656	Apolipoprotein C-III
P02649	Apolipoprotein E
P02787	Serotransferrin

Table 5.6.8. List of proteins annotated to the cytoplasmic region by DAVID. Proteins were identified *via* LC-MS and annotated to the corresponding intracellular compartment with DAVID. Displayed are the Uniprot Accession number and the protein name of each protein.

Cytoplasmatic Region	
Uniprot Accession	**Protein Name**
P60709	Actin_ cytoplasmic 1
P02671	Fibrinogen alpha chain
P02675	Fibrinogen beta chain
P02679	Fibrinogen gamma chain
P49023	Paxillin

Table 5.6.9 List of proteins annotated to the endocytotic vesicle pathway by DAVID. Proteins were identified *via* LC-MS and annotated to the corresponding intracellular compartment with DAVID. Displayed are the Uniprot Accession number and the protein name of each protein.

Endocytotic Vesicle	
Uniprot Accession	**Protein Name**
P02647	Apolipoprotein A-I
P02649	Apolipoprotein E
P00738	Haptoglobin
P0CG47	Polyubiquitin-B
P51153	Ras-related protein Rab-13
P02787	Serotransferrin

Table 5.6.10. List of proteins annotated to the nucleosome by DAVID. Proteins were identified *via* LC-MS and annotated to the corresponding intracellular compartment with DAVID. Displayed are the Uniprot Accession number and the protein name of each protein.

Nucleosome	
Uniprot Accession	**Protein Name**
Q8WYB5	Histone acetyltransferase KAT6B
P10412	Histone H1.4
P16401	Histone H1.5
P04908	Histone H2A type 1-B/E
Q93079	Histone H2B type 1-H
P68431	Histone H3.1
P62805	Histone H4

Table 5.6.11. List of proteins in negative control identified by LC-MS. The negative control cells and tubes were treated in the same way as the samples to ensure that only corona proteins are analyzed and to exclude cell contamination.

Negative Control		
Uniprot Accession	**Protein Name**	**Mol %**
P62736	Actin_ aortic smooth muscle	4,54
P60709	Actin_ cytoplasmic 1	6,94
P05141	ADP/ATP translocase 2	0,36
P12236	ADP/ATP translocase 3	0,41
P25705	ATP synthase subunit alpha_ mitochondrial	0,48
P06576	ATP synthase subunit beta_ mitochondrial	0,29
P00403	Cytochrome c oxidase subunit 2	0,30
Q07065	Cytoskeleton-associated protein 4	0,16
P10412	Histone H1.4	1,55
P16401	Histone H1.5	0,92
P04908	Histone H2A type 1-B/E	13,43
P0C0S5	Histone H2A.Z	0,41
O60814	Histone H2B type 1-K	10,10
P68431	Histone H3.1	5,87
P62805	Histone H4	14,02
P60660	Myosin light polypeptide 6	0,31
O14950	Myosin regulatory light chain 12B	0,22
P35579	Myosin-9	1,35
Q00325	Phosphate carrier protein_ mitochondrial	0,61
Q96DU9	Polyadenylate-binding protein 5	1,45
P0CG47	Polyubiquitin-B	1,76
P02545	Prelamin-A/C	0,33
P35232	Prohibitin	0,17
Q6UXU0	Putative uncharacterized protein	0,26
P06753	Tropomyosin alpha-3 chain	0,57
Q8NEP4	Uncharacterized protein C17orf47	23,96
O95399	Urotensin-2	0,06
P08670	Vimentin	0,30
Q5T200	Zinc finger CCCH domain-containing protein 13	1,35
Q9UHR6	Zinc finger HIT domain-containing protein 2	7,54

6. Exocytosis of magnetic dextran iron oxide nanoparticles from HCT116 cells

This subchapter describes the analysis of the exocytosis of nanoparticles from cells by ICP-OES and LC-MS. In this subchapter unpublished data is shown in the structure of a publication. This work could possibly form the basis of a future publication.

Aim:

The uptake and exocytosis pathways of nanoparticles from cells are important processes in the biodistribution and utilization of nanoparticles. While the uptake pathways are relatively well studied, little focus has been placed on the exocytosis pathways of nanoparticles. In this study, the exocytosis pathways of nanoparticles will be tracked. ICP-OES will be used to quantify the exocytosis and proteomics and LC-MS will be used to analyze the exocytosis pathways. This will help to understand the interactions of nanoparticles with cells in the future.

Contribution:

In this study, I performed the conceptualization, ICP-OES analysis, complete LC-MS analysis, cLSM imaging, and flow cytometry analysis of the iron oxide dextran nanoparticles. XXX performed the flow cytometry experiments with the silica nanocapsules. XXX and XXX supervised the project.

6.1 Introduction

The use of nanoparticles (NPs) for different therapeutic and diagnostic approaches is a steadily growing field in research[2]. However, for their safe application, some barriers must be overcome, such as the nano-bio interface and the uptake into the targeted cells[1]. Nano-bio interactions are the interactions between NPs and tissues, cells, and biomolecules. These interactions determine the biological identity of NPs and influence the therapeutic efficiency of NPs[292]. Upon contact of NPs with biomolecules containing fluids, a so-called biomolecular corona forms around NPs by spontaneous adsorption of these biomolecules on the NPs. This biomolecular corona, or protein corona as it is also called, can influence the blood circulation time, cellular uptake, and exocytosis of NPs[75, 238]. The protein corona is a dynamic system with a constant exchange of proteins when the protein composition in the environment changes. Therefore, the protein corona can be seen as a fingerprint of the intracellular route of the NPs and thereby the intracellular and exocytosis pathways of NPs can be investigated[242].

After the administration of the NPs into an organism, most NPs need to be taken up in cells to achieve their therapeutic or diagnostic goal. The uptake mechanisms of NPs in different cells are well known as well as the influence of the protein corona on it[158]. The fact that NPs can be released from the cells and that this depends on the cell type and the physicochemical properties of the NPS has also been shown[238]. For example, it has been shown that the exocytosis rate of gold NPs from murine embryonic fibroblast was significantly higher than the exocytosis of the same NPs from HeLa and human glioblastoma cells. Moreover, it was previously shown that that the exocytosis of smaller transferrin-coated gold NPs was faster than for bigger gold NPs[293]. One explanation for this observation could be the possibility of NPs with different sizes to enter different exocytosis pathways[294, 295]. Depending on the intended application of the NPs, it is very important to know the intracellular pathways and the exocytosis pathways of the NPs. A NP that is used for diagnostics and imaging should remain in the target cell as long as possible, whereas a NP that is transported across the blood-brain barrier should be exocytosed as quickly as possible. However, very little is known about the exocytosis pathways and often microscopic methods were used for their analysis[239, 240, 260]. The protein corona of excreted NPs could give important insights into the intracellular pathways of NPs which lead to their release. Together with other methods, better and safer targeting of NPs could thus be achieved

Here, we developed a protocol for the analysis of the protein corona of exocytosed magnetic core dextran shell NPs. We performed LC-MS proteomic analysis of the proteins in the protein corona. Moreover, we combined the data with an analysis of the exocytosis rate by inductively coupled plasma optical emission spectrometry (ICP-OES) and flow cytometry. Additionally, the influence of a human blood plasma protein corona was investigated to see if a precoating with extracellular proteins influences the exocytosis pathways of the NPs.

6.2 Materials and Methods

Nanoparticles. Magnetic Dextran-coated iron oxide (mgDex) NPs were obtained from CD Bioparticles. The NPs consist of a magnetite core and a crosslinked dextran shell and have a size of 100 nm. They are equipped with a red fluorescence and an amine functional group on their surface.

Protein Corona Preparation. Protein corona preparation was performed prior to incubation of nanoparticles with the cells as previously described from our group with slight adaptions[67, 169, 296]. Therefore, human blood plasma was taken from healthy donors at the Department of Transfusion Medicine Mainz after physical examination and after obtaining written informed consent in accordance with the Declaration of Helsinki. Plasma of ten donors was pooled and stored at -20 °C. The study was approved by the local ethics committee "Landesärztekammer Rheinland-Pfalz" (Bearbeitungsnummer: 837.439.12 (8540-F)). For the protein corona formation, a ratio of 1 mg of NPs per 1 mL of human blood plasma was chosen. The NPs were incubated for 1 h in the plasma at 37 °C to allow a stable protein corona formation. Afterwards, NPs were isolated by a magnet for 10 min. For cellular uptake studies the NPs were washed twice in PBS and then used for cell incubation. For the protein corona analysis, the NPs were washed three times with 1 mL of PBS to receive the hard protein corona and then the proteins in the protein corona were desorbed by adding 100 µL of desorption buffer (2% SDS in 62.5 mM Tris-HCl). After incubation for 5 min at 95 °C, the proteins were separated by centrifugation (5 000x g, 4°C, 10 min). Protein containing supernatant was collected afterwards and further analyzed by protein quantification, SDS PAGE, and LC-MS.

Cell culture. HCT116 cells were obtained from the DSMZ (German Collection of Microorganisms and Cell Cultures GmbH, Germany) and cultured in Dulbecco's modified eagle medium (DMEM) supplemented with 10% FBS, 100 U/mL penicillin, and 100 mg/mL streptomycin. Cells were grown in a humidified incubator at 37 °C and 5% CO2. The cell viability and count were determined with trypan blue by an automated cell counter (TC10, Bio-Rad). Cells were cultured in flasks and sub-cultured once a week when they reached around 80% of confluence. Cell passage number was kept below 15.

Uptake and Exocytosis. The uptake and exocytosis of the NPs were analyzed by ICP-OES and flow cytometry. For the analysis by ICP-OES cells were seeded at a density of $1x10^6$ cells per well in a six-well plate (Greiner, Germany). Cells were incubated overnight in a humidified incubator (37 °C, 5% CO_2). For the analysis by flow cytometry 150 000 cells were seeded in 24-well plates and incubated overnight. One hour before the treatment of the cells with NPs, the cell culture media was removed and replaced with media without FBS. Afterwards, cells were treated with 300 µg/mL of NPs in DMEM without FBS for either 2 h or 24 h. NPs were used either with a preformed protein corona or without a

protein corona. After the incubation time, the NP solution was removed and the cells were washed twice with PBS (Thermo Fisher Scientific, Germany). For uptake measurements, the cells were harvested afterwards using Trypsin-EDTA (Thermo Fisher Scientific, Germany) and for exocytosis measurements, cells were incubated again in DMEM without FBS for 2, 6, or 24 h and then washed and harvested. Cells were then prepared for flow cytometry or ICP-OES analysis.

Flow Cytometry Analysis. After harvesting, the cells were centrifuged (300× g, 5 min) and the supernatant was removed. Before analysis, a viability staining using Zombie Aqua™ (Biolegend) was applied according to the manufacturer's manual. Therefore, cells were resuspended in a 1:500 dilution of Zombie Aqua™ in PBS and incubated at 4 °C for 15 min. After centrifugation (300× g, 5 min) the supernatant was removed and the cells were resuspended in 1 mL PBS. Analysis was performed at an Attune Nxt Flow cytometer. Therefore, the cell population was selected in a FSC/SSC scatter plot and 10 000 events for the cells were recorded. The NP signal was recorded using the YL 1 channel with an excitation laser of 561 nm and a band-pass filter of 585/16 nm. The viability signal was recorded using the VL2 channel with an excitation laser of 405 nm and a 512/25 nm band pass filter for emission. Data procession and analysis were performed with the Attune NxT Software. For cell viability the % gated cells were analyzed and for nanoparticle uptake the % gated cells and median fluorescence intensity were analyzed.

ICP-OES Analysis. For the analysis of the uptake and exocytosis, cells were centrifuged (300 g, 5 min) and the supernatant was discarded. To get a homogenous solution, the cells were either directly treated with 1 mL of aqua regia or sonicated for 10 min in a sonication bath and afterwards the cell pellet was resuspended in 1 mL nitric acid. After incubation overnight on an orbital shaker (300 rpm), the samples were diluted up to 10 mL with MilliQ water. Iron concentration was determined by ICP-OES (SpectroGreen, Spectro/Ametek, Germany). Calibration was performed using 0.1, 0.5, 1, 5, and 20 ppm iron standard solutions (stock 1000 mg/L, Merck, Germany). To verify the same incubation concentration for the samples with and without protein corona the concentration of the nanoparticle solution was determined as well. Additionally, only cell controls were measured to deduct background signals.

Confocal Laser Scanning Microscopy. cLSM experiment was conducted to verify the intracellular localization of the NPs. For the confocal analysis, cells were seeded at a density of 50 000 cells per well in 8-well ibidi dishes and incubated overnight. The cell incubation with nanoparticles was performed in the same manner as in the flow cytometry and ICP-OES experiment. A Leica Laser Scanning Confocal Microscope (LSM SP5 STED Leica, Germany) equipped with a multi-laser combination and five

detectors (range of 400–800 nm) was used. For the detection of the NPs the 514 nm laser was used, and the emission was detected at 565-600 nm. The cell membrane was stained shortly before measurement using 1:1000 dilution CellMask DeepRed (5 mg/mL ThermoFisher Scientific). The CellMask DeepRed was excited with the 633 nm laser and detected at 650–695 nm. Images were taken using LAS AF 3000 software and processed using Image J.

Exocytosis Pathway Analysis. For the exocytosis pathway analysis, the HCT116 cells were seeded in six-well plates at a density of $1x10^6$ cells and incubated overnight. Cells were treated as described for the exocytosis measurements. Instead of harvesting the cells, the cell culture supernatant with the released nanoparticles was collected. The cells were rinsed one time with 500 µl PBS to collect all released NPs. Afterwards the NPs were collected from the cell culture media using a magnet for 10 min. NPs from three wells were combined and washed twice with PBS. The hard corona proteins were detached from the surface of the NPs using a desorption buffer containing 2% (*w*/*v*) SDS and 62.5 mm Tris-HCl. Then the proteins were collected via centrifugation (5000× *g*, 4 °C, 10 min) and used for protein quantification, SDS PAGE, and LC-MS analysis.

Protein Quantification and SDS-PAGE. Protein quantification was performed with the Pierce 660 nm Protein Assay (Thermo Fisher Scientific) according to the manufacturer's recommendations. Protein concentration was measured in a Tecan Infinite M1000 plate reader (Tecan, Switzerland) with a bovine serum albumin (Merck, Germany) calibration curve. After quantification, the proteins were separated by SDS PAGE. Therefore, 2 µg of protein in 26 µL total volume was mixed with 4 µL of NuPAGE Reducing Agent and 10 µL of NuPage LDS Sample Buffer (both Thermo Fisher Scientific, Germany). Afterwards, the samples were loaded on a 10% Bis-Tris-Protein Gel (Thermo Fisher Scientific, Germany) and as a marker SeeBlue Plus2 Pre-Stained (Invitrogen, USA) was added as well. Gel was run at 100 V for 1.25 h in NuPage MES SDS Running Buffer (Thermo Fisher Scientific, Germany). Afterwards, the gels were stained with Pierce Silver Staining Kit (Thermo Fisher Scientific, Germany) according to the manufacturer's protocol.

In-Solution Digestion, Liquid Chromatography-Mass Spectrometry (LC-MS), and Protein Identification. After collecting the protein corona from human plasma or after exocytosis, the protein corona samples were digested and analyzed by LC-MS. In-solution digestion, LC-MS, and protein identification were performed as previously described from our group[67, 102, 175]. In brief, before the digestion of the proteins, SDS was removed using Pierce Detergent Removal Spin Columns (Thermo Fisher Scientific, Germany) according to the manufacturer's description. Then, the proteins were precipitated with the ProteoExtract protein precipitation kit (Merck, Germany) and then solubilized in

RapiGest SF (Waters, USA) in ammonium bicarbonate buffer (50 mM, Sigma-Aldrich, USA). Before digestion, the proteins were reduced with dithiothreitol (5 mM, Sigma-Aldrich, USA) and then alkylated with iodoacetamide (15 mM, Sigma-Aldrich, USA), both in 50 mM bicarbonate buffer. Tryptic digestion was performed overnight at a ratio of 50:1 for protein:trypsin. The digestion was stopped by lowering the pH with 2 µL hydrochloric acid (Sigma-Aldrich) and degradation products of RapiGest SF were removed by centrifugation (14 000× g; 15 min; 4 °C). For absolute protein quantification, the samples were spiked with 50 fmol/µL Hi3 *E.coli.* (Waters, USA) and diluted with 0.1% formic acid.

LC-MS measurements were performed using a nanoACQUITY UPLY system coupled to a Synapt G2-Si mass spectrometer. The system was operated in a positive resolution mode and data-independent acquisition with ion mobility separation was run. A mass-to-charge range of 50-2000 Da, scan time of 1 s, ramped collision energy from 20 to 40 V, and data acquisition of 120 min was set. As references, Glu-Fibriopeptide (150 fmol/µL) and Leu-Enkephalin (200 pg/µL) were used with a flow rate of 0.5 µL/min. Samples were injected at a flow rate of 0.3 mL/min.

Afterwards, data were processed using MassLynx 4.1 and Progenesis QI 2.0 software. For protein identification, a reviewed database downloaded from Uniprot was used and the thresholds for noise reduction were set at 120, 25, and 750 counts for low energy, high energy, and peptide intensity. Requirements for protein identification were set as at least on assigned fragment per peptide, three assigned fragments per protein, and one assigned peptide per protein. TOP3/HI3 approach was used for absolute quantification of each protein in fmol as described[112].

Protein Annotation. For the analysis of the exocytosis pathways, all protein corona proteins with an enrichment of 1.5-fold compared to cell culture supernatant proteins were identified. Functional protein analysis of the enriched proteins was performed with the annotation tool DAVID (Version DAVID2021, https://david.ncifcrf.gov/home.jsp accessed on 26th September 2022)[287, 288]. Enriched proteins were analyzed by functional annotation clustering with the database for GOTERM-CC_FAT with medium classification stringency. As GOTERMS extracellular vesicles, cytoplasmic vesicle part, membrane region, lysosome, and endosome were considered. In these classes, the protein count and the % of these proteins compared to all identified proteins were analyzed. A detailed list of all identified proteins and the DAVID annotation can be accessed via the following link: https://keeper.mpdl.mpg.de/f/923f1bdb719b452fa59a/.

6.3 Results and Discussion

The influence of the protein corona (PC) on the uptake of NPs has been investigated quite often. However, less is known about the secretion or exocytosis of NPs from the cells and even less is known about the influence of a blood plasma PC on it[209]. In this study, we focused on the influence of a PC on the exocytosis of magnetic core shell NPs with a size of 100 nm. The NPs were composed of a magnetite core with a crosslinked dextran shell. These NPs were used as a model nanocarrier due to their ease to handle and since similar nanocarriers have been used many times before for PC and exocytosis applications which allows easy comparability[69, 169, 297, 298]. Before the analysis of the influence of a PC on the exocytosis, the PC of these NPs in human plasma was investigated. Therefore, we incubated the NPs for 1 h at 37 °C in human plasma and analyzed the proteins in the protein corona by LC-MS. In the left part of Figure 6.3.1, it can be seen that mainly serum albumin, coagulation proteins, and immunoglobulins were bound in the PC. In the right part, it can be seen that two proteins, serum albumin and kininogen-1, make up more than 50% of the proteins in the PC. Kininogen-1 is assigned to the coagulation proteins and thus causes the large share of these proteins in the protein groups. Different immunoglobulins are found as well in the top20 of the proteins in the PC, but their concentration is quite low.

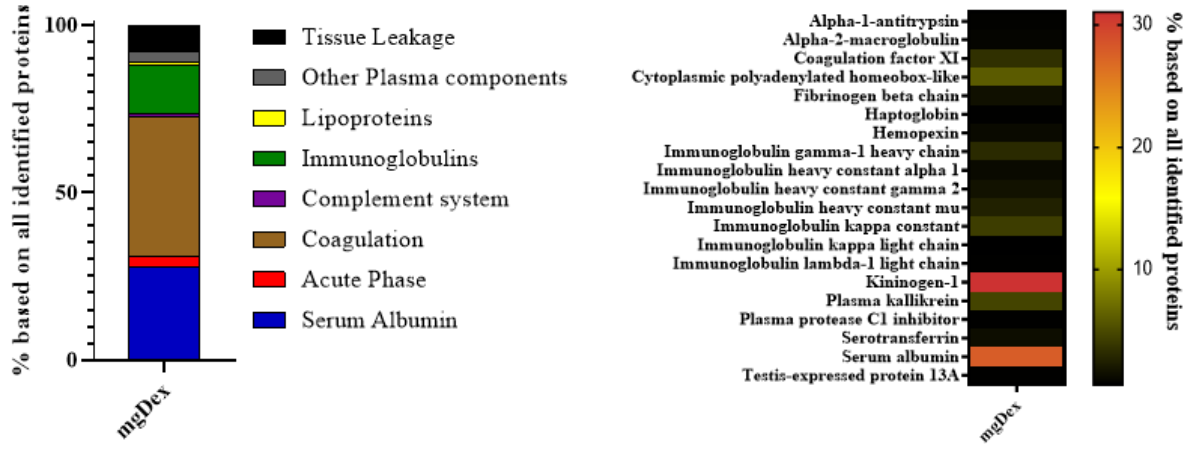

Figure 6.3.1. Proteomic analysis of protein groups and top20 proteins found in the protein corona of mgDex NPs in human plasma. Nanoparticles were incubated in human blood plasma and the protein corona after desorption analyzed by LC-MS. All identified proteins were sorted based on their affiliation to one of the following categories: Serum Albumin, Acute Phase, Coagulation, Complement System, Immunoglobulins, Lipoproteins, Others, Tissue Leakage (staked from bottom to top on the left graphic). Additionally, the top20 proteins in the protein corona are shown in a heatmap (right graphic).

Since the PC is known to influence the uptake and toxicity of NPs, we investigated this effect in the next step (Figure 6.3.2A). The uptake of NPs is usually determined by flow cytometry using the fluorescence properties of the NPs. Here, we tested two different concentrations of the NPs, both with and without PC, and tested two different uptake times as well. This showed that after 2 h of incubation the uptake of the mgDex NPs was higher for the 300 µg/mL incubation solution compared to the lower concentration of 75 µg/mL (Figure 6.3.2A left). However, after 24 h the concentration of the incubation solution

seemed to have no influence anymore and the uptake of the NPs was for both nearly the same. Moreover, the PC did not influence the uptake amount of the NPs and the uptake was the same for the NPs without and with PC. Indeed, it has already been shown that the uptake of dextran coated magnetic NPs is very low and there is no significant difference with a PC[69]. However, no exocytosis measurements have been performed in this study. Viability measurements were performed using ZombieAqua™ as a viability marker. Here, it can be seen that the NPs were not toxic to the cells at both concentrations and at both time points.

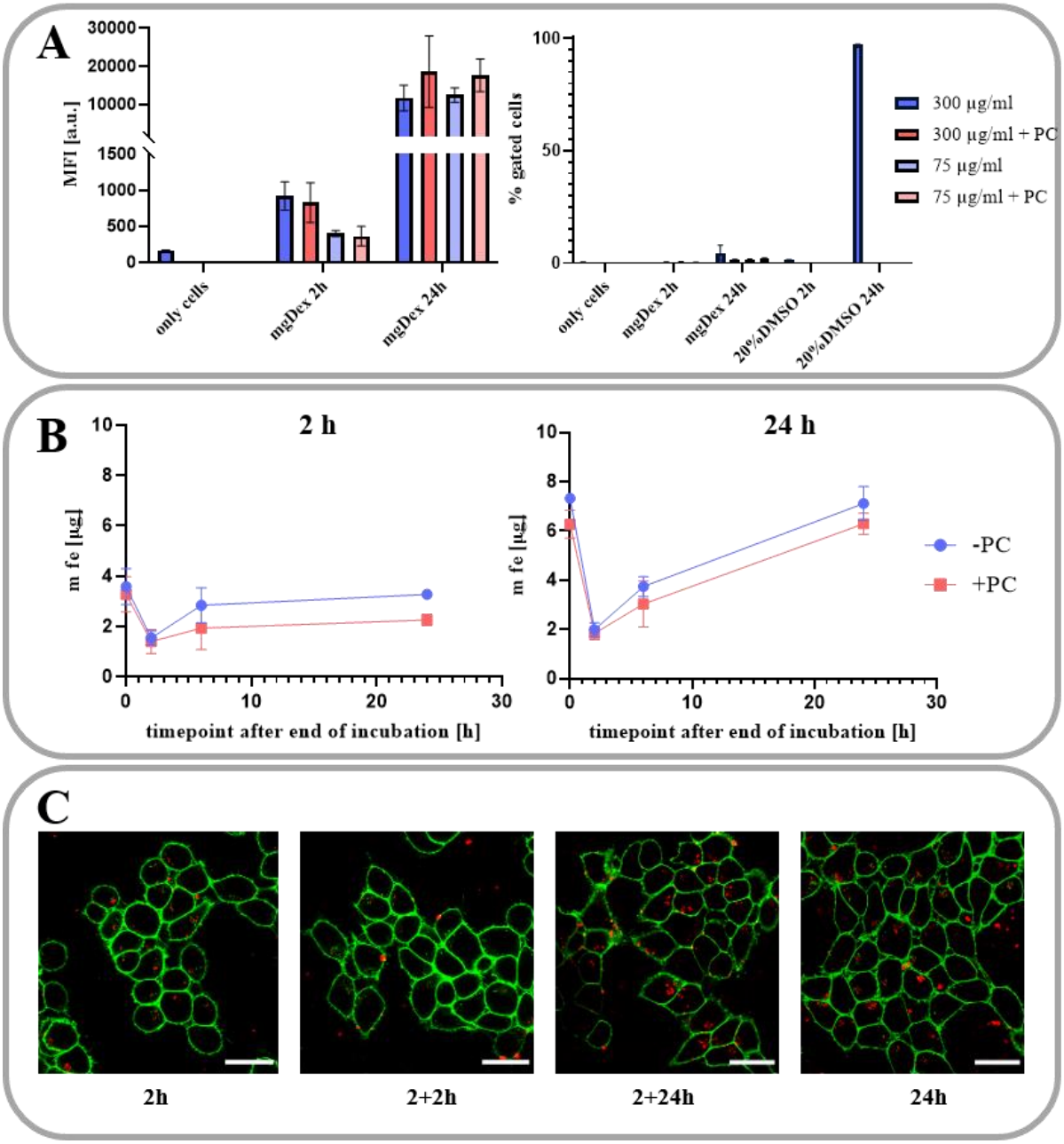

Figure 6.3.2. Uptake and exocytosis analysis of mgDex nanoparticles in HCT116 cells. (A) Uptake (left) and viability (right) analysis of HCT116 cells incubated with either 300 µg/mL or 75 µg/mL of mgDex NPs. Both conditions were analyzed with and without a protein corona from human plasma. Analysis was performed by flow cytometry. n=3 **(B)** Exocytosis analysis of mgDex NPs with ICP-OES. The exocytosis is shown after 2 h of uptake (left) and 24 h of uptake (right) (both incubated with 300µg/mL). In each graph the amount of iron is shown per $1x10^6$ cells. n=3 **(C)** Confocal laser scanning microscopy images of HCT116 cells incubated with mgDex NPs without PC after different time points. The cell membrane was stained with Cellmask Deep Red and is pseudocolored in green. Nanoparticles are pseudocolored in red. PC=Protein corona. Scale bars: 25 µm.

The uptake and exocytosis rate of the mgDex NPs in HCT116 cells should also be analyzed by ICP-OES. This method benefits from its independency of a fluorophore and localization of the NPs intracellular[299]. During the intracellular internalization of the NPs in the cells, the NPs get exposed to different conditions e.g. different pHs[300]. These differences can cause a change in the fluorescence intensity of the fluorophore which could leave to false results. By ICP-OES the elemental composition of the samples is determined independently from the localization of the NPs in the cells and thereby the

amount of NPs in the cells can be quantified. Moreover, besides the cells, also the incubation and wash solutions can be analyzed which allows an analysis of the whole process. Here, the six different fractions (incubation solution, supernatant after uptake, both wash solutions, cells, supernatant after cell centrifugation) that can be generated from the uptake were digested with aqua regia and then the amount of iron in the samples was quantified with ICP-OES. In Figure 6.5.1A it can be seen that the incubation solution contained around 205 µg iron in 1 mL and 185 µg iron in 1 mL for the condition without and with PC respectively. For the preparation of the incubation solution, 300 µg/mL of mgDex NPs were used. However, the NPs consist of an iron oxide core and a dextran shell but here only the iron amount is quantified. This leads to the lower concentration determined here. It can also be seen that the amount of NPs was slightly reduced for the condition with PC. Due to the PC preparation and washing, NPs can get washed away leading to a reduced amount of NPs for incubation. With the ICP-OES we are able to measure the incubation solution which makes it possible to take differences in incubation concentrations into account, whereas with other methods such as flow cytometry, this is not possible.

Next, it can be seen that about 150 µg of iron was not taken up into the cells and was still in the supernatant after 24 h of uptake time. In Figure 6.5.1B the percentage of each fraction compared to the incubation solution was calculated. It shows that 77 % and 79 % of the NPs were left in the cell culture media for the conditions without and with PC respectively. After harvesting the cells with trypsin, the cells were centrifuged again and both, the cell pellet and the supernatant after centrifugation, were analyzed. Around 16 to 17 µg of nanoparticles have been taken up into the cells which make up about 8 to 9 % of the incubation solution. The uptake amount is independent from the PC and also from the slight differences in the NP amount in the incubation solution. This leads to the assumption that the cells are saturated and also with a higher concentration of NPs they would not take up more NPs. This was also shown by flow cytometry in Figure 6.3.2A, where also with a lower concentration of NPs the same amount of NPs were taken up after 24 h of incubation. About 10 % of the NPs were removed during the washing steps. The last fraction analyzed was the cell supernatant after centrifugation. Due to the trypsinization of the cells, loosely bound NPs on the surface of the cells can get released. These NPs are not taken up at this time point and would be with further incubation either taken up or released from the cell surface. However, this fraction makes up only between 3-4 % of NPs from the original solution and as it was shown that the cells are probably already saturated, these NPs will not change the intracellular NP concentration drastically. In total 99.3 % and 101.6 % of the amount of iron without and with PC respectively was quantified in the different fractions. This shows that this method works well to quantify the uptake of the particles into the cells.

Besides the uptake of the NPs into the cells, the exocytosis of them from the cells should be quantified as well. Therefore, the cells were washed twice after the respective uptake time and then further incubated with cell culture media for 2 h, 6 h, or 24 h to allow exocytosis and release of the NPs. Afterwards, the cell culture supernatants and the cells were harvested and then the samples were digested with aqua regia to homogenize the samples. Table 6.5.1 shows the amount of iron determined in the

different fractions of the exocytosis samples. Additionally, the total percentage of the recovered NPs in comparison to the amount of NPs after uptake was calculated. Therefore, the amount of iron determined in the cells and in the supernatant after cell centrifugation was used since these NPs could be possibly taken up with further incubation of the cells. In Table 6.5.1 it can be seen that the amount of iron in the cells decreases significantly two hours after the end of the uptake time. However, with further incubation, the intracellular NP amount increased again and after 24 h of further incubation, the amount was even higher than directly after the end of uptake. This shows that the NPs get released from the cells very quickly but can be retaken up from the cells. Moreover, it indicates that with further incubation of the cells, the NPs seem to reaccumulate in the cells. This has also been shown by XXX for silica nanocapsules in HCT116 cells (Figure 6.5.2, unpublished data). Besides focusing on the intracellular amount of the NPs, the amount of NPs in the supernatant should also be determined. It seemed that the NP concentration in the supernatant after 2 h and 6 h of exocytosis is higher, indicating a high exocytosis rate and it decreases after 24 h indicating the reuptake of the NPs into the cells. However, in total, the amount of iron determined in the exocytosis samples was higher than the amount determined after uptake. This could be due to an inhomogeneity of the samples which results in the incorrect concentration. Therefore, the method for dissolving the samples has been adapted for further experiments.

In the next step we investigated the exocytosis rate of the NPs from the HCT116 cells with an adapted protocol for the digestion of the cells (Figure 6.3.2B). We chose to incubate the cells with 300 µg/mL of NP solution since the uptake of the NPs at this concentration after 2 h was higher and the condition did not show any toxicity. With that, we assume that the higher loading could be better for analysis although when a significant amount of NPs is exocytosed. The dissolution of the cells has been adapted with a sonication of 10 min followed by digestion in nitric acid according to previously reported protocols[239, 301]. This should ensure better homogeneity of the samples. Moreover, the calibration procedure of the ICP-OES was adapted to trace analysis using a sample preparation correction to achieve a higher accuracy. Here, only the intracellular amount of the NPs was determined to investigate the exocytosis behavior of the NPs. In Figure 6.3.2B it can be seen that the intracellular iron amount directly decreases after the uptake. After two hours of exocytosis, the NPs get released from the cells. However, with further incubation, the amount of iron in the cells increases again and reaches after 24 h nearly the same amount as directly after the uptake. This shows that the NPs are released fast from the cells but with further incubation the NPs can get taken up again. Moreover, the absence of reaching a plateau or a second decrease of iron amount might indicate that the NPs then remain stable in the cell. Potentially, this could mean that intracellular pathways are more likely to be involved immediately after uptake, leading to the release of the particles, whereas additional prolonged incubation may favor other pathways that promote longer retention in the cell. The uptake of the NPs with and without PC was nearly the same and the trend of the decrease could be observed both with and without PC. There was a trend, however, that the intracellular particle concentration increased faster and the reuptake was faster

when no PC was present on the particles. The decrease in the intracellular NP amount could also be observed by cLSM (Figure 6.3.2C). After 2+2 h of incubation, the lowest amount of intracellular NPs could be observed but after 2+24 h of incubation again more NPs can be seen.

To analyze which pathways are involved in the secretion of the NPs, we analyzed the PC around the NPs after their exocytosis in the next step. Therefore, we incubated the cells for 2 h or 24 h with the NPs as described and harvested the NPs from the supernatant after the additional incubation for 2 h, 6 h, and 24 h. After desorption of the proteins from the NPs surface, we analyzed the protein composition in a first step by SDS-PAGE. Additionally, the cell culture supernatant without NPs in the solution was analyzed as a reference and a negative control was performed to control the suitability of the process. In Figure 6.3.3 the SDS-PAGEs of the extracellular protein corona (ePC) samples are shown. For the NPs without a PC from human plasma, many different protein bands were detected, and they are very similar at the different time points. Only in condition 24+2 and slightly in condition 2+6 a significantly lower diversity and lower protein concentration is observed. Between 2 h and 24 h of cellular uptake time, the differences are very small. The band pattern of the cell culture supernatant is even more complex than the protein corona samples. This indicates that only specific proteins were bound to the NPs surface. In the negative control, only a few proteins in a low concentration could be detected leading to the assumption that it is most likely that contamination due to sample production can be excluded. Comparing the protein band pattern with the one from the ePC with a PC from human plasma, it can be seen that after 2 h of uptake less bands and proteins were detected for the +PC condition. Only after 2+24 h more bands were detected, and the protein pattern seems to be more complex then. In the +PC samples after 2+2 and 2+6 h, one prominent band can be observed at around 66 kDa. This could be serum albumin which was already shown to be a prominent protein in the PC from human plasma. After the longer uptake time of 24 h, the band pattern is equal to the one without a PC from human plasma. This could indicate that the ePC is initially very similar to the plasma PC, but with a longer incubation period, more and more proteins can be exchanged on the surface and intracellular proteins can accumulate. The fact that the PC is a dynamic process has already been shown as well as that the protein corona is constantly changing intracellularly and adapting to the pathway[242, 243].

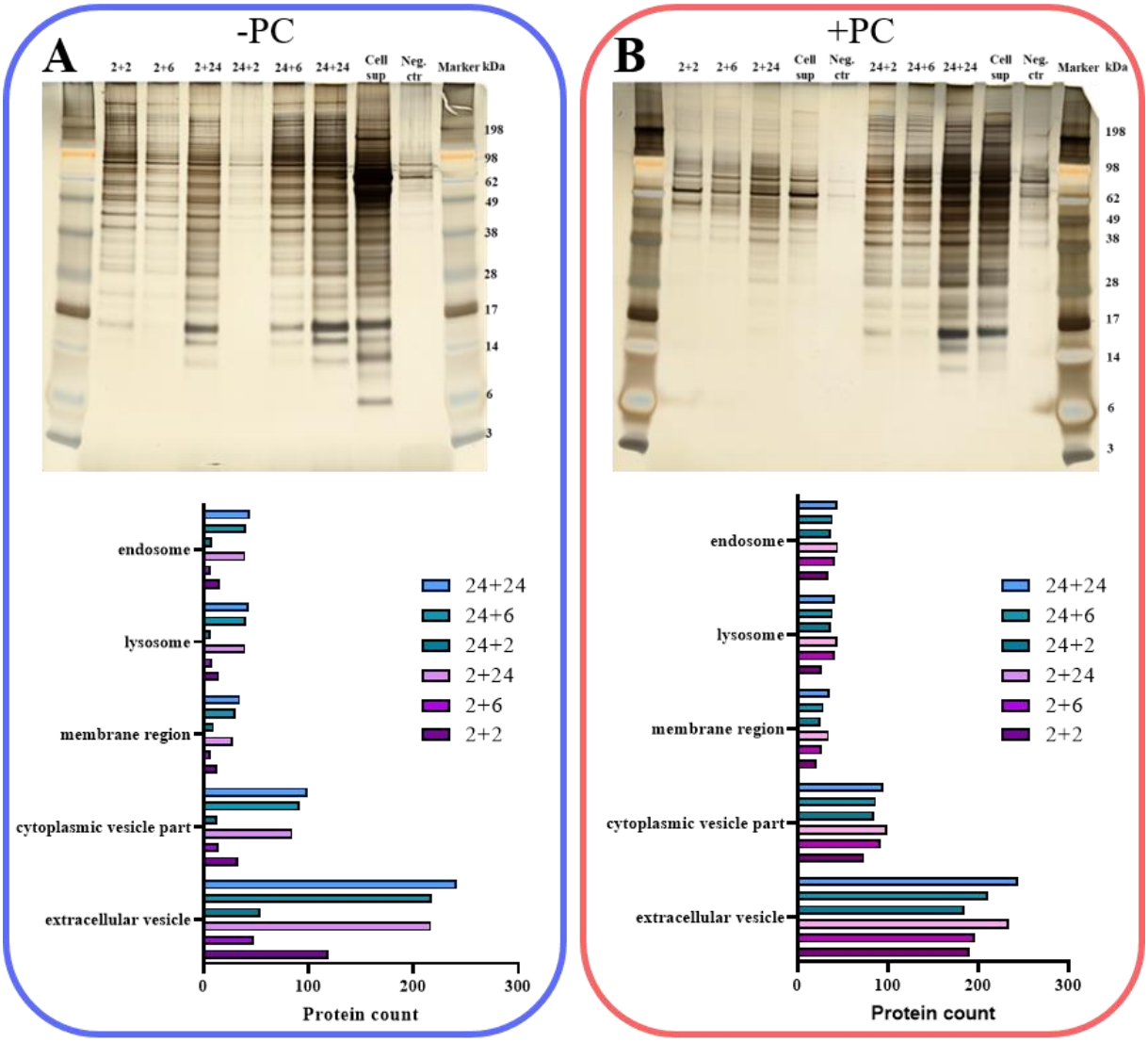

Figure 6.3.3. Protein corona analysis of exocytosed nanoparticles after incubation with HCT116 cells. SDS PAGE and DAVID annotation of proteins in protein corona after incubation of mgDex NPs without (A) or with (B) protein corona in HCT116 cells. For SDS PAGE proteins were desorbed from the released NPs and added onto the SDS PAGE. For DAVID analysis proteins were after desorption analyzed by LC-MS and 1.5-fold enriched proteins were assigned to selected intracellular compartments using DAVID-based functional annotation clustering by GOTERM_CC_FAT. PC=Protein corona.

To analyze the protein composition more in detail, we performed quantitative LC-MS proteomics and determined the proteins that were 1.5-fold enriched in comparison to the cell culture supernatant. Afterwards, the enriched proteins were annotated to the five different GOTERMs extracellular vesicles, cytoplasmic vesicle part, membrane region, lysosome, and endosome using the annotation tool DAVID. We have chosen these GOTERMS since many proteins were assigned to them and because of their importance for the analysis of the exocytosis pathways. In Figure 6.3.3 the protein count for each GOTERM at each time point is shown. For the NPs without a plasma PC (Figure 6.3.3A) it can be seen that the groups with the highest protein count are the extracellular vesicles and cytoplasmic vesicle part. Moreover, it can be seen that the protein count of the enriched proteins varies between the different time points. For the extracellular vesicles, the highest protein count can be observed for the 24+24 condition followed by 24+6 and 2+24 conditions. The lowest protein count can be observed for the 2+6 and 24+2

conditions. The same counts for the other GOTERMS show that at specific time points the ePC is enriched with proteins determining the exocytosis pathway of the NPs. However, when a PC from human plasma has already been present before the uptake of the NPs, the GOTERM with the highest protein count is always extracellular vesicles (Figure 6.3.3B). Moreover, the differences between the time points are not that distinct anymore. The conditions 24+24 and 2+24 still have the highest protein count which suggests that the particles that were exocytosed at this late stage are specifically located in the extracellular vesicles.

As the next step we identified the proteins that were specifically assigned to these GOTERMs and then identified the TOP10 proteins for each time point. In Figure 6.3.4 and Figure 6.5.3-Figure 6.5.6 the heatmaps of the combined TOP10 proteins for each GOTERM are shown. Moreover, the percentage based on all identified proteins for each GOTERM was calculated. As already seen for the protein count, the conditions 2+6 and 24+2 seem to have a different composition of protein concentrations for the GOTERM extracellular vesicles as at the other time points (Figure 6.3.4). Remarkable is that after 2+6 and after 24+2 h for -PC the concentration of plectin, stress-70 protein_mitochondrial and syntaxin-7 is higher than at the other time points. On the opposite, the concentration of heat shock proteins, histones, and actin is decreased at these time points. However, also after 2+2 h, the ePC composition looks slightly different with a high concentration of histone H4 and a high concentration of syntaxin-7 as well. While syntaxin-7 is a protein involved in the exocytosis of lysosomes, heat shock proteins are known to be involved in the secretion of exosomes[302, 303]. Moreover, actin related proteins and histones are as well assigned to be involved in the biogenesis of extracellular vesicles[304, 305]. Depending on the time point of exocytosis different pathways seem to be more favored for the secretion of the NPs. With the human plasma PC on the NPs before, the differences in protein corona get weaker. However, after 2+6 and 24+2 h now serum albumin was detected on the exocytosed NPs. This indicates that these NPs still carry parts of the plasma PC and may have been exocytosed for this reason.

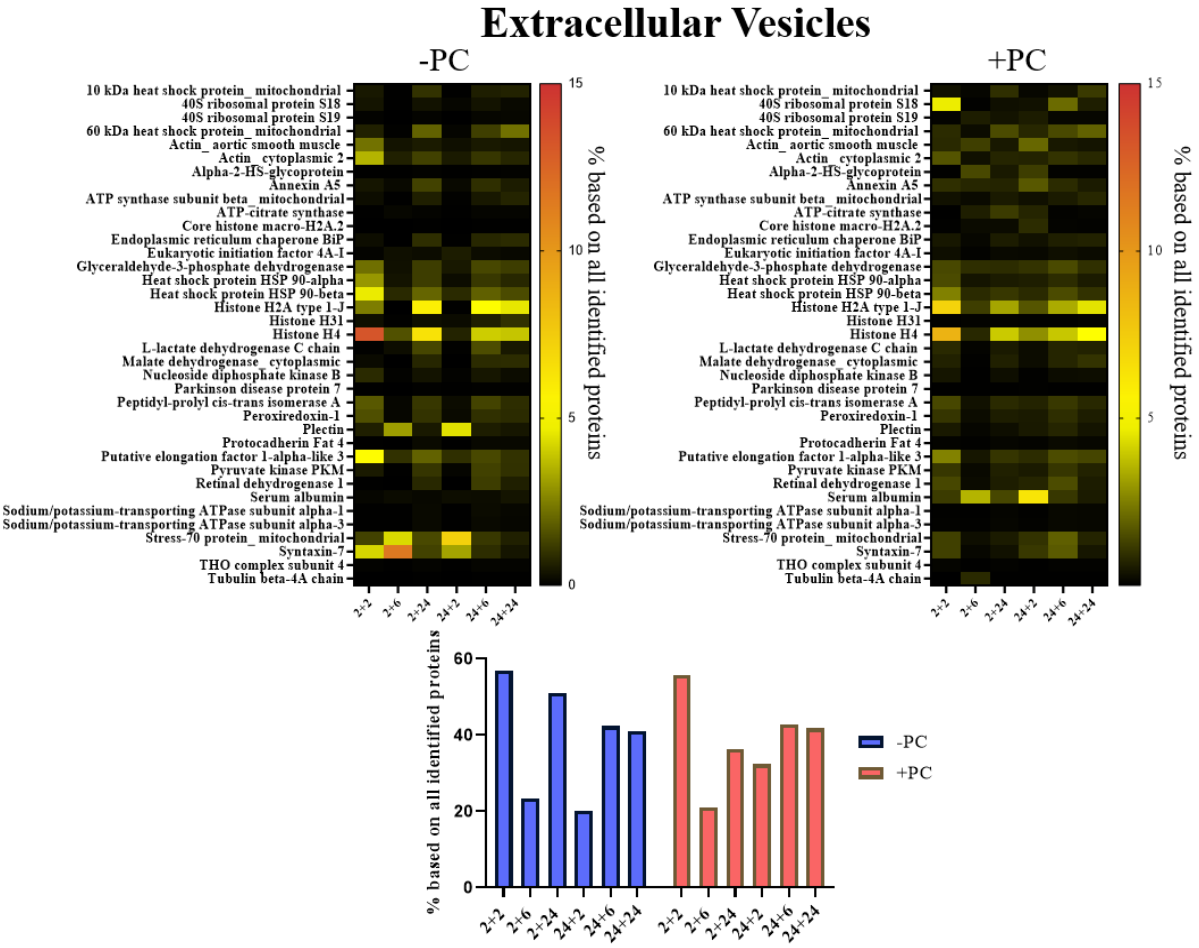

Figure 6.3.4. Annotation of the proteins in the extracellular protein corona of mgDex NPs to the GOTERM extracellular vesicles. Heatmap of all proteins assigned to the extracellular vesicles GOTERM without (left) or with (right) protein corona from human plasma. Different incubation time points are displayed in both heatmaps. Additionally, the % of proteins annotated to extracellular vesicles based on all identified proteins is shown for all conditions. PC=Protein Corona.

Considering the concentration of all the proteins that were assigned to the extracellular vesicles group, interestingly the conditions 2+6 and 24+2 h -PC and 2+6 +PC have the lowest percentage of all identified proteins. After 2 h of uptake and 6 h of exocytosis, the protein amount assigned to extracellular vesicles is low compared to the other exocytosis time points after 2 h of uptake. At this time point, an increasing intracellular NP amount and less exocytosis was measured by ICP-OES. Combining this data, we suggest that at this time point the NPs are more likely to be taken up and be internalized in the cells and not be exocytosed. Moreover, the NPs that get exocytosed at these time points are more likely to be excreted via lysosomal pathways or exocytosis from endosomes as high concentrations of these proteins based on all identified proteins could be found at these time points (Figure 6.5.5 and Figure 6.5.6). A non-specific release of NPs after 2+6 h is also supported by the fact that only very few membrane region proteins could be found at this time point (Figure 6.5.4). Interestingly, the presence of a plasma PC seems to influence the enrichment of specific proteins in the ePC (e.g. syntaxin-7 and V-type protein ATPase) but rather have a low influence on the exocytosis rate and involved exocytosis pathways. Lysosomal secretion of NPs has also been reported by Yanes et al[239]. In this study, the preferred

exocytosis pathway via lysosomal secretion was time independent. However, Ho et al. reported that alkylated gold NPs were mainly exocytosed via extracellular vesicles[240] and Strobel et al. reported the exocytosis of cerium dioxide NPs through endosomes and Golgi transport[301]. However, all these studies were mainly performed by imaging or by the inhibition of specific intracellular pathways. The application of proteomics for tracking the exocytosis pathways could give new insights and can help to better understand the intracellular interactions of NPs and cells.

6.4 Conclusion

Here we demonstrated that the proteomic approach can be used for the tracking of the exocytosis pathways of magnetic dextran nanoparticles. After 2 h of uptake and 6 h of exocytosis the NPs are more likely exocytosed via lysosomal exocytosis and non-vesicle related secretion through endosomal escape. However, after 2 h and 24 h of exocytosis, the nanoparticles are exocytosed in or with extracellular vesicles and the exocytosis rate is the highest after 2 h. The presence of a protein corona from blood plasma did not have a significant influence on the uptake rate or the exocytosis pathways for these NPs. With this study, a first step was made to use proteomics for the exocytosis analysis of NPs. In the future, this may help to better understand the interactions of NPs with cells and their pathways.

6.5 Supporting information

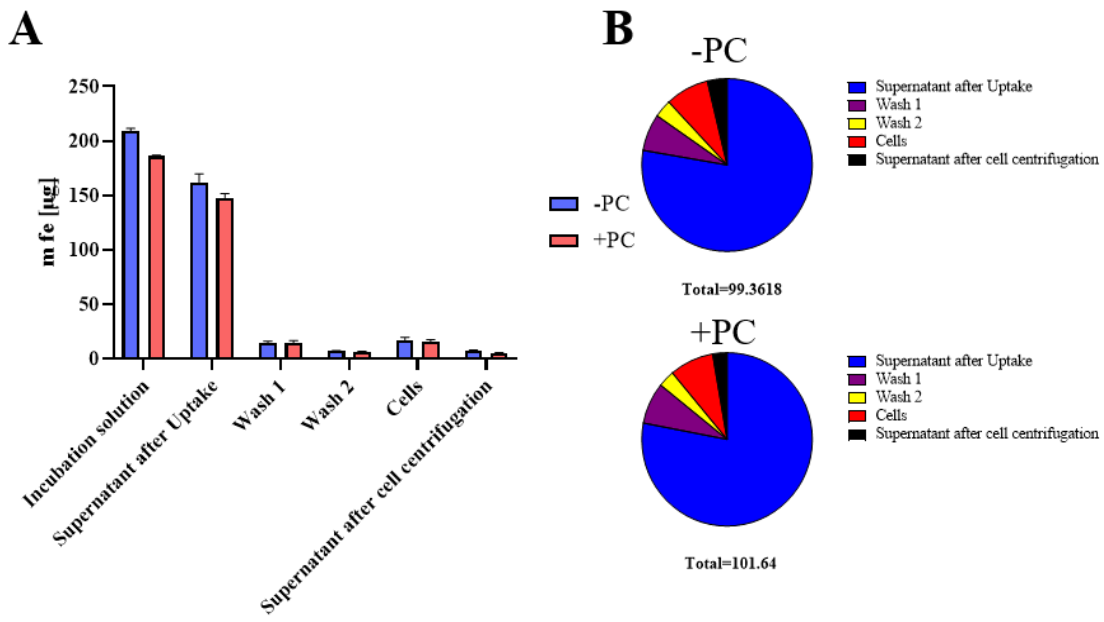

Figure 6.5.1. Uptake analysis of mgDex NPs determined by ICP-OES. (**A**) Analysis of different fractions after incubation with 300 µg/mL of mgDex NPs with HCT116 cells for 24 h. Fractions were harvested and digested with aqua regia before analysis by ICP-OES. All fractions were analyzed without and with a preformed protein corona in human plasma. As fractions the remaining NPs in the supernatant after uptake, both wash solutions, the cells, and the supernatant after cell centrifugation were analyzed. (**B**) Additionally, the percentage of the fractions comparing to the NP incubation solution were calculated. PC=Protein Corona. n=3

Table 6.5.1. Exocytosis analysis of different fractions containing mgDex NPs determined by ICP-OES. HCT116 cells were incubated with 300 mg/mL of mgDex NPs for 24 h without (blue) and with (red) a preformed protein corona in human plasma. Afterwards. NPs were washed away and cells incubated with cell culture media to allow exocytosis. Samples were dissolved in aqua regia for digestion. The amount of iron was then determined in the cells, in the supernatant, and in the cell supernatant after centrifugation. Additionally, the percentage comparing to the uptake was calculated. PC=Protein corona. n=3

	Sample	**Amount in cells [pg/cell]**	**Amount in supernatant (exocytosed) [pg/cell]**	**Amount in supernatant after cell centrifugation [pg/cell]**	**Total (cells + supernatants) [pg/cell]**	**% of uptake**
-PC	Uptake in cells	17.26	-	7.77	25.02	
	2 h Exocytosis	8.59	11.72	5.00	25.31	101.15
	6 h Exocytosis	10.43	16.66	3.90	30.99	123.84
	24 h Exocytosis	19.13	3.45	4.09	26.67	106.59
+PC	Uptake in cells	15.89	-	5.14	21.03	-
	2 h Exocytosis	5.87	12.92	3.13	21.92	104.24
	6 h Exocytosis	7.26	16.20	2.61	26.08	123.98
	24 h Exocytosis	17.49	3.29	2.86	23.65	112.42

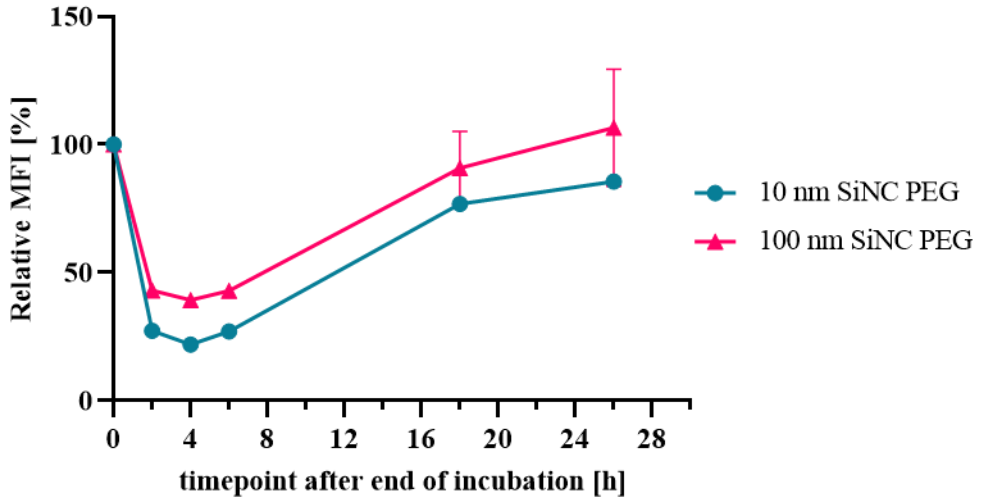

Figure 6.5.2. Uptake and exocytosis of silica nanocapsules from HCT116 cells. Incubation of HCT116 cells with 200 µg/ml of different PEGylated silica nanocapsules (SiNC) for 2h. Afterwards, SiNCs were removed and cells further incubated to allow exocytosis. Intracellular median fluorescence intensity (MFI) was determined by flow cytometry and the MFI after uptake was set as 100%. Values of exocytosis samples were calculated depending on the MFI of the uptake. Results reprinted from XXX (unpublished data). n=3

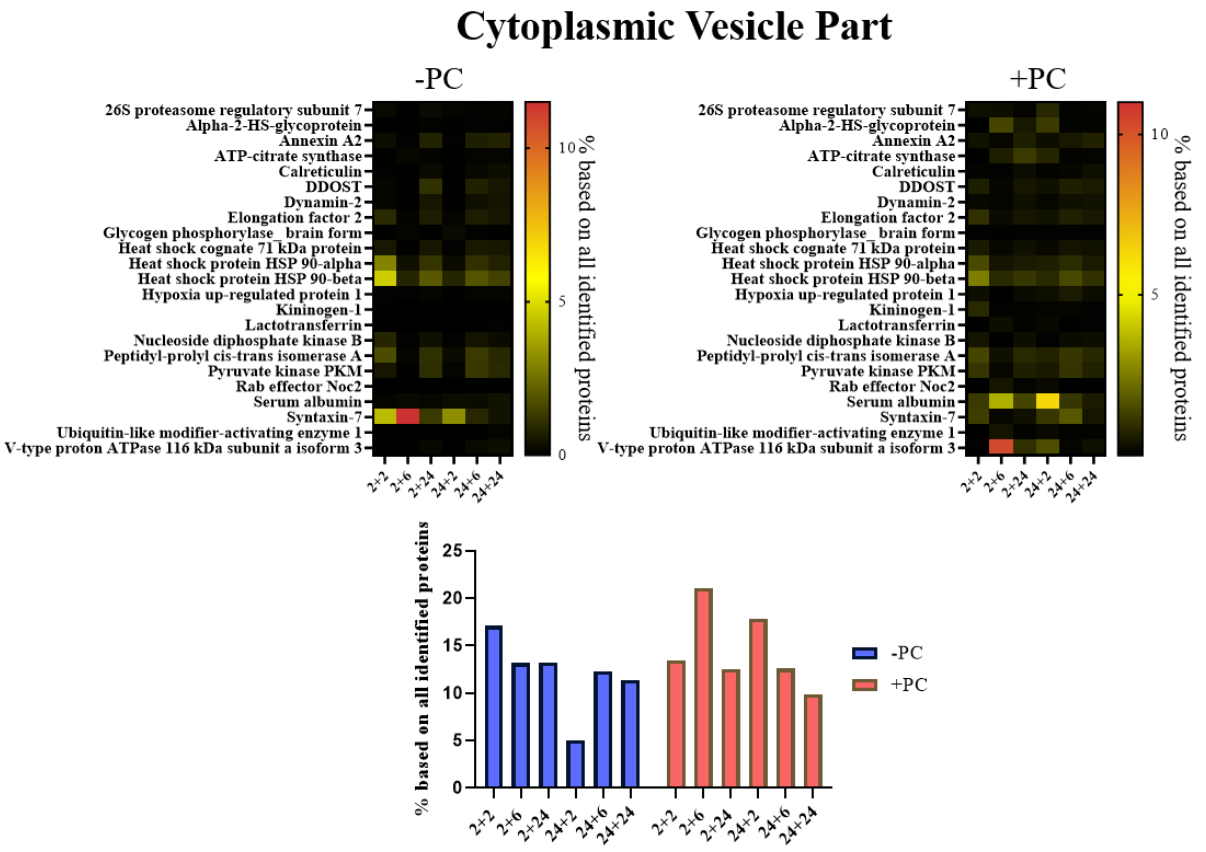

Figure 6.5.3. Annotation of the proteins in the extracellular protein corona to the GOTERM cytoplasmic vesicle part. Heatmap of all proteins assigned to the cytoplasmic vesicle part GOTERM without (left) or with (right) protein corona from human plasma before cell uptake. Different incubation time points are displayed in both heatmaps. Additionally, the % of proteins annotated to cytoplasmic vesicle part based on all identified proteins is shown for all conditions. PC=Protein corona.

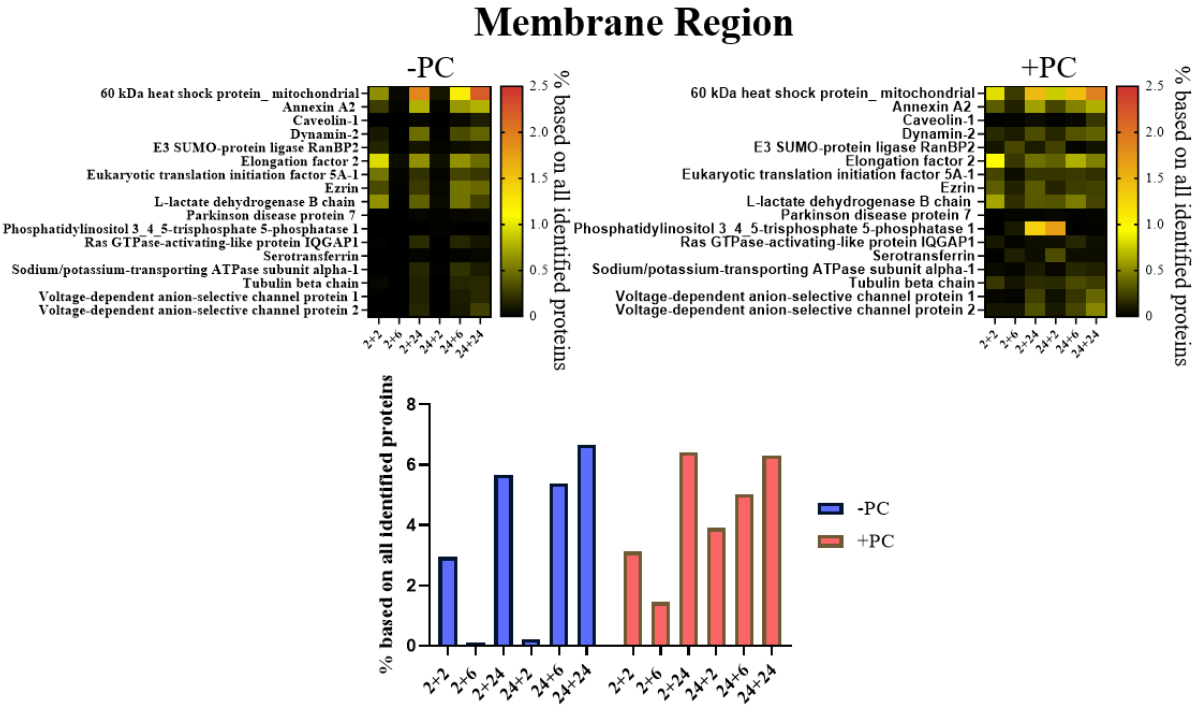

Figure 6.5.4. Annotation of the proteins in the extracellular protein corona of mgDex NPs to the GOTERM membrane region. Heatmap of all proteins assigned to the membrane region GOTERM without (left) or with (right) protein corona from human plasma before cell uptake. Different incubation time points are displayed in both heatmaps. Additionally, the % of proteins annotated to membrane region based on all identified proteins is shown for all conditions. PC=Protein corona.

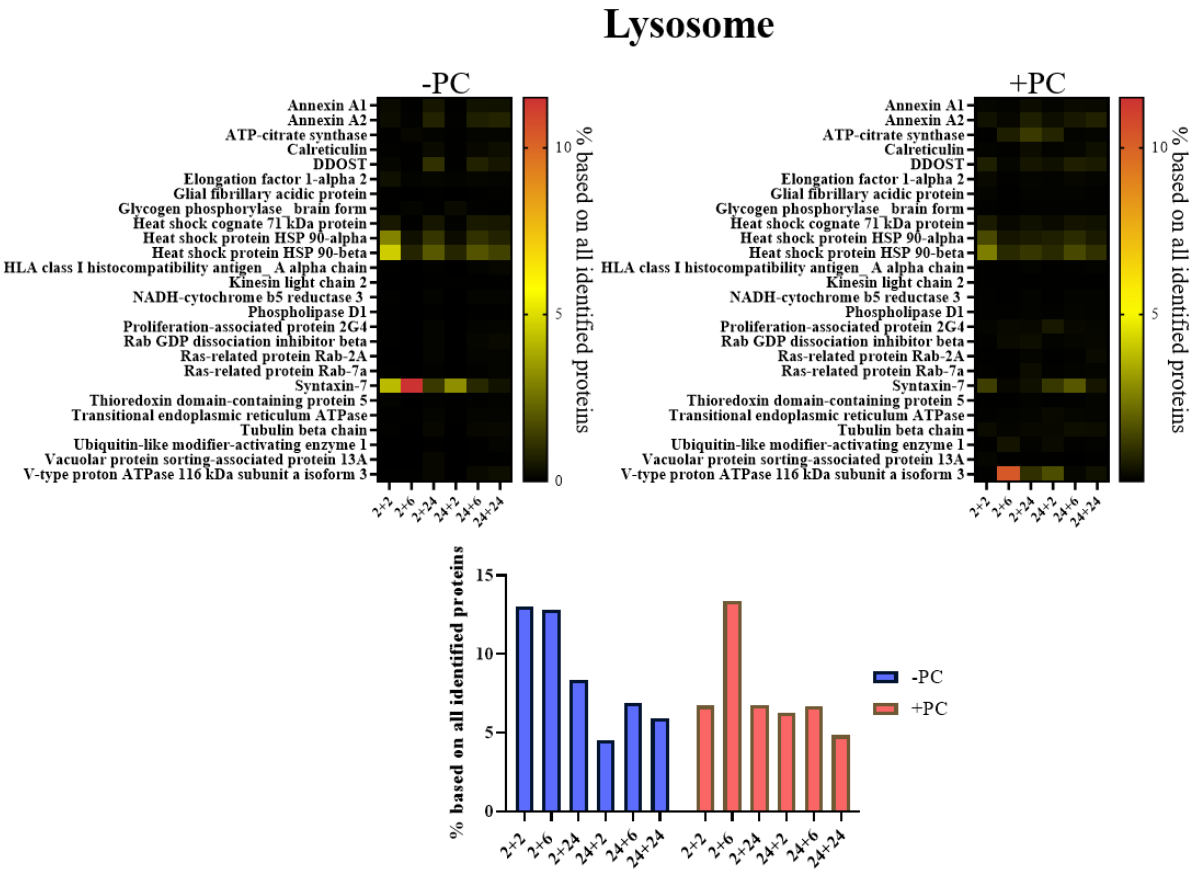

Figure 6.5.5. Annotation of the proteins in the extracellular protein corona of mgDex NPs to the GOTERM lysosome. Heatmap of all proteins assigned to the lysosome GOTERM without (left) or with (right) protein corona from human plasma before cell uptake. Different incubation time points are displayed in both heatmaps. Additionally, the % of proteins annotated to lysosome based on all identified proteins is shown for all conditions. PC=Protein corona.

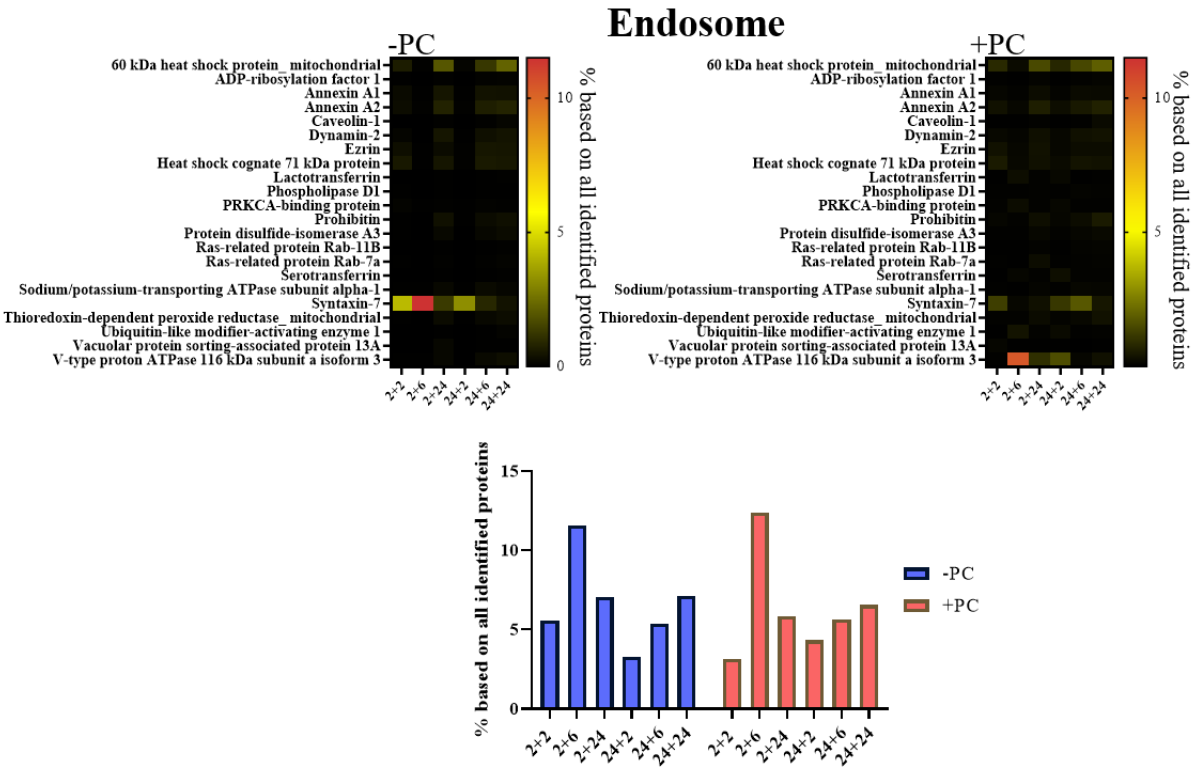

Figure 6.5.6. Annotation of the proteins in the extracellular protein corona of mgDex NPs to the GOTERM endosome. Heatmap of all proteins assigned to the endosome GOTERM without (left) or with (right) protein corona from human plasma before cell uptake. Different incubation time points are displayed in both heatmaps. Additionally, the % of proteins annotated to endosome based on all identified proteins is shown for all conditions. PC=Protein corona.

Chapter C – Further applications of proteomics and ICP-OES

In addition to the applications of ICP-OES and proteomics shown in detail so far, I contributed in different additional projects during my PhD. The results of these projects (Publications [5]-[10]) are either published, submitted, or should be submitted soon. The abstract of these publications and the contribution to the project of each author is indicated.

[5] Amphiphilic dendrimers control protein binding and corona formation on liposome nanocarriers

Copyright:

Abstract:

Amphiphilic polyphenylene dendrimers (PPDs) with distinct lipophilic and positively or negatively charged surface groups were adsorbed onto liposomes and their impact on protein adsorption in blood plasma was studied. The PPD corona reduced binding of specific opsonins and increased the adsorption of proteins controlling cellular uptake based on their surface patches.

Contribution:

I performed the coating and protein corona analysis of the dendrimer coated liposomes with different concentrations. XXX and XXX synthesized the dendrimers. The protein corona analysis of the liposomes and polystyrene nanoparticles coated with the different dendrimers has been performed by XXX. The project was supervised by XXX, XXX, XXX, XXX, and XXX.

[6] Transparent polycarbonate coated with CeO_2 nanozymes repel *Pseudomonas aeruginosa* PA14 biofilms

Copyright:

The following part is based on the publication: XXX, XXX, XXX, **Jennifer Oberländer**, XXX, XXX, XXX, XXX, XXX, XXX, XXX, XXX. Transparent polycarbonate coated with CeO_2 nanozymes repel *Pseudomonas aeruginosa* PA14 biofilms. *Nanoscale*, **2022**, 14 (1), 86-98.

Abstract:

Highly transparent CeO_2/polycarbonate surfaces were fabricated that prevent adhesion, proliferation, and the spread of bacteria. CeO_2 nanoparticles with diameters of 10–15 nm and lengths of 100–200 nm for this application were prepared by oxidizing aqueous dispersions of $Ce(OH)_3$ with H_2O_2 in the presence of nitrilotriacetic acid (NTA) as the capping agent. The surface-functionalized water-dispersible CeO_2 nanorods showed high catalytic activity in the halogenation reactions, which makes them highly efficient functional mimics of haloperoxidases. These enzymes are used in nature to prevent the formation of biofilms through the halogenation of signaling compounds that interfere with bacterial cell–cell communication ("quorum sensing"). Bacteria-repellent CeO_2/polycarbonate plates were prepared by dip-coating plasma-treated polycarbonate plates in aqueous CeO_2 particle dispersions. The quasi-enzymatic activity of the CeO_2 coating was demonstrated using phenol red enzyme assays. The monolayer coating of CeO_2 nanorods (1.6 $\mu g/cm^2$) and the bacteria repellent properties were demonstrated by atomic force microscopy, biofilm assays, and fluorescence measurements. The engineered polymer surfaces have the ability to repel biofilms as green antimicrobials on plastics, where H_2O_2 is present in humid environments such as automotive parts, greenhouses, or plastic containers for rainwater.

Contribution:

I performed the cell viability measurement for the CeO_2 nanoparticles under the supervision of XXX. XXX developed the concept, performed the plasma treatment, contact angle measurements, SEM images, and together with XXX TLCMS measurements. XXX synthesized the nanoparticles, performed the haloperoxidase assay, TEM, BET surface area and ζ-potential measurement. XXX performed the biological evaluation and XXX AFM measurements. XXX did the HRTEM measurements and the ICP-MS analysis was performed by XXX and XXX. Manuscript correction and scientific supervision was done by XXX and XXX.

[7] A new methodology combining QCM-D and proteomic profiling enables characterization of protein adsorption on 2D surfaces

Copyright:

Abstract:

One of the critical features of biomedical material design is controlling the plasma protein adsorption to modulate the material behavior in biological media. Protein adsorption is highly influenced by the material surfaces and the proteins present in the biological medium. Thus, it is necessary to study protein-surface interactions that eventually take place on nanomaterials introduced into the body by the use of human plasma. However, very little information is available about human plasma interaction with planar surfaces under physiological conditions. Due to the limitation of the current characterization techniques to investigate the complicated interaction between the complex milieu of plasma proteins and planar materials, most efforts have focused on single proteins. To face this challenge, we have developed a new methodology based on the combination of quartz crystal microbalance with dissipation monitoring (QCM-D) and liquid chromatography coupled with mass spectrometry (LC-MS) to obtain information about protein-surface interactions on planar surfaces. First, QCM-D allowed us to determine the adsorbed protein mass and layer thickness. After detaching the proteins by a surfactant treatment, LC-MS analysis revealed the proteomic profile. Here, we have investigated three base materials, polystyrene (PS), gold (Au), and silica (SiO2) with or without precoating and compared the protein profiles.

Contribution:

I and XXX performed the protein corona analysis by LC-MS. XXX developed the concept, prepared the manuscript and protein corona samples, and performed QCM-D experiments. The project was supervised by XXX, XXX, and XXX.

[8] Proteomics-guided intracellular trafficking analysis reveals time-dependent protein corona changes and the intracellular pathway.

Copyright:

Abstract:

The intracellular protein corona remains poorly investigated within the field of nanotechnology-biology (nano-bio) interactions. To deeply understand the intracellular protein corona formation and dynamics, we established a workflow to isolate the intracellular protein corona of different nanoparticles - magnetic hydroxyethyl starch nanoparticles (HES NPs) and magnetic human serum albumin nanocapsules (HSA NCs) - and after different uptake time points. This intracellular protein corona defines the direct molecular contact partners of the nanocarrier and is, therefore, a prime target for further drug development We performed label-free quantitative LC MS proteomics to analyze the composition of this intracellular protein corona and correlated our findings to conventional methods for intracellular trafficking of nanocarriers, such as flow cytometry, transmission electron microscopy (TEM), and confocal microscopy (cLSM). In sum, we demonstrated the evolution of intracellular protein corona. The protein corona differed within the different timepoints for the HES NPs with a slow uptake but less for the HSA NCs with a rapid uptake. Furthermore, we selectively identified proteins of interest for intracellular trafficking. These proteins served as an effective “fingerprint” and allowed for a more detailed intracellular pathway reconstruction than the conventional methods. Thus, the analysis of the intracellular protein corona will provide a powerful resource in investigating the intracellular trafficking of nanocarriers for efficient drug delivery or intracellular applications.

Contribution:

In this project, I performed the ICP-OES analysis and the processing of the cLSM images. XXX developed the concept, prepared the manuscript, performed the cLSM imaging, protein corona analysis and uptake studies. XXX synthesized the HSA nanocapsules. XXX supervised the TEM imaging. The project was under supervision of XXX and XXX.

[9] Protein Corona Bio-Inspired Mesenchymal Stem Cells Derived Extracellular Vesicles for Specific Liver Cells Targeting.

Copyright:

Abstract:

Therapeutic potentials of extracellular vesicles (EVs) derived from mesenchymal stem cells (MSCs) have been supported by several liver clinical trials and pre-clinical studies due to their regenerative and immunomodulatory properties. We have previously demonstrated liver accumulation of intravenously administered EVs but knowledge about their cell type-specific distribution in the liver is lacking in addition to concerns being raised regarding rapid clearance by phagocytic cells. Herein, we explore EVs derived using two culturing methods allowing pre-exposure of EVs to different protein environments. We hypothesise that this method can influence EVs' pharmacokinetics by modulating its protein corona (PC). Herein, we report two types of MSC EVs cultured without and with serum, in two-dimensional and three-dimensional cultures, offering EV2D and EV3D, respectively. EVs exhibited matching physico/biochemical properties but different protein compositions. Incubation of EVs with fetal bovine serum (FBS), simulating protein corona (PC) formation upon systemic delivery, resulted in further resolved PC-EV complex patterns, determined by liquid chromatography-mass spectrometry. In healthy mouse models, EV3D and EV2D accumulated in the liver and kidney, respectively. Both EVs showed comparable uptake in Kupffer cells. EV3D, however, exhibited higher uptake in hepatocytes, liver sinusoidal endothelial cells, and stellate cells, compared to EV2D, shown by flow cytometry of digested livers from intravenously injected mice. Quantitative proteomics, gene ontology enrichment analysis, and principal component analysis suggested that the significant enrichment of "influencer" protein in the EVs was responsible for those differences. The finding from this work offers a solution to a critical challenge facing intravenously administered EVs and paves the way towards effortlessly tailoring the PC-EV complex for immune evasion and non-phagocytic cell targeting in the liver and other organs in the future.

Contribution:

XXX developed the concept, performed the experiments, and wrote the manuscript. XXX, XXX, XXX, and XXX supervised the project and provided experimental support. I performed the LC-MS experiments and analysis under the supervision of XXX. XXX developed the concept, designed and supervised the experiments and wrote the manuscript.

[10] Formation of a protein corona on HCT116 extracellular vesicles leads to an increased uptake into human monocytes.

Copyright:

Abstract:

The influence of a protein corona on the uptake of nanoparticles in cells has been demonstrated in various publications over the last years. Extracellular vesicles (EVs), which are natural nanoparticles, attract growing attention as therapeutically effective nanoparticles for different diseases. However, EVs are produced under different cell culture conditions and only less is known about the protein corona of EVs and its influence on the cell uptake. Here, we use a proteomic approach in order to analyze the protein composition of the EVs itself and the protein composition of a human blood plasma protein corona around EVs. Moreover, we analyze the influence of the protein corona on EV uptake into human monocytes and compare it with the influence on the uptake of engineered liposomes. We show that the presence of a protein corona increases the uptake of EVs in human monocytes. This can be attributed to the presence of complement system proteins and immunoglobulins in the protein corona. Our results demonstrate the importance of the protein corona for EV uptake, which helps to use them as a therapeutic reagent in future.

Contribution:

XXX and I performed the conceptualization. XXX isolated and stained the extracellular vesicles and performed protein corona preparation and flow cytometry analysis. I performed the LC-MS preparation and analysis. XXX prepared the liposomes. The project was supervised by XXX and XXX.

Conclusion and outlook

In today's research nanomedicine is attracting more and more attention due to its broad applicability and therefore new nanoparticle formulations are being developed constantly. However, there is still a gap between the development of new nanoparticle formulations and their applicability *in vivo*. One concern is the behavior of nanoparticles after their contact with biomolecule containing fluids and cells. This nano-bio-interface causes that many nanoparticle formulations do not reach their intended goal. Detailed analysis of the interactions of nanoparticles with biomolecules and cells is needed to bridge the gap between the synthesis and the application of new nanoparticles. Therefore, this work focuses on the protein corona around nanoparticles and its influence on the exocytosis of nanoparticles from cells.

In this work, two major topics about the nano-bio interface have been addressed. The formation of a protein corona around nanoparticles is one of the obstacles nanoparticles have to face in their application in medicine. The understanding of this protein corona is essential to understand the behavior of nanoparticles under physiological conditions (**Chapter A**). Furthermore, controlled cellular interactions and controlled retention time in cells are needed for the safe applicability of nanoparticles. Besides their uptake into targeted cells also the release and exocytosis from these cells need to be fully investigated and understood (**Chapter B**). In the following, the main message of each chapter will be highlighted.

In **chapter A** the temperature-dependent protein corona was investigated. We demonstrated in a first study that the incubation of nanoparticles at different concentrations or temperatures led to a change in the uptake amount in HeLa and HUVEC cells. We analyzed the concentration- and temperature-dependent protein corona of five different polystyrene nanoparticles with different surface functionalization and surfactants. With an increasing plasma concentration and temperature, the uptake of the nanoparticles was reduced. This could be attributed to a change in the protein composition in the protein corona. This highlights how important it is to control the conditions of protein corona formation *in vitro* to mimic the *in vivo* situation as best as possible. This ensures a better transferability from pre-clinical studies to *in vivo* studies.

In the second study of **chapter A,** we showed that we were able to specifically catch apolipoproteins from human blood plasma with temperature-responsive nanoparticles. Therefore, we synthesized polystyrene core and poly(N-isopropylacrylamide) (PNIPAM) shell nanoparticles. PNIPAM possesses a lower critical solution temperature in the physiological range which enables its applicability for the catch of proteins. While at temperatures below the lower critical solution temperature the surface of the PNIPAM nanoparticles is hydrophilic, the surface of the nanoparticles is at temperatures above the lower critical solution temperature hydrophobic. This allowed the specific binding of apolipoprotein J (clusterin) from human blood plasma at 25 °C and the catch of apolipoprotein E and apolipoprotein A1 at 37 °C in the protein corona. Moreover, the influence on the stealth effect of the enrichment of apolipoproteins in the protein corona could be shown by analysis of the uptake in HeLa and RAW264.7

cells. Using temperature-responsive materials which enable a specific protein binding on their surface could be used for providing a stealth effect on nanoparticles and for drug delivery applications in the future.

Chapter B deals with the exocytosis of nanoparticles from cells. Depending on the application of nanoparticles, it is necessary that they either remain stable in the cell or are released from the cell. In the first study of this chapter, we investigated the exocytosis of gold nanoparticles from human mesenchymal-like stromal cells. Labeling cells with nanoparticles before the cells are injected into a human body would allow a better tracking of the *in vivo* fate and interactions of these cells. However, therefore the nanoparticles must remain in the cells for a longer time without being exocytosed. We showed that with a longer and higher loading of the nanoparticles in the cells the exocytosis of these particles was significantly reduced compared to a shorter and lower loading. Additionally, we showed through the analysis of the intracellular formed protein corona, that the proteins in the corona change from extracellular FBS proteins to intracellular proteins with time which could lead to the reduced exocytosis. By enabling a more stable and higher loading of cells with nanoparticles, the *in vivo* fate of cells can be better understood in the future.

Ultimately, the last subchapter aims to analyze the influence of a blood plasma protein corona on the exocytosis pathway of nanoparticles from cells. Therefore, a protocol for the analysis of the protein corona of exocytosed nanoparticles was developed. Moreover, with inductively coupled plasma optical emission spectrometry the intracellular amount of nanoparticles could be determined. It could be shown that after a short uptake time and 6 h of exocytosis time the nanoparticles are more likely to be exocytosed *via* lysosomal secretion or non-vesicle related secretion. However, after 2 h, when the exocytosis rate is the highest, the nanoparticles are more likely to be exocytosed *via* a late endosomal and vesicle-related pathway. Moreover, for this nanoparticle and cell combination, it was shown that the protein corona did not influence the exocytosis pathways. This method to analyze the protein corona of exocytosed nanoparticles could help to better understand the intracellular and exocytosis pathways of nanoparticles in the future.

In the future, more work is needed to fully understand the interactions of biomolecules with nanoparticles to reach an efficient translation from the synthesis of nanoparticles to their application. Additionally, new strategies to analyze the intracellular fate and exocytosis of nanoparticles in cells are needed. Nanomedicine offers such a wide range of possibilities and applications and a better understanding of the nano-bio-interface would help to exploit this potential

References

1. Blanco, E.; Shen, H.; Ferrari, M., Principles of nanoparticle design for overcoming biological barriers to drug delivery. *Nature biotechnology* **2015,** *33*, 941-951.
2. Patra, J. K.; Das, G.; Fraceto, L. F.; Campos, E. V. R.; Rodriguez-Torres, M. d. P.; Acosta-Torres, L. S.; Diaz-Torres, L. A.; Grillo, R.; Swamy, M. K.; Sharma, S., Nano based drug delivery systems: recent developments and future prospects. *Journal of nanobiotechnology* **2018,** *16*, 1-33.
3. Hahn, M. A.; Singh, A. K.; Sharma, P.; Brown, S. C.; Moudgil, B. M., Nanoparticles as contrast agents for in-vivo bioimaging: current status and future perspectives. *Analytical and bioanalytical chemistry* **2011,** *399*, 3-27.
4. Pollard, C.; Rejman, J.; De Haes, W.; Verrier, B.; Van Gulck, E.; Naessens, T.; De Smedt, S.; Bogaert, P.; Grooten, J.; Vanham, G., Type I IFN counteracts the induction of antigen-specific immune responses by lipid-based delivery of mRNA vaccines. *Molecular Therapy* **2013,** *21*, 251-259.
5. Geall, A. J.; Verma, A.; Otten, G. R.; Shaw, C. A.; Hekele, A.; Banerjee, K.; Cu, Y.; Beard, C. W.; Brito, L. A.; Krucker, T., Nonviral delivery of self-amplifying RNA vaccines. *Proceedings of the National Academy of Sciences* **2012,** *109*, 14604-14609.
6. Gebre, M. S.; Brito, L. A.; Tostanoski, L. H.; Edwards, D. K.; Carfi, A.; Barouch, D. H., Novel approaches for vaccine development. *Cell* **2021,** *184*, 1589-1603.
7. Mahmoudi, M.; Lohse, S. E.; Murphy, C. J.; Fathizadeh, A.; Montazeri, A.; Suslick, K. S., Variation of protein corona composition of gold nanoparticles following plasmonic heating. *Nano letters* **2014,** *14*, 6-12.
8. Berrecoso, G.; Crecente-Campo, J.; Alonso, M. J., Unveiling the pitfalls of the protein corona of polymeric drug nanocarriers. *Drug Delivery and Translational Research* **2020,** *10*, 730-750.
9. Hadjidemetriou, M.; Kostarelos, K., Evolution of the nanoparticle corona. *Nature nanotechnology* **2017,** *12*, 288-290.
10. Farokhzad, O. C.; Langer, R., Impact of nanotechnology on drug delivery. *ACS nano* **2009,** *3*, 16-20.
11. Mitchell, M. J.; Billingsley, M. M.; Haley, R. M.; Wechsler, M. E.; Peppas, N. A.; Langer, R., Engineering precision nanoparticles for drug delivery. *Nature Reviews Drug Discovery* **2021,** *20*, 101-124.
12. Zielińska, A.; Carreiró, F.; Oliveira, A. M.; Neves, A.; Pires, B.; Venkatesh, D. N.; Durazzo, A.; Lucarini, M.; Eder, P.; Silva, A. M.; Santini, A.; Souto, E. B., Polymeric Nanoparticles: Production, Characterization, Toxicology and Ecotoxicology. *Molecules* **2020,** *25*, 3731.
13. Mitragotri, S.; Lammers, T.; Bae, Y. H.; Schwendeman, S.; De Smedt, S. C.; Leroux, J. C.; Peer, D.; Kwon, I. C.; Harashima, H.; Kikuchi, A., Drug delivery research for the future: expanding the nano horizons and beyond. Elsevier: 2017; pp 183-184.
14. Mahmoudi, M., Debugging nano–bio interfaces: systematic strategies to accelerate clinical translation of nanotechnologies. *Trends in biotechnology* **2018,** *36*, 755-769.
15. Onishchenko, N.; Tretiakova, D.; Vodovozova, E., Spotlight on the protein corona of liposomes. *Acta Biomaterialia* **2021,** *134*, 57-78.
16. Vroman, L., Effect of adsorbed proteins on the wettability of hydrophilic and hydrophobic solids. *Nature* **1962,** *196*, 476-477.
17. Mahmoudi, M.; Moore, A., Implications of biomolecular corona for molecular imaging. *Molecular Imaging and Biology* **2021,** *23*, 1-10.
18. Monopoli, M. P.; Åberg, C.; Salvati, A.; Dawson, K. A., Biomolecular coronas provide the biological identity of nanosized materials. *Nature nanotechnology* **2012,** *7*, 779-786.
19. Mahmoudi, M.; Bertrand, N.; Zope, H.; Farokhzad, O. C., Emerging understanding of the protein corona at the nano-bio interfaces. *Nano Today* **2016,** *11*, 817-832.
20. Monopoli, M. P.; Walczyk, D.; Campbell, A.; Elia, G.; Lynch, I.; Baldelli Bombelli, F.; Dawson, K. A., Physical− chemical aspects of protein corona: relevance to in vitro and in vivo

biological impacts of nanoparticles. *Journal of the American Chemical Society* **2011,** *133*, 2525-2534.
21. Charbgoo, F.; Nejabat, M.; Abnous, K.; Soltani, F.; Taghdisi, S. M.; Alibolandi, M.; Shier, W. T.; Steele, T. W.; Ramezani, M., Gold nanoparticle should understand protein corona for being a clinical nanomaterial. *Journal of controlled release* **2018,** *272*, 39-53.
22. Liu, Y.; Zhong, R.; Zhang, P.; Ma, Y.; Yun, X.; Gong, P.; Wei, J.; Zhao, X.; Zhang, F., Understanding the robust physisorption between bovine serum albumin and amphiphilic polymer coated nanoparticles. *ACS Applied Materials & Interfaces* **2016,** *8*, 2478-2485.
23. Walczyk, D.; Bombelli, F. B.; Monopoli, M. P.; Lynch, I.; Dawson, K. A., What the cell "sees" in bionanoscience. *Journal of the American Chemical Society* **2010,** *132*, 5761-5768.
24. Casals, E.; Pfaller, T.; Duschl, A.; Oostingh, G. J.; Puntes, V., Time evolution of the nanoparticle protein corona. *ACS nano* **2010,** *4*, 3623-3632.
25. Vroman, L.; Adams, A.; Fischer, G.; Munoz, P., Interaction of high molecular weight kininogen, factor XII, and fibrinogen in plasma at interfaces. *Blood* **1980,** *55*, 438.
26. Tenzer, S.; Docter, D.; Kuharev, J.; Musyanovych, A.; Fetz, V.; Hecht, R.; Schlenk, F.; Fischer, D.; Kiouptsi, K.; Reinhardt, C., Rapid formation of plasma protein corona critically affects nanoparticle pathophysiology. In *Nano-Enabled Medical Applications*, Jenny Stanford Publishing: 2020; pp 251-278.
27. Wang, H.; Lin, Y.; Nienhaus, K.; Nienhaus, G. U., The protein corona on nanoparticles as viewed from a nanoparticle-sizing perspective. *Wiley Interdisciplinary Reviews: Nanomedicine and Nanobiotechnology* **2018,** *10*, e1500.
28. Corbo, C.; Molinaro, R.; Parodi, A.; Toledano Furman, N. E.; Salvatore, F.; Tasciotti, E., The impact of nanoparticle protein corona on cytotoxicity, immunotoxicity and target drug delivery. *Nanomedicine* **2016,** *11*, 81-100.
29. Cedervall, T.; Lynch, I.; Lindman, S.; Berggård, T.; Thulin, E.; Nilsson, H.; Dawson, K. A.; Linse, S., Understanding the nanoparticle–protein corona using methods to quantify exchange rates and affinities of proteins for nanoparticles. *Proceedings of the National Academy of Sciences* **2007,** *104*, 2050-2055.
30. Aggarwal, P.; Hall, J. B.; McLeland, C. B.; Dobrovolskaia, M. A.; McNeil, S. E., Nanoparticle interaction with plasma proteins as it relates to particle biodistribution, biocompatibility and therapeutic efficacy. *Advanced drug delivery reviews* **2009,** *61*, 428-437.
31. Lesniak, A.; Fenaroli, F.; Monopoli, M. P.; Åberg, C.; Dawson, K. A.; Salvati, A., Effects of the presence or absence of a protein corona on silica nanoparticle uptake and impact on cells. *ACS nano* **2012,** *6*, 5845-5857.
32. Lesniak, A.; Salvati, A.; Santos-Martinez, M. J.; Radomski, M. W.; Dawson, K. A.; Åberg, C., Nanoparticle adhesion to the cell membrane and its effect on nanoparticle uptake efficiency. *Journal of the American Chemical Society* **2013,** *135*, 1438-1444.
33. Mirshafiee, V.; Kim, R.; Park, S.; Mahmoudi, M.; Kraft, M. L., Impact of protein pre-coating on the protein corona composition and nanoparticle cellular uptake. *Biomaterials* **2016,** *75*, 295-304.
34. Mirshafiee, V.; Mahmoudi, M.; Lou, K.; Cheng, J.; Kraft, M. L., Protein corona significantly reduces active targeting yield. *Chemical communications* **2013,** *49*, 2557-2559.
35. Francia, V.; Yang, K.; Deville, S.; Reker-Smit, C.; Nelissen, I.; Salvati, A., Corona composition can affect the mechanisms cells use to internalize nanoparticles. *ACS nano* **2019,** *13*, 11107-11121.
36. von Roemeling, C.; Jiang, W.; Chan, C. K.; Weissman, I. L.; Kim, B. Y., Breaking down the barriers to precision cancer nanomedicine. *Trends in biotechnology* **2017,** *35*, 159-171.
37. Mahon, E.; Salvati, A.; Bombelli, F. B.; Lynch, I.; Dawson, K. A., Designing the nanoparticle–biomolecule interface for "targeting and therapeutic delivery". *Journal of Controlled Release* **2012,** *161*, 164-174.
38. Pulido-Reyes, G.; Leganes, F.; Fernández-Piñas, F.; Rosal, R., Bio-nano interface and environment: A critical review. *Environmental toxicology and chemistry* **2017,** *36*, 3181-3193.
39. Verma, A.; Stellacci, F., Effect of surface properties on nanoparticle–cell interactions. *small* **2010,** *6*, 12-21.

40. Bilardo, R.; Traldi, F.; Vdovchenko, A.; Resmini, M., Influence of surface chemistry and morphology of nanoparticles on protein corona formation. *Wiley Interdisciplinary Reviews: Nanomedicine and Nanobiotechnology* **2022**, e1788.
41. Docter, D.; Westmeier, D.; Markiewicz, M.; Stolte, S.; Knauer, S.; Stauber, R., The nanoparticle biomolecule corona: lessons learned–challenge accepted? *Chemical Society Reviews* **2015,** *44*, 6094-6121.
42. Giulimondi, F.; Digiacomo, L.; Pozzi, D.; Palchetti, S.; Vulpis, E.; Capriotti, A. L.; Chiozzi, R. Z.; Laganà, A.; Amenitsch, H.; Masuelli, L., Interplay of protein corona and immune cells controls blood residency of liposomes. *Nature communications* **2019,** *10*, 1-11.
43. Gräfe, C.; von der Lühe, M.; Weidner, A.; Globig, P.; Clement, J. H.; Dutz, S.; Schacher, F. H., Protein corona formation and its constitutional changes on magnetic nanoparticles in serum featuring a polydehydroalanine coating: effects of charge and incubation conditions. *Nanotechnology* **2019,** *30*, 265707.
44. Meesaragandla, B.; García, I.; Biedenweg, D.; Toro-Mendoza, J.; Coluzza, I.; Liz-Marzán, L. M.; Delcea, M., H-Bonding-mediated binding and charge reorganization of proteins on gold nanoparticles. *Physical Chemistry Chemical Physics* **2020,** *22*, 4490-4500.
45. Sakulkhu, U.; Mahmoudi, M.; Maurizi, L.; Coullerez, G.; Hofmann-Amtenbrink, M.; Vries, M.; Motazacker, M.; Rezaee, F.; Hofmann, H., Significance of surface charge and shell material of superparamagnetic iron oxide nanoparticle (SPION) based core/shell nanoparticles on the composition of the protein corona. *Biomaterials science* **2015,** *3*, 265-278.
46. Mosquera, J. s.; García, I.; Henriksen-Lacey, M.; Martínez-Calvo, M.; Dhanjani, M. n.; Mascareñas, J. L.; Liz-Marzán, L. M., Reversible control of protein corona formation on gold nanoparticles using host–guest interactions. *ACS nano* **2020,** *14*, 5382-5391.
47. Shao, Q., A computational avenue towards understanding and design of zwitterionic anti-biofouling materials. *Molecular Simulation* **2019,** *45*, 1211-1222.
48. Gessner, A.; Lieske, A.; Paulke, B. R.; Müller, R. H., Functional groups on polystyrene model nanoparticles: influence on protein adsorption. *Journal of Biomedical Materials Research Part A: An Official Journal of The Society for Biomaterials, The Japanese Society for Biomaterials, and The Australian Society for Biomaterials and the Korean Society for Biomaterials* **2003,** *65*, 319-326.
49. Gessner, A.; Waicz, R.; Lieske, A.; Paulke, B.-R.; Mäder, K.; Müller, R., Nanoparticles with decreasing surface hydrophobicities: influence on plasma protein adsorption. *International journal of pharmaceutics* **2000,** *196*, 245-249.
50. Srivastava, I.; Khan, M. S.; Dighe, K.; Alafeef, M.; Wang, Z.; Banerjee, T.; Ghonge, T.; Grove, L. M.; Bashir, R.; Pan, D., On-Chip electrical monitoring of real-time "soft" and "hard" protein Corona formation on carbon nanoparticles. *Small Methods* **2020,** *4*, 2000099.
51. Encinas, N.; Angulo, M.; Astorga, C.; Colilla, M.; Izquierdo-Barba, I.; Vallet-Regí, M., Mixed-charge pseudo-zwitterionic mesoporous silica nanoparticles with low-fouling and reduced cell uptake properties. *Acta biomaterialia* **2019,** *84*, 317-327.
52. Li, B.; Jain, P.; Ma, J.; Smith, J. K.; Yuan, Z.; Hung, H.-C.; He, Y.; Lin, X.; Wu, K.; Pfaendtner, J., Trimethylamine N-oxide–derived zwitterionic polymers: A new class of ultralow fouling bioinspired materials. *Science advances* **2019,** *5*, eaaw9562.
53. Liu, X.; Jin, Q.; Ji, Y.; Ji, J., Minimizing nonspecific phagocytic uptake of biocompatible gold nanoparticles with mixed charged zwitterionic surface modification. *Journal of Materials Chemistry* **2012,** *22*, 1916-1927.
54. Lima, T.; Bernfur, K.; Vilanova, M.; Cedervall, T., Understanding the lipid and protein corona formation on different sized polymeric nanoparticles. *Scientific reports* **2020,** *10*, 1-9.
55. Partikel, K.; Korte, R.; Stein, N. C.; Mulac, D.; Herrmann, F. C.; Humpf, H.-U.; Langer, K., Effect of nanoparticle size and PEGylation on the protein corona of PLGA nanoparticles. *European Journal of Pharmaceutics and Biopharmaceutics* **2019,** *141*, 70-80.
56. Marichal, L.; Klein, G.; Armengaud, J.; Boulard, Y.; Chédin, S.; Labarre, J.; Pin, S.; Renault, J.-P.; Aude, J.-C., Protein corona composition of silica nanoparticles in complex media: Nanoparticle size does not matter. *Nanomaterials* **2020,** *10*, 240.
57. Pant, K.; Pufe, J.; Zarschler, K.; Bergmann, R.; Steinbach, J.; Reimann, S.; Haag, R.; Pietzsch, J.; Stephan, H., Surface charge and particle size determine the metabolic fate of dendritic polyglycerols. *Nanoscale* **2017,** *9*, 8723-8739.

58. Yu, J.; Kim, H.-J.; Go, M.-R.; Bae, S.-H.; Choi, S.-J., ZnO interactions with biomatrices: Effect of particle size on ZnO-protein corona. *Nanomaterials* **2017,** *7*, 377.
59. Lundqvist, M.; Stigler, J.; Elia, G.; Lynch, I.; Cedervall, T.; Dawson, K. A., Nanoparticle size and surface properties determine the protein corona with possible implications for biological impacts. *Proceedings of the National Academy of Sciences* **2008,** *105*, 14265-14270.
60. Piloni, A.; Wong, C. K.; Chen, F.; Lord, M.; Walther, A.; Stenzel, M. H., Surface roughness influences the protein corona formation of glycosylated nanoparticles and alter their cellular uptake. *Nanoscale* **2019,** *11*, 23259-23267.
61. García-Álvarez, R.; Hadjidemetriou, M.; Sánchez-Iglesias, A.; Liz-Marzán, L. M.; Kostarelos, K., In vivo formation of protein corona on gold nanoparticles. The effect of their size and shape. *Nanoscale* **2018,** *10*, 1256-1264.
62. Madathiparambil Visalakshan, R.; González García, L. E.; Benzigar, M. R.; Ghazaryan, A.; Simon, J.; Mierczynska-Vasilev, A.; Michl, T. D.; Vinu, A.; Mailänder, V.; Morsbach, S., The influence of nanoparticle shape on protein corona formation. *Small* **2020,** *16*, 2000285.
63. Yu, Q.; Zhao, L.; Guo, C.; Yan, B.; Su, G., Regulating protein corona formation and dynamic protein exchange by controlling nanoparticle hydrophobicity. *Frontiers in bioengineering and biotechnology* **2020,** *8*, 210.
64. Capjak, I.; Šupraha Goreta, S.; Domazet Jurašin, D.; Vinković Vrček, I., How protein coronas determine the fate of engineered nanoparticles in biological environment. **2017**.
65. Lee, B.-J., Protein corona: a new approach for nanomedicine design. *International journal of nanomedicine* **2017,** *12*, 3137.
66. Sempf, K.; Arrey, T.; Gelperina, S.; Schorge, T.; Meyer, B.; Karas, M.; Kreuter, J., Adsorption of plasma proteins on uncoated PLGA nanoparticles. *European Journal of Pharmaceutics and Biopharmaceutics* **2013,** *85*, 53-60.
67. Simon, J.; Wolf, T.; Klein, K.; Landfester, K.; Wurm, F. R.; Mailander, V., Hydrophilicity Regulates the Stealth Properties of Polyphosphoester-Coated Nanocarriers. *Angew Chem Int Ed Engl* **2018,** *57*, 5548-5553.
68. Ritz, S.; Schottler, S.; Kotman, N.; Baier, G.; Musyanovych, A.; Kuharev, J.; Landfester, K.; Schild, H.; Jahn, O.; Tenzer, S.; Mailander, V., Protein corona of nanoparticles: distinct proteins regulate the cellular uptake. *Biomacromolecules* **2015,** *16*, 1311-21.
69. Vogt, C.; Pernemalm, M.; Kohonen, P.; Laurent, S.; Hultenby, K.; Vahter, M.; Lehtiö, J.; Toprak, M. S.; Fadeel, B., Proteomics analysis reveals distinct corona composition on magnetic nanoparticles with different surface coatings: implications for interactions with primary human macrophages. *PLoS One* **2015,** *10*, e0129008.
70. Furumoto, K.; Ogawara, K.-i.; Nagayama, S.; Takakura, Y.; Hashida, M.; Higaki, K.; Kimura, T., Important role of serum proteins associated on the surface of particles in their hepatic disposition. *Journal of controlled release* **2002,** *83*, 89-96.
71. Müller, R. H.; Rühl, D.; Lück, M.; Paulke, B., Influence of fluorescent labelling of polystyrene particles on phagocytic uptake, surface hydrophobicity, and plasma protein adsorption. *Pharmaceutical research* **1997,** *14*, 18-24.
72. Blunk, T.; Hochstrasser, D. F.; Sanchez, J. C.; Müller, B. W.; Müller, R. H., Colloidal carriers for intravenous drug targeting: plasma protein adsorption patterns on surface-modified latex particles evaluated by two-dimensional polyacrylamide gel electrophoresis. *Electrophoresis* **1993,** *14*, 1382-1387.
73. Dobrovolskaia, M. A.; Aggarwal, P.; Hall, J. B.; McNeil, S. E., Preclinical studies to understand nanoparticle interaction with the immune system and its potential effects on nanoparticle biodistribution. *Molecular pharmaceutics* **2008,** *5*, 487-495.
74. Walkey, C. D.; Olsen, J. B.; Guo, H.; Emili, A.; Chan, W. C., Nanoparticle size and surface chemistry determine serum protein adsorption and macrophage uptake. *Journal of the American Chemical Society* **2012,** *134*, 2139-2147.
75. Schottler, S.; Becker, G.; Winzen, S.; Steinbach, T.; Mohr, K.; Landfester, K.; Mailander, V.; Wurm, F. R., Protein adsorption is required for stealth effect of poly(ethylene glycol)- and poly(phosphoester)-coated nanocarriers. *Nat Nanotechnol* **2016,** *11*, 372-7.
76. Bertrand, N.; Grenier, P.; Mahmoudi, M.; Lima, E. M.; Appel, E. A.; Dormont, F.; Lim, J.-M.; Karnik, R.; Langer, R.; Farokhzad, O. C., Mechanistic understanding of in vivo protein

corona formation on polymeric nanoparticles and impact on pharmacokinetics. *Nature communications* **2017,** *8*, 1-8.

77. Samaridou, E.; Kalamidas, N.; Santalices, I.; Crecente-Campo, J.; Alonso, M. J., Tuning the PEG surface density of the PEG-PGA enveloped Octaarginine-peptide Nanocomplexes. *Drug Delivery and Translational Research* **2020,** *10*, 241-258.
78. Gref, R.; Lück, M.; Quellec, P.; Marchand, M.; Dellacherie, E.; Harnisch, S.; Blunk, T.; Müller, R., 'Stealth'corona-core nanoparticles surface modified by polyethylene glycol (PEG): influences of the corona (PEG chain length and surface density) and of the core composition on phagocytic uptake and plasma protein adsorption. *Colloids and Surfaces B: Biointerfaces* **2000,** *18*, 301-313.
79. Partikel, K.; Korte, R.; Mulac, D.; Humpf, H. U.; Langer, K., Serum type and concentration both affect the protein-corona composition of PLGA nanoparticles. *Beilstein J Nanotechnol* **2019,** *10*, 1002-1015.
80. Müller, L. K.; Simon, J.; Rosenauer, C.; Mailänder, V.; Morsbach, S.; Landfester, K., The transferability from animal models to humans: challenges regarding aggregation and protein corona formation of nanoparticles. *Biomacromolecules* **2018,** *19*, 374-385.
81. Mahmoudi, M.; Abdelmonem, A. M.; Behzadi, S.; Clement, J. H.; Dutz, S.; Ejtehadi, M. R.; Hartmann, R.; Kantner, K.; Linne, U.; Maffre, P.; Metzler, S.; Moghadam, M. K.; Pfeiffer, C.; Rezaei, M.; Ruiz-Lozano, P.; Serpooshan, V.; Shokrgozar, M. A.; Nienhaus, G. U.; Parak, W. J., Temperature: the "ignored" factor at the NanoBio interface. *ACS Nano* **2013,** *7*, 6555-62.
82. Mahmoudi, M.; Shokrgozar, M. A.; Behzadi, S., Slight temperature changes affect protein affinity and cellular uptake/toxicity of nanoparticles. *Nanoscale* **2013,** *5*, 3240-3244.
83. Chetwynd, A. J.; Wheeler, K. E.; Lynch, I., Best practice in reporting corona studies: Minimum information about Nanomaterial Biocorona Experiments (MINBE). *Nano Today* **2019,** *28*, 100758.
84. Kamaly, N.; Farokhzad, O. C.; Corbo, C., Nanoparticle protein corona evolution: from biological impact to biomarker discovery. *Nanoscale* **2022,** *14*, 1606-1620.
85. Kruszewska, J.; Zajda, J.; Matczuk, M., How to effectively prepare a sample for bottom-up proteomic analysis of nanoparticle protein corona? A critical review. *Talanta* **2021,** *226*, 122153.
86. Böhmert, L.; Voß, L.; Stock, V.; Braeuning, A.; Lampen, A.; Sieg, H., Isolation methods for particle protein corona complexes from protein-rich matrices. *Nanoscale Advances* **2020,** *2*, 563-582.
87. Weber, C.; Morsbach, S.; Landfester, K., Possibilities and limitations of different separation techniques for the analysis of the protein corona. *Angewandte Chemie International Edition* **2019,** *58*, 12787-12794.
88. Capriotti, A. L.; Caracciolo, G.; Caruso, G.; Cavaliere, C.; Pozzi, D.; Samperi, R.; Laganà, A., Analysis of plasma protein adsorption onto DC-Chol-DOPE cationic liposomes by HPLC-CHIP coupled to a Q-TOF mass spectrometer. *Analytical and bioanalytical chemistry* **2010,** *398*, 2895-2903.
89. Bonvin, D.; Chiappe, D.; Moniatte, M.; Hofmann, H.; Ebersold, M. M., Methods of protein corona isolation for magnetic nanoparticles. *Analyst* **2017,** *142*, 3805-3815.
90. Brückner, M.; Simon, J.; Jiang, S.; Landfester, K.; Mailänder, V., Preparation of the protein corona: How washing shapes the proteome and influences cellular uptake of nanocarriers. *Acta Biomaterialia* **2020,** *114*, 333-342.
91. Weber, C.; Simon, J.; Mailänder, V.; Morsbach, S.; Landfester, K., Preservation of the soft protein corona in distinct flow allows identification of weakly bound proteins. *Acta biomaterialia* **2018,** *76*, 217-224.
92. Ashby, J.; Schachermeyer, S.; Pan, S.; Zhong, W., Dissociation-based screening of nanoparticle–protein interaction via flow field-flow fractionation. *Analytical chemistry* **2013,** *85*, 7494-7501.
93. Wang, Y.; Olesik, S. V., Separation of PEGylated gold nanoparticles by micellar enhanced electrospun fiber based ultrathin layer chromatography. *Analytical chemistry* **2018,** *90*, 2662-2670.

94. Capriotti, A. L.; Caracciolo, G.; Cavaliere, C.; Colapicchioni, V.; Piovesana, S.; Pozzi, D.; Laganà, A., Analytical methods for characterizing the nanoparticle–protein corona. *Chromatographia* **2014,** *77*, 755-769.
95. Contado, C., Field flow fractionation techniques to explore the "nano-world". *Analytical and bioanalytical chemistry* **2017,** *409*, 2501-2518.
96. Gossmann, R.; Fahrländer, E.; Hummel, M.; Mulac, D.; Brockmeyer, J.; Langer, K., Comparative examination of adsorption of serum proteins on HSA-and PLGA-based nanoparticles using SDS–PAGE and LC–MS. *European Journal of Pharmaceutics and Biopharmaceutics* **2015,** *93*, 80-87.
97. Kim, H. R.; Andrieux, K.; Gil, S.; Taverna, M.; Chacun, H.; Desmaële, D.; Taran, F.; Georgin, D.; Couvreur, P., Translocation of poly (ethylene glycol-co-hexadecyl) cyanoacrylate nanoparticles into rat brain endothelial cells: role of apolipoproteins in receptor-mediated endocytosis. *Biomacromolecules* **2007,** *8*, 793-799.
98. Docter, D.; Distler, U.; Storck, W.; Kuharev, J.; Wünsch, D.; Hahlbrock, A.; Knauer, S. K.; Tenzer, S.; Stauber, R. H., Quantitative profiling of the protein coronas that form around nanoparticles. *Nature protocols* **2014,** *9*, 2030-2044.
99. Maiolo, D.; Bergese, P.; Mahon, E.; Dawson, K. A.; Monopoli, M. P., Surfactant titration of nanoparticle–protein corona. *Analytical chemistry* **2014,** *86*, 12055-12063.
100. Leroux, J. C.; Gravel, P.; Balant, L.; Volet, B.; Anner, B. M.; Allémann, E.; Doelker, E.; Gurny, R., Internalization of poly (D, L-1actic acid) nanoparticles by isolated human leukocytes and analysis of plasma proteins adsorbed onto the particles. *Journal of biomedical materials research* **1994,** *28*, 471-481.
101. Zhang, H.; Peng, J.; Li, X.; Liu, S.; Hu, Z.; Xu, G.; Wu, R. a., A nano-bio interfacial protein corona on silica nanoparticle. *Colloids and Surfaces B: Biointerfaces* **2018,** *167*, 220-228.
102. Kokkinopoulou, M.; Simon, J.; Landfester, K.; Mailander, V.; Lieberwirth, I., Visualization of the protein corona: towards a biomolecular understanding of nanoparticle-cell-interactions. *Nanoscale* **2017,** *9*, 8858-8870.
103. Karpievitch, Y. V.; Polpitiya, A. D.; Anderson, G. A.; Smith, R. D.; Dabney, A. R., Liquid chromatography mass spectrometry-based proteomics: biological and technological aspects. *The annals of applied statistics* **2010,** *4*, 1797.
104. Faserl, K.; Chetwynd, A. J.; Lynch, I.; Thorn, J. A.; Lindner, H. H., Corona isolation method matters: capillary electrophoresis mass spectrometry based comparison of protein corona compositions following on-particle versus in-solution or in-gel digestion. *Nanomaterials* **2019,** *9*, 898.
105. Bonvin, D.; Aschauer, U.; Alexander, D. T.; Chiappe, D.; Moniatte, M.; Hofmann, H.; Mionić Ebersold, M., Protein corona: impact of lymph versus blood in a complex in vitro environment. *Small* **2017,** *13*, 1700409.
106. Müller, J.; Simon, J.; Rohne, P.; Koch-Brandt, C.; Mailänder, V.; Morsbach, S.; Landfester, K., Denaturation via surfactants changes composition of protein corona. *Biomacromolecules* **2018,** *19*, 2657-2664.
107. Blume, J. E.; Manning, W. C.; Troiano, G.; Hornburg, D.; Figa, M.; Hesterberg, L.; Platt, T. L.; Zhao, X.; Cuaresma, R. A.; Everley, P. A., Rapid, deep and precise profiling of the plasma proteome with multi-nanoparticle protein corona. *Nature communications* **2020,** *11*, 1-14.
108. Capriotti, A. L.; Caracciolo, G.; Caruso, G.; Cavaliere, C.; Pozzi, D.; Samperi, R.; Laganà, A., Label-free quantitative analysis for studying the interactions between nanoparticles and plasma proteins. *Analytical and bioanalytical chemistry* **2013,** *405*, 635-645.
109. Morris, C. B.; Poland, J. C.; May, J. C.; McLean, J. A., Fundamentals of ion mobility-mass spectrometry for the analysis of biomolecules. *Ion Mobility-Mass Spectrometry* **2020**, 1-31.
110. Distler, U.; Kuharev, J.; Navarro, P.; Tenzer, S., Label-free quantification in ion mobility–enhanced data-independent acquisition proteomics. *Nature protocols* **2016,** *11*, 795-812.
111. Neilson, K. A.; Ali, N. A.; Muralidharan, S.; Mirzaei, M.; Mariani, M.; Assadourian, G.; Lee, A.; Van Sluyter, S. C.; Haynes, P. A., Less label, more free: approaches in label-free quantitative mass spectrometry. *Proteomics* **2011,** *11*, 535-553.
112. Silva, J. C.; Gorenstein, M. V.; Li, G. Z.; Vissers, J. P.; Geromanos, S. J., Absolute quantification of proteins by LCMSE: a virtue of parallel MS acquisition. *Mol. Cell. Proteomics* **2006,** *5*, 144-56.

113. Rabe, M.; Verdes, D.; Seeger, S., Understanding protein adsorption phenomena at solid surfaces. *Advances in colloid and interface science* **2011,** *162*, 87-106.
114. Vroman, L.; Adams, A. L., Findings with the recording ellipsometer suggesting rapid exchange of specific plasma proteins at liquid/solid interfaces. *Surface Science* **1969,** *16*, 438-446.
115. Daly, S. M.; Przybycien, T. M.; Tilton, R. D., Coverage-dependent orientation of lysozyme adsorbed on silica. *Langmuir* **2003,** *19*, 3848-3857.
116. Jackler, G.; Steitz, R.; Czeslik, C., Effect of temperature on the adsorption of lysozyme at the silica/water interface studied by optical and neutron reflectometry. *Langmuir* **2002,** *18*, 6565-6570.
117. Kiesel, I.; Paulus, M.; Nase, J.; Tiemeyer, S.; Sternemann, C.; Rüster, K.; Wirkert, F. J.; Mende, K.; Büning, T.; Tolan, M., Temperature-driven adsorption and desorption of proteins at solid–liquid interfaces. *Langmuir* **2014,** *30*, 2077-2083.
118. Qiao, S.; Wang, H., Temperature-responsive polymers: Synthesis, properties, and biomedical applications. Nano Res 11: 5400–5423. 2018.
119. Zarrintaj, P.; Jouyandeh, M.; Ganjali, M. R.; Hadavand, B. S.; Mozafari, M.; Sheiko, S. S.; Vatankhah-Varnoosfaderani, M.; Gutiérrez, T. J.; Saeb, M. R., Thermo-sensitive polymers in medicine: A review. *European Polymer Journal* **2019,** *117*, 402-423.
120. Bordat, A.; Boissenot, T.; Nicolas, J.; Tsapis, N., Thermoresponsive polymer nanocarriers for biomedical applications. *Advanced drug delivery reviews* **2019,** *138*, 167-192.
121. Kim, Y.-J.; Matsunaga, Y. T., Thermo-responsive polymers and their application as smart biomaterials. *Journal of Materials Chemistry B* **2017,** *5*, 4307-4321.
122. Niskanen, J.; Tenhu, H., How to manipulate the upper critical solution temperature (UCST)? *Polymer Chemistry* **2017,** *8*, 220-232.
123. Xue, C.; Yonet-Tanyeri, N.; Brouette, N.; Sferrazza, M.; Braun, P. V.; Leckband, D. E., Protein adsorption on poly(N-isopropylacrylamide) brushes: dependence on grafting density and chain collapse. *Langmuir* **2011,** *27*, 8810-8.
124. Kanazawa, H.; Okano, T., Temperature-responsive chromatography for the separation of biomolecules. *Journal of Chromatography A* **2011,** *1218*, 8738-8747.
125. Zhang, Y.; Cai, J.; Li, C.; Wei, J.; Liu, Z.; Xue, W., Effects of thermosensitive poly (N-isopropylacrylamide) on blood coagulation. *Journal of Materials Chemistry B* **2016,** *4*, 3733-3749.
126. Miceli, E.; Kuropka, B.; Rosenauer, C.; Osorio Blanco, E. R.; Theune, L. E.; Kar, M.; Weise, C.; Morsbach, S.; Freund, C.; Calderon, M., Understanding the elusive protein corona of thermoresponsive nanogels. *Nanomedicine (Lond)* **2018,** *13*, 2657-2668.
127. Walkey, C. D.; Chan, W. C., Understanding and controlling the interaction of nanomaterials with proteins in a physiological environment. *Chemical Society Reviews* **2012,** *41*, 2780-2799.
128. Saptarshi, S. R.; Duschl, A.; Lopata, A. L., Interaction of nanoparticles with proteins: relation to bio-reactivity of the nanoparticle. *Journal of nanobiotechnology* **2013,** *11*, 1-12.
129. Wang, J.; Ayano, E.; Maitani, Y.; Kanazawa, H., Enhanced cellular uptake and gene silencing activity of siRNA using temperature-responsive polymer-modified liposome. *International Journal of Pharmaceutics* **2017,** *523*, 217-228.
130. Okano, T.; Yamada, N.; Okuhara, M.; Sakai, H.; Sakurai, Y., Mechanism of cell detachment from temperature-modulated, hydrophilic-hydrophobic polymer surfaces. *Biomaterials* **1995,** *16*, 297-303.
131. Nagase, K.; Yamato, M.; Kanazawa, H.; Okano, T., Poly (N-isopropylacrylamide)-based thermoresponsive surfaces provide new types of biomedical applications. *Biomaterials* **2018,** *153*, 27-48.
132. Tang, Z.; Akiyama, Y.; Okano, T., Recent development of temperature-responsive cell culture surface using poly (N-isopropylacrylamide). *Journal of Polymer Science Part B: Polymer Physics* **2014,** *52*, 917-926.
133. Heffernan, J. M.; Overstreet, D. J.; Srinivasan, S.; Le, L. D.; Vernon, B. L.; Sirianni, R. W., Temperature responsive hydrogels enable transient three-dimensional tumor cultures via rapid cell recovery. *Journal of Biomedical Materials Research Part A* **2016,** *104*, 17-25.
134. Yamato, M.; Akiyama, Y.; Kobayashi, J.; Yang, J.; Kikuchi, A.; Okano, T., Temperature-responsive cell culture surfaces for regenerative medicine with cell sheet engineering. *Progress in Polymer Science* **2007,** *32*, 1123-1133.

135. Lesniak, A.; Campbell, A.; Monopoli, M. P.; Lynch, I.; Salvati, A.; Dawson, K. A., Serum heat inactivation affects protein corona composition and nanoparticle uptake. *Biomaterials* **2010,** *31*, 9511-8.
136. Simon, J.; Muller, J.; Ghazaryan, A.; Morsbach, S.; Mailander, V.; Landfester, K., Protein denaturation caused by heat inactivation detrimentally affects biomolecular corona formation and cellular uptake. *Nanoscale* **2018,** *10*, 21096-21105.
137. Soltis, R. D.; Hasz, D.; Morris, M.; Wilson, I., Studies on the nature of heat-labile anti-complementary activity in normal human serum. *Clinical and Experimental Immunology* **1979,** *37*, 310.
138. Cunliffe, D.; de las Heras Alarcón, C.; Peters, V.; Smith, J. R.; Alexander, C., Thermoresponsive surface-grafted poly (N− isopropylacrylamide) copolymers: effect of phase transitions on protein and bacterial attachment. *Langmuir* **2003,** *19*, 2888-2899.
139. Tu, Y.; Peng, F.; Sui, X.; Men, Y.; White, P. B.; van Hest, J.; Wilson, D. A., Self-propelled supramolecular nanomotors with temperature-responsive speed regulation. *Nature chemistry* **2017,** *9*, 480-486.
140. Müller, R. H., *Colloidal carriers for controlled drug delivery and targeting: Modification, characterization and in vivo distribution*. Taylor & Francis: 1991.
141. Xiao, Y.; Wiesner, M. R., Characterization of surface hydrophobicity of engineered nanoparticles. *Journal of hazardous materials* **2012,** *215*, 146-151.
142. Cao, Z.; Tsai, S. N.; Zuo, Y. Y., An optical method for quantitatively determining the surface free energy of micro-and nanoparticles. *Analytical chemistry* **2019,** *91*, 12819-12826.
143. Song, F.; Wang, X.-L.; Wang, Y.-Z., Fabrication of novel thermo-responsive electrospun nanofibrous mats and their application in bioseparation. *European polymer journal* **2011,** *47*, 1885-1892.
144. Psarra, E.; König, U.; Ueda, Y.; Bellmann, C.; Janke, A.; Bittrich, E.; Eichhorn, K.-J.; Uhlmann, P., Nanostructured biointerfaces: nanoarchitectonics of thermoresponsive polymer brushes impact protein adsorption and cell adhesion. *ACS applied materials & interfaces* **2015,** *7*, 12516-12529.
145. Choi, S.; Choi, B.-C.; Xue, C.; Leckband, D., Protein adsorption mechanisms determine the efficiency of thermally controlled cell adhesion on poly (N-isopropyl acrylamide) brushes. *Biomacromolecules* **2013,** *14*, 92-100.
146. Zelzer, M.; Albutt, D.; Alexander, M. R.; Russell, N. A., The role of albumin and fibronectin in the adhesion of fibroblasts to plasma polymer surfaces. *Plasma Processes and Polymers* **2012,** *9*, 149-156.
147. Horbett, T. A., Fibrinogen adsorption to biomaterials. *Journal of biomedical materials research Part A* **2018,** *106*, 2777-2788.
148. O'Brien, J.; Shea, K. J., Tuning the protein corona of hydrogel nanoparticles: the synthesis of abiotic protein and peptide affinity reagents. *Accounts of chemical research* **2016,** *49*, 1200-1210.
149. Wischerhoff, E.; Uhlig, K.; Lankenau, A.; Börner, H. G.; Laschewsky, A.; Duschl, C.; Lutz, J. F., Controlled cell adhesion on PEG-based switchable surfaces. *Angewandte Chemie International Edition* **2008,** *47*, 5666-5668.
150. Badi, N., Non-linear PEG-based thermoresponsive polymer systems. *Progress in Polymer Science* **2017,** *66*, 54-79.
151. Kitano, H.; Kondo, T.; Suzuki, H.; Ohno, K., Temperature-responsive polymer-brush constructed on a glass substrate by atom transfer radical polymerization. *Journal of colloid and interface science* **2010,** *345*, 325-331.
152. Murakami, D.; Kitahara, Y.; Kobayashi, S.; Tanaka, M., Thermosensitive polymer biocompatibility based on interfacial structure at biointerface. *ACS Biomaterials Science & Engineering* **2018,** *4*, 1591-1597.
153. Becherer, T.; Heinen, S.; Wei, Q.; Haag, R.; Weinhart, M., In-depth analysis of switchable glycerol based polymeric coatings for cell sheet engineering. *Acta Biomaterialia* **2015,** *25*, 43-55.
154. Gaertner, F. C.; Luxenhofer, R.; Blechert, B.; Jordan, R.; Essler, M., Synthesis, biodistribution and excretion of radiolabeled poly (2-alkyl-2-oxazoline) s. *Journal of Controlled Release* **2007,** *119*, 291-300.

155. Koshkina, O.; Lang, T.; Thiermann, R.; Docter, D.; Stauber, R. H.; Secker, C.; Schlaad, H.; Weidner, S.; Mohr, B.; Maskos, M., Temperature-triggered protein adsorption on polymer-coated nanoparticles in serum. *Langmuir* **2015,** *31*, 8873-8881.
156. Hajipour, M. J.; Aghaverdi, H.; Serpooshan, V.; Vali, H.; Sheibani, S.; Mahmoudi, M., Sex as an important factor in nanomedicine. *Nature Communications* **2021,** *12*, 1-11.
157. Hayashi, Y.; Miclaus, T.; Murugadoss, S.; Takamiya, M.; Scavenius, C.; Kjaer-Sorensen, K.; Enghild, J. J.; Strähle, U.; Oxvig, C.; Weiss, C., Female versus male biological identities of nanoparticles determine the interaction with immune cells in fish. *Environmental Science: Nano* **2017,** *4*, 895-906.
158. Behzadi, S.; Serpooshan, V.; Tao, W.; Hamaly, M. A.; Alkawareek, M. Y.; Dreaden, E. C.; Brown, D.; Alkilany, A. M.; Farokhzad, O. C.; Mahmoudi, M., Cellular uptake of nanoparticles: journey inside the cell. *Chemical Society Reviews* **2017,** *46*, 4218-4244.
159. Akimoto, J.; Nakayama, M.; Sakai, K.; Okano, T., Thermally controlled intracellular uptake system of polymeric micelles possessing poly (N-isopropylacrylamide)-based outer coronas. *Molecular pharmaceutics* **2010,** *7*, 926-935.
160. Hiruta, Y.; Shimamura, M.; Matsuura, M.; Maekawa, Y.; Funatsu, T.; Suzuki, Y.; Ayano, E.; Okano, T.; Kanazawa, H., Temperature-responsive fluorescence polymer probes with accurate thermally controlled cellular uptakes. *ACS Macro Letters* **2014,** *3*, 281-285.
161. Kobayashi, J.; Kikuchi, A.; Aoyagi, T.; Okano, T., Cell sheet tissue engineering: cell sheet preparation, harvesting/manipulation, and transplantation. *Journal of biomedical materials research Part A* **2019,** *107*, 955-967.
162. Farjadian, F.; Ghasemi, A.; Gohari, O.; Roointan, A.; Karimi, M.; Hamblin, M. R., Nanopharmaceuticals and nanomedicines currently on the market: challenges and opportunities. *Nanomedicine* **2019,** *14*, 93-126.
163. Manzari, M. T.; Shamay, Y.; Kiguchi, H.; Rosen, N.; Scaltriti, M.; Heller, D. A., Targeted drug delivery strategies for precision medicines. *Nature Reviews Materials* **2021,** *6*, 351-370.
164. Tonigold, M.; Simon, J.; Estupiñán, D.; Kokkinopoulou, M.; Reinholz, J.; Kintzel, U.; Kaltbeitzel, A.; Renz, P.; Domogalla, M. P.; Steinbrink, K., Pre-adsorption of antibodies enables targeting of nanocarriers despite a biomolecular corona. *Nature nanotechnology* **2018,** *13*, 862-869.
165. Yu, L.; Xu, M.; Xu, W.; Xiao, W.; Jiang, X.-h.; Wang, L.; Gao, H., Enhanced cancer-targeted drug delivery using precoated nanoparticles. *Nano Letters* **2020,** *20*, 8903-8911.
166. Lara, S.; Alnasser, F.; Polo, E.; Garry, D.; Lo Giudice, M. C.; Hristov, D. R.; Rocks, L.; Salvati, A.; Yan, Y.; Dawson, K. A., Identification of receptor binding to the biomolecular corona of nanoparticles. *ACS nano* **2017,** *11*, 1884-1893.
167. Ke, P. C.; Lin, S.; Parak, W. J.; Davis, T. P.; Caruso, F., A decade of the protein corona. *ACS nano* **2017,** *11*, 11773-11776.
168. Schottler, S.; Landfester, K.; Mailander, V., Controlling the Stealth Effect of Nanocarriers through Understanding the Protein Corona. *Angew. Chem. Int. Ed. Engl.* **2016,** *55*, 8806-15.
169. Simon, J.; Kuhn, G.; Fichter, M.; Gehring, S.; Landfester, K.; Mailänder, V., Unraveling the In Vivo Protein Corona. *Cells* **2021,** *10*, 132.
170. Cedervall, T.; Lynch, I.; Foy, M.; Berggard, T.; Donnelly, S. C.; Cagney, G.; Linse, S.; Dawson, K. A., Detailed identification of plasma proteins adsorbed on copolymer nanoparticles. *Angew Chem Int Ed Engl* **2007,** *46*, 5754-6.
171. Yoshimatsu, K.; Lesel, B. K.; Yonamine, Y.; Beierle, J. M.; Hoshino, Y.; Shea, K. J., Temperature-responsive "catch and release" of proteins by using multifunctional polymer-based nanoparticles. *Angew Chem Int Ed Engl* **2012,** *51*, 2405-8.
172. Gräfe, C.; Weidner, A.; vd Lühe, M.; Bergemann, C.; Schacher, F. H.; Clement, J. H.; Dutz, S., Intentional formation of a protein corona on nanoparticles: Serum concentration affects protein corona mass, surface charge, and nanoparticle–cell interaction. *The international journal of biochemistry & cell biology* **2016,** *75*, 196-202.
173. Van Hong Nguyen, B.-J. L., Protein corona: a new approach for nanomedicine design. *International journal of nanomedicine* **2017,** *12*, 3137.
174. Aoyama, M.; Hata, K.; Higashisaka, K.; Nagano, K.; Yoshioka, Y.; Tsutsumi, Y., Clusterin in the protein corona plays a key role in the stealth effect of nanoparticles against phagocytes. *Biochemical and biophysical research communications* **2016,** *480*, 690-695.

175. Simon, J.; Muller, L. K.; Kokkinopoulou, M.; Lieberwirth, I.; Morsbach, S.; Landfester, K.; Mailander, V., Exploiting the biomolecular corona: pre-coating of nanoparticles enables controlled cellular interactions. *Nanoscale* **2018,** *10*, 10731-10739.
176. Urban, M.; Freisinger, B.; Ghazy, O.; Staff, R.; Landfester, K.; Crespy, D.; Musyanovych, A., Polymer Janus nanoparticles with two spatially segregated functionalizations. *Macromolecules* **2014,** *47*, 7194-7199.
177. Jiang, S.; Prozeller, D.; Pereira, J.; Simon, J.; Han, S.; Wirsching, S.; Fichter, M.; Mottola, M.; Lieberwirth, I.; Morsbach, S.; Mailander, V.; Gehring, S.; Crespy, D.; Landfester, K., Controlling protein interactions in blood for effective liver immunosuppressive therapy by silica nanocapsules. *Nanoscale* **2020,** *12*, 2626-2637.
178. Schwartz, R. S. a. C., C. L. Blood. https: //www .britannica.com/science/blood-biochemistry. Accessed 16 November 2021.
179. Firkowska-Boden, I.; Zhang, X.; Jandt, K. D., Controlling Protein Adsorption through Nanostructured Polymeric Surfaces. *Adv Healthc Mater* **2018,** *7*.
180. Yang, S. T.; Liu, Y.; Wang, Y. W.; Cao, A., Biosafety and bioapplication of nanomaterials by designing protein–nanoparticle interactions. *Small* **2013,** *9*, 1635-1653.
181. Doane, T. L.; Burda, C., The unique role of nanoparticles in nanomedicine: imaging, drug delivery and therapy. *Chemical Society Reviews* **2012,** *41*, 2885-2911.
182. Gustafson, H. H.; Holt-Casper, D.; Grainger, D. W.; Ghandehari, H., Nanoparticle uptake: the phagocyte problem. *Nano today* **2015,** *10*, 487-510.
183. Johnson, R. L.; Schmidt-Rohr, K., Quantitative solid-state 13C NMR with signal enhancement by multiple cross polarization. *Journal of Magnetic Resonance* **2014,** *239*, 44-49.
184. Thurmond, C. D., Control of dust in solution for turbidimetry. *Journal of Polymer Science* **1952,** *8*, 607-609.
185. Rausch, K.; Reuter, A.; Fischer, K.; Schmidt, M., Evaluation of nanoparticle aggregation in human blood serum. *Biomacromolecules* **2010,** *11*, 2836-2839.
186. Brouwer, A. M., Standards for photoluminescence quantum yield measurements in solution (IUPAC Technical Report). *Pure and Applied Chemistry* **2011,** *83*, 2213-2228.
187. Rusconi, F.; Valton, É.; Nguyen, R.; Dufourc, E., Quantification of sodium dodecyl sulfate in microliter-volume biochemical samples by visible light spectroscopy. *Analytical biochemistry* **2001,** *295*, 31-37.
188. Bewersdorff, T.; Gruber, A.; Eravci, M.; Dumbani, M.; Klinger, D.; Haase, A., Amphiphilic nanogels: influence of surface hydrophobicity on protein corona, biocompatibility and cellular uptake. *International journal of nanomedicine* **2019,** *14*, 7861.
189. Lu, Y.; Ballauff, M., Thermosensitive core–shell microgels: From colloidal model systems to nanoreactors. *Progress in Polymer Science* **2011,** *36*, 767-792.
190. Winzen, S.; Schwabacher, J. C.; Müller, J.; Landfester, K.; Mohr, K., Small surfactant concentration differences influence adsorption of human serum albumin on polystyrene nanoparticles. *Biomacromolecules* **2016,** *17*, 3845-3851.
191. Mohr, K.; Sommer, M.; Baier, G.; Schöttler, S.; Okwieka, P.; Tenzer, S.; Landfester, K.; Mailänder, V.; Schmidt, M.; Meyer, R. G., Aggregation behavior of polystyrene-nanoparticles in human blood serum and its impact on the in vivo distribution in mice. *Journal of Nanomedicine & Nanotechnology* **2014,** *5*.
192. Hiruta, Y.; Nagumo, Y.; Suzuki, Y.; Funatsu, T.; Ishikawa, Y.; Kanazawa, H., The effects of anionic electrolytes and human serum albumin on the LCST of poly (N-isopropylacrylamide)-based temperature-responsive copolymers. *Colloids and Surfaces B: Biointerfaces* **2015,** *132*, 299-304.
193. Rizzo, L. Y.; Theek, B.; Storm, G.; Kiessling, F.; Lammers, T., Recent progress in nanomedicine: therapeutic, diagnostic and theranostic applications. *Current opinion in biotechnology* **2013,** *24*, 1159-1166.
194. Han, X.; Xu, K.; Taratula, O.; Farsad, K., Applications of nanoparticles in biomedical imaging. *Nanoscale* **2019,** *11*, 799-819.
195. Vargo, K. B.; Zaki, A. A.; Warden-Rothman, R.; Tsourkas, A.; Hammer, D. A., Superparamagnetic iron oxide nanoparticle micelles stabilized by recombinant oleosin for targeted magnetic resonance imaging. *Small* **2015,** *11*, 1409-1413.

196. Wu, S.-C.; Chen, Y.-J.; Lin, Y.-J.; Wu, T.-H.; Wang, Y.-M., Development of a mucin4-targeting SPIO contrast agent for effective detection of pancreatic tumor cells in vitro and in vivo. *Journal of medicinal chemistry* **2013,** *56*, 9100-9109.
197. Park, I.-K.; Ng, C.-P.; Wang, J.; Chu, B.; Yuan, C.; Zhang, S.; Pun, S. H., Determination of nanoparticle vehicle unpackaging by MR imaging of a T2 magnetic relaxation switch. *Biomaterials* **2008,** *29*, 724-732.
198. Liu, G.; Wang, Z.; Lu, J.; Xia, C.; Gao, F.; Gong, Q.; Song, B.; Zhao, X.; Shuai, X.; Chen, X., Low molecular weight alkyl-polycation wrapped magnetite nanoparticle clusters as MRI probes for stem cell labeling and in vivo imaging. *Biomaterials* **2011,** *32*, 528-537.
199. Kim, J.; Chhour, P.; Hsu, J.; Litt, H. I.; Ferrari, V. A.; Popovtzer, R.; Cormode, D. P., Use of nanoparticle contrast agents for cell tracking with computed tomography. *Bioconjugate chemistry* **2017,** *28*, 1581-1597.
200. Chien, C.-C.; Chen, H.-H.; Lai, S.-F.; Hwu, Y.; Petibois, C.; Yang, C.; Chu, Y.; Margaritondo, G., X-ray imaging of tumor growth in live mice by detecting gold-nanoparticle-loaded cells. *Scientific reports* **2012,** *2*, 1-6.
201. Ahn, S.; Jung, S. Y.; Seo, E.; Lee, S. J., Gold nanoparticle-incorporated human red blood cells (RBCs) for X-ray dynamic imaging. *Biomaterials* **2011,** *32*, 7191-7199.
202. Tao, Y.; Li, M.; Kim, B.; Auguste, D. T., Incorporating gold nanoclusters and target-directed liposomes as a synergistic amplified colorimetric sensor for HER2-positive breast cancer cell detection. *Theranostics* **2017,** *7*, 899.
203. Winter, P. M.; Caruthers, S. D.; Kassner, A.; Harris, T. D.; Chinen, L. K.; Allen, J. S.; Lacy, E. K.; Zhang, H.; Robertson, J. D.; Wickline, S. A., Molecular imaging of angiogenesis in nascent Vx-2 rabbit tumors using a novel αvβ3-targeted nanoparticle and 1.5 tesla magnetic resonance imaging. *Cancer research* **2003,** *63*, 5838-5843.
204. Bazak, R.; Houri, M.; El Achy, S.; Kamel, S.; Refaat, T., Cancer active targeting by nanoparticles: a comprehensive review of literature. *Journal of cancer research and clinical oncology* **2015,** *141*, 769-784.
205. Attia, M. F.; Anton, N.; Wallyn, J.; Omran, Z.; Vandamme, T. F., An overview of active and passive targeting strategies to improve the nanocarriers efficiency to tumour sites. *Journal of Pharmacy and Pharmacology* **2019,** *71*, 1185-1198.
206. Torchilin, V., Tumor delivery of macromolecular drugs based on the EPR effect. *Advanced drug delivery reviews* **2011,** *63*, 131-135.
207. D Friedman, A.; E Claypool, S.; Liu, R., The smart targeting of nanoparticles. *Current pharmaceutical design* **2013,** *19*, 6315-6329.
208. Foroozandeh, P.; Aziz, A. A., Insight into cellular uptake and intracellular trafficking of nanoparticles. *Nanoscale research letters* **2018,** *13*, 1-12.
209. Oh, N.; Park, J. H., Endocytosis and exocytosis of nanoparticles in mammalian cells. *Int J Nanomedicine* **2014,** *9 Suppl 1*, 51-63.
210. Mahmoudi, M.; Meng, J.; Xue, X.; Liang, X. J.; Rahman, M.; Pfeiffer, C.; Hartmann, R.; Gil, P. R.; Pelaz, B.; Parak, W. J., Interaction of stable colloidal nanoparticles with cellular membranes. *Biotechnology advances* **2014,** *32*, 679-692.
211. Chou, L. Y.; Ming, K.; Chan, W. C., Strategies for the intracellular delivery of nanoparticles. *Chemical Society Reviews* **2011,** *40*, 233-245.
212. Iversen, T.-G.; Skotland, T.; Sandvig, K., Endocytosis and intracellular transport of nanoparticles: Present knowledge and need for future studies. *Nano today* **2011,** *6*, 176-185.
213. Makaraci, P.; Kim, K., trans-Golgi network-bound cargo traffic. *European journal of cell biology* **2018,** *97*, 137-149.
214. Sahay, G.; Alakhova, D. Y.; Kabanov, A. V., Endocytosis of nanomedicines. *Journal of controlled release* **2010,** *145*, 182-195.
215. Hillaireau, H.; Couvreur, P., Nanocarriers' entry into the cell: relevance to drug delivery. *Cellular and molecular life sciences* **2009,** *66*, 2873-2896.
216. Patel, A. A.; Ginhoux, F.; Yona, S., Monocytes, macrophages, dendritic cells and neutrophils: an update on lifespan kinetics in health and disease. *Immunology* **2021,** *163*, 250-261.
217. Swanson, J. A., Shaping cups into phagosomes and macropinosomes. *Nature reviews Molecular cell biology* **2008,** *9*, 639-649.

218. Aderem, A.; Underhill, D. M., Mechanisms of phagocytosis in macrophages. *Annual review of immunology* **1999,** *17*, 593-623.
219. Ferguson, J. P.; Huber, S. D.; Willy, N. M.; Aygün, E.; Goker, S.; Atabey, T.; Kural, C., Mechanoregulation of clathrin-mediated endocytosis. *Journal of Cell Science* **2017,** *130*, 3631-3636.
220. Lu, R.; Drubin, D. G.; Sun, Y., Clathrin-mediated endocytosis in budding yeast at a glance. *Journal of Cell Science* **2016,** *129*, 1531-1536.
221. Conner, S. D.; Schmid, S. L., Regulated portals of entry into the cell. *Nature* **2003,** *422*, 37-44.
222. Xiang, S.; Tong, H.; Shi, Q.; Fernandes, J. C.; Jin, T.; Dai, K.; Zhang, X., Uptake mechanisms of non-viral gene delivery. *Journal of controlled release* **2012,** *158*, 371-378.
223. Schmid, E. M.; Ford, M. G. J.; Burtey, A.; Praefcke, G. J. K.; Peak-Chew, S.-Y.; Mills, I. G.; Benmerah, A.; McMahon, H. T., Role of the AP2 β-appendage hub in recruiting partners for clathrin-coated vesicle assembly. *PLoS biology* **2006,** *4*, e262.
224. Parton, R. G.; Simons, K., The multiple faces of caveolae. *Nature reviews Molecular cell biology* **2007,** *8*, 185-194.
225. Rothberg, K. G.; Heuser, J. E.; Donzell, W. C.; Ying, Y.-S.; Glenney, J. R.; Anderson, R. G., Caveolin, a protein component of caveolae membrane coats. *Cell* **1992,** *68*, 673-682.
226. Parton, R. G.; Del Pozo, M. A., Caveolae as plasma membrane sensors, protectors and organizers. *Nature reviews Molecular cell biology* **2013,** *14*, 98-112.
227. Rejman, J.; Conese, M.; Hoekstra, D., Gene transfer by means of lipo-and polyplexes: role of clathrin and caveolae-mediated endocytosis. *Journal of liposome research* **2006,** *16*, 237-247.
228. Rauch, J.; Kolch, W.; Laurent, S.; Mahmoudi, M., Big signals from small particles: regulation of cell signaling pathways by nanoparticles. *Chemical reviews* **2013,** *113*, 3391-3406.
229. Jovic, M.; Sharma, M.; Rahajeng, J.; Caplan, S., The early endosome: a busy sorting station for proteins at the crossroads. *Histology and histopathology* **2010,** *25*, 99.
230. Park, M.; Salgado, J. M.; Ostroff, L.; Helton, T. D.; Robinson, C. G.; Harris, K. M.; Ehlers, M. D., Plasticity-induced growth of dendritic spines by exocytic trafficking from recycling endosomes. *Neuron* **2006,** *52*, 817-830.
231. Huotari, J.; Helenius, A., Endosome maturation. *The EMBO journal* **2011,** *30*, 3481-3500.
232. Martens, T. F.; Remaut, K.; Demeester, J.; De Smedt, S. C.; Braeckmans, K., Intracellular delivery of nanomaterials: how to catch endosomal escape in the act. *Nano Today* **2014,** *9*, 344-364.
233. Dominska, M.; Dykxhoorn, D. M., Breaking down the barriers: siRNA delivery and endosome escape. *Journal of cell science* **2010,** *123*, 1183-1189.
234. Anding, A. L.; Baehrecke, E. H., Cleaning house: selective autophagy of organelles. *Developmental cell* **2017,** *41*, 10-22.
235. Mizushima, N., Autophagy: process and function. *Genes & development* **2007,** *21*, 2861-2873.
236. Mahmoudi, M.; Saeedi-Eslami, S. N.; Shokrgozar, M. A.; Azadmanesh, K.; Hassanlou, M.; Kalhor, H. R.; Burtea, C.; Rothen-Rutishauser, B.; Laurent, S.; Sheibani, S., Cell "vision": complementary factor of protein corona in nanotoxicology. *Nanoscale* **2012,** *4*, 5461-5468.
237. Azhdarzadeh, M.; Saei, A. A.; Sharifi, S.; Hajipour, M. J.; Alkilany, A. M.; Sharifzadeh, M.; Ramazani, F.; Laurent, S.; Mashaghi, A.; Mahmoudi, M., Nanotoxicology: advances and pitfalls in research methodology. *Nanomedicine* **2015,** *10*, 2931-2952.
238. Sakhtianchi, R.; Minchin, R. F.; Lee, K.-B.; Alkilany, A. M.; Serpooshan, V.; Mahmoudi, M., Exocytosis of nanoparticles from cells: role in cellular retention and toxicity. *Advances in colloid and interface science* **2013,** *201*, 18-29.
239. Yanes, R. E.; Tarn, D.; Hwang, A. A.; Ferris, D. P.; Sherman, S. P.; Thomas, C. R.; Lu, J.; Pyle, A. D.; Zink, J. I.; Tamanoi, F., Involvement of lysosomal exocytosis in the excretion of mesoporous silica nanoparticles and enhancement of the drug delivery effect by exocytosis inhibition. *Small* **2013,** *9*, 697-704.
240. Ho, L. W. C.; Chan, C. K. W.; Han, R.; Lau, Y. F. Y.; Li, H.; Ho, Y.-P.; Zhuang, X.; Choi, C. H. J., Mammalian Cells Exocytose Alkylated Gold Nanoparticles via Extracellular Vesicles. *ACS nano* **2022,** *16*, 2032-2045.
241. Bertoli, F.; Davies, G. L.; Monopoli, M. P.; Moloney, M.; Gun'ko, Y. K.; Salvati, A.; Dawson, K. A., Magnetic nanoparticles to recover cellular organelles and study the time resolved nanoparticle-cell interactome throughout uptake. *Small* **2014,** *10*, 3307-3315.

242. Wang, C.; Chen, B.; He, M.; Hu, B., Composition of Intracellular Protein Corona around Nanoparticles during Internalization. *ACS nano* **2021,** *15*, 3108-3122.
243. Hofmann, D.; Tenzer, S.; Bannwarth, M. B.; Messerschmidt, C.; Glaser, S. F.; Schild, H.; Landfester, K.; Mailander, V., Mass spectrometry and imaging analysis of nanoparticle-containing vesicles provide a mechanistic insight into cellular trafficking. *ACS Nano* **2014,** *8*, 10077-88.
244. Nölte, J., *ICP Emissionsspektrometrie für Praktiker: Grundlagen, Methodenentwicklung, Anwendungsbeispiele*. John Wiley & Sons Hobooken, NJ, USA: 2003.
245. Kocherlakota, N., Factors to be considered in the preparation of single and multi-element standards for inductively coupled plasma optical emission spectrometry. *Analyst* **1992,** *117*, 401-406.
246. Ammann, A. A., Inductively coupled plasma mass spectrometry (ICP MS): a versatile tool. *Journal of mass spectrometry* **2007,** *42*, 419-427.
247. Khan, K. F., Application, principle and operation of ICP-OES in pharmaceutical analysis. *The Pharmaceutical Innovation Journal* **2019,** *8*, 281-282.
248. Nomizu, T.; Kaneco, S.; Tanaka, T.; Ito, D.; Kawaguchi, H.; Vallee, B. T., Determination of calcium content in individual biological cells by inductively coupled plasma atomic emission spectrometry. *Analytical Chemistry* **1994,** *66*, 3000-3004.
249. Mueller, L.; Traub, H.; Jakubowski, N.; Drescher, D.; Baranov, V. I.; Kneipp, J., Trends in single-cell analysis by use of ICP-MS. *Analytical and bioanalytical chemistry* **2014,** *406*, 6963-6977.
250. Prohaska, C.; Pomazal, K.; Steffan, I., Determination of Ca, Mg, Fe, Cu, and Zn in blood fractions and whole blood of humans by ICP-OES. *Fresenius' journal of analytical chemistry* **2000,** *367*, 479-484.
251. Haraguchi, H., Metallomics: Integrated biometal science. In *Metallomics*, Springer: 2017; pp 3-39.
252. Ohayon-Courtès, C.; Passagne, I.; De Portal, C.; Pouvreau, C.; Cambar, J.; L'Azou, B., ICP/OES application for assessing cadmium uptake (or toxicity) in glomerular cells: influence of extracellular calcium. *Journal of Toxicology and Environmental Health, Part A* **2007,** *70*, 750-759.
253. Parsons, J.; Tiemann, K.; Peralta-Videa, J.; Gardea-Torresdey, J., Sorption of uranyl cations onto inactivated cells of alfalfa biomass investigated using chemical modification, ICP-OES, and XAS. *Environmental science & technology* **2006,** *40*, 4181-4188.
254. Riedel, F.; Hönle, W.; Göske, J.; Kachler, W.; Holzwarth, U.; Schuh, A., Examination of granuloma of revised cemented or cementless total hip arthroplasties using inductively coupled plasma atomic emission spectrometry (ICP-OES). *Biomedizinische Technik. Biomedical Engineering* **2006,** *51*, 15-20.
255. Liu, Y.; Shipton, M. K.; Ryan, J.; Kaufman, E. D.; Franzen, S.; Feldheim, D. L., Synthesis, stability, and cellular internalization of gold nanoparticles containing mixed peptide− poly (ethylene glycol) monolayers. *Analytical chemistry* **2007,** *79*, 2221-2229.
256. Ferrati, S.; Mack, A.; Chiappini, C.; Liu, X.; Bean, A. J.; Ferrari, M.; Serda, R. E., Intracellular trafficking of silicon particles and logic-embedded vectors. *Nanoscale* **2010,** *2*, 1512-1520.
257. Asharani, P.; Hande, M. P.; Valiyaveettil, S., Anti-proliferative activity of silver nanoparticles. *BMC cell biology* **2009,** *10*, 1-14.
258. Ho, L. W. C.; Yin, B.; Dai, G.; Choi, C. H. J., Effect of surface modification with hydrocarbyl groups on the exocytosis of nanoparticles. *Biochemistry* **2020,** *60*, 1019-1030.
259. Oh, N.; Park, J.-H., Surface chemistry of gold nanoparticles mediates their exocytosis in macrophages. *ACS nano* **2014,** *8*, 6232-6241.
260. Wang, Y.; Wu, Q.; Sui, K.; Chen, X.-X.; Fang, J.; Hu, X.; Wu, M.; Liu, Y., A quantitative study of exocytosis of titanium dioxide nanoparticles from neural stem cells. *Nanoscale* **2013,** *5*, 4737-4743.
261. Han, Y.; Li, X.; Zhang, Y.; Han, Y.; Chang, F.; Ding, J., Mesenchymal stem cells for regenerative medicine. *Cells* **2019,** *8*, 886.
262. Motiei, M.; Dreifuss, T.; Sadan, T.; Omer, N.; Blumenfeld-Katzir, T.; Fragogeorgi, E.; Loudos, G.; Popovtzer, R.; Ben-Eliezer, N., Trimodal Nanoparticle Contrast Agent for CT, MRI

and SPECT Imaging: Synthesis and Characterization of Radiolabeled Core/Shell Iron Oxide@Gold Nanoparticles. *Chemistry Letters* **2019,** *48*, 291-294.
263. Chemla, Y.; Betzer, O.; Markus, A.; Farah, N.; Motiei, M.; Popovtzer, R.; Mandel, Y., Gold nanoparticles for multimodal high-resolution imaging of transplanted cells for retinal replacement therapy. *Nanomedicine* **2019,** *14*, 1857-1871.
264. Barthélémy, I.; Thibaud, J.-L.; de Fornel, P.; Cassano, M.; Punzón, I.; Mauduit, D.; Vilquin, J.-T.; Devauchelle, P.; Sampaolesi, M.; Blot, S., In vivo stem cell tracking using scintigraphy in a canine model of DMD. *Scientific reports* **2020,** *10*, 1-13.
265. Glover, J. C.; Aswendt, M.; Boulland, J.-L.; Lojk, J.; Stamenković, S.; Andjus, P.; Fiori, F.; Hoehn, M.; Mitrecic, D.; Pavlin, M., In vivo cell tracking using non-invasive imaging of iron oxide-based particles with particular relevance for stem cell-based treatments of neurological and cardiac disease. *Molecular Imaging and Biology* **2020,** *22*, 1469-1488.
266. Chithrani, B. D.; Ghazani, A. A.; Chan, W. C., Determining the size and shape dependence of gold nanoparticle uptake into mammalian cells. *Nano letters* **2006,** *6*, 662-668.
267. Senut, M. C.; Zhang, Y.; Liu, F.; Sen, A.; Ruden, D. M.; Mao, G., Size-dependent toxicity of gold nanoparticles on human embryonic stem cells and their neural derivatives. *Small* **2016,** *12*, 631-646.
268. Meir, R.; Shamalov, K.; Betzer, O.; Motiei, M.; Horovitz-Fried, M.; Yehuda, R.; Popovtzer, A.; Popovtzer, R.; Cohen, C. J., Nanomedicine for cancer immunotherapy: tracking cancer-specific T-cells in vivo with gold nanoparticles and CT imaging. *ACS nano* **2015,** *9*, 6363-6372.
269. Yu, C.; Bao, H.; Chen, Z.; Li, X.; Liu, X.; Wang, W.; Huang, J.; Zhang, Z., Enhanced and long-term CT imaging tracking of transplanted stem cells labeled with temperature-responsive gold nanoparticles. *Journal of Materials Chemistry B* **2021,** *9*, 2854-2865.
270. Bao, H.; Xia, Y.; Yu, C.; Ning, X.; Liu, X.; Fu, H.; Chen, Z.; Huang, J.; Zhang, Z., CT/Bioluminescence Dual-Modal Imaging Tracking of Mesenchymal Stem Cells in Pulmonary Fibrosis. *Small* **2019,** *15*, 1904314.
271. Ning, X.; Bao, H.; Liu, X.; Fu, H.; Wang, W.; Huang, J.; Zhang, Z., Long-term in vivo CT tracking of mesenchymal stem cells labeled with Au@ BSA@ PLL nanotracers. *Nanoscale* **2019,** *11*, 20932-20941.
272. Ramot, Y.; Meiron, M.; Toren, A.; Steiner, M.; Nyska, A., Safety and biodistribution profile of placental-derived mesenchymal stromal cells (PLX-PAD) following intramuscular delivery. *Toxicologic pathology* **2009,** *37*, 606-616.
273. Zahavi-Goldstein, E.; Blumenfeld, M.; Fuchs-Telem, D.; Pinzur, L.; Rubin, S.; Aberman, Z.; Sher, N.; Ofir, R., Placenta-derived PLX-PAD mesenchymal-like stromal cells are efficacious in rescuing blood flow in hind limb ischemia mouse model by a dose-and site-dependent mechanism of action. *Cytotherapy* **2017,** *19*, 1438-1446.
274. Norgren, L.; Weiss, N.; Nikol, S.; Hinchliffe, R. J.; Lantis, J. C.; Patel, M. R.; Reinecke, H.; Ofir, R.; Rosen, Y.; Peres, D., PLX-PAD cell treatment of critical limb ischaemia: rationale and design of the PACE trial. *European Journal of Vascular and Endovascular Surgery* **2019,** *57*, 538-545.
275. Chatterjee, P.; Chiasson, V. L.; Pinzur, L.; Raveh, S.; Abraham, E.; Jones, K. A.; Bounds, K. R.; Ofir, R.; Flaishon, L.; Chajut, A., Human placenta-derived stromal cells decrease inflammation, placental injury and blood pressure in hypertensive pregnant mice. *Clinical Science* **2016,** *130*, 513-523.
276. Rubinstein, L.; Paul, A. M.; Houseman, C.; Abegaz, M.; Tabares Ruiz, S.; O'Neil, N.; Kunis, G.; Ofir, R.; Cohen, J.; Ronca, A. E., Placenta-expanded stromal cell therapy in a rodent model of simulated weightlessness. *Cells* **2021,** *10*, 940.
277. Prather, W. R.; Toren, A.; Meiron, M.; Ofir, R.; Tschope, C.; Horwitz, E. M., The role of placental-derived adherent stromal cell (PLX-PAD) in the treatment of critical limb ischemia. *Cytotherapy* **2009,** *11*, 427-434.
278. Barkama, R.; Mayo, A.; Paz, A.; Solopov, A.; Mann, T.; Vadasz, Z.; Appel, T.; Ofir, R.; Shani, L.; Sheleg, M., Placenta-derived cell therapy to treat patients with respiratory failure due to coronavirus disease 2019. *Critical care explorations* **2020,** *2*.
279. Winkler, T.; Perka, C.; von Roth, P.; Agres, A. N.; Plage, H.; Preininger, B.; Pumberger, M.; Geissler, S.; Hagai, E. L.; Ofir, R.; Pinzur, L.; Eyal, E.; Stoltenburg-Didinger, G.; Meisel, C.; Consentius, C.; Streitz, M.; Reinke, P.; Duda, G. N.; Volk, H. D., Immunomodulatory

placental-expanded, mesenchymal stromal cells improve muscle function following hip arthroplasty. *J Cachexia Sarcopenia Muscle* **2018,** *9*, 880-897.
280. Maleitzke, T.; Reinke, P.; Agres, A. N.; Alves, S. A.; Akyüz, L.; Fleckenstein, F. N.; Bichmann, A.; Ofir, R.; Perka, C.; Duda, G. N., Intramuscular and intratendinous placenta-derived mesenchymal stromal-like cell treatment of a chronic quadriceps tendon rupture. *Journal of Cachexia, Sarcopenia and Muscle* **2022,** *13*, 434-445.
281. Papait, A.; Vertua, E.; Magatti, M.; Ceccariglia, S.; De Munari, S.; Silini, A. R.; Sheleg, M.; Ofir, R.; Parolini, O., Mesenchymal stromal cells from fetal and maternal placenta possess key similarities and differences: potential implications for their applications in regenerative medicine. *Cells* **2020,** *9*, 127.
282. Consentius, C.; Akyüz, L.; Schmidt-Lucke, J.; Tschöpe, C.; Pinzur, L.; Ofir, R.; Reinke, P.; Volk, H. D.; Juelke, K., Mesenchymal stromal cells prevent allostimulation in vivo and control checkpoints of Th1 priming: migration of human DC to lymph nodes and NK cell activation. *Stem cells* **2015,** *33*, 3087-3099.
283. Lahiani, A.; Zahavi, E.; Netzer, N.; Ofir, R.; Pinzur, L.; Raveh, S.; Arien-Zakay, H.; Yavin, E.; Lazarovici, P., Human placental eXpanded (PLX) mesenchymal-like adherent stromal cells confer neuroprotection to nerve growth factor (NGF)-differentiated PC12 cells exposed to ischemia by secretion of IL-6 and VEGF. *Biochimica et Biophysica Acta (BBA)-Molecular Cell Research* **2015,** *1853*, 422-430.
284. Ding, L.; Yao, C.; Yin, X.; Li, C.; Huang, Y.; Wu, M.; Wang, B.; Guo, X.; Wang, Y.; Wu, M., Size, shape, and protein corona determine cellular uptake and removal mechanisms of gold nanoparticles. *Small* **2018,** *14*, 1801451.
285. Renz, P.; Kokkinopoulou, M.; Landfester, K.; Lieberwirth, I., Imaging of polymeric nanoparticles: hard challenge for soft objects. *Macromolecular Chemistry and Physics* **2016,** *217*, 1879-1885.
286. Bradshaw, R. A.; Burlingame, A. L.; Carr, S.; Aebersold, R., Reporting protein identification data: the next generation of guidelines. *Molecular & Cellular Proteomics* **2006,** *5*, 787-788.
287. Huang, D. W.; Sherman, B. T.; Lempicki, R. A., Systematic and integrative analysis of large gene lists using DAVID bioinformatics resources. *Nature protocols* **2009,** *4*, 44-57.
288. Huang, D. W.; Sherman, B. T.; Lempicki, R. A., Bioinformatics enrichment tools: paths toward the comprehensive functional analysis of large gene lists. *Nucleic acids research* **2009,** *37*, 1-13.
289. Cao, Y., The toxicity of nanoparticles to human endothelial cells. *Cellular and molecular toxicology of nanoparticles* **2018**, 59-69.
290. Nokes, R. L.; Fields, I. C.; Collins, R. N.; Fölsch, H., Rab13 regulates membrane trafficking between TGN and recycling endosomes in polarized epithelial cells. *The Journal of cell biology* **2008,** *182*, 845-853.
291. Morimoto, S.; Nishimura, N.; Terai, T.; Manabe, S.; Yamamoto, Y.; Shinahara, W.; Miyake, H.; Tashiro, S.; Shimada, M.; Sasaki, T., Rab13 mediates the continuous endocytic recycling of occludin to the cell surface. *Journal of Biological Chemistry* **2005,** *280*, 2220-2228.
292. Donahue, N. D.; Acar, H.; Wilhelm, S., Concepts of nanoparticle cellular uptake, intracellular trafficking, and kinetics in nanomedicine. *Advanced drug delivery reviews* **2019,** *143*, 68-96.
293. Chithrani, B. D.; Chan, W. C., Elucidating the mechanism of cellular uptake and removal of protein-coated gold nanoparticles of different sizes and shapes. *Nano letters* **2007,** *7*, 1542-1550.
294. Buckmaster, M. J.; Braico Jr, D. L.; Ferris, A. L.; Storrie, B., Retention of pinocytized solute by CHO cell lysosomes correlates with molecular weight. *Cell biology international reports* **1987,** *11*, 501-507.
295. Swanson, J. A.; Yirinec, B. D.; Silverstein, S. C., Phorbol esters and horseradish peroxidase stimulate pinocytosis and redirect the flow of pinocytosed fluid in macrophages. *The Journal of cell biology* **1985,** *100*, 851-859.
296. Oberländer, J.; Champanhac, C.; da Costa Marques, R.; Landfester, K.; Mailänder, V., Temperature, concentration, and surface modification influence the cellular uptake and the protein corona of polystyrene nanoparticles. *Acta Biomaterialia* **2022,** *148*, 271-278.
297. Sakulkhu, U.; Mahmoudi, M.; Maurizi, L.; Salaklang, J.; Hofmann, H., Protein corona composition of superparamagnetic iron oxide nanoparticles with various physico-chemical properties and coatings. *Scientific reports* **2014,** *4*, 1-9.

298. Serda, R. E.; Mack, A.; Van De Ven, A. L.; Ferrati, S.; Dunner Jr, K.; Godin, B.; Chiappini, C.; Landry, M.; Brousseau, L.; Liu, X., Logic-Embedded Vectors for Intracellular Partitioning, Endosomal Escape, and Exocytosis of Nanoparticles. *Small* **2010,** *6*, 2691-2700.
299. Doerr, A., A flow cytometry revolution. *Nature methods* **2011,** *8*, 531-531.
300. Rivera_Gil, P.; Nazarenus, M.; Ashraf, S.; Parak, W. J., pH-sensitive capsules as intracellular optical reporters for monitoring lysosomal pH changes upon stimulation. *Small* **2012,** *8*, 943-948.
301. Strobel, C.; Oehring, H.; Herrmann, R.; Förster, M.; Reller, A.; Hilger, I., Fate of cerium dioxide nanoparticles in endothelial cells: exocytosis. *Journal of Nanoparticle Research* **2015,** *17*, 1-14.
302. Van Niel, G.; d'Angelo, G.; Raposo, G., Shedding light on the cell biology of extracellular vesicles. *Nature reviews Molecular cell biology* **2018,** *19*, 213-228.
303. Ono, K.; Eguchi, T.; Sogawa, C.; Calderwood, S. K.; Futagawa, J.; Kasai, T.; Seno, M.; Okamoto, K.; Sasaki, A.; Kozaki, K. i., HSP-enriched properties of extracellular vesicles involve survival of metastatic oral cancer cells. *Journal of cellular biochemistry* **2018,** *119*, 7350-7362.
304. Mallia, A.; Gianazza, E.; Zoanni, B.; Brioschi, M.; Barbieri, S. S.; Banfi, C., Proteomics of extracellular vesicles: update on their composition, biological roles and potential use as diagnostic tools in atherosclerotic cardiovascular diseases. *Diagnostics* **2020,** *10*, 843.
305. Choi, D. S.; Kim, D. K.; Kim, Y. K.; Gho, Y. S., Proteomics of extracellular vesicles: exosomes and ectosomes. *Mass spectrometry reviews* **2015,** *34*, 474-490.

Acknowledgements

First, I want to thank Prof. XXX and Prof. XXX for giving me the opportunity to carry out my PhD thesis on these interesting topics. I am very grateful for their supervision and support during the three years of my PhD. I am especially grateful that despite the pandemic, both have always tried to make it possible to work safely.

Further, I would like to thank Prof. XXX and Prof. XXX for being my second expert and for being my referee. Additionally, many thanks go to all my cooperation partners in the European Project nTrack and from the VISTEC institute in Thailand for the exciting collaborations during my doctoral studies.

Many thanks to the members and former members of XXX´s group and the small subgroup of XXX at the Max Planck Institute and at the PKZI. Thank you for the great working atmosphere, fun activities, and scientific discussions. Special thanks to all the technicians from AK XXX for their support, especially to XXX for cell cultivation and Biolab assistance, XXX for performing DLS measurements, XXX for TEM measurements, XXX for nanoparticle synthesis, and XXX for the help with the creation of different graphics and figures. In addition, I would like to thank Dr. XXX who supervised me at the beginning of my PhD and trained me at the LC-MS.

Finally, I would like to thank my family and friends, especially my parents, my sister, and my boyfriend for their support during my studies and doctoral work. Without your support, this thesis would not have been possible.